Earth-Science Reviews 216 (2021) 103577

Contents lists available at ScienceDirect

Earth-Science Reviews

journal homepage: www.elsevier.com/locate/earscirev

Freshening of the Mediterranean Salt Giant: controversies and certainties around the terminal (Upper Gypsum and Lago-Mare) phases of the Messinian Salinity Crisis

F. Andreetto [a,*], G. Aloisi [b], F. Raad [c], H. Heida [d], R. Flecker [e], K. Agiadi [f], J. Lofi [c], S. Blondel [g], F. Bulian [h], A. Camerlenghi [g], A. Caruso [i], R. Ebner [j], D. Garcia-Castellanos [d], V. Gaullier [k], L. Guibourdenche [b], Z. Gvirtzman [l,m], T.M. Hoyle [a,n], P.T. Meijer [j], J. Moneron [l,m], F.J. Sierro [h], G. Travan [k], A. Tzevahirtzian [i], I. Vasiliev [o], W. Krijgsman [a]

[a] Paleomagnetic Laboratory "Fort Hoofddijk", Dept. of Earth Sciences, Utrecht University, Budapestlaan 17, 3584 CD Utrecht, The Netherlands
[b] Université de Paris, Institut de physique du globe de Paris, CNRS, F-75005 Paris, France
[c] Géosciences Montpellier, CNRS, Université de Montpellier, Montpellier, France
[d] Geosciences Barcelona, GEO3BCN, CSIC, Solé i Sabarís s/n, Barcelona, Spain
[e] BRIDGE, School of Geographical Sciences and Cabot Institute, University of Bristol, University Road, Bristol BS8 1SS, United Kingdom
[f] Department of Palaeontology, University of Vienna, Althanstraße 14 (UZA II), 1090 Vienna, Austria
[g] Istituto Nazionale di Oceanografia e di Geofisica Sperimentale (OGS), Trieste, Italy
[h] Department of Geology, University of Salamanca, Salamanca, Spain
[i] Dipartimento di Scienze della Terra e del Mare, Università degli studi di Palermo, via Archirafi 20-22, 90123 Palermo, Italy
[j] Department of Earth Sciences, Utrecht University, Utrecht, The Netherlands
[k] Univ. Lille, CNRS, Univ. Littoral Côte d'Opale, UMR 8187, LOG, Laboratoire d'Océanologie et de Géosciences, F 59000, Lille, France
[l] Geological Survey of Israel, Jerusalem 95501, Israel
[m] Institute of Earth Sciences, The Hebrew University of Jerusalem, Israel
[n] CASP, West Building, Madingley Rise, Madingley Road, Cambridge CB3 0UD, United Kingdom
[o] Senckenberg Research Biodiversity and Climate Research Centre, Senckenberganlage 25, 60325 Frankfurt am Main, Germany

ARTICLE INFO

Keywords:
Messinian Salinity Crisis
Mediterranean stratigraphy
Connectivity proxies
Paleogeography
Paratethys
Lago-Mare

ABSTRACT

The late Miocene evolution of the Mediterranean Basin is characterized by major changes in connectivity, climate and tectonic activity resulting in unprecedented environmental and ecological disruptions. During the Messinian Salinity Crisis (MSC, 5.97-5.33 Ma) this culminated in most scenarios first in the precipitation of gypsum around the Mediterranean margins (Stage 1, 5.97-5.60 Ma) and subsequently > 2 km of halite on the basin floor, which formed the so-called Mediterranean Salt Giant (Stage 2, 5.60-5.55 Ma). The final MSC Stage 3, however, was characterized by a "low-salinity crisis", when a second calcium-sulfate unit (Upper Gypsum; substage 3.1, 5.55-5.42 Ma) showing (bio)geochemical evidence of substantial brine dilution and brackish biota-bearing terrigenous sediments (substage 3.2 or Lago-Mare phase, 5.42-5.33 Ma) deposited in a Mediterranean that received relatively large amounts of riverine and Paratethys-derived low-salinity waters. The transition from hypersaline evaporitic (halite) to brackish facies implies a major change in the Mediterranean's hydrological regime. However, even after nearly 50 years of research, causes and modalities are poorly understood and the original scientific debate between a largely isolated and (partly) desiccated Mediterranean or a fully connected and filled basin is still vibrant. Here we present a comprehensive overview that brings together (chrono)stratigraphic, sedimentological, paleontological, geochemical and seismic data from all over the Mediterranean. We summarize the paleo-environmental, paleohydrological and paleoconnectivity scenarios that arose from this cross-disciplinary dataset and we discuss arguments in favour of and against each scenario.

* Corresponding author.
E-mail address: f.andreetto@uu.nl (F. Andreetto).

https://doi.org/10.1016/j.earscirev.2021.103577
Received 1 November 2020; Received in revised form 4 February 2021; Accepted 25 February 2021
Available online 3 March 2021

1. Introduction

At the end of the Miocene, orbital and tectonic drivers combined to alter the amount of water delivered to the Mediterranean Basin by the Atlantic Ocean from the west, the brackish Eastern Paratethys (i.e. Euxinic-Caspian Basin system) from the east and the major peri-Mediterranean freshwater drainage systems (e.g. African rivers and Rhône; Griffin, 2002; Gladstone et al., 2007; Van der Laan et al., 2006; Hilgen et al., 2007; Ryan, 2009; Flecker et al., 2015; Marzocchi et al., 2015, 2016, 2019; Simon et al., 2017; Krijgsman et al., 2018; Capella et al., 2020). The changes in extra and intrabasinal connectivity resulted in unprecedented paleoceanographic and paleohydrological budget changes that led to a relatively short-lived environmental and ecological crisis (approx. 660 kyr; 5.97-5.33 Ma), for which the term Messinian Salinity Crisis (MSC) was coined (Selli, 1954, 1960). Most conspicuous was the rapid accumulation of several kilometers of halite (i.e. ~1 million km^3) on the Mediterranean abyssal plains (e.g. Hsü, 1972; Ryan, 1973; Montadert et al., 1978; Haq et al., 2020). This happened within 50 kyr, from 5.60-5.55 Ma, according to Roveri et al. (2014a) and Manzi et al. (2018), or in >300 kyr, when starting at 5.97 Ma, as put forward by Meilijson et al. (2018, 2019).

During the ~200 kyr lapse (i.e. MSC Stage 3 following Roveri et al., 2014a; Fig. 1a) between the end of salt precipitation (5.55 Ma) and the restoration of the still enduring marine conditions (5.33 Ma), the Mediterranean underwent a sequence of paleohydrological and base-level changes that are the topic of intense and long-standing debates. The initial and still widely endorsed hypothesis was that the Mediterranean Sea, following the major drawdown event that led to halite deposition (i.e. Stage 2), maintained the isolated, deeply-desiccated geography containing a series of hypersaline (substage 3.1; 5.55-5.42 Ma) and hyposaline (substage 3.2; 5.42-5.33 Ma) ponds which only received water from local streams and were colonized by Black Sea organisms carried by aquatic migratory birds (Fig. 1b; e.g. Ruggieri, 1967; Decima and Sprovieri, 1973; Decima and Wezel, 1971, 1973; Cita et al., 1978; Müller et al., 1990; Benson and Rakic-El Bied, 1991; Benson et al., 1991; Müller and Mueller, 1991; Butler et al., 1995; Orszag-Sperber et al., 2000; Rouchy et al., 2001; Kartveit et al., 2019; Madof et al., 2019; Camerlenghi et al., 2019; Caruso et al., 2020; Raad et al., 2021). As morphological and seismic reflection studies at the Strait of Gibraltar documented a ~400 km long erosional trough connecting the Gulf of Cadiz (Atlantic Ocean) to the Mediterranean Sea, this scenario of a lowered Mediterranean Sea was promptly linked to the termination of the MSC (McKenzie, 1999; Blanc, 2002; Garcia-Castellanos et al., 2009, 2020). This conclusion has recently been reinforced by the discovery of vast chaotic deposits sitting at the claimed Miocene/Pliocene transition in the area of the Malta Escarpment-Ionian Abyssal Plain (Micallef et al., 2018, 2019; Spatola et al., 2020).

In more recent years, the desiccated basin model was challenged by the observation of deposits that are uniform in terms of sedimentology and stratigraphic architecture (Roveri et al., 2008a), ostracod content (Gliozzi et al., 2007; Stoica et al., 2016) and geochemistry (McCulloch and De Deckker, 1989; García-Veigas et al., 2018; Andreetto et al., 2021) throughout the Mediterranean marginal belt and of $\delta D_{n\text{-alkanes}}$ and $\delta D_{alkenones}$ sharing similarities with the coeval Atlantic Ocean and Black Sea, respectively (Vasiliev et al., 2017). A model of a (relatively) full Mediterranean Sea developed (Fig. 1c), where the debate mainly concerns the provenance of the hydrological fluxes and the resultant hydrochemical composition of the water mass. In this scenario, the Mediterranean was first, during substage 3.1, transformed into a new gypsum-precipitating basin filled with marine and continent-derived

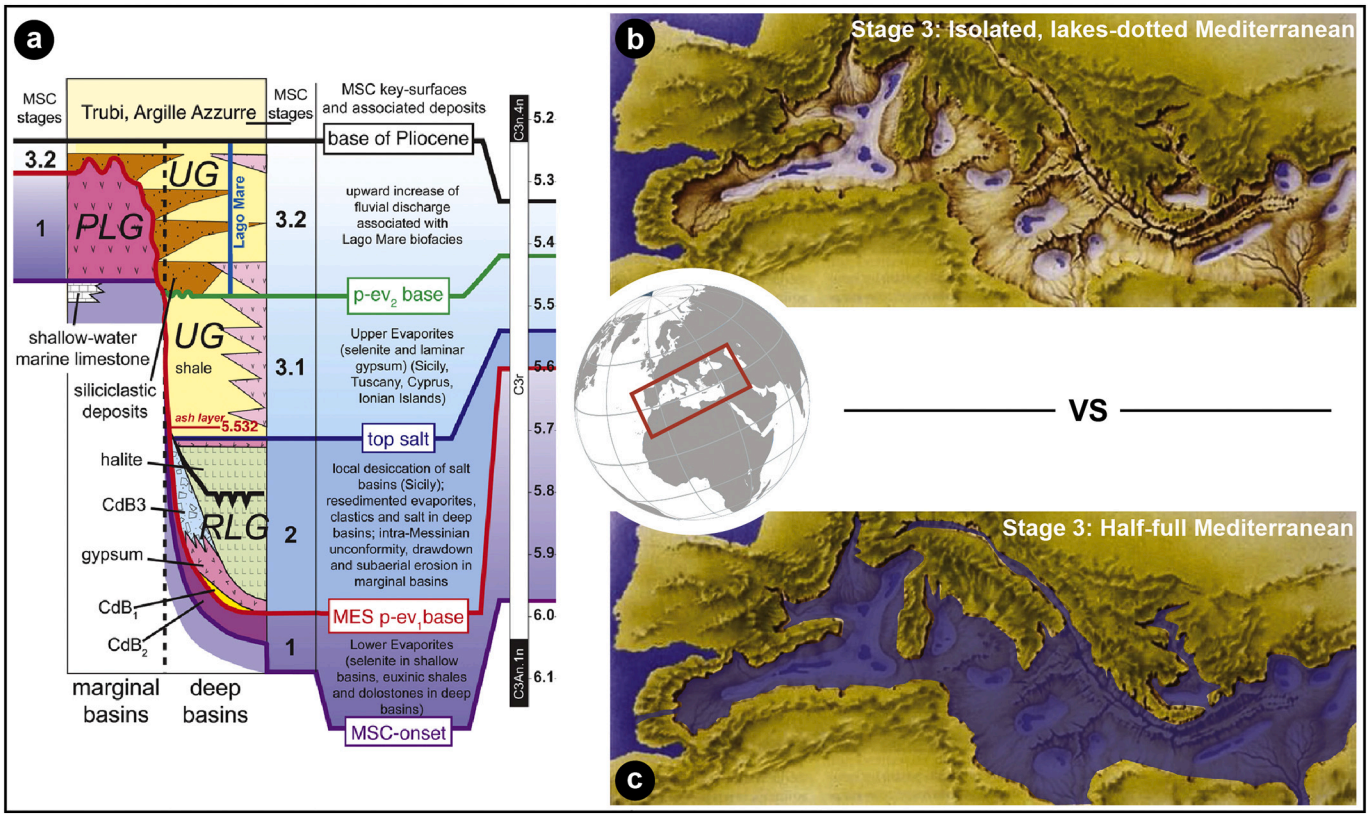

Fig. 1. (a) Consensus chronostratigraphic model for the MSC events (Roveri et al., 2014a). Stage 3, here of interest, spans between 5.55 Ma and 5.332 Ma, the astronomical ages of the base of the Upper Gypsum Unit (following Manzi et al., 2009) and Trubi Formation (Van Couvering et al., 2000) in the Sicilian Eraclea Minoa section, respectively. CdB: Calcare di Base; PLG: Primary Lower Gypsum; RLG: Resedimented Lower Gypsum; UG: Upper Gypsum. (b), (c) Map of the Mediterranean region showing the two extreme and mutually exclusive paleoenvironmental scenarios proposed to have featured the Mediterranean during Stage 3 (see discussion in Chapter 7; modified after Krijgsman et al., 2018).

waters (e.g. Manzi et al., 2009; Roveri et al., 2014c; Flecker et al., 2015; Vasiliev et al., 2017; García-Veigas et al., 2018; Grothe et al., 2020). Then, during substage 3.2, it became a brackish lake-sea comparable to the present-day Black Sea or Caspian Sea (Roveri et al., 2008a; Stoica et al., 2016; Andreetto et al., 2021), depending on whether a marine connection with the Atlantic was active (Manzi et al., 2009; Roveri et al., 2014b, 2014c; Flecker et al., 2015; Marzocchi et al., 2016; Vasiliev et al., 2017; García-Veigas et al., 2018) or not (e.g. McCulloch and De Deckker, 1989; Roveri et al., 2008a), and with a base-level fluctuating by hundreds of meters with precessional periodicity (Fortuin and Krijgsman, 2003; Ben Moshe et al., 2020; Andreetto et al., 2021). In the relatively full scenario, the revival of marine conditions is ascribed to either connectivity changes (Marzocchi et al., 2016) or to a moderate sea-level rise (Andreetto et al., 2021). In contrast, Carnevale et al. (2006a, 2006b, 2008, 2018) and Grunert et al. (2016), based on the recovery of fish remains ascribed to marine species, proposed that fully marine conditions were in force in the Mediterranean already at the end of substage 3.1.

After nearly 50 years of research on both onshore and offshore localities (Fig. 2), the observations backing up the competing desiccated and full-basin Mediterranean models remain extremely difficult to reconcile. Uncertainties regarding the chronostratigraphic framework of Stage 3 deposits, the origin and migration of its characteristic biota, the meaning of the data derived from the applied geochemical techniques

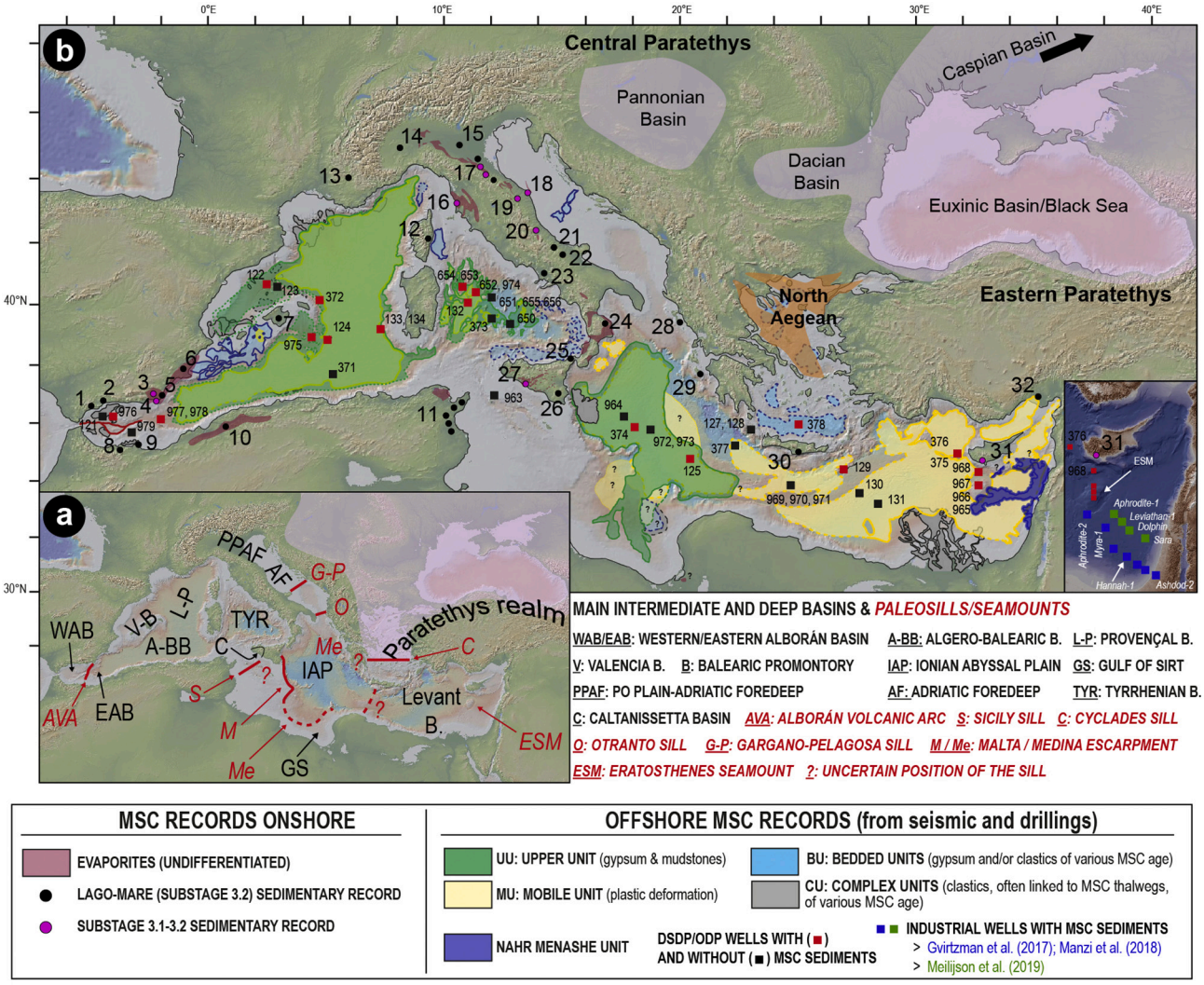

Fig. 2. Map of the Mediterranean Basin (modified from Lofi, 2018) showing: a) the location of the key intermediate and deep basins as well as physical thresholds that influenced the connectivity history of the Mediterranean; b) the onshore (i.e. basins and/or sections) and offshore (DSDP/ODP/Industrial drill sites) localities where deposits attributed to MSC Stage 3 have been studied. Mixed assemblages of Paratethyan-like ostracods and foraminifera are known from all mentioned onshore localities and some offshore locations (see text). The present-day spatial extent of the MSC seismic units, except for the Lower Unit, is also shown. The paleogeography of the (Eastern and Central) Paratethys and of the North Aegean domain is contoured after Van Baak et al. (2017) and Krijgsman et al. (2020a), respectively. W-E onshore localities: 1-6 Betic Cordillera (SE Spain): 1-Marbella and 2-Malaga basins (Guerra-Merchán et al., 2010); 3-Sorbas Basin (Roveri et al., 2009, 2019a); 4-Nijar Basin (Fortuin and Krijgsman, 2003); 5-Vera Basin (Fortuin et al., 1995); 6-Bajo Segura Basin (Soria et al., 2005, 2008a, 2008b); 7-Mallorca (Mas and Fornós, 2020); 8-Melilla Basin (Rouchy et al., 2003); 9-Boudinar Basin (Merzeraud et al., 2019); 10-Chelif Basin (Rouchy et al., 2007); 11-Sahel area (Frigui et al., 2016); 12-Aléria Basin and 13-Rhône Valley (Carbonnel, 1978); 14-Piedmont Basin (Dela Pierre et al., 2011, 2016); 15-Po Plain (Ghielmi et al., 2010, 2013; Amadori et al., 2018); 16-Fine Basin (Cava Serredi section; Carnevale et al., 2006a, 2008). 17-21 Apennine system: Romagna sections (17, Roveri et al., 1998), Trave section (18, Iaccarino et al., 2008), Maccarone section (19, Bertini, 2006, Grossi et al., 2008; Sampalmieri et al., 2010; Pellen et al., 2017), Colle di Votta (20)-Fonte dei Pulcini (21)-Stingeti (22) sections (Cosentino et al., 2005, 2012, 2013, 2018), Mondragone 1 well (23, Cosentino et al., 2006), Crotone Basin (24, Roveri et al., 2008a); 25-27 Sicily: Villafranca Tirrena (25) and Licodia Eubea (26) sections (Sciuto et al., 2018), Caltanissetta Basin (27, Manzi et al., 2009); 28-Corfu (Pierre et al., 2006); 29-Zakinthos (Karakitsios et al., 2017b); 30-Crete (Cosentino et al., 2007); 31-Cyprus (Rouchy et al., 2001; Manzi et al., 2016a); 32-Adana Basin (Radeff et al., 2016).

and the relationship between the Mediterranean and its surrounding water bodies (i.e. Atlantic Ocean, Indian Ocean and Paratethys) all inhibit a clear understanding of the Mediterranean base-level and its hydrochemical structure.

In this paper we attempt to summarize all the existing, but heavily scattered, data resulting from ~50 years of cross-disciplinary studies with the aim of providing a comprehensive overview of the stratigraphic arrangement of Stage 3 onshore and offshore deposits, as well as of their sedimentological, paleontological, geochemical and seismic properties. Subsequently, we assemble the observations favoring both end-member scenarios of a relatively desiccated and relatively full Mediterranean. Finally, we focus on novel future analytical techniques and approaches that have the potential to constrain Mediterranean base-level during MSC Stage 3 as well as the changing hydrological fluxes and connectivity phases between the intra-Mediterranean basins and the neighboring Atlantic Ocean and Paratethyan domains as a mean of reconstructing the state of the art of the complex history of this enigmatic period of the Mediterranean history once and for all.

2. The terminal Stage 3 of the MSC

2.1. Historic overview of nomenclature and concepts

The final phase of the MSC (i.e. substage 3.2), also known as “Lago-Mare”, finds its sedimentary expression in cyclically-arranged terrigenous and evaporitic sediments hosting unique faunal assemblages of ostracods, mollusks and dinoflagellate cysts (dinocysts). They are related, at species level, to those inhabiting, during the Miocene, the brackish basins of the Paratethys realm (e.g. Gliozzi et al., 2007; Stoica et al., 2016). But what exactly is the “Lago-Mare”? This widely employed expression in the MSC literature encompasses a variety of meanings that make its application doubtful and misleading. The root of the wording “Lago-Mare” is to be found in the Russian scientific literature of the late 1800s. Nikolai Andrusov (1890) used the corresponding Russian term with a geographical and chronological connotation in reference to the series of central-eastern European basins that during the Miocene turned from marine settings to desalinized semi-isolated lakes with an endemic fresh-brackish water biota association (e.g. Popov et al., 2006 and references therein). The original monograph of Andrusov (1890) was not widely available outside Russia, but his attendance of international conferences allowed his research to spread outside the Russian borders. From the publications of the French geologists Suzette Gillet (Gillet, 1932, 1933) and Maurice Gignoux (Gignoux, 1936a) we can state with relative certainty that the original meaning of the word “Lago-Mare” (here reported with the French counterpart “Lac-Mer”) had its provenance in the Russian literature:

> *“[…] An isolation of the basin, that became a brackish, isolated basin. Then, a uniform fauna populated this immense lac-mer which was divided […] into Pannonian basin, […] Dacique Basin, and Euxin and Caspian basin […]”* (Gillet, 1932).
>
> *“[…] During the Volhynien (Sarmatique inferior) there was a lac-mer of uniform fauna that extended through all the eastern Europe. […] and the fauna of the eastern regions of that huge lac-mer was completely differenciated* [sic] *from the one in the western regions. […]”* (Gillet, 1933).
>
> *“[…] The Pontien fauna is not anymore a fauna characteristic of an internal saline sea, as in the Sarmantien, but is a fauna of a “desalinated lagoon”, a lac-mer, as the Russian geologists named it. […]”* (Gignoux, 1936b).

In the late 19th (Capellini, 1880) and 20th century (Ogniben, 1955; Ruggieri, 1962, 1967; Decima, 1964), late Messinian ostracod- and mollusk-bearing deposits in the Mediterranean were described at several Italian localities. Initially, the expressions “*Congeria* beds” (Capellini, 1880) and "*Melanopsis* beds" (Ruggieri, 1962) were used. Later on, Ruggieri (1967) pointed out the affinity of these faunal elements with those of the Pontian of the Paratethys. Consequently, he speculated on a feasible Paratethys-like paleoenvironmental configuration for the Mediterranean in the latest Messinian and he coined the Italian translation (i.e. "Lago-Mare") from the French “Lac-Mer” in reference to the shallow-water lakes claimed to be widely distributed across the Mediterranean. Progress in the 1970s in onshore and offshore exploration highlighted the temporally well-constrained distribution of the Paratethyan organisms in the Mediterranean (Carbonnel, 1978). On this premise, Hsü et al. (1978a) proposed to use "Lago-Mare" to "*designate the latest Messinian oligohaline environment, postdating evaporite deposition and predating Pliocene marine sedimentation […] in order to distinguish it from "lac mer" which, strictly speaking, was a Paratethyan environment*". Notwithstanding the new definition, in various parts of the text they used "Lago-Mare" to refer to the Paratethyan lakes (pp. 1071-1072: "*[…] The upper Messinian Mediterranean was floored by a series of desert basins, some with salt lakes, prior to inundation by the Lago-Mare.*"), thus giving rise to the confusion on how to use the term properly.

In the most recent stratigraphic overview of the MSC (Fig. 1a; Roveri et al., 2014a), the terminal MSC stage is called Stage 3, which is in turn subdivided into substages 3.1 and 3.2 (also termed Lago-Mare). Beside such a chronostratigraphic definition, the term “Lago-Mare” has also been used for a typical biofacies of the late Messinian Mediterranean (e.g. Fortuin et al., 1995; Gliozzi, 1999; Gliozzi and Grossi, 2008; Sciuto et al., 2018), for the pelitic beds encasing the Paratethyan-related fauna (i.e. a lithofacies; e.g. Fortuin and Krijgsman, 2003; Sciuto et al., 2018), as the name of an informal lithostratigraphic unit (usually distinguished by its fossil content) sandwiched between the Sicilian Upper Gypsum and the Arenazzolo Fm. (Fig. 4b; Clauzon et al., 2005; Londeix et al., 2007; Popescu et al., 2009; Bache et al., 2012) and to denote multiple (3 to 4) spilling events of the Paratethys into the Mediterranean (Clauzon et al., 2005, 2015; Popescu et al., 2007, 2009, 2015; Suc et al., 2011; Bache et al., 2012; Do Couto et al., 2014; Frigui et al., 2016; Mas and Fornós, 2020).

This being a review, we use the widely employed definition of the model of Roveri et al., 2014a) (Fig. 1a) and regard the Lago-Mare as a “phase of massive biota migration from the Paratethys realm, cyclostratigraphically constrained between 5.42 Ma and 5.332 Ma (Roveri et al., 2008a; Grossi et al., 2011), during which the Mediterranean sedimentary environments underwent an impressive freshening”. Nevertheless, we call for caution in the use of this definition of “Lago-Mare” in future studies, since 5.42 Ma as the (astronomical) age of the first entrance of Paratethyan organisms into the Mediterranean is likely to be incorrect (see subsection 5.1) and evidence of ‘impressive freshening’ are already present much earlier (e.g. at Eraclea Minoa; Vasiliev et al., 2017; García-Veigas et al., 2018).

2.2. Development of a chronostratigraphic framework

Issues of the timing and duration of the MSC only began to be tackled in the 1990s, in parallel with discussion concerning the nature of its extreme paleoenvironments (Schmalz, 1969; Hsü et al., 1973a, 1973b, 1973c, Hsü et al., 1978a, 1978b; Nesteroff, 1973; De Benedetti, 1982). While published models (Butler et al., 1995; Clauzon et al., 1996; Krijgsman et al., 1999a; Rouchy and Caruso, 2006) mostly converged on the (astronomical) age of the marine replenishment at the beginning of the Pliocene (5.332 Ma; Van Couvering et al., 2000), there were disagreements about the age of the onset of the MSC (synchronous vs diachronous) and of specific events within it (see discussion in Roveri et al., 2014a). Among these, the work of Krijgsman et al. (1999a) has obtained wide consensus. Their cyclostratigraphic tuning and correlation of continuous and bio-magnetostratigraphically constrained pre-evaporitic sections in Spain (Sorbas), Sicily (Gibliscemi/Falconara) and Greece (Metochia) resulted in a synchronous age of 5.96±0.02 Ma for the MSC onset (later refined to 5.97 Ma by Manzi et al., 2013). The astronomical ages for the onset (Krijgsman et al., 1999a) and termination (Van Couvering et al., 2000) of the MSC are not contentious since

the characteristic sedimentary cyclicity and sediments' properties (e.g. color of the lithologies and biota content) of the pre- and post-MSC successions fit robustly with the insolation curve (see also Van der Laan et al., 2006 and Topper and Meijer, 2015).

The cyclic arrangement of the MSC sediments (Fig. 3a) led scientists to interpret that the same cyclostratigraphic approach could be used to gain precise dates for events within the MSC (e.g. Hilgen et al., 1995; Vai, 1997; Krijgsman et al., 1999b, 2001), bypassing the challenge posed by the unsuitability of the classic biomagnetostratigraphic tools for the MSC successions. Characteristic interference patterns of eccentricity and precession have been tentatively recognized in the Sicilian Eraclea Minoa section (see subsection 3.8; Van der Laan et al., 2006). However, clear orbital signals are typically poorly expressed in MSC records and, when they are present, like in Sicily, they are not (vertically) repeated with sufficient frequency to establish clear phase relations with the astronomical cyclicity. For this reason, the simple counting of cycles with no analysis of cyclostratigraphic pattern in proxy records has mostly been employed as a correlation method (Roveri et al., 2008a; Manzi et al., 2009; Manzi et al., 2016a; Cosentino et al., 2013).

The age of the base of Stage 3 is largely determined by correlating the sedimentary cycles of the Upper Gypsum unit (UG) at Eraclea Minoa (Sicily) with the astronomical curve La2004 (Laskar et al., 2004). The UG sedimentary cyclicity consists of alternating gypsum and mudstone beds of variable thickness (Figs. 5g-i; see subsection 3.8). Precessional variation of the Mediterranean freshwater budget tied tightly to the African monsoon and Atlantic storms are the drivers interpreted to lie behind the gypsum-mudstone cycles (e.g. Marzocchi et al., 2015, 2019; Simon et al., 2017). Variations of the freshwater discharge cause the pycnocline to shift vertically, resulting in brine concentration and gypsum precipitation during to the arid/dry phases of the precession cycles (precession maxima-insolation minima) and brine dilution and mudstone deposition during the humid/wet phases (precession minima-insolation maxima) (Van der Laan et al., 2006; Manzi et al., 2009). Two different tuning options exist in literature (Van der Laan et al., 2006 versus Manzi et al., 2009; Fig. 3a):

1. Van der Laan et al. (2006) tentatively recognized sedimentary patterns that they correlated with the astronomical curves by using the same phase relationships between the sedimentary cycles and the astronomical cycles as are seen in Plio-Pleistocene sapropel-bearing marine successions of the Mediterranean (Hilgen, 1991). The four closely spaced gypsum beds III to VI were regarded as a cluster, i.e. the sedimentary expression of a 100 kyr eccentricity maximum (Hilgen, 1991; Strasser et al., 2006), whereas the preceding and following evaporite-free marly interval were attributed to a phase of low-amplitude precession oscillations caused by a 100 kyr eccentricity minimum (Fig. 3a). Tuning downward from the conformable Miocene/Pliocene boundary (Fig. 6d) and arguing that the precession peak at ~5.38 Ma, which has an extremely low amplitude, is not expressed in the sedimentary record, Van der Laan et al. (2006) correlated gypsums III to VI with the four successive precession/insolation peaks of the 100 kyr eccentricity maximum dated around 5.44 Ma and the overlying and underlying gypsum-free marly interval fell within 100 kyr eccentricity minimum cycles (Fig. 3a, right log). This tuning resulted in an astronomical age of ~5.51 Ma for the first gypsum bed in their log (i.e. gypsum II in the log of Manzi et al., 2009), and an approximate duration of 175 kyr for Stage 3 as whole.
2. An alternative tuning by Manzi et al., 2009; Fig. 3a, left log) argued that every precessional/insolation peak must have an expression in the rock record. Manzi et al. (2009) agreed with the solution of Van

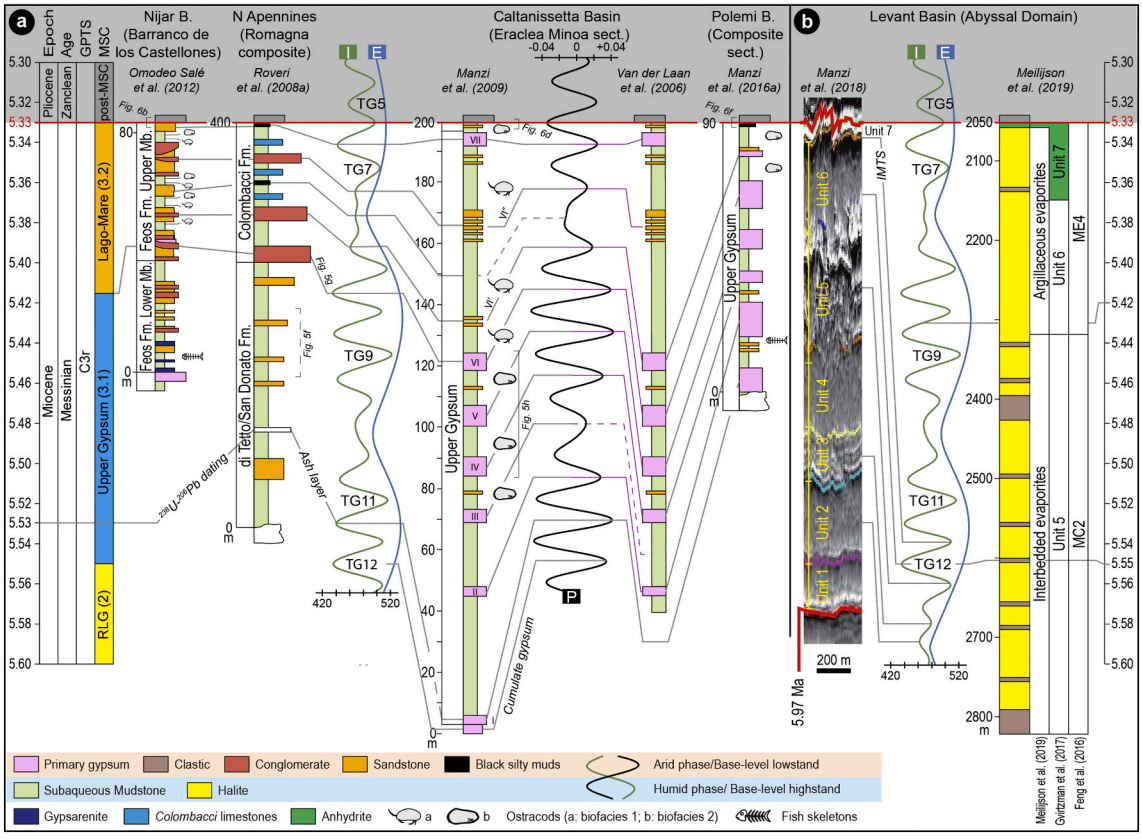

Fig. 3. (a), (b) Available astronomical tunings to astronomic curves of climatic precession (P), 100 kyr eccentricity (E) and 65°N insolation curve (I) of Laskar et al. (2004) of the lithological cyclicity of onshore Stage 3sections (a) and of the seismic cycles and/or well logs (gamma ray and resistivity) of the MU in the Levant Basin (b). Tunings of onshore sections in (a) are carried out downward from the M/P boundary (conformable in all sections). Astronomically-tuned glacial (even numbers) and interglacial (odd numbers) stages (i.e. TG) as defined by Hodell et al. (1994) are also indicated.

der Laan et al. (2006) on the sedimentary inexpressiveness of the (barely visible) insolation minima peak at ~5.38 Ma. However, these authors considered the insolation minima peaks immediately above and below of too low amplitude to promote the conditions required for gypsum precipitation, but also too high not to have some sedimentary expression. They therefore identified sandstone horizons VI' and VI" as the sedimentary response to these weak insolation/precession signals. The addition of two precessional cycles (i.e. a total of 9) resulted in an astronomical solution that was adjusted one precessional cycle lower than that of Van der Laan et al. (2006), translating into an age of 5.53 Ma for the base of the UG and a total duration of ~200 kyr for Stage 3. But the more conspicuous difference between the two astronomical solutions discussed lies in the timing at which gypsum precipitation occurred, restricted to the 100 kyr eccentricity maxima according to Van der Laan et al. (2006), extended to the 100 kyr eccentricity minima by Manzi et al. (2009).

An age of 5.53 Ma for the first gypsum bed was also obtained by the astronomical tuning of the Upper Gypsum in Cyprus (Manzi et al., 2016a), but there the tuning is performed just by following the recognition, from the base up, of 6 gypsum beds just like in Sicily and therefore arguing for a bed-to-bed correlation with the Sicilian gypsums I-VI. In the consensus model of Roveri et al. (2014a) the base of Stage 3 coincides with the base of the Sicilian UG, placed by Manzi et al. (2009) at 5.55 Ma (Fig. 1A). However, in the model of Manzi et al. (2009) this age is attributed to a cumulate gypsum horizon interpreted as laterally equivalent of the Halite (i.e. Stage 2), and therefore implying the kickoff of Stage 3 at 5.53 Ma (Fig. 3a).

The post-evaporitic successions of the Romagna (Cusercoli and Sapigno sections; Roveri et al., 1998) and Marche (e.g. Trave and Maccarone sections; Iaccarino et al., 2008; Cosentino et al., 2013) areas provided evidence that led to the splitting of Stage 3 into substage 3.1 and 3.2. In the resulting composite section (Roveri et al., 2008a), a shift in the sedimentary facies and stacking pattern is observed (see description in subsection 3.7). Correlation of the sedimentary cyclicity in Romagna was from the (conformable) base of the Pliocene downwards (or from an U-Pb-dated ash layer upward; Cosentino et al., 2013) and linked three fluvial conglomerates and two black mudstone layers of unknown sedimentological significance to the arid phases of the precession cycles (Fig. 3a; Roveri et al., 2008a). The greater thickness of the oldest conglomerate was possibly assumed to be evocative of an oscillation of the amplitude of the corresponding precession minima peak rather than the amplitude of the peaks responsible for the formation of the other facies. This approach resulted in an age of 5.42 Ma for the first conglomerate (i.e. the substage 3.1/3.2 transition; Fig. 5g) and an approximate duration of 90 kyr for substage 3.2 (the Lago-Mare phase). The same astronomical age is obtained by tuning the Upper Member of the Feos Formation in the Nijar Basin (Omodeo-Salé et al., 2012), where four pelite-conglomerate cycles plus one sandstone capped by the Miocene/Pliocene boundary mark the interval attributed to Stage 3.2 (Fortuin and Krijgsman, 2003).

Although the substage 3.1/3.2 transition is linked to a major Mediterranean-scale hydrological re-organization possibly coinciding with the migration of the Paratethyan biota (Roveri et al., 2008a; Grossi et al., 2011), the facies change used for its definition is hardly recognizable elsewhere (see Chapter 3). As such, other tools have been used to equip fragmentary and/or lithological cyclicity-lacking sections with an age model: the (highly controversial) ostracod biozonation (see subsection 5.1; e.g. Stoica et al., 2016; Karakitsios et al., 2017a; Cosentino et al., 2018; Caruso et al., 2020) and the astronomical tuning of magnetic susceptibility records (e.g. Fonte dei Pulcini section, Central Apennines; Cosentino et al., 2012).

Comparison of Atlantic oxygen isotope records (Van der Laan et al., 2005, 2006) and the chronostratigraphy of Roveri et al. (2014a) revealed that Stage 3 sedimentation started during a prominent global eustatic lowstand associated with oxygen isotope (glacial) stage TG12, followed by a latest Messinian deglacial interval which comprised multiple obliquity- and possibly precession-forced global eustatic phases. As documented by Hodell et al. (2001) (later revised by Drury et al., 2018), Van der Laan et al. (2006) and Roveri et al. (2014a), the marine replenishment of the Mediterranean did not coincide with any major deglaciation, so non-eustatic causes of the Zanclean megaflood hypothesis are required.

3. Onshore domain: key sections, sedimentary expression and faunal content

3.1. The Alborán region

The westernmost outcrops of Stage 3 deposits in the Mediterranean are located in the Alborán region, close to the present-day Strait of Gibraltar (Fig. 2b). MSC deposits on the margins of this region are poorly developed, possibly because of a late Tortonian uplift that raised the margins above the Mediterranean water level (López-Garrido and Sanz de Galdeano, 1999). Near Malaga, however, two facies associations consisting of m-thick conglomerate-sandstone beds alternating with laminated pelites are documented in the Rio Mendelín section (informally referred to as "LM unit"; Guerra-Merchán et al., 2010) and attributed to (part of) the Lago-Mare phase (Fig. 4a) based on their paleontological content. These sediments are squeezed between the Paleozoic basement units, with an erosive contact and associated angular unconformity, and the Pliocene, from which they are separated by another erosional surface draped by conglomeratic accumulations (Fig. 6a). A well-preserved and diverse *in situ* Paratethyan-type ostracod and molluskan fauna (i.e. *Lymnocardiinae* and *Dreissenidae*) typical of shallow waterbodies (up to 100 m deep; Grossi et al., 2008; Gliozzi and Grossi, 2008) with low salinities (5-18‰) is reported from the pelitic units (Guerra-Merchán et al., 2010). The overlying Pliocene in the deeper depocenters starts with 30 m-thick littoral conglomerates with marine mollusks passing progressively upwards into deeper water facies, while fan deltas developed at the basin margins (López-Garrido and Sanz de Galdeano, 1999; Guerra-Merchán et al., 2010, 2014). Notably, the overall thickness of the Pliocene deposits reaches 600 m. The detailed regional studies by López-Garrido and Sanz de Galdeano (1999) and Guerra-Merchán et al. (2014) concluded that accommodation space was created during (Zanclean) sedimentation by local fault-driven subsidence, and that movement on these faults only reversed at the end of the Zanclean causing uplift.

An alternative scenario, based on the finding of (a few) specimens of the nannofossil *Ceratolithus acutus*, ascribed the LM unit of Guerra-Merchán et al. (2010) to the earliest Zanclean (Fig. 4b; Do Couto et al., 2014).

On the southern Alborán margin in Morocco, latest Messinian deposits are reported from the Boudinar and Melilla basins (Fig. 2b). Up to 100 m-thick chaotic deposits containing selenite gypsum fragments, azoic conglomerates, sandstones yielding planktic foraminifera and nannofossils and lacustrine limestones are capped by early Pliocene marine marls (Rouchy et al., 2003; Azdimousa et al., 2006; Cornée et al., 2016; Merzeraud et al., 2019). Due to their stratigraphic position, these continental to lacustrine deposits are interpreted as the local expression of the Lago-Mare phase (Cornée et al., 2016) or alternatively as Zanclean successions (Azdimousa et al., 2006).

3.2. Algeria

The Chelif Basin in Algeria (Fig. 2b) displays the typical marginal Messinian succession comprising Tortonian to lower Messinian blue marls, diatomite-bearing sediments (Tripoli unit), cyclically-arranged primary evaporites (13 couplets), ostracod-rich post-evaporitic deposits and Zanclean foraminiferal marls (Rouchy et al., 2007). The post-evaporitic sediments show a great lateral variability in both thickness (from few meters up to 125 m) and facies. They are mainly dominated by

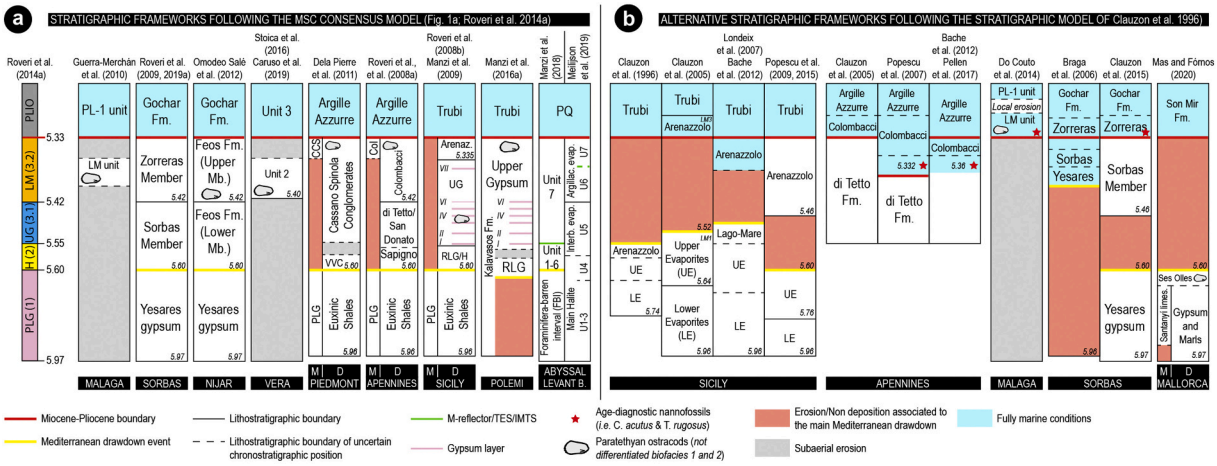

Fig. 4. Schematic overview of different chronostratigraphic models for some of the Messinian successions presented in Chapter 3. Note the large controversies in timing, duration and chronostratigraphic position of the main erosion phase between models in (a) and (b). Models in (a) follow the recently established MSC chronostratigraphic model of Roveri et al. (2014a), according to which the Mediterranean base-level dropped and halite deposited on sea floor during Stage 2 and the Upper Gypsum/Upper Evaporites-Lago-Mare sequence followed. Models in (b) were proposed following the alternative scenario of Clauzon et al. (1996, 2005), which envisaged two Lago-Mare episodes (LM1 and LM3) that occurred before and after the main Mediterranean drawdown event, during which LM2 was deposited in the deep desiccated basins (Do Couto et al., 2014; Popescu et al., 2015; see Roveri et al., 2008c and Grothe et al., 2018 for further explanations). Note, in (b), the shifting of the position of the main erosional phase in Sicily through time as well as the time of the marine replenishment in the Apennines.

terrigenous clastic lithologies, associated in the marginal areas with sandy carbonates and stromatolitic limestones. A mixed faunal assemblage of non-marine (Paratethyan-like ostracods) and marine (benthic and planktic foraminifera) organisms is present, showing an increase in ostracod species diversity from the bottom to the top (Rouchy et al., 2007).

3.3. *Neogene basins of the Eastern Betics (Spain)*

The external Neogene basins (Sorbas, Nijar, Vera and Bajo Segura) of the eastern Betic Cordillera (SE Spain; Fig. 2b) represent an important laboratory for understanding Messinian events. In particular, the Sorbas and Nijar basins preserve two allegedly continuous successions spanning the entire MSC (e.g. Roveri et al., 2009; Omodeo-Salé et al., 2012). The two basins are similar in many respects. Their stratigraphic organization, for example, suggests they were connected for much of the late Miocene up until MSC Stage 1 (Fortuin and Krijgsman, 2003), which is represented by the gypsiferous Yesares Member (e.g. Lu, 2006). However, facies differences are prominent in the Stage 3 formations according to the chronostratigraphic frameworks of Roveri et al. (2009) for the Sorbas Basin and Omodeo-Salé et al. (2012) for the Nijar Basin (Fig. 4a). Lithostratigraphically, two members are discerned between the Yesares Member and the basal Zanclean: the Sorbas and Zorreras members in the Sorbas Basin (Figs. 4a, 5a) and the lower and upper members of the Feos Fm. in Nijar (Figs. 3a, 4a; Roep et al., 1998; Krijgsman et al., 2001; Fortuin and Krijgsman, 2003; Braga et al., 2006; Roveri et al., 2009, 2019a; Omodeo-Salé et al., 2012).

The Sorbas Member (see Roep et al., 1998 and Aufgebauer and McCann, 2010 for a more detailed sedimentological description) consists of three overlapping coarsening-upward depositional sequences made of offshore clays and marls passing upward into shelf muds and coastal sandstone bodies. Still unclear is the chemistry of the subaqueous environment during the formation of the Sorbas Member and the provenance of the water fluxes. These shallow-water deposits are conformably replaced upward by the Zorreras Member that comprises alternations of reddish siltstones and sandstones (Fig. 5a) organized in five (or eight) lithological cycles expressing continental environments (Martín-Suárez et al., 2000; Aufgebauer and McCann, 2010). Up to four lenticular white limestone beds bearing brackish Paratethyan-like ostracods (*Cyprideis, Loxocorniculina djafarovi* and freshwater species of the family Limnocytheridae), bivalves and *Chara* oogonia (Roep and Harten, 1979; Aufgebauer and McCann, 2010) are found interrupting the fluviatile sequence (Fig. 5a) and are linked to either episodic flooding by local rivers (Braga et al., 2006; Aufgebauer and McCann, 2010) or episodic Mediterranean ingressions (Fortuin and Krijgsman, 2003; Andreetto et al., 2021). A correct interpretation of the paleodepositional environment of these limestone beds is crucial for the discussion concerning the Mediterranean base-level position during the Lago-Mare phase. In fact, if the Sorbas Basin was relatively shallow during Zorreras deposition (50-100 m; Roveri et al., 2019a, 2020), repeated and sudden Mediterranean incursions would indicate that the Mediterranean Basin was relatively full and that its base level was oscillating, possibly with precessional periodicity (Andreetto et al., 2021). The contact between the Zorreras Mb. and the overlying nearshore Pliocene (<50 m depositional paleodepth; Roveri et al., 2019a) in the Sorbas Basin is conformable and expressed differently around the basin, ranging from a bivalves-rich bed overlain by a yellow, fossiliferous calcarenite floored by a gravelly lag deposit (Mather et al., 2001) to a grey marl horizon with marine foraminifera assemblages followed by a second shell-rich bed (Roveri et al., 2019a). Similar to the situation in Malaga, the rare identification of *Ceratolithus acutus* in sediments of the continental Zorreras Mb. led Clauzon et al. (2015) to put forward an alternative chronostratigraphic and paleoenvironmental interpretation for the Sorbas MSC succession, shifting the Zorreras Mb. into the Pliocene (Fig. 4b) and thus associating the presence of brackish Paratethyan-like ostracods with exchanges between the Mediterranean and Paratethys following the Mediterranean re-filling, at high sea level.

In the Nijar Basin (Fig. 2b), the latest Messinian Feos Formation is bracketed at the base and top by an erosional surface along the basin margins and its correlative conformity in the deeper parts (Fig. 3a; Fortuin and Krijgsman, 2003; Aguirre and Sánchez-Almazo, 2004; Omodeo-Salé et al., 2012). The Lower Feos Member consists of azoic, graded and locally slumped siliciclastic-carbonate beds alternating with gypsarenites and gypsiltites and including a laterally continuous Mn-rich bed (Fortuin and Krijgsman, 2003; Omodeo-Salé et al., 2012). In the basin center (e.g. Barranco de los Castellones section; Fig. 3a) the Upper Feos member comprises four complete lithological cycles of m-thick conglomerate to sandstone beds alternating with laminated pelites (Fig. 5b), and one incomplete cycle, which only consists of a sandstone horizon conformably capped by the Pliocene Cuevas Fm. (Fig. 6b;

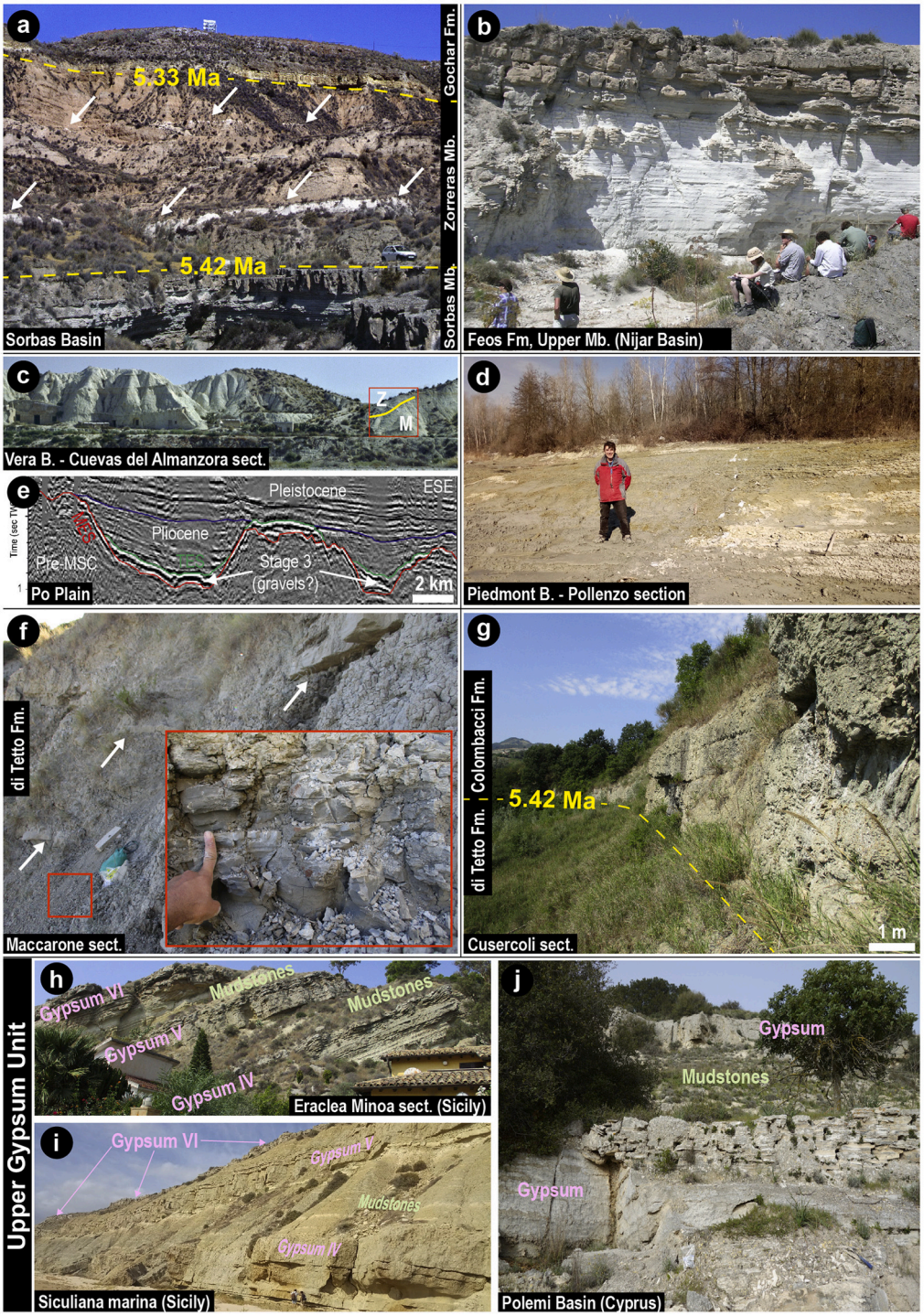

Fig. 5. Sedimentary expression of Stage 3 from selected onshore Mediterranean localities. (a) Photograph from the Sorbas Basin showing the red continental sediments of the Zorreras member with intercalated white limestones (white arrows; from Andreetto et al., 2021). The conformable resting of the Zorreras Mb. above the Sorbas Mb. and underneath the Gochar Fm. of Pliocene age is also appreciable. Car for scale. (b) One typical lithological (and precessional) cycle of the Upper Mb. of the Feos Fm. in the Nijar Basin, here constituted by an ostracod-bearing, white and laminated mudstone bed overlain by an azoic fluvial sandstone (courtesy of Anne Fortuin). (c) Panoramic view of the Cuevas del Almanzora section (from Andreetto et al., 2021). Red rectangle indicates the position of the section straddling the Messinian (M)/Zanclean (Z) transition and studied by Fortuin et al. (1995), Stoica et al. (2016), Caruso et al. (2020) and Andreetto et al. (2021). Buildings for scale. (d) The sub-unit a of the Piedmont Basin composed of azoic grey mudstones grading into yellowish, mammal-rich overbank deposits. (e) WNW-ESE seismic profile in the Po Plain showing incised valleys filled during Stage 3 by suggested clastic deposits and sealed by deep-water turbidites in the Zanclean (modified from Amadori et al., 2018). (f) Typical aspect of the di Tetto/San Donato Formation in the Northern Apennines composed by grey mudstones (detail in the inset) with interbedded sandstone bodies (white arrows). The picture is taken from the Maccarone section. (g) The di Tetto Fm.-Colombacci Fm. transition in the Cusercoli area (Eastern Romagna, Fig. 2b), defined by the facies change underlined by the appearance of a fluvial conglomerate. This lithostratigraphic boundary also corresponds to substage 3.1/3.2 boundary of Roveri et al. (2014a). (h), (i), (l) Lithological cycles of the Upper Gypsum Unit in Eraclea Minoa (h), Siculiana Marina (i) and Polemi (l) sections. Cycles are several m-thick and primarily composed by beds of primary gypsum alternating with mudstones bearing Paratethyan ostracods (at least in Eraclea Minoa).

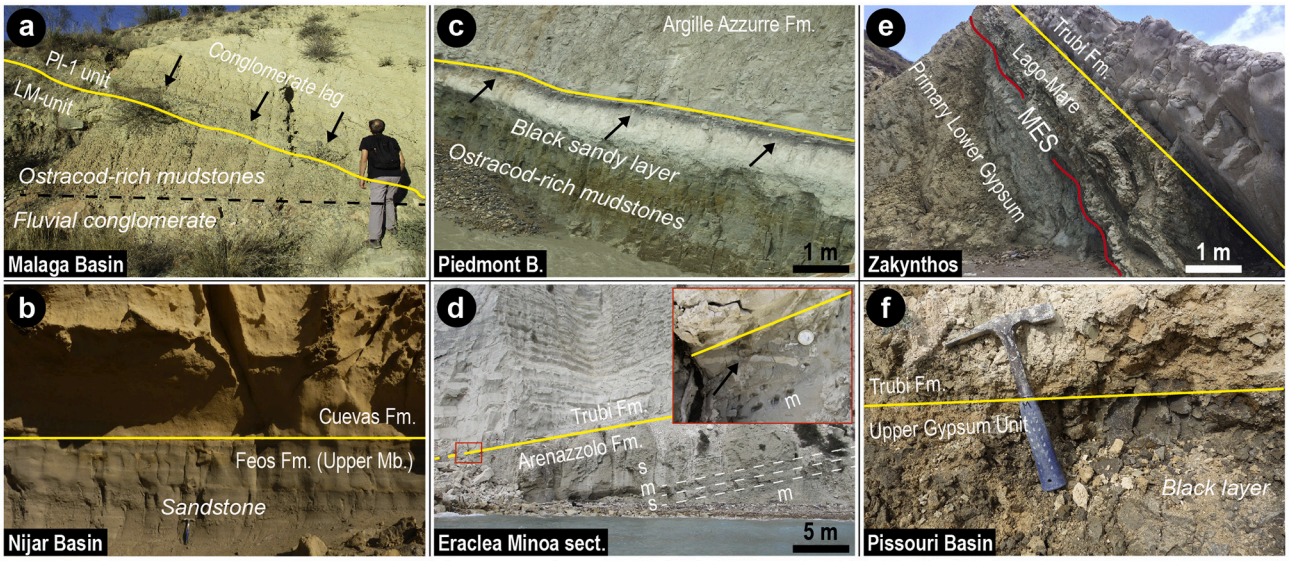

Fig. 6. Photographs of the Miocene/Pliocene boundary (yellow lines) from selected onshore Mediterranean localities. (a) Erosive M/P transition in the Mendelín section (Malaga Basin). Note the conglomeratic lag draping the erosional surface and sharply overlain by foraminifera-rich marls. (b) Conformable stratigraphic contact between the uppermost Messinian sandstone of the Feos Fm. and the Zanclean biocalcarenites of the Cuevas Fm. in the Barranco de los Castellones section, Nijar Basin (hammer for scale; modified from Andreetto et al., 2021). (c) The Messinian/Zanclean boundary in the Pollenzo section (Piedmont Basin) marked by a characteristic black layer interbedded between Paratethyan ostracods-rich mudstones and marine foraminifera-rich marls (modified from Dela Pierre et al., 2016). (d) Uppermost segment of the Eraclea Minoa section (Caltanissetta Basin, Sicily) displaying the (non erosive) contact between the Pliocene Trubi Formation above and the sandy Arenazzolo Formation below. The inset is a close view of the transition, which occurs above a ~50 cm-thick burrowed mudstone horizon rich in Paratethyan ostracods and marine foraminifera. (e) Lago-Mare sediments in the Kalamaki section (Zakynthos) unconformable, through an erosional surface (i.e. the Messinian Erosional Surface, MES), over the PLG unit and also unconformable beneath the Trubi Fm. (modified from Karakitsios et al., 2017b). (f) Close view of the M/P boundary in the Pissouri Basin, where the foraminifera-rich Trubi marls lie above a black layer (paleosol according to Rouchy et al., 2001).

Fortuin and Krijgsman, 2003). A rich fauna of mixed brackish ostracods and marine foraminifera is found in all four pelitic beds (Bassetti et al., 2006). Its origin is questionable. These ostracods were regarded as endemic to the Mediterranean and inhabiting endorheic lakes by Bassetti et al. (2006). However, later they were shown to have been misidentified and were instead considered Paratethys-derived by Stoica et al. (2016; see subsection 5.1). Planktonic and deep-water benthic foraminifera are widely considered reworked by Fortuin and Krijgsman (2003), Bassetti et al. (2006) and Omodeo-Salé et al. (2012), in place by Aguirre and Sánchez-Almazo (2004).

In the Vera Basin (Fig. 2b), in situ gypsum deposits are missing because of widespread erosion or non-deposition and MSC deposits are only represented by ~12 m of laminated varicolored marly clays (Unit 2 Fig. 4a), which are best exposed in the Cuevas del Almanzora section (Fortuin et al., 1995; Fig. 5c). These clays contain a well-preserved and diversified *in situ* fauna of Paratethyan-like ostracod and shallow-water, benthic foraminifera mixed with physically reworked (mostly from the lower Messinian Abad marls) planktic and deep-water benthic foraminifera (Fortuin et al., 1995; Stoica et al., 2016; Caruso et al., 2020). The marly clays are assigned by Stoica et al. (2016) and Caruso et al. (2020) to (roughly) the whole late Messinian Lago-Mare phase (Fig. 4a) based on the ostracod biozonation of Grossi et al. (2011) and are considered to represent either sedimentation in an isolated lake subject to base-level and salinity fluctuations (Caruso et al., 2020) or deposition in a coastal lagoon that was connected to the water mass filling the open Mediterranean (Stoica et al., 2016; Andreetto et al., 2021). Similar to Malaga, these sediments are topped by an erosive surface draped by a conglomeratic accumulation which is overlain by the open marine fauna-rich sediments of the basal Zanclean (Fortuin et al., 1995; Caruso et al., 2020). This erosion feature likely indicates that the Miocene/Pliocene transition followed a base-level lowstand in the Vera Basin.

Stage 3 deposits (Garrucha Fm.) in the easternmost basin of the Betic Cordillera, the Bajo Segura Basin (Fig. 2b), are bounded below and above by two erosional surfaces related to lowered Mediterranean base-levels and discontinuously present due to the widespread fluvial erosion that occurred at the Miocene/Pliocene boundary (Soria et al., 2005, 2008a, 2008b). The Garrucha Fm. shows a maximum thickness of 100 m in its type section (Soria et al., 2007, 2008b). It consists of 20-50 cm thick sandstone bodies interrupting a dominantly marly succession deposited in a subaqueous environment inhabited by *Cyprideis* sp. and euryhaline, shallow-water benthic foraminifera (*Ammonia beccarii*, *Elphidium granosum*, *Elphidium macellum*, *Haynesina germanica* and *Quinqueloculina laevigata*). Planktic foraminifera are also observed and for a long time were considered to be physically reworked (Soria et al., 2005, 2008b). However, some stratigraphic levels contain dwarf tests of long-ranging taxa such as *Globoturborotalita decoraperta*, *Globigerina bulloides*, and *Neogloboquadrina spp*. which recently have been interpreted as being *in-situ* mostly due to the absence of notable signs of reworking (Corbí and Soria, 2016). Among these dwarf taxa is *Neogloboquadrina acostaensis* (dextral; Corbí and Soria, 2016). Since this group is mainly dextral in the latest Messinian Atlantic successions (e.g. Sierro et al., 1993; Bassetti et al., 2006), this may indicate that Atlantic inflow to the Mediterranean occurred during the late Messinian and the base level of the Mediterranean was high enough to reach the marginal Bajo Segura Basin. The Miocene/Pliocene boundary is, once again, marked by an erosional surface which outlines up to 200 m deep paleovalleys engraved down into the pre-MSC sediments and filled with conglomerates and sandstones of claimed coastal and shallow marine environments (Soria et al., 2005, 2008b; García-García et al., 2011; Corbí et al., 2016).

3.4. Mallorca

Mallorca, which constitutes an emerged segment of the Balearic Promontory (Fig. 2), does not expose the classical MSC evaporite sequence. Instead, two main MSC-related units are found above late Tortonian-Messinian reefal carbonates (Reef Complex Unit) and beneath the Pliocene: the Santanyí limestones and the Ses Olles Formation (Mas

and Fornós, 2020 and references therein). The Santanyí limestones are microbialites and oolite-dominated sediments in which a baleen whale neurocranium has been found (Mas et al., 2018a). This unit was interpreted either as a Terminal Carbonate Complex (TCC) laterally equivalent to the Primary Lower Gypsum (PLG) which has been drilled in the deeper parts of the bay of Palma (Mas and Fornós, 2020) or as time-equivalent to the Reef Complex Unit (e.g. Arenas and Pomar, 2010; Suárez-González et al., 2019). The Ses Olles Formation consists of marls, sandy-marls and marly-calcareous lacustrine deposits rich in in-situ freshwater *Chara* spp., brackish water Paratethyan-like mollusks and ostracods and littoral benthic foraminifera (*Elphidium* sp., *Ammonia* sp.).

The upper contact of the Ses Olles Formation with the Pliocene corresponds to an erosional ravinement surface draped by a transgressive lag of coastal deposits usually containing coquinas and/or conglomerates (Mas, 2013, 2015; Mas and Fornós, 2020). The lower contact of the Ses Olles Formation with the Santanyí limestones is sporadically marked by a well-developed reddish paleosol (Mas, 2013, 2015; Mas and Fornós, 2020), which indicates that a (unquantified) period of subaerial exposure occurred before the emplacement of the Ses Olles Fm. However, in their more recent study, Mas and Fornós (2020) surprisingly conclude that the Ses Olles Formation has a conformable contact with the Santanyí limestones, ascribed to part of Stage 1. This led Mas and Fornós (2020) to conclude that the emplacement of the Ses Olles Fm. pre-dated the MSC peak and that the erosional surface marking the Miocene/Pliocene boundary is associated with a 270 kyr hiatus linked to the main MSC base-level drawdown (Fig. 4b). This conclusion is, however, in disagreement with the unconformity at the base of the Ses Olles Fm., which instead points to the deposition of the Ses Olles Fm. (and therefore to the arrival of the Paratethyan fauna in Mallorca) at some point during Stage 3 of Roveri et al. (2014a).

3.5. Piedmont Basin

The Piedmont Basin (NW Italy) contains the northernmost record of the MSC (Fig. 2b). The terminal MSC sediments (i.e. the Cassano Spinola Conglomerates Fm.) overlay pre-MSC units, the PLG deposits (Gessoso Solfifera Fm.) or reworked evaporites (Valle Versa chaotic complex, VVC) and underly the Zanclean marls of the Argille Azzurre Fm. (Dela Pierre et al., 2011).

The Cassano Spinola Conglomerates is splitted in two sub-units by Dela Pierre et al. (2016). Sub-unit *a* consists of azoic grey mudstones turning to yellowish silty mudstones (Fig. 5d) typified by in situ root traces, paleosols and mud cracks and including three/four intercalated lens-shaped, cross-bedded conglomeratic layers (Ghibaudo et al., 1985; Dela Pierre et al., 2011, 2016). Abundant land plant leaves and a diverse terrestrial vertebrate fauna are found in the yellowish siltstones, which have been interpreted as overbank deposits (Harzhauser et al., 2015; Colombero et al., 2017 and references therein). In this continental interval, a low-diversity fish fauna consisting of otoliths of marine and Paratethyan species is found (Grunert et al., 2016; Carnevale et al., 2018; Schwarzhans et al., 2020). These otoliths were Sr-dated to the early-middle Miocene (Grunert et al., 2016). Nevertheless, they were concluded not to be physically reworked, but rather to have been transported by large marine predators, therefore implying a Piedmont Basin-(marine) Mediterranean connection was in force (Grunert et al., 2016; see subsection 5.6). Sub-unit *b* (i.e. Strati a Congeria *sensu*Sturani, 1973) is made of grey mudstones bearing a mixture of in-situ brackish water mollusks (Sturani, 1973; Esu, 2007) and ostracods (Trenkwalder et al., 2008) of Paratethyan affinity along with physically reworked foraminifera and calcareous nannofossils (Trenkwalder et al., 2008; Violanti et al., 2009). The transition to the Pliocene Argille Azzurre Fm. is sharp above a characteristic black and azoic sandy layer (Fig. 6c) rich in terrigenous and intrabasinal (i.e., glaucony and phosphates) grains and disarticulated valves of both brackish-water and continental bivalves, but barren of in-situ fossils (Trenkwalder et al., 2008). The occurrence, at its top and directly below the Argille Azzurre Fm., of abundant *Thalassinoides* trace fossils filled with Pliocene sediments led Trenkwalder et al. (2008) and Dela Pierre et al. (2016) to interpret the top surface of this layer as an omission surface. This surface indicates a period of basin starvation (and therefore a hiatus) due to a sudden increase in water-depth, ascribed by Trenkwalder et al. (2008) to the Zanclean reflooding. This hiatus may have lasted for only part of the late Messinian (Violanti et al., 2009; Dela Pierre et al., 2016) or may have endured into the Pliocene (Trenkwalder et al., 2008).

3.6. Po Plain

To the east, the Messinian sediments in the Piedmont Basin disappear beneath the km-thick Plio-Quaternary succession of the Po Plain-Adriatic Foredeep (PPAF; Fig. 2a). By definition of Ghielmi et al. (2010) and Amadori et al. (2018), the PPAF includes two main elongated depocenters enclosed within the northern Apennines to the South and the Southern Alps to the North: the easternmost portion of the Po Plain and the whole present-day northern Adriatic Sea. Here, for simplicity, we include in the definition of PPAF also its westernmost depocenters of the Western Po Plain Foredeep.

The Messinian-Pleistocene sedimentary sequence, studied through the integration of seismic and borehole observations, is mostly represented by thick sequences of turbidite deposits in the foreland depocenter passing, towards the margins, to fluvial and deltaic systems related to the proximity of the marginal thrust-fold-belts (Cipollari et al., 1999; Ghielmi et al., 2010, 2013; Rossi et al., 2015a; Rossi, 2017). During MSC Stage 1, primary evaporites and dolomicrites were deposited in some shallow-water settings, while evaporitic deposition was inhibited in the deep-water settings, where it was replaced by deposition of anoxic mudstones (Ghielmi et al., 2010). Instead, the post-evaporitic deposits consist of large thicknesses (up to 1 km) and volumes of coarse-grained clastics (LM1 and LM2 of Rossi and Rogledi, 1988; ME3 or Fusignano Fm. of Ghielmi et al., 2010; ME4 of Ghielmi et al., 2013; ME3b and possibly ME3a of Rossi et al., 2015a). Several authors (Ghielmi et al., 2010, 2013; Rossi et al., 2015a; Amadori et al., 2018; Cazzini et al., 2020) showed that these post-evaporitic sediments are the infilling of ca. N-S and NW-SE trending, V-shaped valleys (Fig. 5e). These valleys were carved at least as far as 50 km into the Alps, to a depth up to 1 km into the pre- and syn-evaporitic Messinian deposits and nicely shape the present-day river network of the southern Alps (Amadori et al., 2018).

Different mechanisms for the incision have been proposed, with major implications for the desiccated vs full Mediterranean controversy (Figs. 1b-c). Ghielmi et al. (2010, 2013), Rossi et al. (2015a), Amadori et al. (2018) and Cazzini et al. (2020) ascribed the valley incision along the PPAF northern margin to fluvial erosion, whose basinward shifting was triggered by the Stage 2 Mediterranean drawdown, estimated to have been around 800-900 m (Ghielmi et al., 2013; Amadori et al., 2018). In this case, Stage 3 deposition in the PPAF occurred in endorheic lakes fed by the Alpine rivers and kept isolated until the Zanclean, when the sudden sea-level rise following the Zanclean reflooding was enough to bypass morphological highs (e.g. Gargano-Pelagosa and/or Otranto paleosills) located in the southern Adriatic foredeep (Fig. 2a; see Pellen et al., 2017; Amadori et al., 2018; Manzi et al., 2020). Conversely, Winterberg et al. (2020) suggested that the over-deepened valleys on the southern slope of the Alps are related to Pleistocene glacial erosion. Although Winterberg et al. (2020) do not address the paleoenvironment during the Messinian, this interpretation does not rule out the possibility that (at least part of) Stage 3 sedimentation occurred in a PPAF connected to the Mediterranean water mass and that no catastrophic reflooding occurred at the Miocene/Pliocene boundary. The conclusion of a non-catastrophic refilling was also drawn by Pellen et al. (2017) on the basis of the onshore Adriatic record (see subsection 3.7).

3.7. Apennine system

The Messinian deposits resurface to the south of the PPAF sector and extensive sections are found in several basins on both the foreland domain (Adriatic side of the partially uplifted Apennine chain), subjected to compressional tectonics during the late Messinian, and the back-arc domain (Tyrrhenian side), contemporaneously affected by extension (Fig. 2b; Cipollari et al., 1999; Schildgen et al., 2014; Cosentino et al., 2018). Overall, the MSC record of the Apennines is subdivided into an evaporitic and post-evaporitic interval squeezed in between two marine units (Messinian Euxinic Shales Fm. at the base and Zanclean Argille Azzurre Fm. atop; Fig. 4a). Different vertical motions related to ongoing Apenninic tectonics resulted in the deposition of Stage 3 sediments with highly variable sedimentary expression and stratigraphic resolution from basin to basin. The post-evaporitic deposits are alternatively found resting unconformably, with an erosional contact associated to an angular unconformity, above the alternations of the Gessoso Solfifera Fm./PLG, or conformably above evaporitic-free cycles lateral equivalent of the marginal PLG (Fig. 4a; e.g. Roveri et al., 1998, 2008a). This led to the conclusion that both shallow and deep-water successions are present in the Apennine foredeep system (Roveri et al., 2001).

The physical-stratigraphic model developed for the post-evaporitic interval in the Romagna area (i.e. Northern Apennines) and applied to the whole Apennine domain was subdivided into two allounits (named p-ev$_1$ and p-ev$_2$) based on a basin-wide shift in facies, overall stacking patterns and depositional trends (i.e. progradational and retrogradational, respectively; Roveri et al., 1998, 2001, 2005, 2008a; Manzi et al., 2005, 2007, 2020). Allounit p-ev$_1$ only accumulated in deep-water settings (e.g. Cusercoli, Sapigno, Maccarone and Trave sections; Roveri et al., 1998; Iaccarino et al., 2008; Cosentino et al., 2013) during the subaerial exposure of the basin margins (e.g. Vena del Gesso Basin, Monticino quarry, Pellen et al., 2017). It starts with resedimented clastic evaporites (i.e. Sapigno Fm.) followed by a coarsening- and shallowing-upward succession (i.e. di Tetto or San Donato Fm.) of mudstones with intercalated turbiditic sandstones (Fig. 5f) and a volcaniclastic marker bed dated initially by ^{40}Ar-^{39}Ar at ~5.5 Ma (Odin et al., 1997) and later by ^{238}U-^{206}Pb at 5.5320±0.0046/0.0074 Ma (Cosentino et al., 2013; Fig. 3a). Allounit p-ev$_2$ (i.e. Colombacci Fm.) occurs in the deeper depocenters in 4/5 sedimentary cycles consisting of three > 5 m-thick coarse-grained bodies (conglomerates and sandstones) and two black-colored mudstone beds alternating with fine-grained mudstones/clays with intercalated three micritic limestones (known in literature as *Colombacci* limestones; Figs. 3a, 5g; Bassetti et al., 2004). By contrast, an incomplete Colombacci Fm. deposited in the shallower thrust-top basins (e.g. Vena del Gesso Basin and Molise sections; Pellen et al., 2017; Cosentino et al., 2018). The p-ev$_2$ cycles have been interpreted as reflecting the alternation of wet (mudstones and Colombacci limestones in Eastern Romagna) and dry (coarse-grained facies and Colombacci limestones in the Maccarone section) phases controlled by Milankovitch-driven climatic factors (Fig. 3a; Roveri et al., 2008a; Cosentino et al., 2013) and, as such, they have been used for the astronomical tuning of the Colombacci Fm. to the Lago-Mare phase (Figs. 3a, 4a; see subsection 2.2). By contrast, Clauzon et al. (2005) and Popescu et al. (2007) moved the Colombacci Fm. into the Pliocene (Fig. 4b). However, this conclusion has been proven to rely on wrong stratigraphic and paleontological arguments (see Roveri et al., 2008c, Grothe et al., 2018 and subsection 5.5). Substage 3.2 records in the Apennines do not always contain the three prominent conglomeratic facies as in Romagna, but only laminated to massive clays with sandy intercalations equivalent to the ones typifying substage 3.1 records (e.g. Maccarone section; Sampalmieri et al., 2010; Cosentino et al., 2013; Fig. 5f). The absence of a lithological cyclicity that clearly mimics an orbital signal largely hampered the astronomical tuning of these clay-dominated sections, although an attempt has been made with the Maccarone section (Cosentino et al., 2013). The only exception is represented by the Fonte dei Pulcini section, which has been equipped with an age framework by astronomical tuning of the magnetic susceptibility record (Cosentino et al., 2012). Despite the lack of outstanding lithological changes these sections are often provided with a lithostratigraphic subdivision using the same nomenclature as in the Romagna area. When applied, the di Tetto Fm.-Colombacci Fm. boundary is placed high in the sections, i.e. few tens of meters underneath the Miocene/Pliocene boundary, resulting in a much different thickness of the formations compared to the Romagna area.

Stage 3 sediments are poorly exposed on the Tyrrhenian Sea onshore side of Italy (Fig. 2b). The best known succession crops out in the Cava Serredi quarry in the Fine Basin (Tuscany; Bossio et al., 1978, 1993; Carnevale et al., 2006b, 2008). Here the MSC has a thickness of ~150 m, of which only the uppermost ~100 m are attributed, without clear arguments, to Stage 3 by Carnevale et al. (2006b). The lowermost ~40 m of the Stage 3 unit consists of mudstone with alternating sandstone bodies which have been attributed to Roveri et al. (1998)'s p-ev$_1$ allounit, while the uppermost ~60 m form the p-ev$_2$ allounit and include two prominent conglomerate bodies alternating with mudstones interbedded with sandstone horizons and black, organic-rich layers (Carnevale et al., 2006b). A few and more fragmented sections are also described on the Tyrrhenian Sea side of Italy by Cipollari et al. (1999).

The Miocene/Pliocene boundary is variably expressed through the Apennine system: unconformable above the ostracod-bearing clays and highlighted by erosional surfaces draped by conglomeratic accumulations (e.g. Stingeti section in Molise; Cosentino et al., 2018), conformable above 0.5-1 m-thick black mudstones similar to how it is observed in Piedmont and of equally unknown paleoenvironmental significance (e.g. Romagna area and Maccarone section; Roveri et al., 1998; Gennari et al., 2008) or conformable above the ostracod-rich mudstones (e.g. Maccarone and Fonte dei Pulcini sections; Cosentino et al., 2005, 2012, 2013; Sampalmieri et al., 2010).

All p-ev$_1$ deposits studied are almost devoid of in-situ biota, except for fish otoliths and three fish skeletons found in the upper substage 3.1 part of Cava Serredi (Carnevale et al., 2006b). The p-ev$_2$/Colombacci deposits, instead, host typical Paratethyan assemblages of brackish-water mollusks, ostracods, dinocysts and fish (Bassetti et al., 2003; Bertini, 2006; Popescu et al., 2007; Grossi et al., 2008; Iaccarino et al., 2008; Cosentino et al., 2012, 2018; Schwarzhans et al., 2020). A diverse array of marine fossils (benthic and planktic foraminifera, calcareous nannofossils, dinocysts and fish otoliths and skeletons) has also been reported from the horizons containing these Paratethyan taxa (Bertini, 2006; Carnevale et al., 2006a; Popescu et al., 2007; Pellen et al., 2017). While the autochthony of ostracods, when considered, is unquestioned, the allochthonous vs autochthonous character of the other mentioned fossils is disputed and still unclear (see Chapter 5).

3.8. Sicily

The MSC record is widely exposed on Sicily, mainly in the Caltanissetta Basin and in scattered locations on the Hyblean Plateau (i.e. Ragusa-Siracusa area) and the Messina area (Fig. 2b; Butler et al., 1995; Manzi et al., 2009; Sciuto et al., 2018). Like the Northern Apennines, it shows a complex distribution and variable stratigraphy that mirrors the structuring of Sicily into basins with different characters, geometries and depocenters which subsided at different times and rates (Butler et al., 1995; Catalano et al., 2013). This structural setting permitted the simultaneous deposition of shallow and intermediate-water sediments (Roveri et al., 2008b). Mostly found in the Caltanissetta Basin, these intermediate-water successions have for decades been considered the onshore counterpart of the offshore evaporitic trilogy seen in seismic data from the Western Mediterranean Basin (Decima and Wezel, 1973). More recently, Raad et al. (2021) attempted a similar onshore-offshore correlation but with the intermediate Central Mallorca Depression. The currently endorsed stratigraphic model (Fig. 4a), refined over the years by Decima and Wezel (1971, 1973), Decima et al. (1988), Butler et al. (1995), García-Veigas et al. (1995), Rouchy and Caruso (2006),

Roveri et al. (2008b) and Manzi et al. (2009), envisages two 'evaporitic cycles'. The 'First cycle', overlying both alluvial and deep-water sediments (Tripoli Fm., Licata Fm. and Terravecchia Fm.; see Maniscalco et al., 2019 and references therein), comprises the disputed Calcare di Base (Manzi et al., 2011, 2016b vs Caruso et al., 2015), PLG or Gessi di Cattolica Fm. (Decima and Wezel, 1973; Lugli et al., 2010) and the Halite Unit (Lugli et al., 1999). The 'Second cycle' comprises the Upper Gypsum (UG) or Gessi di Pasquasia Fm., which is only present in depocenters of the Caltanissetta Basin (see Manzi et al., 2009 for a detailed overview), sporadically overlain by the siliciclastic Arenazzolo Fm. (Decima and Wezel, 1973; Cita and Colombo, 1979). The whole succession is sealed by the Pliocene marine Trubi Fm. (Fig. 4a). The two evaporite cycles are separated by an erosional surface (MES) associated with an angular discordance broadly linked to the main Mediterranean drawdown event (e.g. Butler et al., 1995; Roveri et al., 2008b). Clauzon et al. (1996), however, placed the MES at the Arenazzolo Fm.-Trubi Fm. transition, implying that the entire evaporitic deposition in the Caltanissetta Basin pre-dated the offshore one, but they do not provide evidence of erosion at that level. In more recent publications from the same research group, the MES is shifted towards the base of the Arenazzolo Fm. (e.g. Bache et al., 2012), again without evidence of major erosion, and different ages are assigned (see Fig. 4b and Grothe et al., 2018 for details).

The Upper Gypsum successions are commonly incomplete in many of the Caltanissetta Basin sections (Pasquasia-Capodarso, Casteltermini, Alimena, Nicosia, Siculiana-Marina; Decima and Sprovieri, 1973; Rouchy and Caruso, 2006; Manzi et al., 2009; Fig. 5i). In the most complete section, Eraclea Minoa (Fig. 3a), the Upper Gypsum Unit consists of 6 (Van der Laan et al., 2006) to 7 (Manzi et al., 2009) primary gypsum beds with a repetitive internal organization of facies (see Schreiber, 1997 and Manzi et al., 2009 for facies description) interbedded with marls and lenticular terrigenous sandstone bodies, gypsarenites and gypsrudites (Fig. 5h). Two of the terrigenous sandstone bodies are highlighted by Manzi et al. (2009) in the thick (~60 m), *Cyprideis agrigentina*-rich (Grossi et al., 2015), marly interval dividing gypsum VI and VII for its alleged astronomical significance (Fig. 3a; see subsection 2.2). A mixed (physically reworked) marine (foraminifera and dinocysts) and (*in-situ*) brackish biota (ostracods and dinocysts) of Paratethyan origin characterizes the marly interbeds from at least gypsum III upwards (following the investigations carried on the Eraclea Minoa section; Bonaduce and Sgarrella, 1999; Rouchy and Caruso, 2006; Londeix et al., 2007; Grossi et al., 2015; Fig. 3a). Calcareous nannofossils have been found along with the above organisms in a more northerly location by Maniscalco et al. (2019) and considered reworked. Above the last gypsum, the ~6-7 m-thick Arenazzolo Fm. is found, represented by reddish arkosic cross-laminated and poorly consolidated sand (Bonaduce and Sgarrella, 1999; Roveri et al., 2008b) and interpreted as the expression of a shallow-water delta, albeit without a sedimentological investigation (e.g. Decima and Wezel, 1973; Cita and Colombo, 1979). The whole Stage 3 sequence is conformably overlain by the Zanclean marine Trubi Fm. in the basin center (e.g. at Eraclea Minoa and Capo Rossello; Fig. 6d; Brolsma, 1975; Cita and Colombo, 1979; Van Couvering et al., 2000; Rouchy and Caruso, 2006; Manzi et al., 2009; Fig. 6d) and unconformably in the shallower, marginal areas (Manzi et al., 2009; Roveri et al., 2019b). Only Decima and Wezel (1973) and Raad et al. (2021) report the Miocene/Pliocene transition in the key, intermediate water-representative section of Eraclea Minoa as erosive. However, they do not provide evidence (e.g. photographic documentation) for the presence of an erosional unconformity and, moreover, Raad et al. (2021) erroneously refer to Cita and Colombo (1979), where no erosion is mentioned at the M/P boundary in Eraclea Minoa.

The bathymetric jump between the <100 m of water depth during the late Messinian and the >200 m at the base of the Trubi Fm. is often regarded as a key onshore evidence of the sudden and catastrophic Mediterranean-Atlantic re-connection at the Miocene/Pliocene boundary (e.g. Caruso et al., 2020). However, the real depth of the base of the Trubi is all but obvious. In fact, variable estimates have been proposed based on the observed benthic foraminifera and/or psychrospheric ostracods at Capo Rossello and Eraclea Minoa: 200-500 m (Decima and Wezel, 1973), 600-800 m (Sgarrella et al., 1997, 1999; Barra et al., 1998), 1400-2400 m (Cita and Colombo, 1979).

3.9. Greece

Several MSC localities are reported from the Greek Ionian Islands (Corfu, Cephalonia and Zakynthos) and from Crete (Fig. 2b).

On the NW coast of Corfu (Aghios Stefanos section), the PLG unit is missing and only a 32 m-thick cyclically-arranged terrigenous succession is present comprising three m-thick conglomerate beds alternating with fine-grained deposits rich in unspecified species of brackish water ostracods (Pierre et al., 2006).

In the southern part of Zakynthos, an evaporitic succession composed of eight gypsum cycles (Kalamaki section) occurs above marine marly deposits (Karakitsios et al., 2017b). These gypsum beds were initially ascribed to the UG unit (Pierre et al., 2006) and later to the PLG (Karakitsios et al., 2017b). The gypsum unit is overlain by approximately ~13 m of siltstones and marls with scattered, cm-thick beds of sandstones, conglomerates and carbonates with nodular texture (Pierre et al., 2006; Karakitsios et al., 2017b). Although no ostracods are reported from this interval, due to its stratigraphic position the post-evaporitic unit is correlated to the Lago-Mare phase (Karakitsios et al., 2017b). Except for the rare presence of marine nannofossils (*Ceratolithus acutus* together with *Reticulofenestra zancleana)* just below the Miocene/Pliocene boundary, only reworked marine fauna has been reported from the post-evaporitic package (Karakitsios et al., 2017b). This dominantly terrigenous succession is unconformably overlain by the Zanclean Trubi Formation (Fig. 6e; Karakitsios et al., 2017b).

MSC deposits on Crete (e.g. Meulenkamp et al., 1979; Delrieu et al., 1993; Cosentino et al., 2007; Roveri et al., 2008a; Zachariasse et al., 2008, 2011) were deposited in Miocene extensional, fault-bound basins driven by tectonic subsidence that ceased in the late Pliocene and Pleistocene (Van Hinsbergen and Meulenkamp, 2006). Because of the strong tectonic and eustatic sea-level-related fragmentation of the stratigraphic record, reconstructing the late Miocene stratigraphy of Crete has not been straightforward (Zachariasse et al., 2008, 2011). Several primary and clastic gypsum facies are recognized, but their correlation with the MSC stratigraphy is disputed (see Cosentino et al., 2007; Roveri et al., 2008a, 2014a; Zachariasse et al., 2008). Coarse-grained, mammal-bearing terrigenous facies irregularly alternating with marls are in places found unconformably overlying the gypsum and separated from the Pliocene facies by an erosion surface (see Meulenkamp et al., 1979; Delrieu et al., 1993; Cosentino et al., 2007). In two localities on the Messarà Plain, Cosentino et al. (2007) described a highly diversified ostracod fauna with Paratethyan affinity in some marly intervals.

Messinian evaporites and/or Lago-Mare deposits are also reported from the North Aegean region onshore in the Strymon Basin (Snel et al., 2006; Suc et al., 2015; Karakitsios et al., 2017a) and Dardanelles region (Melinte-Dobrinescu et al., 2009) and offshore (Prinos-Nestos Basin; Karakitsios et al., 2017a), but recent integrated studies suggested that the sections studied by the above listed authors are older than the MSC (see Krijgsman et al., 2020a, 2020b). In particular, Krijgsman et al. (2020a) proposed that for most, if not all, of the MSC the North Aegean was a brackish water, mostly Paratethyan-fed basin restricted by the Cyclades sill to the south (Fig. 2a) and forming a passageway for Paratethyan overspill waters towards the Mediterranean.

3.10. Cyprus

MSC deposits on Cyprus outcrop in the Pissouri, Psematismenos, Mesaoria and Polemi basins on the southerly fringe of the Troodos massif (Fig. 2b; Rouchy et al., 2001; Manzi et al., 2016a). According to

Rouchy et al. (2001) and Orszag-Sperber et al. (2009), sediments belonging to all MSC stages of Roveri et al. (2014a) are preserved in the Cypriot basins. By contrast, Robertson et al. (1995) and Manzi et al. (2016a) considered that PLG evaporites on Cyprus are only present as fragments reworked within a chaotic unit (the Lower Gypsum and Intermediate breccia units of Orszag-Sperber et al., 2009) and that the only *in situ* evaporites belong to the overlying Upper Gypsum Unit, which encompasses the whole of Stage 3 (Figs. 3a, 4a). A continuous, Eraclea Minoa-like section is not known in Cyprus (Manzi et al., 2016a). The best exposure of the lower 60 m of this unit is found in the Polemi Basin (Manzi et al., 2016a). It comprises up to six gypsum beds (the lower three of which are mainly selenitic, while the upper three are predominantly laminated; Fig. 3a). Gypsum beds range in thickness from 1 to 6 m and are separated by laminated marls (Fig. 5j) occasionally interbedded with conglomerates and sandstones (e.g. between the 5th and 6th gypsum layers; Rouchy, 1982; Rouchy et al., 2001; Manzi et al., 2016a). The sixth gypsum bed is reported by Rouchy et al. (2001) to be hollowed in the upper part with the cavities filled with overlying sediments. The similarity of the cyclicity and facies association of this Cyprus succession with the substage 3.1 interval of the Sicilian UG led Manzi et al. (2016a) to propose a bed-to-bed correlation and to recognize the substage 3.1/3.2 boundary at the top of the last gypsum bed (Fig. 3a). According to Orszag-Sperber et al. (2000) and Rouchy et al. (2001), this chronostratigraphic boundary coincides with a Mediterranean-scale sea-level drop, a conclusion that arises from the interpretation of the cavities in the uppermost gypsum as the product of karstic dissolution following a prolonged period of subaerial exposure.

The sedimentary sequence overlying the last gypsum bed and assigned by Manzi et al. (2016a) to the Lago-Mare phase lacks a clear and rhythmic sedimentary cyclicity. In the Pissouri Basin this interval (up to 25-30 m-thick) mostly consists of conglomerates, sandstones, limestones, paleosols (which appear as dm to m-thick dark marly horizons, in one case with pulmonated gastropods) and subordinated clay-marly horizons (Rouchy et al., 2001). By contrast, in the Polemi sections the clay-marly facies dominates this interval (Rouchy et al., 2001). *In situ* fresh-brackish water species of articulated mollusks (*Limnocardiidae*, *Melanopsis*), Paratethyan (*Loxocorniculina djafarovi*, *Euxynocythere praebaquana*) and Mediterranean (*Cyprideis agrigentina*) ostracods and foraminifera (*Ammonia beccarii*), *Characeae*, abundant fragments of the marine euryhaline fish *Clupeidae* and a fish skeleton of the euryhaline *Aphanius crassicaudus* are described from some of the substage 3.1 and 3.2 fine-grained facies and within the terrigenous laminae of some *balatino* gypsum (Orszag-Sperber et al., 2000; Rouchy et al., 2001; Orszag-Sperber, 2006; Manzi et al., 2016a). The upward change in diversity of the ostracod fauna seen elsewhere (e.g. Malaga, Nijar, Vera, Apennines and Eraclea Minoa) is not reported in Cyprus but this may be because no detailed study of ostracod assemblages in Stage 3 sediments has been published. The Miocene/Pliocene boundary, near Polemi village is described by Manzi et al. (2016a) as a sharp contact above a dark, organic-rich layer (Fig. 6f). It appears to be similar to the boundary reported from Piedmont (Fig. 6c; Trenkwalder et al., 2008; Dela Pierre et al., 2016) and Northern Apennines (Gennari et al., 2008; Grossi et al., 2008), if not for the presence, in Cyprus, of (possibly) in-situ *Cyprideis agrigentina* (Manzi et al., 2016a). A layer with the same field appearance, thickness (~ 1 m) and stratigraphic position is reported in Pissouri by Rouchy et al. (2001), which they interpreted as a paleosol based on mottling, oxidized roots, carbonate concretions and plant fragments.

3.11. Southern Turkey

The tectonically active, during the Miocene, thrust-top basin of Adana in southern Turkey (Radeff et al., 2017) retains the most complete and better exposed easternmost successions of the MSC (Fig. 2b), whose deposits were attributed to the Handere Fm. (Cosentino et al., 2010; Radeff et al., 2016).

MSC Stage 3 finds expression in a >1 km thick continental unit unconformable, through an erosional surface, above the pre-evaporitic, Stage 1 anhydrite-shale alternations (Radeff et al., 2016) and resedimented gypsum-bearing Stage 2 deposits (Cosentino et al., 2010; Cipollari et al., 2013). This unit mainly consists of fluvial coarse- and fine-grained deposits representing channel fill and overbank deposits. Sporadically, some fine-grained intercalations are found containing a mixed brackish (ostracod) and marine (foraminifera and calcareous nannofossils) fauna. The ostracod fauna has affinity with the Paratethyan fauna but, unlike to many other Mediterranean onshore localities, is poorly diversified, with monospecific assemblages of *Cyprideis agrigentina* (Avadan section and T-191 borehole; Cipollari et al., 2013) or with *Cyprideis agrigentina* accompanied by rare to abundant specimens of *Loxoconcha muelleri*, *Euxinocyhere* (*Maeotocythere*) *praebaquana*, and *Loxoconcha* sp. (Adana section; Faranda et al., 2013). Ostracods are often associated with *Ammonia beccarii* and rare *Elphidium* and *Cribroelphidium*, which are the only foraminifera considered as autochthonous. Conversely, the entire nannoflora is interpreted as physically reworked (Cipollari et al., 2013; Faranda et al., 2013).

The Handere Fm. is followed by early Zanclean marine sediments (Avadan Fm.) deposited, according to the paleoecology of the benthic foraminifera species recognized, at bathymetries ranging from 200 to 500 m (Cipollari et al., 2013). The lithological nature of the Miocene/Pliocene boundary in the Adana Basin is not clear, but it occurs either above the continental or subaqueous, ostracod-bearing facies.

A similar stratigraphic sequence is present in the subsurface. Here, however, chaotic gypsum-bearing deposits are not found and two halite bodies ~20 and ~170 m-thick are present, separated and followed by fluvial gravels, sands and silts (Cipollari et al., 2013).

3.12. Summary of the onshore Stage 3 record

Most of the onshore Stage 3 records formed in shallow marginal Mediterranean basins, which underwent substantial uplift from the Messinian till nowadays and are assumed to have had their depocenter at ~200 to 50 m below the Atlantic level during the late Messinian (Roveri et al., 2014a, 2019a; Radeff et al., 2016, 2017). The Caltanissetta Basin (Sicily), some basins along the Apennines and (possibly) Cyprus represent, instead, possible onshore representative of intermediate basins. The nature and duration of these records is quite variable, and there are only six sections that may record an entire Stage 3 sequence (i.e. Sorbas, Nijar, Northern Apennines, Eraclea Minoa and Cyprus; Fig. 3a). Reasons for the fragmentary nature of the Stage 3 sedimentary record include different durations of subaerial exposure following the Stage 2 drawdown, local tectonics and associated syn-depositional erosion and deposition. One of the consequences of this is that any sedimentary cyclicity that resulted from orbital fluctuations is typically either less well developed or poorly preserved, making the chronology of Stage 3 rather uncertain or controversial in places.

Despite this variability, several fairly consistent characteristics are widely expressed. These are:

1) Stage 3 sedimentation follows a period of intensive tectonic and/or eustatic-driven erosion of the margins, as demonstrated by the frequent presence of erosional unconformities and/or chaotic Stage 2 deposits (RLG unit);
2) Stage 3 lithologies are mostly terrigenous (conglomerates, sandstones and mudstones) and deposited in a variety of continental (fan delta, fluvial channels and alluvial plains) and shallow water environments (endorheic lakes or water bodies connected with the Mediterranean water mass is the riddle). Carbonate intercalations are sometimes present (e.g. Sorbas Basin and *Colombacci* limestones in the Apennines). Stage 3 gypsum is only found in deeper-water intermediate basins of Caltanissetta in Sicily and Cyprus.
3) A diversified fossil assemblage with Paratethyan affiliation (ostracods, dinocysts, mollusks) is commonly found in the shallow-water

sediments of Lago-Mare successions. Only in the intermediate Caltanissetta Basin (Sicily) do these diversified Paratethyan forms (only ostracods) occur earlier, in the sediments from substage 3.1. Where these have been studied in detail, these assemblages typically show an increase in diversity with time (possibly every wet phase of the precession cycles). Some of these sediments also contain marine fossils and there is controversy over whether these are *in situ* and contemporaneous or reworked.

4) In outcrop, the Miocene/Pliocene boundary has four main sedimentary expressions: erosive and followed by a conglomeratic lag (e.g. Malaga, Vera, Mallorca; Fig. 6a); conformable above continental facies (e.g. Nijar Basin; Fig. 6b); conformable above ostracod-rich mudstones (e.g. Eraclea Minoa; Fig. 6d); sharp contact above a black layer of still largely unknown paleoenvironmental significance (Piedmont, Apennines and Cyprus; Fig. 6c, f).

For a better understanding of how Stage 3 developed across the Mediterranean these marginal records now need to be considered alongside the evidence from intermediate to deep offshore settings.

We note that alternative chronostratigraphic frameworks have been proposed for several onshore (Malaga, Sorbas, Mallorca, Apennines, Sicily) and offshore (Sites 134B, 976B, 978A) locations (see Fig. 4b for references), but we have omitted them as they are shown to rely on incorrect (bio)stratigraphic arguments (see Roveri et al., 2008c, Grothe et al., 2018 and subsection 5.5).

4. Offshore domain

The offshore Mediterranean is a complex array of variable-depth and morphologically complex subbasins framed by morphological highs or sills. Traditionally it is divided into two main domains (Fig. 2a), the Western and Eastern Mediterranean, with the intervening divide (or Sicily sill) situated in the Sicily channel at present with a maximum depth of 316 m. The Alborán Basin, the depressions on the Balearic Promontory, the Corsica, Valencia, Algero-Balearic, Liguro (or Sardo)-Provençal and Tyrrhenian basins belong to the "Western Mediterranean" (Fig. 2a). The Adriatic foredeep, the Ionian, Sirte, Aegean and Levant basins belong in the "Eastern Mediterranean" (Fig. 2a). Smaller-sized depressions, again surrounded by sills of variable depth, are identified and labelled within each of these subbasins.

Although the exact topography and hypsometry of the Messinian Mediterranean is difficult to reconstruct, this present-day geography is generally assumed to have been in place, with five main differences: (1) the Alborán Basin was split into a Western (WAB) and Eastern Alborán (EAB) by a volcanic arc (Booth-Rea et al., 2018); (2) the Tyrrhenian Basin was only partly opened (Lymer et al., 2018); (3) the precise depth and width of the ancient Sicily Sill are difficult to estimate, but may have been much deeper than today (~300 m; Meijer and Krijgsman, 2005Jolivet et al., 2006). Paleodepth estimations for the Messinian configuration range from 380 m (Just et al., 2011) to 430 m (Garcia-Castellanos et al., 2009); (4) one or two sills were present at the southern termination of the Adriatic foredeep (Pellen et al., 2017; Amadori et al., 2018; Manzi et al., 2020); (5) the North Aegean was partially isolated from the Mediterranean by the Cyclades Sill and with high Paratethys affinity (Krijgsman et al., 2020a). Following the schematic classification of the Messinian sub-basins by Roveri et al. (2014a), all these subbasins are regarded as either intermediate (i.e. relatively deep-water, 200–1000 m) or deep (water depth > 1000 m).

Compared with the onshore domain, the offshore basins hold a far greater percentage of the total volume of MSC sediments (Ryan, 1973; Haq et al., 2020). The architecture, geometry and main lithologies of the MSC and younger deposits are well known thanks to the high density of seismic data and the fact that evaporites (halite particularly) are easily identified on seismic profiles due to their unusual seismic properties, especially compared to those of terrigenous and carbonate sediments (see Lofi et al., 2011a, 2011b; Lofi, 2018; Haq et al., 2020). However, the detailed lithological, sedimentological, paleontological and geochemical nature and their chronostratigraphy are still poorly constrained offshore because these cannot be univocally defined on the basis of seismic data alone (Roveri et al., 2019b) and direct information about these deep MSC successions is limited to a small number of cores (16) drilled during the DSDP (Ryan et al., 1973; Hsü et al., 1978b) and ODP (Kastens et al., 1987; Comas et al., 1996; Emeis et al., 1996) drilling campaigns that penetrated exclusively the uppermost tens of meters of the deep MSC suite in very scattered localities (Fig. 2b). Only recently, access to industrial boreholes crossing the base of the halite in the deep Levant Basin has been granted, providing a rare glimpse of the deep MSC deposits in the easternmost part of the Mediterranean (Gvirtzman et al., 2017; Manzi et al., 2018; Meilijson et al., 2018, 2019).

The MSC is commonly described as tripartite ('Messinian trilogy' after Montadert et al., 1978) in the Western Mediterranean (Lower-Mobile-Upper units: LU-MU-UU, respectively). However, in the Ionian Basin is described as bipartite (MU-UU) by Camerlenghi et al. (2019) while according to Lofi et al. (2011a), Gvirtzman et al. (2013, 2017), Lofi (2018) and Camerlenghi et al. (2019), the Levant Basin consists of the MU and the UU is only present locally and possibly represented by evaporite-free terrigenous accumulations (Kartveit et al., 2019; Madof et al., 2019). The lack of many age constraints within the offshore MSC successions hampers unambiguous correlation with onshore sequences (Fig. 1a; Roveri et al., 2014a). Nevertheless, different authors have proposed onshore-offshore correlation of specific events (e.g. onset, Ochoa et al., 2015; and termination of the MSC, Biscaye et al., 1972, Iaccarino et al., 1999) and stratigraphic schemes (Decima and Wezel, 1971; Raad et al., 2021) based on and biostratigraphic evidence (Cosentino et al., 2006), $^{87}Sr/^{86}Sr$ isotope ratios (Roveri et al., 2014b; Gvirtzman et al., 2017; Manzi et al., 2018) and astronomical tuning of the deep seismic record (Ochoa et al., 2015, 2018; Manzi et al., 2018; Meilijson et al., 2018, 2019). Here we focus on the seismic and geological (core-derived)[1] properties of the Upper Unit (and laterally grading/interfingering sediments when present), stratigraphically below the Plio-Quaternary deposits (PQ) suggesting that it belongs to (at least part of) Stage 3.

4.1. Western Alborán Basin and westernmost East Alborán Basin

The Alborán Basin has received particular attention because of its proximity to the Gibraltar Corridor (Estrada et al., 2011; Popescu et al., 2015 and references therein). Evaporites only occur on the eastern side of the EAB (which is treated in subsection 4.2; Fig. 2a). To the west of the volcanic archipelago (Booth-Rea et al., 2018, i.e. the WAB) and immediately to the east on the western side of the EAB only terrigenous sediments occur in the MSC interval (Booth-Rea et al., 2018; de la Peña et al., 2020). Sediments at the Miocene/Pliocene boundary appear in the seismic reflection data as parallel reflectors with increasing reflectivity (Comas et al., 1996, 1999; Booth-Rea et al., 2018). Locally, just below the M discontinuity, some of the reflectors suggest a chaotic seismic facies (Fig. 7a; Booth-Rea et al., 2018; Bulian et al., 2021). Miocene sediments with a maximum thickness of 100 m have been recovered from two out of nine holes drilled in the region (ODP 976B, 978A; Comas et al., 1996, 1999). These sediments mostly consist of claystones, siltstones and sandstones with *Chondrites* and *Zoophycos* ichnofacies at site 976B and include a conglomerate close to the Miocene/Pliocene boundary at Site 978A. The lack of age-diagnostic fossils hampers their correlation with the Geologic Time Scale (GTS). However, the presence,

[1] Lithostratigraphic and biostratigraphic information from DSDP and ODP cores are primarily extracted from the Scientific Shipboard Party documents, accessible from https://www.marum.de/en/Research/Cores-at-BCR.html. These documents are referenced in the text as follows: Ryan et al. (1973): DSDP 120-134; Hsü et al. (1978b): DSDP 371-378; Kastens et al. (1987): ODP 650-656; Comas et al. (1996): ODP 974-979; Emeis et al. (1996): ODP 963-973.

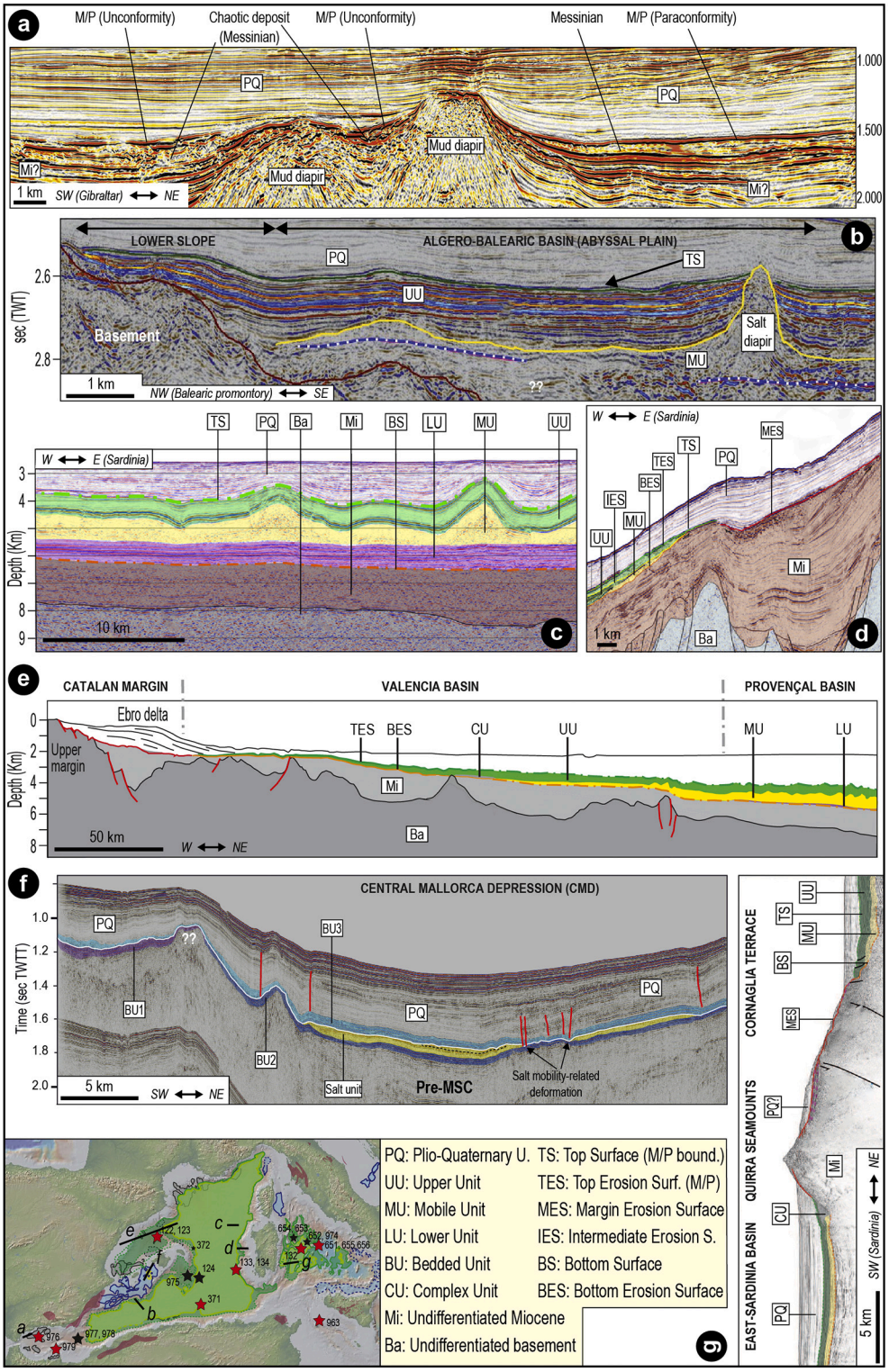

Fig. 7. Seismic profiles from intermediate-deep Western Mediterranean basins containing MSC markers/units. (a) Seismic reflection line CAB01-104 from the WAB (modified from Booth-Rea et al., 2018). The line shows the variable geometry of the inferred M/P boundary, erosive in proximity of mud diapirs, (para)conformable in tectonically undisturbed sectors. Chaotic reflectors are occasionally imaged below the inferred M/P boundary. (b) Seismic profile SF12-09 imaging the lower slope of the south Algero-Balearic margin and part of the Algero-Balearic abyssal plain (modified from Mocnik et al., 2014). Here a high reflecting and horizontally stratified UU covers a thin layer of MU evidenced by salt diapirism. Note the concordant deformation of the UU and MU. (c) Line MS-39 from the abyssal plain of the Liguro-Provençal Basin showing the Messinian trilogy and non-erosive bottom and top surfaces (BS and TS; Dal Cin et al., 2016). Halokinesis of MU gives rise to domes that deform the UU and PQ units. (d) Interpreted seismic profile from the lower-middle slope of the west Sardinian margin (modified from Dal Cin et al., 2016). Thin MU and UU are present on the lower slope, while on the middle slope (and upper slope here not shown) they converge in the margin erosion surface MES. (e) Line drawing of seismic line imaging from the Catalan margin (or Ebro Basin) to the abyss of the Liguro-Provençal basin (modified from Maillard et al., 2011b). Note the pinch out of the MU in the Valencia Basin and of the UU in the Ebro Basin, which is MSC free. (f) Interpreted seismic profile Simbad 15 crossing the depocenter of the CMD showing all the MSC units and erosional surfaces (modified from Raad et al., 2021). (g) Interpreted seismic profile MYS40 illustrating the MU-UU-PQ units in the East-Sardinia Basin and Cornaglia Terrace, separated by the MSC deposits-free Quirra Seamounts (modified from Lymer et al., 2018).

high in the Miocene section, of an oligotypic association of ostracods (*Candona* sp., *Loxoconcha muelleri*, and *Cyprideis* sp.) with different stages of growth (Site 978A; Iaccarino and Bossio, 1999) and Paratethyan dinocysts (including *Galeacysta etrusca*; see subsection 5.2; Popescu et al., 2015) indicates a latest Messinian (substage 3.2) age and brackish paleodepositional conditions. Foraminifera and nannofossils are also present, but all species recognized are of no help in narrowing down the paleoenvironmental interpretation because they are considered either definitely or likely to be reworked (Iaccarino and Bossio, 1999). By contrast, Popescu et al. (2015) interpreted some species of calcareous nannofossils (*Reticulofenestra pseudoumbilicus*, *Discoaster quinqueramus*, *Ceratolithus acutus*, *Triquetrorhabdulus rugosus*, *Amaurolithus primus*) and marine dinocysts as autochthonous.

The nature of the Miocene/Pliocene boundary is also uncertain. According to some authors, the "M" discontinuity is a high-amplitude reflector with evidence of erosion attributed to subaerial processes (Estrada et al., 2011; Urgeles et al., 2011) and locally (e.g. close to Site 121; Ryan et al., 1973) associated with an angular unconformity that

abruptly truncates the upper Miocene deposits and morphological highs (Comas et al., 1999; Estrada et al., 2011; Garcia-Castellanos et al., 2020). Although the M-reflector was drilled at Sites 976B, 977A and 978A, a lithological contact was only recovered at Site 976B coinciding with a major erosional surface between the early Messinian and the base of the Pliocene (Bulian et al., 2021). Only at Site 978A (and possibly 977A) was a few meters of what may be the contact interval recovered (Comas et al., 1996). This comprises a 25 m-thick cemented succession containing pebbles of volcanic and sedimentary rocks likely to derive from the Alborán substrate (46R, 620.9-630.67 mbsf, between the Pliocene-bearing core 45R and the Messinian-bearing core 47R; Comas et al., 1996). In contrast, Booth-Rea et al. (2018) concluded that the M-reflector is an unconformity only close to the mud diapirs and owes its erosive shape and angular discordance to the activity of these structures (Fig. 7a). In more undisturbed sectors these authors argue that the boundary is a paraconformity with no evidence of erosion (Fig. 7a). The lack of Messinian erosion in the shallow regions of the WAB margins has prompted the hypothesis that this area did not desiccate during the MSC (Booth-Rea et al., 2018; de la Peña et al., 2020). This contradicts much of the interpretation made of the DSDP and ODP cores of this interval in the Alborán Sea. The succession recovered by drilling from beneath the Pliocene comprises gravels that contain a mixed Miocene fauna. These sediments and their faunal content are thought to have been reworked from older sediments exposed as Alborán substrate with no evidence of an extensive wet Lago Mare interval immediately before the Zanclean (Comas et al., 1996).

Two W-E-aligned erosional channels straddling the Strait of Gibraltar and stretching for 390 km from the easternmost Gulf of Cádiz (Atlantic Ocean) into the Alborán Basin are clearly observed in seismic profiles (Garcia-Castellanos et al., 2009; Estrada et al., 2011). There is disagreement, however, concerning the timing and nature of their formation. These incisions are classically considered to occur at the very top of the MSC suite (when present) and to be the consequence of the Zanclean megaflood (Garcia-Castellanos et al., 2009, 2020; Estrada et al., 2011 among others). More recently, Krijgsman et al. (2018) highlighted that an accurate age determination for these channel incisions is lacking and that they might have been formed earlier during the MSC as a result of the Mediterranean-Atlantic gateway currents. Interpretation of E-W seismic profiles across the Alborán Basin combined with mammal records in Africa and Iberia led Booth-Rea et al. (2018) to suggest the existence of an emergent volcanic archipelago that temporarily connected southeastern Iberia with northern Africa, separating an open marine, Atlantic-influenced West Alborán Basin realm from a restricted, hydrologically complex Mediterranean realm to the east.

4.2. Eastern Alborán, Algero-Balearic and Liguro-Provençal basins

From the eastern margin of the EAB as far east as the Tyrrhenian coast of Italy, the Messinian (evaporites-bearing) trilogy LU-MU-UU is found and sealed by the PQ. The MU and UU are interpreted to fill the deepest depocenters (Algero-Balearic, Valencia and Liguro-Provençal basins; with minor interruptions due to seamounts) and the lower slope domain, where they comprise ~500 to ~800 m of UU and ~1000 m of MU/halite (Figs. 7b-d; Camerlenghi et al., 2009; Lofi et al., 2011a, 2011b; Geletti et al., 2014; Mocnik et al., 2014; Dal Cin et al., 2016; Lofi, 2018). Upslope, a thinner, possibly incomplete UU is locally described on the middle-upper continental slopes of Western Corsica (Guennoc et al., 2011) and Sardinia (Mocnik et al., 2014; Dal Cin et al., 2016) and the northern (Maillard et al., 2006) and southern (Maillard and Maufret, 2013; Mocnik et al., 2014; Dal Cin et al., 2016) flanks of the Balearic Promontory, even though the structural settings of these locations are mostly dominated by erosion (Fig. 7d). MSC evaporites are absent on the continental shelves bordering the deep Algero-Balearic and Liguro-Provençal basins, where the PQ directly overlies the MES which, in turn, cuts through the middle Miocene deposits (Gorini et al., 2005; Lofi et al., 2005). The only late Messinian sediments are present as Complex Units (Gulf of Lion, Bessis, 1986; Gorini et al., 2005; Lofi et al., 2005; Algerian Basin, Medaouri et al., 2014; Arab et al., 2016; Fig. 7e). CUs can have various origin (Lofi et al., 2011a, 2011b), but when identified at the outlet of drainage systems, they are commonly interpreted as Messinian clastics supplied by rivers (Lofi et al., 2005). In the Gulf of Lion, the MES is a high angle unconformity with substantial erosion along highly rugged relief thought to have been generated by fluvial incision (Lofi et al., 2005). In contrast, Roveri et al. (2014c) suggested that the drainage networks visible on the seismic could be of subaqueous origin.

When not involved in MU-related deformation processes, the UU appears as a highly reflective series of flat reflectors alternating with less reflective, but concordant, reflectors (Figs. 7b-c; Lofi et al., 2011a, 2011b) aggrading in the basin center and onlapping the margins (Fig. 7b; Camerlenghi et al., 2009; Lofi et al., 2011a, 2011b; Geletti et al., 2014; Mocnik et al., 2014; Dal Cin et al., 2016). The aggrading nature, shelf-ward thinning and the onlap terminations of the UU are interpreted as evidence of sedimentation in a lake with fluctuating base level (e.g. Lofi et al., 2005; Lofi et al., 2011a). In the abyssal plains (Figs. 2a, 7c), nine to ten cycles have been interpreted on high resolution seismic profiles as corresponding to gypsum-marl alternations (Geletti et al., 2014; Mocnik et al., 2014). At Sites 124 and 372, ~40-50 m of the UU have been drilled at the feet of the east Menorca continental rise and the northern Menorca slope, where 3-4 gypsum-marl cycles are recognized (Fig. 2b; Ryan et al., 1973; Hsü et al., 1978a). Primary gypsum facies are widely overprinted by post-depositional diagenetic processes, but the still recognizable laminated and clastic primary textures indicate precipitation at the water-air interface and emplacement by gravity flows, respectively (Lugli et al., 2015). The marl interbeds are made from stiff to firm dolomitic mud containing substantial quantities of detrital material intercalated with current-bedded sandstones and, at Site 124, with diatomites (Ryan et al., 1973). *Cyprideis* sp. specimens are reported from some mudstone interbeds at Site 372, while dwarf planktonic foraminifera are present just below the Miocene/Pliocene boundary at Site 124 (Ryan et al., 1973).

The Miocene/Pliocene boundary coincides with the top of the UU where present (labelled TES when erosional and TS when conformable; Lofi et al., 2011a, 2011b). In the abyssal plain-lower slope domain it appears to be undulating, although this geometry is related to the deformation of the underlying salt (Figs. 7b-c), and it actually corresponds to a sharp surface lacking signs of erosion (Lofi et al., 2011a, 2011b; Geletti et al., 2014; Mocnik et al., 2014). By contrast, the UU-PQ boundary commonly appears strongly erosional in the middle-upper slope and shelf domain, where it coincides with the MES (Fig. 7d; Lofi et al., 2005; Maillard et al., 2006; Geletti et al., 2014; Mocnik et al., 2014). Among the six DSDP-ODP Sites drilled in this region (Fig. 2b), only Hole 975B recovered the Miocene/Pliocene boundary (Iaccarino and Bossio, 1999; Marsaglia and Tribble, 1999). Here the Messinian is a few centimeters thick and consists of banded micritic silty clays with minor calcareous siltstones to sandstones typified by a diverse faunal assemblage consisting of dwarf planktonic foraminifera, *Ammonia tepida* tests and brackish Paratethyan ostracods (*Loxocorniculina djafarovi*, *Euxinocythere praebaquana*, *Amnicythere idonea*, *Leptocythere limbate*, *Candona* sp., and *Cyprideis* sp.; Iaccarino and Bossio, 1999).

Halite is present at the bottom of Hole 134 drilled within the UU (Ryan et al., 1973; Sage et al., 2005; Lugli et al., 2015). High-resolution seismic profiles from both the Algero-Balearic and Ligurian-Provençal basins confirm the presence of a halite layer high in the UU sequence (Geletti et al., 2014; Mocnik et al., 2014). This layer is up to 50 m thick (Dal Cin et al., 2016) and is correlated with an erosional surface (called IES: Intermediate Erosional Surface by Lofi et al., 2011a, 2011b) associated with an angular unconformity which is better developed on the lower slope (Fig. 7d). Geletti et al. (2014) and Mocnik et al. (2014) interpreted this layer as autochtonous and indicative of at least one important sea level drop during UU deposition. However, this intra UU halite layer is always described from areas strongly affected by salt

diapirism (just like in the Ionian Abyssal Plain; see subsection 4.6.1) and is never found in adjacent, undisturbed areas (see Camerlenghi et al., 2009; Geletti et al., 2014; Mocnik et al., 2014; Dal Cin et al., 2016), two features that may suggest it has an allochthonous origin.

Site 134 shows evidence of a "desiccation crack" cutting through a sandy silt layer interbedded with unaffected laminated halite (Hsü et al., 1973c). Unfortunately, the core photograph of this crack has been published in two different orientations (Hsü et al., 1973a, 1973b), leading both Hardie and Lowenstein (2004) and Lugli et al. (2015) to question the evidence for subaerial desiccation. Because of these ambiguities, we suggest to dismiss this example from the book of evidence.

4.3. Valencia Basin

The Valencia Basin (VB; Fig. 2a) is an aborted rift formed during the late Oligocene-early Miocene opening of the back-arc Liguro-Provençal Basin (e.g. Jolivet et al., 2006). It is located between the Spanish Ebro Margin to the west and the Balearic Promontory to the east, while it grades into the Liguro-Provençal Basin to the E/NE (Fig. 7e; Maillard and Mauffret, 2006; Maillard et al., 2006).

Numerous exploratory boreholes exist on the western Ebro margin. These boreholes, tied to seismic data, confirm that MSC-related sediments on the northwestern shelf are missing (Fig. 7e; Urgeles et al., 2011; Pellen et al., 2019). The only MSC feature present is a prominent erosional surface (the MES) incising Serravallian-early Messinian sediments (Urgeles et al., 2011). By contrast, on the southwestern and southern part of the margin, well data show the presence of evaporitic sediments (e.g. Delta L and Golfo de Valencia D1 boreholes; Del Olmo, 2011; Del Olmo and Martín, 2016; Lozano, 2016). Del Olmo and Martín (2016) described these evaporites as primary selenites and ascribed them to MSC Stage 1 (their unit M7). Lozano (2016) described the same evaporitic deposits in the same boreholes as 'white anhydrites', leaving open the question as to whether the anhydrite is primary (sabhka's) or secondary at the expense of a primary gypsum facies. On the eastern margin of the VB boreholes and seismic studies suggest there are no MSC units with only a prominent MES cutting pre-MSC sediments (Driussi et al., 2015; Raad et al., 2021). All authors conclude that the shelves of VB were exposed to subaerial erosion during and following the main drawdown.

MSC deposits are also absent along the slopes and, where present, consist of coarse- and fine-grained terrigenous facies filling valleys largely related to fluvial incision (Fig. 7e; Stampfli and Höcker, 1989).

A different situation features in the depocenter. Despite its present-day depth of $>$ 2000 m, no MU is observed in the depocenter, as the salt pinches-out at the edge of the deeper Provençal Basin (Fig. 7e). Only the seismic properties of UU suggest that it is roughly continuous from the Provençal Basin into the VB (Fig. 7e; see subsection 4.2), although it thins from ~1000 m to $<$ 500 m. The UU is characterized by aggrading and onlapping geometries towards the slopes, where it also thins out until it disappears along the middle-upper slope (Fig. 7e; Maillard et al., 2006; Cameselle and Urgeles, 2017). Maillard et al. (2006), Urgeles et al. (2011), Cameselle et al. (2014) and Cameselle and Urgeles (2017) all stated that the UU formed during an important Mediterranean-level lowstand (~1000 m). Several Complex Units (CU), with different origin, have been observed and described as belonging to the MSC (Cameselle and Urgeles, 2017).

DSDP Site 122, drilled at the mouth of a valley incision, recovered a few meters of sand-gravels made of well-rounded basalt, marine limestones, nodules of crystalline gypsum and mollusk fragments in a clay-silty matrix rich in deep-water benthonic foraminifera and early Pliocene nannofossils, all interpreted as erosional products of the VB seabed (Ryan et al., 1973). The uppermost Messinian in two industrial wells (Ibiza Marino and Cabriel boreholes; see Lozano, 2016) is represented by intercalations of clastic gypsum/anhydrite and marls (unit M8-P1 of Del Olmo and Martín, 2016). These are interpreted as turbidites sourced from the shelf and/or slope during a lowstand phase of the Mediterranean base level (Del Olmo, 2011; Del Olmo and Martín, 2016; Cameselle and Urgeles, 2017).

In seismic profiles, the UU/PQ transition (M-reflector or TES) is locally both sharp and smooth (in more distal settings) and erosional (in more proximal settings; Fig. 7e). Maillard and Mauffret (2006) indicate that the smooth parts have been caused by increasing fresh water influx during the Lago-Mare phase, leading to dissolution of the evaporites, and the rough erosional segments are of subaerial origin. For Cameselle and Urgeles (2017), the top of the UU is a smooth and conformable downlap surface, representing the rapid inundation of the basin with only local minor erosional features.

4.4. Balearic Promontory

Sticking out from the surrounding deep-water locations, the Balearic Promontory (BP; Fig. 2a) is a continental high that has undergone tectonic extension since the late Serravallian (Roca and Guimera, 1992; Sabat et al., 2011). During the Messinian, it comprised in topographic lows/subbasins at different water depths and separated by structural highs/sills (Maillard et al., 2014; Driussi et al., 2015; Roveri et al., 2019b; Raad et al., 2021). The area has been the subject of multiple studies (Maillard et al., 2014; Driussi et al., 2015; Ochoa et al., 2015; Roveri et al., 2019b; Raad et al., 2021) and several controversies arose after the publication of Roveri et al. (2019b).

The first controversy concerns the Messinian paleodepth of the BP's subbasins. According to Roveri et al. (2019b) the subbasins were shallow during the Messinian and acquired today's paleodepths following a strong post-MSC subsidence; Maillard and Mauffret (2011), Maillard et al. (2014) and Raad et al. (2021), instead, consider the tectonic movements in the BP to have been minor since the late Miocene (Messinian) and the region to have been already structured as it is today during the MSC. Well-to-seismic ties in the shallower basins closer to the Spanish coast (i.e. Bajo Segura, San Pedro and Elche basins) comprise up to 14 Stage 1 primary gypsum-marl cycles similar to the onshore PLG unit (Lugli et al., 2010) truncated at the top by the MES (Soria et al., 2008a, 2008b; Ochoa et al., 2015). At first, Ochoa et al. (2015) concluded that all sediments overlying the MES are Pliocene in age. A later re-appraisal of the same downhole logging data and cuttings led Ochoa et al. (2018) to attribute the first ~13 m-thick micritic and evaporite-free sediments to the late Messinian (stage 2 or 3 of the MSC according to the authors). The MSC stratigraphy of the shallowest offshore basins of the BP closely resembles that described from cores and outcrops onshore Mallorca (see subsection 3.4; Roveri et al., 2019b).

High resolution seismic reflection data in the Central Mallorca Depression (CMD) highlighted up to 500 m of MSC deposits made of a Bedded Unit (BU) and a thin salt layer (Maillard et al., 2014; Driussi et al., 2015). This BU has never been drilled and, therefore, lacks lithological and chronostratigraphic constraints. Two contrasting chronostratigraphic and lithological interpretations are proposed: Roveri et al. (2019b) ascribed these sediments to Stage 2 and 3 and suggested that only reworked evaporites and halite are present. By contrast, following the seismostratigraphic description of Maillard et al. (2014), Ochoa et al. (2015) and Raad et al. (2021) inferred the presence of Stage 1 gypsum also in the CMD.

Raad et al. (2021) made a step forward by disclosing a possible tripartition of the BU unit (Fig. 7f). In their seismostratigraphic framework, Raad et al. (2021) noticed that the uppermost evaporite-bearing unit (called BU3), ~120 m-thick in the CMD, has geometric, stratigraphic and facies analogies with the astronomically-tuned UG unit of the Caltanissetta Basin (Fig. 3a) that endorse its attribution to Stage 3. Similar to the UU in the deepest basins (see subsection 4.2), BU3 consists of up to 9 low- and medium-amplitude reflectors that are interpreted as alternating terrigenous and gypsum beds (Maillard et al., 2014; Raad et al., 2021). Reflectors are parallel and continuous in the more distal areas, while they appear more chaotic in the more proximal sectors (Raad et al., 2021). The base of BU3 coincides with the erosional top of the salt,

interpreted as created by salt exposure, dissolution and locally salt gliding towards the depocenter (Fig. 7f; Raad et al., 2021). By contrast, the top of BU3, which corresponds to the Miocene/Pliocene boundary, is largely flat without signs of erosion (Fig. 7f; Maillard et al., 2014; Raad et al., 2021). An irregular geometry is sometimes visible, but is likely to be related to deformation of the underlying salt (Fig. 7f; Raad et al., 2021).

4.5. Tyrrhenian Basin

The Tyrrhenian Basin to the east of Sardinia is a back-arc basin that opened by continental rifting and oceanic spreading related to the eastward migration of the Apennine subduction system from middle Miocene to Pliocene times (Gaullier et al., 2014; Lymer et al., 2018; Loreto et al., 2020 and references therein). Three main domains are traditionally identified (Lymer et al., 2018 and references therein): 1) the East Sardinia Basin, with present-day water depths between 200-2000 m consisting of a system of seamounts and depressions that do not contain MSC sediments (Lymer et al., 2018); 2) the Cornaglia Terrace (2000-3000 m deep), a wide, flat area with dispersed structural highs; 3) the Tyrrhenian Basin *s.s.*, with water depths varying from 3000-3600 m. Whether the Tyrrhenian Basin acquired the present-day topography and hypsometry before the MSC (Lymer et al., 2018) or at least part of it (e.g. Eastern Sardinia margin, where Site 654 is located, and Northern Tyrrhenian) was much shallower (possibly comparable to the Caltanissetta Basin; Roveri et al., 2014b) and underwent extension and subsidence during the Messinian-Pliocene (e.g. Kastens and Mascle, 1990; Loreto et al., 2020) is still unresolved.

The MSC units in seismic profiles from the Tyrrhenian Basin (Fig. 7g) are very similar to the ones described in the Algero-Balearic and Liguro-Provençal basins (Fig. 7b-c; Gaullier et al., 2014; Lymer et al., 2018). ODP Sites 652, 653 and 654 confirmed the seismic-inferred lithological nature of UU as consisting, of gypsum-mudstone alternations (8 are counted at Site 654; Kastens et al., 1987; Borsetti et al., 1990; Roveri et al., 2014b). Intercalations of ripple–cross-laminated, fine-grained, azoic sandstones occur within the mudstone intervals in places (Cita et al., 1990; Iaccarino and Bossio, 1999). In some mudstone samples, the ostracod *Cyprideis* sp. (Site 654) and *Candona* sp. (DSDP Hole 974B) and the foraminifera *Ammonia beccarii* and *Ammonia tepida* have been found, indicating a shallow-water (< 50 m) brackish environment (see subsections 5.1 and 5.4; Cita et al., 1990; Iaccarino and Bossio, 1999). $^{87}Sr/^{86}Sr$ isotope ratios of UU gypsum and planktic foraminifera of the overlying Pliocene (Unit 1 at Site 654) show values much lower (from 0.708627 to 0.708745) and roughly equivalent (from 0.708935 to 0.709112) to coeval ocean water (~0.709020-30; McArthur et al., 2012), respectively (Müller et al., 1990; Müller and Mueller, 1991). Similar $^{87}Sr/^{86}Sr$ values were obtained from the gypsum cored at Site 652 (0.708626-0.708773; Müller and Mueller, 1991).

The Miocene/Pliocene boundary at DSDP Site 132 is placed above a cross-bedded sand rich in quartz, mica, pyrite, rounded fragments of gypsum and specimens of *Ammonia beccarii* and *Elphidium macellus* (Ryan et al., 1973). In the adjacent ODP Site 653 a similar sandstone is found slightly below the biostratigraphically-defined Messinian/Pliocene boundary and ~70 cm of grey mudstones with foraminifera and nannofossils of undisclosed provenance are squeezed in between (Cita et al., 1990). These mudstones also contain rare dwarf planktic foraminifera (*Globorotalia acostaensis*, *Orbulina universa*, and *Globigerina bulbosa*; Cita et al., 1990).

Overall, the uppermost Messinian sediments of the Tyrrhenian Basin are interpreted as having been deposited in lakes with periodic episodes of increased salinity and dilution under the strong influence of high energy rivers and, perhaps ocassionally, of the Atlantic (Cita et al., 1990; Müller et al., 1990; Müller and Mueller, 1991).

4.6. Ionian Basin

The deepest basin in the Mediterranean today is the Ionian Basin, with its lowest point at 5,267 meters. The so-called Ionian Abyssal Plain (IAP) is bounded on all sides by pre-MSC structural highs (Fig. 2a; Camerlenghi et al., 2019): the Malta Escarpment to the west; the Medina Escarpment to the south separating it from the Gulf of Sirt (Fig. 8a); the Gargano-Pelagosa and/or Otranto sill to the north dividing it from the Adriatic Foreland and, finally, an unnamed sill to the east, separating the IAP from the Levant Basin. Evidence from recent high-resolution seismic studies across the region have been used to support Stage 3 desiccation models (e.g. Hsü et al., 1978a, 1978b; Bowman, 2012; Micallef et al., 2018, 2019; Camerlenghi et al., 2019; Spatola et al., 2020).

4.6.1. Ionian Abyssal Plain

The typical "trilogy" of seismic units representing the MSC deposition in the Western Mediterranean is recognized also in the IAP by Gallais et al. (2018) and Mocnik et al. (2018). However, Camerlenghi et al. (2019) states the MSC sequence in the IAP is ~1,300 m-thick and composed of only two units (Fig. 8a). The lowermost 150-700 m-thick Mobile Unit (MU) is seismically transparent without discernible bedding and with diapiric structures, all features diagnostic of halite. By contrast, the 350-1,000 m-thick Upper Unit (UU) alternates highly reflective with acoustically transparent reflectors (Figs. 8a-b), similar to those described of the UU sequences of the Western Mediterranean (Figs. 7b-c). These are therefore assumed to represent gypsum-mudstone cycles (Camerlenghi et al., 2019). The uppermost 80 m of UU has been recovered from DSDP Site 374 (Hsü et al., 1978b), confirming the presence of gypsum (both primary cumulate and clastic; Lugli et al., 2015) alternating with mudstones (Unit III; Hsü et al., 1978b). These mudstones are largely barren of *in situ* fossils. However, the presence of some foraminifera and siliceous microfossils led Cita et al. (1978) and Hsü et al. (1978a) to suggest that sporadic marine incursions, possibly from the Indian Ocean, took place during Stage 3. Similar to Site 372, the basal part of Hole 374 intercepted one thin (~3.5 m) halite layer within the UU (Hsü et al., 1978b).

The UU and the overlying Zanclean (subunit PQc of Camerlenghi et al., 2019) reflectors are conformably folded throughout most of the abyssal plain, locally showing chaotic internal structure, irregular folding mimicking V-shaped incisions and truncations (Fig. 8b; Camerlenghi et al., 2019). These features are interpreted by Camerlenghi et al. (2019) as fluvial valleys carved in subaerially exposed evaporites by the Eso-Sahabi fluvial system, the closest fluvial drainage network to the area (see Micallef et al., 2018) that drained Libya in the late Miocene (Griffin, 2002) and has been traced across the Gulf of Sirt offshore (Sabato Ceraldi et al., 2010; Bowman, 2012). Several arguments counteract this interpretation: 1) the coherent, deformation, mostly of post-Messinian age, of both the UU and the lower Zanclean; 2) the absence of fluvial facies above the bottom of the "valleys", which instead correspond to a mudstone interval that underwent post-depositional dolomitization (Unit II; see below; Fig. 8b); 3) the unlikelihood that the Eso-Sahabi fluvial system managed to bypass the Medina Ridge divide (Fig. 8a). Alternatively, the apparent incisions at the M/P boundary in the IAP may represent post-sedimentary folds resulting from post-Messinian tectonic and/or salt movements-driven deformation (e.g. Mocnik et al., 2018). At Site 374 the Miocene/Pliocene boundary has been recovered (Unit II), but its primary nature (likely a mudstone) is obscured by diagenesis (cementation by dolomite; Hsü et al., 1978b). A lithified dolostone at the (seismic) predicted depth of the M-Horizon is a characteristic of several sites. Sometimes this interval has been recovered (e.g. Sites 125 and 374; Ryan et al., 1973; Hsü et al., 1978b; Comas et al., 1996); at others the hard lithology is inferred by the torqueing of the drill string (resistance to turning) accompanied by bouncing of the drill bit at the (e.g. Sites 122, 124, 125, 132, 133 and 134; Ryan et al., 1973). Dolomitization was (Hsü et al., 1973a, 1973b; Ryan et al., 1973) and still is (e.g. Ryan, 2009) largely considered a

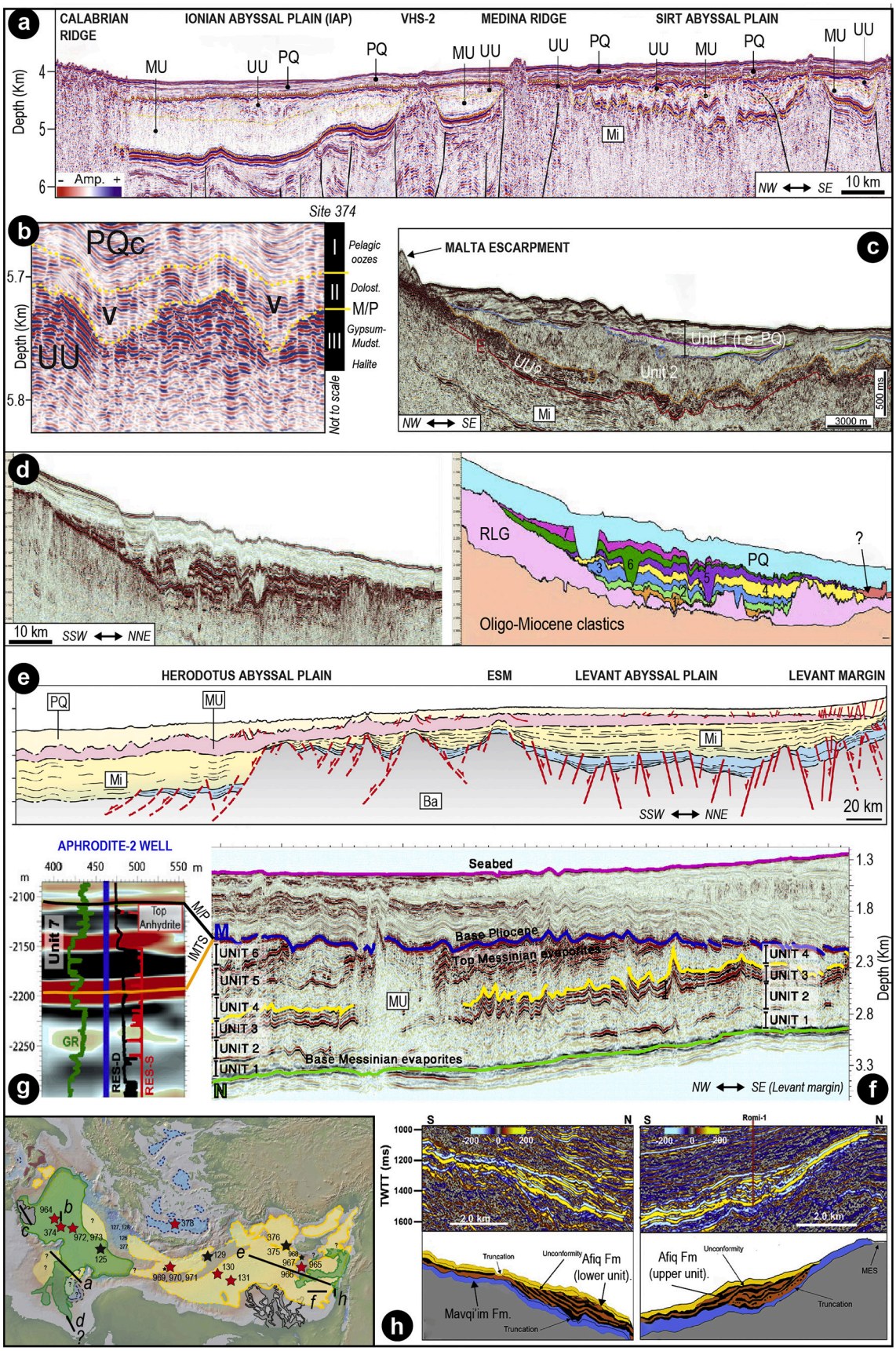

(caption on next page)

Fig. 8. Seismic profiles from intermediate-deep Eastern Mediterranean basins containing MSC markers/units (see Fig. 7 for abbreviations). (a) High-resolution seismic line MS27 imaging the PQ and the uppermost MSC's UU and MU in the Ionian Abyssal Plain and Gulf of Sirt (modified from Camerlenghi et al., 2019). Note how the MSC units are thinner, more difficult to distinguish and more deformed in the Sirt Abyssal Plain than in the IAP. PQ, UU and MU all onlap the structural highs of the Medina Ridge and VHS-2 sill. (b) High-resolution imaging of the lower part of the Plio-Quaternary (PQc unit) and upper part of the Messinian (UU) in the IAP (Camerlenghi et al., 2019). The MSC-PQ boundary is a highly irregular surface, describing apparent V-shaped incisions (symbol V) of controversial origin (see subsection 4.6.1 for insights). Note the coherent deformation of PQc with the underlying MSC sequence and the absence of fluvial facies within the incisions (Unit II is made of lower Pliocene dolomitic marls recovered in Site 374 drilled nearby the seismic line; see text). (c) Multichannel seismic reflection profile MEM-07-203 running approximately parallel to the Malta Escarpment and showing the relationship between Unit 2 of Micallef et al. (2018) with the overlying and underlying Zanclean and Messinian sediments, respectively (modified from Spatola et al., 2020). (d) Uninterpreted (left) and interpreted (right) seismic profiles showing the cyclic and channelized nature of the uppermost Messinian observed in the offshore Sirt Basin (modified from Bowman, 2012). (e) Interpreted 2D regional WNW–ESE seismic profile crossing the continental shelf and offshore Levant Basin and the Herodotus Abyssal Plain (Jagger et al., 2020). Note the lateral continuity of the Messinian MU. (f) Seismic profile from the Levant Basin showing the 6 sub-units distinguished inside the MU as well as its lower (N-reflector) and upper (M-reflector) boundaries (modified from Gvirtzman et al., 2013). (g) High-resolution seismic reflection image with wireline logs from Aphrodite-2 well illustrating that M-reflector previously considered as top evaporitic sequence and M/P boundary here consists of a ~100-m-thick unit (i.e. Unit 7 of Gvirtzman et al., 2017) in which different layers are distinguished (modified from Gvirtzman et al., 2017). (h) Interpreted and uninterpreted seismic profiles imaging the Mavqi'im and Afiq formations described in the canyons on the Levant continental margin (modified from Ben Moshe et al., 2020).

"*diagnostic feature of tidal (sabkha) sediments*" (Friedman, 1973, *pp.* 705). Its occurrence at locations with present-day water depth exceeding 2000 m was therefore considered strong evidence that the Mediterranean floor was subaerially exposed prior to the Zanclean marine replenishment (e.g. Ryan et al., 1973). It is, however, now widely accepted that dolomite precipitation is not exclusive of sabkha environments, but rather is a common process also in bottom sediments under a relatively deep water column (see Dela Pierre et al., 2012, 2014 and references therein). In the specific case of the offshore Mediterranean's M/P boundary on the Ionian Abyssal Plain, already in the '70s dolomitization was thought to have occurred after burial (Hsü et al., 1978b), a conclusion recently reinforced by McKenzie et al. (2017).

4.6.2. Malta Escarpment

At the foot of the Malta Escarpment, Micallef et al. (2018, 2019) and Spatola et al. (2020) amalgamated the MU and UU into one seismic unit, Unit 3, which is separated from the Plio-Quaternary marine sediments (Unit 1) by Unit 2, a chaotic transparent seismic package (Fig. 8c). Unit 2 has a maximum thickness of 760-860 m, a volume of 1430–1620 km^3 and a wedge-shaped geometry that thins eastwards, disappearing before reaching the IAP (Micallef et al., 2018). Micallef et al. (2018) and Spatola et al. (2020) proposed a lithological/sedimentological interpretation of this chaotic body, suggesting it is composed of well-sorted sediments of the Pelagian Platform to the west of the Malta Escarpment, with coarser material at the mouth grading into more distal finer sediments. This chaotic body has recently been attributed to the Zanclean megaflood during its passage from the western to the eastern Mediterranean via a gateway located in south-eastern Sicily (Micallef et al., 2018, 2019; Spatola et al., 2020). Given the rapidity of the reflooding ($\leq$ 2 years, Garcia-Castellanos et al., 2009, 2020), this interpretation implies rapid mass deposition. Other interpretations of this Unit 2 include being the result of extensive marine mass movement (Polonia et al., 2011), being folded UU (Butler et al., 2015) or being a complex unit built during lower sea level phases (Lofi et al., 2011a, 2011b).

4.6.3. Gulf of Sirt

The Gulf of Sirt (or Sirt embayment; Figs. 2a, 8a), the offshore extension of the Sirt Basin onshore Libya (Griffin, 2002 and references therein), is cross-cut by high-density seismic and well datasets as a result of oil potential of the region (Fiduk, 2009). However, only few studies have tackled the MSC (e.g. Hallett, 2002; Fiduk, 2009; Bowman, 2012).

In the Sirt embayment the MSC unit(s) is unevenly distributed in sub-basins controlled by a pre-existing topography, there is little distinction between the MU and UU, the overall thickness of the MSC unit(s) is lower and the degree of deformation is higher than in the adjacent IAP (Fig. 8a; Camerlenghi et al., 2019). The presence of halite in the Sirt embayment is debated, but most authors think it is absent (see Fiduk, 2009; Sabato Ceraldi et al., 2010; Lofi, 2018; Jagger et al., 2020; Fig. 2b). Bowman (2012) distinguishes seven seismic units within the MSC-related sequence (Fig. 8d). On the basis of high-resolution 3D and 2D data, each seismic unit has been interpreted consisting of clastics filling erosional channels cutting up to 100 m deep and wide (Fig. 8d) and evaporites (gypsum and anhydrite) alternating with precessional cyclicity (Bowman, 2012). The presence of anhydrite in the topmost part of the sequence is confirmed by the B1 NC 35A well (Hallett, 2002). Sabato Ceraldi et al. (2010) and Bowman (2012) envisaged a three-step evolution of each unit: 1) evaporitic deposition during precession maxima in a dried out Sirt embayment; 2) erosion of the valleys during the arid-wet transition fed by the Eso-Sahabi paleofluvial system; 3) filling of the valleys with the fluvial sediments during the wet phase. Based on this chronostratigraphic interpretation, the evaporite cycles should be time equivalent to most of Stage 3, with the upper four seismic units reflecting the Lago-Mare phase (Fig. 1a).

4.7. Levant Basin

4.7.1. Abyssal plain

Old seismic data in the Levant Basin show an up to 2 km-thick, high velocity, acoustically transparent sequence bounded by the N-reflector at the base and the M-reflector at the top (Figs. 8e-f; Ryan, 1978; Netzeband et al., 2006). This sequence thickens and extends for tens of kilometers towards WNW and thins eastward along the continental margin (Fig. 8e), where the N and M-reflectors converge forming the condensed MSC section of the Mavqiim and Afiq formations (described in subsection 4.7.2; Gvirtzman et al., 2017; Manzi et al., 2018). High resolution 2D and 3D industrial seismic and well data from the southern Levant Basin revealed that this transparent sequence is largely made of pure halite with internal stratification picked out by diatomite, clay- and clastic-rich layers that allowed the division of the sequence into six sub-units, basinward-tilted and truncated at the top by the flat TES (Fig. 8f; Gvirtzman et al., 2013, 2015, 2017; Feng et al., 2016, 2017; Manzi et al., 2018; Meilijson et al., 2018, 2019). Clastic beds ~3 to 20 m-thick are abundant in the highly reflective and chaotic Unit 5 (i.e. Interbedded evaporites of Meilijson et al., 2019; MC2 unit of Feng et al., 2016; Figs. 3b, 4a), where they are interbedded with evaporites (probably halite with minor occurrences of anhydrite) varying in thickness from ~6 to 30 m (Manzi et al., 2018; Meilijson et al., 2019). Paleontological analyses of cuttings probably belonging to one of the clastic beds revealed the presence of a few mollusk fragments, ostracods, echinoid spines and a relatively rich assemblage of benthic and planktic foraminifera which Meilijson et al. (2019) concluded to be reworked. Based on seismic and well-log data, clastic intercalations (probably of clays, silts and sands) within a halite-dominated sequence are thought to persist in the overlying Unit 6, although they diminish in thickness and frequency (Gvirtzman et al., 2013; Feng et al., 2016; Meilijson et al., 2019). The expression of the end of the MSC is highly controversial. Until recently, the M-reflector of Ryan (1978) (later renamed as the Top Erosion Surface, TES; Lofi et al., 2011a, 2011b) bounding Unit 6 at the top was

considered to be the Miocene/Pliocene boundary (Fig. 8f; Ryan, 1978; Gvirtzman et al., 2013; Feng et al., 2016). Instead, Gvirtzman et al. (2017) showed that in higher resolution seismic data the M-reflector/TES is a bundle of reflectors forming a distinct layer (Unit 7) overlying a truncation surface (i.e. Unit 6/7 boundary) that they re-labelled intra-Messinian truncation surface (IMTS; Fig. 8g) and ascribed to subaqueous dissolution rather than subaerial incision (e.g. Bertoni and Cartwright, 2007; Lofi et al., 2011a, 2011b; Kartveit et al., 2019; Madof et al., 2019). This conclusion was recently corroborated by the independent study of Kirkham et al. (2020). Analysis of gamma-ray and resistivity logs in three deep basin wells (Aphrodite-2, Myra-1, Sara-1; Fig. 2b) and correlation with the Or-South-1 well (located between the deep basin and the shelf) showed that Unit 7 maintains a constant thickness of ~100 m-thick and consists of clastic-rich anhydrite of undisclosed provenance. Meilijson et al. (2019)'s lithological interpretation of industrial boreholes slightly farther to the NE (Fig. 2b) give Unit 7 a significantly smaller thickness (5 m; Fig. 3b). Independent studies offshore Lebanon and Syria (Kartveit et al., 2019; Madof et al., 2019) describe a unit (Nahr Menashe complex) interpreted as a thicker (up to 300 m; Madof et al., 2019), but lateral equivalent of Gvirtzman et al. (2017)'s Unit 7. Based on its channelized morphology identified upslope near the Lebanese coast, Kartveit et al. (2019) and Madof et al. (2019) interpreted the Nahr Menashe Unit and the IMTS underneath as fluvial in origin, deposited/formed on a subaerially exposed floor of the Levant Basin. Six (Madof et al., 2019) to eight (Madof and Connell, 2018) lobes were identified and are proposed to have stacked with precessional frequency. The Nahr Menashe sequence has been correlated by the same authors with the Abu Madi Fm. located within the Messinian canyons offshore Egypt (Abdel Aal et al., 2000; Loncke et al., 2006; Abdel-Fattah, 2014), the Handere Formation offshore Turkey (Radeff et al., 2017) and with the Eosahabi deposits offshore Libya (Bowman, 2012). This interpretation implies a low base-level during the final stage of the MSC.

Manzi et al. (2018) and Meilijson et al. (2018, 2019) attempted astronomical dating of the abyssal MSC succession of the Levant Basin by integrating biostratigraphy on the pre-MU succession, reflector counting within the MU (only Meilijson et al., 2019) and well-log data (Fig. 3b). They achieved two contrasting results that gave rise to an outstanding controversy (Figs. 3b, 4a). Manzi et al. (2018) proposed that Stage 1 in the deep Levant is represented by a foraminifera-barren, evaporite-free shales interval labelled FBI (foraminifer barren interval) observed in the deep Aprodite-2 well and in the more proximal Myra-1 well. In this interpretation Unit 7 comprises the whole of Stage 3 (with the IMTS corresponding to the Stage 2/3 transition) and all halite deposition took place in ~50 kyr estimated during Stage 2 of the MSC (Fig. 1a; Roveri et al., 2014a). By contrast, the FBI is not present in the Dolphin well targeted by Meilijson et al. (2019), which is located in an intermediate position between the Aprodite-2 and Myra-1 wells studied by Manzi et al., 2018; Fig. 2b). Instead, in the Dolphin well a relatively open-marine, foraminifera-rich sequence extends below the (conformable) base of the MU, placed in correspondence to a ~2 to 5.5 m-thick anhydrite/shale (Unit 0; Manzi et al., 2018 and Meilijson et al., 2018, respectively). Astronomical tuning of the ~33 cycles counted in the MU in the Dolphin well, which are assumed to be precessional, results in the Main Halite body (i.e. Unit 0-4 of Gvirtzman et al., 2013 and Manzi et al., 2018) spanning MSC Stage 1 and 2, the Interbedded Evaporites/Unit 5 covering substage 3.1 and the Argillaceous Evaporites/Unit 6-7 to encompass the Lago-Mare phase (Figs. 3b, 4a). In this interpretation from Meilijson et al. (2019), halite deposition in the Levant Basin started in Stage 1 and persisted throughout the entire MSC, including Stage 3, during which more allochthonous material was delivered to the basin (Fig. 3b). Madof and Connell (2018) and Madof et al. (2019) also attempted an astronomical tuning of the Nahr Menashe Unit, concluding that it spans throughout substage 3.2 and part of substage 3.1. Feng et al. (2016) claim, however, that the impressive thickness of clastics found in the Levantine MU is more indicative of distinct short-term events (shorter than the precession cycle) associated with transport of extraordinary power and magnitude.

Late Messinian sediments have also been recovered at several DSDP (129, 375, 376; Ryan et al., 1973; Hsü et al., 1978b) and ODP Sites (965, 967, 968; Emeis et al., 1996), but the assignment of the retrieved sediments to seismostratigraphic units is problematic. Nevertheless, they provide several key nuggets of precious information about the Stage 3 paleoenvironment:

- Sites 965 and 966, located roughly on the crest of the Eratosthenes Seamount, just south of Cyprus (Fig. 2b), recovered soil structures above the evaporites indicating exposure above sea level (Robertson, 1998a, 1998b; Maillard et al., 2011a; Reiche et al., 2016).
- ODP Sites 967 and 968, located at the base of the northern and southern slope of Eratosthenes Seamount (Fig. 2b), respectively, revealed the presence, within the MSC interval, of calcareous turbidites with Cyprus-derived clasts and clays containing *Ammonia tepida*, *Cyprideis pannonica* and *pulmonate gastropods* (Blanc-Valleron et al., 1998; Robertson, 1998a,b; Reiche et al., 2016).
- Abundant *Cyprideis pannonica* specimens were also recovered from DSDP Sites 375 and 376 drilled on the crest of the Florence Rise, west of Cyprus (Fig. 2b; Hsü et al., 1978b).
- Abundant, well-preserved *Ammonia* tests and *Cyprideis* specimens are also known from Site 129A (Fig. 2b), occurring with dwarf planktonic foraminifera (Ryan et al., 1973).

All the evidence listed above suggest that a base-level fall leading to subaerial exposure occurred at some point(s) during Stage 3 in the Eastern Mediterranean (Ryan, 2009). However, it must be kept in mind that both the Florence Rise and Eratosthenes Seamount are likely to have been much more elevated during the Messinian than they are today because of Pliocene-Quaternary subsidence related to the Cyprus subduction zone (Robertson, 1998a, 1998b; Maillard et al., 2011a; Reiche et al., 2016).

Sites 375 and 376 display several discrete layers of primary and clastic gypsum interbedded in the *Cyprideis*-rich mudstones (McCulloch and De Deckker, 1989; Lugli et al., 2015). This succession shares several similarities with sites drilled in the Western Mediterranean (e.g. ODP 654A) and Ionian Basin (DSDP 374), where they have been correlated with the seismic Upper Unit (see subsections 4.5 and 4.6). This may suggest that a Western Mediterranean-like gypsum-bearing UU was also locally deposited in the easternmost abyss of the Mediterranean (see Güneş et al., 2018).

4.7.2. Levant continental margin

Evaporitic and non-evaporitic deposits are buried beneath PQ deposits (Yafo Formation) along the Levant continental margin, where they are mostly preserved within canyons carved underwater in pre-Messinian time (Druckman et al., 1995; Lugli et al., 2013). Within the Afiq canyon, Druckman et al. (1995) distinguished three formations in the Messinian sequence: the evaporitic Mavqi'im Formation, 115 m-thick and mostly composed of anhydrite in places interbedded with micritic limestones; the Be'eri Formation, cmprising gypsum; the Afiq Formation, varying in thickness from 30 to 90 m and consisting of conglomerates, sandstones and marls interpreted as representing fluvial and lacustrine-marsh environments (Druckman et al., 1995). The Afiq Fm. is only present in the deepest portions of the canyon where it overlies the Mavqi'im Fm. By contrast, the Be'eri gypsum is only found along the canyon shoulders covered by the Pliocene, at elevations > 600 m with respect to the Mavqi'im Fm. Based on Sr values, Druckman et al. (1995) attributed the Mavqi'im Fm. to MSC Stage 1, the Be'eri Fm. to substage 3.1 and the Afiq Fm. to the Lago-Mare phase. These authors also suggested that gypsum precipitation occurred under subaqueous conditions, with the water level ~600 m (i.e. the difference in altitude between the Mavqi'im and Be'eri fms.) higher during the deposition of the Be'eri Fm. Two base-level falls of approximately the same magnitude are thought to have occurred between the evaporitic phases and after

Mavqi'im deposition. A lowstand phase was therefore in force during Afiq deposition (Druckman et al., 1995).

However, combining stratigraphic, sedimentological and geochemical (Sr isotopes) considerations, Lugli et al. (2013) revealed the clastic nature of both the Mavqi'im and Be'eri evaporites and suggested the persistent drowning of the canyon(s), filled with turbidites (Lugli et al., 2013). Due to the presence of clastic evaporites, Gvirtzman et al. (2017) suggested that the Mavqiim Formation is a condensed section encompassing MSC Stage 2 and early Stage 3, while the evaporite-free Afiq Formation represents the Lago-Mare phase.

Ben Moshe et al. (2020) ascribed (at least part of) the Afiq Fm. to the whole of Stage 3 as a wedge-shape clastic complex lying on top of the Mavqi'im Fm. and with the basal surface corresponding to the correlative conformity of the MES developed landward, at the expense of the Mavqi'im Fm (Fig. 8h). Ben Moshe et al. (2020) distinguished a lower sub-unit composed of clastic gypsum and with fore-stepping and down-stepping internal geometry typical of progradational wedges, and an upper sub-unit containing anhydrite fragments and marls with Lago-Mare fauna (e.g. *Cyprideis torosa*; Rosenfeld, 1977) and with seismic characteristics typical of a transgressive systems tract. Incisions are reported throughout the Afiq Fm. at different depths, while erosional surfaces bound both sub-units (Ben Moshe et al., 2020). In particular, the surface capping the upper subunit and correlated to the M horizon or TES basinward (see subsection 4.7.1) shows dendritic drainage patterns of gullies and channels (Ben Moshe et al., 2020).

Ben Moshe et al. (2020) identify the variation of base level specifically during Stage 3 by analyzing the morphology of truncation surfaces bounding the Afiq Formation on the continental margin of the Levant Basin. This suggests high amplitude fluctuations of base-level in the order of one hundred meters, with development of subaerial erosion surfaces and the deposition of clastics and incision by fluvial drainage systems that occurred during the lowstand phases, while aggradational units (of unknown lithological nature) accumulated during the highstand phases. According to their analysis, base level dropped down to a maximum 535 m during Afiq deposition (i.e. below the maximum 430 m estimated paleodepth of the Sicily Sill; Garcia-Castellanos et al., 2009), implying hydrological disconnection between the Eastern and Western basins at various times during Stage 3. A regression to 615-885 m is proposed to have occurred at the top of the Afiq Fm., pre-dating the abrupt refilling at the base of the Zanclean (e.g. Micallef et al., 2018, 2019; Garcia-Castellanos et al., 2020; Spatola et al., 2020).

4.8. Summary of the offshore Stage 3 record

Knowledge of the Stage 3 sequence offshore is mainly based on the integration of seismic interpretations and analysis of material recovered from fragmentary and unevenly distributed DSDP/ODP/industrial cores.

- MSC sediments are absent on the eroded continental shelves bordering the deep basins, except in the Messinian thalwegs and at their mouth. Here the PQ lies directly above the MES which, in turn, cuts through the pre-MSC deposits (Fig. 7e). A similar stratigraphic arrangement is found along the middle-upper slopes (Fig. 7d), although the presence of a thin, possibly incomplete UU in morphological depressions is sometimes postulated. Seamounts also lack MSC Stage 3 sediments and are strongly incised by the MES (Fig. 7g).
- The thick UU is widespread and roughly present everywhere in the abyssal plains from west of the Alborán volcanic arc to the eastern edge of the Ionian Basin (Fig. 2b). In the abyssal plains its seismic facies appears homogeneous, comprising parallel and relatively continuous high amplitude reflections (Figs. 7b-c). The UU pinches out towards the foot of continental slopes and seamounts (Figs. 7b, d-g), where it can be irregularly bedded or relatively well bedded (Lofi et al., 2011a, 2011b). The uppermost part of the Bedded Units (defined in depressions physically disconnected from the abyssal plains and, therefore, from the UU; e.g. CMD and Corsica Basin; Maillard et al., 2014; Thinon et al., 2016; Raad et al., 2021) shows seismic features comparable to those of the UU.
- Drill Sites revealed that the reflections of relatively high amplitude in seismic profiles correspond to gypsum and mudstone alternations with sporadic intercalations of massive to cross-bedded sandstones. Some mudstone interbeds contain low-diversity assemblages of benthic organisms (ostracods, foraminifera and diatoms) indicative of shallow to neritic environments. Except for dwarfed forms of planktonic foraminifera and the monospecific nannofossil assemblages described by Castradori (1998), the rest of planktonic foraminifera and nannofossils are largely regarded as reworked.
- The deep Levant Basin contains a ~1.8-2.0 km-thick MU (Figs. 8e-f), consisting of 6 to 7 seismic units depending on the resolution of the seismic employed. In high resolution seismic data, the lateral equivalent of part of the UU is identified as a ~100-m-thick, clastic-rich, anhydrite layer (Unit 7 of Gvirtzman 1207) offshore Israel, thickening to 300 m offshore Lebanon (Nahr Menashe complex, Madof et al., 2019). The Levant Basin still has major controversies concerning the timing of halite deposition (~50 kyr vs ~550 kyr; Manzi et al., 2018 vs Meilijson et al., 2019), the origin of the clastic accumulations overlying the halite (fluvial vs subaqueous) and the presence or absence of gypsum-mudstone cycles.
- Apart from the halite flow-related deformation, the Miocene/Pliocene boundary (i.e. UU/PQ transition) is conformable in intermediate (e.g. Balearic Promontory) and deep (WAB, EAB, Algero-Balearic, Liguro-Provençal, Tyrrhenian, Ionian and Levant) depocenters, while it shows signs of erosion on the shelf domain and along the upper-middle continental slopes and seamounts. Clear arguments of floor exposure at the M/P boundary are absent in all drill sites but 978A.

5. The paleontological perspective

Paleontological data have been used to define and identify Stage 3 sediments, but have also been a source of profound contention over the interpretation of its paleoenvironmental and paleohydrological nature. Biotic groups impacted by the evolution of the gateways linking the Mediterranean with the Atlantic, Indian Ocean and Paratethys include marine species (e.g. foraminifera, calcareous nannofossils, fish) and brackish water-species (ostracods, fish, mollusks and dinocysts endemic or with affinity to species of the Paratethys region) that were unable to migrate when these corridors were closed, and terrestrial species (e.g. mammals) that, conversely, got across the gateway during periods of exposure (see Colombero et al., 2017; Booth-Rea et al., 2018; Mas et al., 2018b). Analysis of these faunal datasets provides key insights into likely gateway dimensions and the timing of their opening, restriction and closure (e.g. Palcu et al., 2017). Furthermore, they are a key constraint on the water sources likely to have been affecting the Mediterranean during MSC Stage 3.

5.1. Ostracods

Ostracods are by far the most prolific faunal group during Stage 3. Brackish species are known from both land sections and deep-sea cores across the whole Mediterranean (see Fig. 2b for sites and references; Fig. 9a). Two characteristic biofacies are commonly distinguished: Biofacies 1 (Bonaduce and Sgarrella, 1999) or *Cyprideis* assemblage (Iaccarino and Bossio, 1999) consists of an monospecific population of *Cyprideis* species or of an oligotypic population dominated by *Cyprideis* species alongside rare specimens of *Tyrrhenocythere ruggierii*, *Loxoconcha kochi*, *Loxoconcha muelleri* and *Caspiocypris alta*); Biofacies 2 (Bonaduce

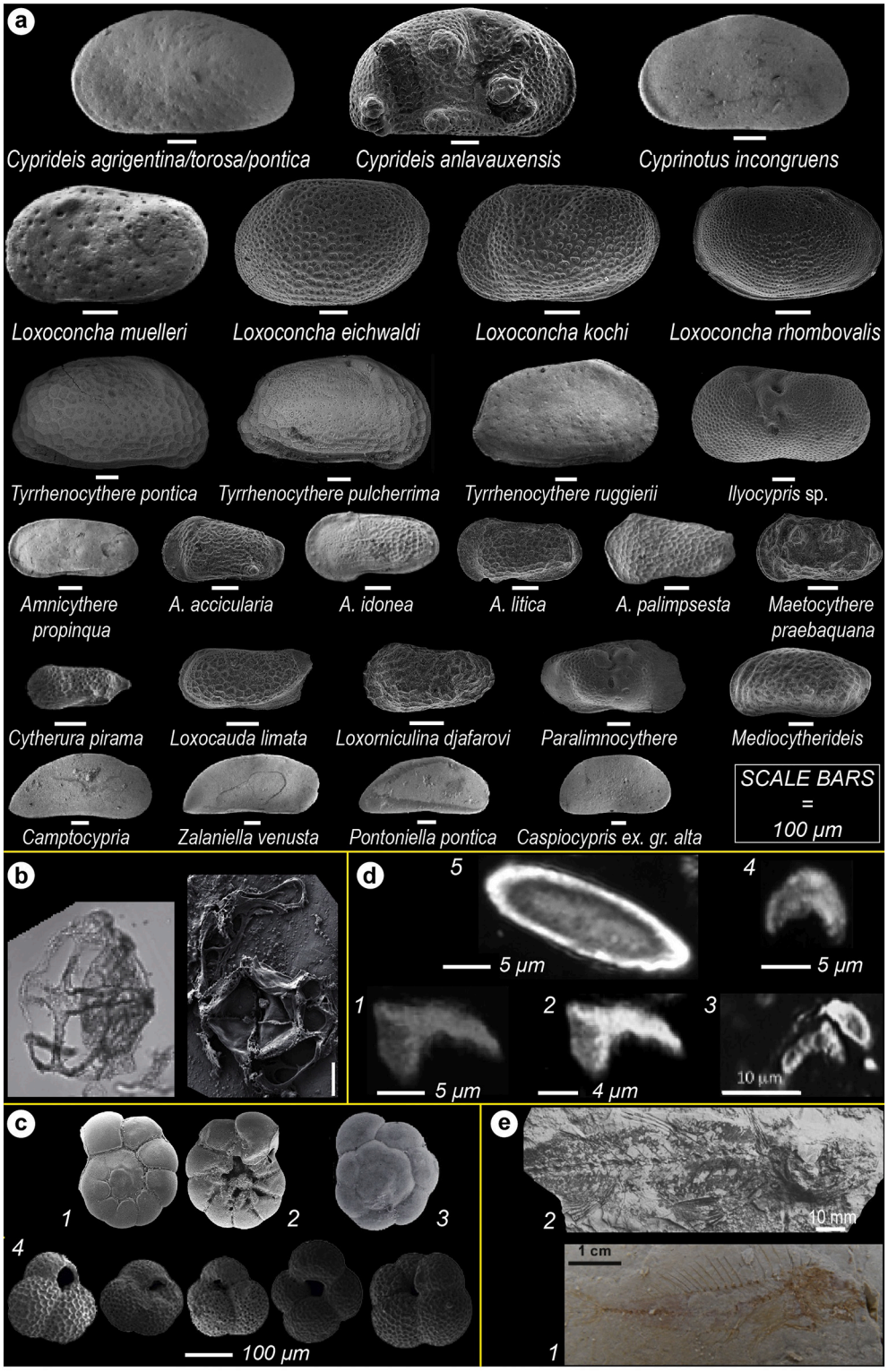

Fig. 9. Photomicrographs of the key micro- and macrofossils featuring Stage 3 sediments. (a) Scanning electron microscope (SEM) photographs of the more common Paratethyan ostracod species in substage 3.1 and 3.2 sediments (compiled from Stoica et al., 2016, Cosentino et al., 2018 and Sciuto et al., 2018). (b) Photomicrographs of the Paratethyan dinoflagellate cyst *Galeacysta etrusca* under the optical microscope (left) and SEM (right) (modified from Do Couto et al., 2014 and Grothe et al., 2018). Scale=20 µm. (c) SEM microphotographs of the euryhaline, shallow-water benthic foraminifera *Ammonia beccarii* (1-spiral side, 2-umbilical side) and *Ammonia tepida* (3-spiral side; Carnevale et al., 2019) and of the dwarf fauna of planktonic foraminifera from the Bajo Segura Basin (4; Corbí and Soria, 2016). (d) Photographs in polarized light (crossed nicols) of some specimens of *Ceratolithus acutus* (1-3) described in the Lago-Mare unit of Malaga (1-Do Couto et al., 2014), the Zorreras Mb. of Sorbas (2-Clauzon et al., 2015) and of the Colombacci Fm. of the Northern Apennines (3-Popescu et al., 2017) and of destroyed (4) and intact (5) ascidian spicules of *Micrascidiscus* sp. (Golovina et al., 2019). Note that *C. acutus* specimens closely resemble ascidian spicules of *Micrascidiscus* sp., which may lead to misinterpretation of the C. acutus (see Golovina et al., 2019), and that pictures 1 and 2 are identical, despite they are attributed to samples taken from two different localities. (e) Articulated skeletons of marine fish from substage 3.1 mudstone horizons in Cyprus (1-*Aphanius crassicaudus*; Manzi et al., 2016a) and substage 3.2 deposits in Cava Serredi (2-*Mugil cf. cephalus*; Carnevale et al., 2018).

and Sgarrella, 1999) or *Loxocorniculina djafarovi* assemblage (Iaccarino and Bossio, 1999) has a higher species diversity characterized by the abundant occurrence of truly Paratethyan species belonging to the genera *Amnicythere*, *Loxoconcha*, *Loxocauda*, *Cytheromorpha*, *Cyprinotus* and *Tyrrenhocythere* (see species names in Fig. 9a). The number of species reported in the onshore sections is variable, ranging from a dozen (e.g. Caruso et al., 2020) to more than sixty (e.g. Gliozzi et al., 2007; Grossi et al., 2008). This variability is not explained, but it may result from the application of different taxonomic concepts that resulted in the recognition of more or fewer species (Stoica et al., 2016) or from local environmental conditions that differed from basin to basin and resulted in different patterns of colonization.

Compared to the onshore domain, the ostracod fauna offshore is impoverished. Monospecific assemblages of *Cyprideis* sp. (Sites 372, 129A, 376, 654A, 967, 968; Ryan et al., 1973; Cita et al., 1990) or oligospecific assemblages dominated by *Cyprideis* and rare specimens of

Candona sp. (Hole 974B, Iaccarino and Bossio, 1999) and L. *muelleri* (Hole 978, Iaccarino and Bossio, 1999) are the more widely reported. Interestingly, these assemblages are always associated with *Ammonia* sp. tests and, in some cases, with other species of shallow-water, euryhaline benthic foraminifera (see subsection 5.4). Only in Hole 975, close to the M/P boundary is a more heterotypic ostracod assemblage found (*Euxinocythere praebaquana*, *Amnicythere idonea*, *Leptocythere limbate, Loxocorniculina djafarovi, Candona sp.,* and *Cyprideis* sp.; Iaccarino and Bossio, 1999) and lacking of euryhaline benthic foraminifera. The likely cause of the widespread barrenness of ostracods in most of the offshore samples is perhaps because environmental conditions in the deep basins (depth and/or salinity) where not suitable to permit population by this benthic fauna (see below for the ecological requirements; e.g. Hsü et al., 1978b in reference to Site 374). Finally, one must bear in mind that studying these organisms require much more material (some hundreds of grams) than the quantity of core sediments usually processed (i.e. ~10 cm^3; Iaccarino and Bossio, 1999).

The paleoecology (salinity and depth ranges) of Stage 3 ostracods has been based on both observations of few species that still live in the Caspian and Black seas today and have affinities with the Stage 3 species and on the interpretation of sedimentological, geochemical and mineralogical data of the surrounding sediments (see Gliozzi and Grossi, 2008 and Grossi et al., 2008 for insights). Biofacies 1 is thought to represent very shallow water environments (i.e. <15 m) with salinity fluctuating between mesohaline and hypersaline when the euryhaline *Cyprideis* is dominant. Instead, more stable oligo-mesohaline water is inferred when the other species are more abundant in Biofacies 1. The variegated Biofacies 2, on the other hand, is thought to represent somewhat deeper environments (up to 100 m) and less salty conditions (oligo-low mesohaline; Gliozzi and Grossi, 2008; Grossi et al., 2008; Caruso et al., 2020).

Some authors consider the time when the Paratethyan ostracods arrived in the Mediterranean to be well constrained (e.g. Roveri et al., 2008a; Grossi et al., 2011; Cosentino et al., 2018) by the scarce occurrence of the first Paratethyan immigrant *Loxoconcha muelleri* 20 cm below the ash layer in the Colla di Votta section, which has a ^{238}U-^{206}Pb age of 5.5320±0.0074 Ma (Cosentino et al., 2013), and in the chaotic deposits of the Adana Basin, ascribed to Stage 2 (Faranda et al., 2013). Instead, the first appearance of *Loxocorniculina djafarovi* has been considered to coincide with the biofacies 1-2 shift and to have occurred Mediterranean-wide synchronously at 5.40 Ma (Roveri et al., 2008a; Grossi et al., 2011; Cosentino et al., 2013). Roveri et al. (2008a) also showed Biofacies 2 diversity as increasing linearly through the Lago-Mare phase, reaching its maximum diversity just beneath the Miocene/Pliocene boundary and before disappearing in the Pliocene. Following the claimed synchronicity of the FO of both *Loxoconcha muelleri* and *Loxocorniculina djafarovi*, Roveri et al. (2008a) and Grossi et al. (2011) recognized one biozone in each biofacies: the *Loxoconcha muelleri* Biozone, spanning from 5.59 to 5.40 Ma, and the *Loxocorniculina djafarovi* Biozone, whose boundaries correspond respectively to the first (5.40 Ma) and last occurrence (5.33 Ma) of *L. djafarovi* in the Mediterranean. This biozonation, erected by Grossi et al. (2011), is often used for dating incomplete successions (e.g. Vera Basin; Stoica et al., 2016; Caruso et al., 2020). However, the first appearance of a diversified ostracod assemblage (including *Loxocorniculina djafarovi*) occurred in already cycle 3 of the Sicilian Upper Gypsum at Eraclea Minoa (Fig. 3a; Grossi et al., 2015), which has an astronomical age of 5.45 Ma (Van der Laan et al., 2006) or 5.47 Ma (Manzi et al., 2009). Furthermore, the sudden appearance of Biofacies 2 and its linear, upward increase in diversity have not been recognized in localities like Nijar and Malaga, where biofacies 1 and 2 are found stacked in more than one lithological (possibly precession-controlled) cycle in the Lago-Mare succession (Bassetti et al., 2006; Guerra-Merchán et al., 2010). These findings argue that the appearance of Paratethyan ostracods in the Mediterranean may not have been synchronous, therefore casting serious doubts upon the biostratigraphic relevance of the Mediterranean ostracods.

Except for *Cyprideis* specimens, where species attribution is debated (see discussion in Stoica et al., 2016), the affinity of all other ostracod species observed in Mediterranean Stage 3 sediments (Fig. 9a) with those of the Eastern Paratethys basins (i.e. Dacian, Euxinic and Caspian) has been demonstrated in several publications (e.g. Ruggieri, 1967; Gliozzi et al., 2007; Stoica et al., 2016; Sciuto et al., 2018). Only Bassetti et al. (2003, 2006) have questioned the Paratethyan affinity by suggesting that species from the Northern Apennines and Nijar Basin have ambiguous affinities with Paratethyan fauna as described in the mainly Russian literature from the '60-'70s. However, these differences between the late Messinian Mediterranean and Paratethyan ostracods resulted from misidentifications and/or a different use of species nomenclature (Stoica et al., 2016). Recently acquired knowledge of the Pontian assemblages of the Dacian, Euxinic and Caspian basins now permit to trace the provenance of Mediterranean Stage 3 ostracod species from the entire Black Sea region (Stoica et al., 2016) and, for a few species, from the Dacian (Stoica et al., 2013; Lazarev et al., 2020), Caspian (Van Baak et al., 2016) and North Aegean (see references in Krijgsman et al., 2020a) basins.

The means by which the ostracods travelled from the Paratethys to and across the Mediterranean during Stage 3 is as crucial for reconstructing the Stage 3 paleoenvironment as it is poorly addressed in onshore studies or overlooked in seismic and computational studies. Two migratory mechanisms have been suggested:

1) the aerial dispersion of ostracods through the migration of aquatic birds (Benson, 1978; Caruso et al., 2020); this hypothesis was proposed because, in a Mediterranean concluded to have been desiccated, it was the only possible migration mechanism.

2) direct aqueous migration by the ostracods themselves (which are planktonic in the larval stage) through the establishment of similar paleoenvironmental conditions; by this mechanism, the dispersion of Paratethyan ostracod fauna from right across the Mediterranean requires E-W intraconnection and a Mediterranean water-level high enough to reach the marginal basins (Gliozzi et al., 2007; Stoica et al., 2016; Sciuto et al., 2018; Sciuto and Baldanza, 2020).

Finally, Carnevale et al. (2006a, 2006b, 2008, 2018) recognized the Paratethyan affinity of the Mediterranean Stage 3 species but, in view of their occurrence with *in-situ* species of marine fish, they suggested that Stage 3 ostracods descended from a Paratethyan stock that migrated into the Mediterranean well before the MSC and survived the extreme salinity conditions of Stage 1 and 2 in marginal, fresher water refugia. In this scenario the brackish water ostracod assemblages found in Stage 3 have no paleoecological significance for Stage 3 paleoenvironment (Carnevale et al., 2006a, 2006b, 2008, 2018). However, there are two, unflagged problems with this hypothesis: 1) the Mediterranean-Central Paratethys connection through the Trans-Tethyan gateway in Slovenia already closed in the early Tortonian (Kováč et al., 2007; Sant et al., 2017; Palcu et al., 2017); 2) No Paratethyan ostracod species have been found in the Mediterranean before the MSC (see Gliozzi et al., 2007).

5.2. Dinoflagellate cysts

Dinoflagellate cysts (dinocysts) are the fossil remains of unicellular protists that live in the upper water column of many water bodies (e.g. Zonneveld et al., 2013; Mudie et al., 2017). They can be used as paleoenvironmental indicators and for biostratigraphy, providing the ages of speciation and extinction events, as well as supplying evidence of age diagnostic dispersals of characteristic taxa/assemblages. Influxes of these microorganisms into a basin may occur as the result of interconnection with another basin and dinocysts can therefore be useful indicators of the open gateways between adjacent basins and the resultant changes in conditions (e.g. Grothe et al., 2018). In the case of the MSC, presence of *in situ* marine and/or Paratethys dinocyst assemblages in a marginal basin are likely to indicate the presence of Atlantic and/or Eastern Paratethys water (respectively) in the Mediterranean and (relatively) high water level conditions (e.g. Pellen et al., 2017).

Palynological studies on the late Messinian Mediterranean dinocysts

record are rather scarce, confined to a limited number of outcrops (Malaga Basin, Do Couto et al., 2014; Northern Apennines, Bertini, 2006; Popescu et al., 2007; Iaccarino et al., 2008; Cosentino et al., 2012; Pellen et al., 2017; Caltanissetta Basin, Londeix et al., 2007) and deep wells (976B, 977A, 978A and 134B, Popescu et al., 2015). These studies describe substage 3.1 as being barren of dinocysts. By contrast, substage 3.2 dinocyst assemblages are diverse particularly a few meters/tens of meters below the Miocene/Pliocene boundary and show recurrent vertical variation in abundance between brackish, Paratethyan-type taxa and marine stenohaline and euryhaline species. Taxa with Paratethyan affinities are largely considered to be autochthonous by all aforementioned authors. The extent to which reworking may have affected the marine assemblages is more controversial and debated between none (in Malaga and in the Apennines; Popescu et al., 2007; Do Couto et al., 2014; Pellen et al., 2017), partial (in the uppermost part of the Sicilian Upper Gypsum; Londeix et al., 2007) and total (in the Apennines; e.g. Bertini, 2006; Iaccarino et al., 2008; Cosentino et al., 2012). Given the extent of the implications (i.e. re-establishment of a Mediterranean-Atlantic flow or connection earlier than the Zanclean; e.g. Pellen et al., 2017), this is an issue that will require further clarification.

A key dinocyst influencing our understanding of the late Miocene Lago-Mare phase is *Galeacysta etrusca* (Fig. 9b; see Bertini and Corradini, 1998; Popescu et al., 2009 and Grothe et al., 2018 for more insights). This species was originally described from sediments in the Mediterranean (Corradini and Biffi, 1988), but has since been discovered in much older deposits in Paratethys (Magyar et al., 1999a, 1999b). The earliest recorded occurrence of *Galeacysta etrusca* is in sediments from the Pannonian Basin dated at ~8 Ma (Magyar et al., 1999a, 1999b). It subsequently dispersed throughout Paratethys at ~6 Ma and was present in the Black Sea throughout the MSC interval (Grothe et al., 2014, 2018). Despite a Mediterranean-Eastern Paratethys connection that is thought to have been established at ~6.1 Ma (Krijgsman et al., 2010; Van Baak et al., 2016; Grothe et al., 2020), *G. etrusca* is not found in the Mediterranean during MSC Stages 1, 2 and 3.1 (5.97-5.42 Ma; Bertini, 2006, Londeix et al., 2007, Manzi et al., 2007, Iaccarino et al., 2008, Gennari et al., 2013) and is only reported in the uppermost part of the Lago-Mare phase, very close to the transition to the Pliocene (e.g. Bertini, 2006; Londeix et al., 2007; Popescu et al., 2007; Iaccarino et al., 2008; Cosentino et al., 2012; Pellen et al., 2017). This implies that *Galeacysta etrusca* may have migrated from Paratethys into the Mediterranean after 5.42 Ma or that environmental conditions in the Mediterranean and in its marginal basins were only suitable for this species (and more generally the whole dinocysts Paratethyan contingent) to proliferate in the uppermost Messinian. Several authors report multiple occurrences of *Galeacysta etrusca* within the Zanclean (e.g. Clauzon et al., 2005; Londeix et al., 2007; Popescu et al., 2007, 2015; Do Couto et al., 2014; Clauzon et al., 2015), but these interpretations are based on the use of an alternative stratigraphic model for the MSC sections (Fig. 4b; see Grothe et al., 2018 for details).

5.3. Diatoms

Among the fresh-brackish organisms found in Stage 3 sediments are also species of diatoms. To date (and to our knowledge), there are no onshore studies that have ever looked for these organisms. By contrast, two samples from DSDP Site 124 in the Algero-Balearic Basin (Fig. 2b) revealed the presence of littoral planktonic forms accompanied by brackish water, and even freshwater, euryhaline, benthonic, and epiphytic species in considerable numbers (Hajós, 1973). Diatoms of undisclosed paleoecological significance are also reported from the ~60 cm-thick mudstone bed between an anhydrite and halite bed found in the last core of Site 134 (Ryan et al., 1973). According to Hajós (1973) and Ryan (2009), the diatoms found in these drill cores attest to an extremely low salinity and a base level in the Balearic and Valencia basins below wave action. Further study of these indicative species and a wider distribution is required to apply this interpretation more generally.

5.4. Foraminifera

A reasonably diverse benthic and planktic foraminiferal assemblage containing no age-diagnostic taxa have been found co-occurring with the brackish Paratethyan fauna in both the onshore and offshore record throughout the Mediterranean (Fig. 2b for localities and references).

The benthic foraminifera assemblage is dominated by euryhaline representatives of the genus *Ammonia*, which today dwell in marginal marine (lagoons, estuaries, fjords and deltas) and lacustrine environments at depths < 50 m and tolerate salinities of up to 50‰ (Milker and Schmiedl, 2012; Consorti et al., 2020). *Ammonia tepida* and *Ammonia beccari* (Fig. 9c) are by far the most abundant species in both onshore (see Fig. 2b for localities and references) and offshore (e.g. Site 968A, Blanc-Valleron et al., 1998; Sites 375, 376, 965-968, Orszag-Sperber, 2006) localities, where they co-occur with ostracods belonging to Biofacies 1. Other commonly occurring benthic euryhaline taxa are *Elphidium* sp., *Cribroelphidium excavatum*, *Haynesina* sp., *Nonion* sp., *Quinqueloculina* sp., *Discorbis* sp. and T*richohyalus* sp., *Brizalina dentellata*, *Bulimina echinate* and *Bolivina* spp. (Ryan et al., 1973; Hsü et al., 1978a, 1978b; Rouchy et al., 2001, 2003, 2007; Iaccarino et al., 2008; Caruso et al., 2020). These species are frequently mixed with poorly preserved and older in age bathyal species (e.g. Caruso et al., 2020).

Planktic foraminifera are represented both by species whose last occurrence pre-dates the MSC (e.g. *Praeorbulina* spp., *Paragloborotalia partimlabiata*, P. *siakensis*, *Neogloquadrina atlantica praeatlantica*, *Globigerinoides subquadratus*, *Globorotalia saheliana, Globorotalia conomiozea, Acarinina sp., Hedbergella sp.*) and by taxa with extended biostratigraphic ranges (e.g. *Sphaeroidinellopsis seminulina, Turborotalita quinqueloba*, *Globorotalia miotumida, Globoturborotalita decoraperta*, *Neogloboquadrina acostaensis*, *Neogloboquadrina* spp., *Orbulina universa*, *Globigerinoides trilobus, Globigerinoides obliquus, Globorotalia scitula, Globigerina bulloides*, *G. Mediterranea* and *G. humerosa*; see Fig. 2b for references).

The mixing of foraminifera species with different ecological and salinity requirements and the widespread agreement that the brackish Paratethyan fauna are autochthonous (see subsection 5.1) has always complicated the interpretation of the origin of the foraminiferal assemblages. Among the benthic species, *Ammonia* taxa and the other benthic euryhaline taxa are generally considered autochthonous because they are typically well-preserved and their ecological and salinity requirements could be compatible with those of the Paratethyan ostracods.

The habitat of these benthic foraminifera today in environments both influenced by and disconnected from the open ocean indicates that the Stage 3 sediments in which they occur were deposited in a shallow-water environment subject to salinity fluctuations (Caruso et al., 2020 and references therein), but they do not provide insights into the water provenance. By contrast, the poor preservation, older age and low diversity of the bathyal taxa strongly suggest that these species are reworked (Bassetti et al., 2006; Iaccarino et al., 2008; Caruso et al., 2020). Their mode of life is also incompatible with the shallower water elements of the faunal assemblage. The planktic species which went extinct before the MSC are also undoubtedly reworked (Iaccarino et al., 2008; Caruso et al., 2020). It is more challenging to discriminate between *in situ* and reworked specimens of the long range Neogene taxa. Most of them are considered to be reworked because of their scarcity, their occurrence with *in-situ* brackish organisms and their poor preservation (e.g. Iaccarino et al., 2008; Caruso et al., 2020). A more complex controversy surrounds the long-range dwarf specimens (Fig. 9c) occurring in onshore substage 3.1 (di Tetto Fm. in the Trave section; Iaccarino et al., 2008) and Lago-Mare sediments (Upper Mb. of the Nijar Feos Fm., Fortuin and Krijgsman, 2003; Aguirre and Sánchez-Almazo, 2004; Bassetti et al., 2006; Sorbas Basin, Roveri et al., 2019a; Bajo Segura Basin, Corbí and Soria, 2016; Colombacci Fm. in Northern Apennines localities, Casati et al., 1976; Colalongo et al., 1976; Rio and Negri, 1988;

Popescu et al., 2007; Cyprus, Rouchy et al., 2001) and in some offshore localities (e.g. Sites 124, 125, 129A, 132, 134, 372, 376, 653, 974B, 975, 978; Cita, 1973; Cita et al., 1978; Kastens et al., 1987; Cita et al., 1990; Iaccarino and Bossio, 1999). This fauna is variably interpreted as:

1) reworked and size-sorted during transport, therefore lacking any paleoenvironmental significance (e.g. Kastens et al., 1987; Iaccarino and Bossio, 1999; Fortuin and Krijgsman, 2003; Bassetti et al., 2006);

2) *in situ* and indicating normal marine conditions (Aguirre and Sánchez-Almazo, 2004; Braga et al., 2006) or temporary Atlantic incursions (Rouchy et al., 2001);

3) *in situ* and indicative of high-stress environments (Keller and Abramovich, 2009), such as restricted and/or diluted marine environments (Corbí and Soria, 2016; Corbí et al., 2016, 2020). However, the paleoecological significance of dwarfism in foraminifer tests is not well understood and, given its potential implications for the Lago-Mare environment, it needs to be explored in greater detail.

5.5. Calcareous nannofossils and the C. acutus conundrum

Calcareous nannofossils are the fossil remains of coccolithophores, single-celled marine algae which dwell in the eutrophic and photic zone of the ocean (e.g. Ziveri et al., 2004). The potential recognition of marine calcareous nannofossils in marginal Stage 3 deposits would therefore have implications for the Mediterranean base-level and the hydrological riddle of MSC Stage 3. However, like foraminifera and dinocysts, the *in situ* versus reworking issue also impacts the nannoflora.

MSC Stage 3 is crossed by three important nannofossil bio-events astronomically calibrated in the ocean record: the top of *Discoaster quinqueramus* at 5.537 Ma, the base of *Ceratolithus acutus* at 5.36 Ma and the top of *Triquetrorhabdulus rugosus* at 5.231 Ma (Backman et al., 2012; Agnini et al., 2017). Most of the (few) studies that addressed the nannoflora component of Stage 3 deposits did not report taxa belonging to the biozones defined by these bio-events, but only taxa of Cenozoic and Cretaceous age, clearly physically reworked (e.g. Sites 132, 134, 653, 654A, 967A, 969B, Ryan et al., 1973; Hsü et al., 1978b; Müller et al., 1990; Castradori, 1998; Piedmont Basin, Trenkwalder et al., 2008; Violanti et al., 2009; Trave, Fonte dei Pulcini and Stingeti sections and Mondragone well in the Apennines, Cosentino et al., 2006, 2012, 2018; Iaccarino et al., 2008). An exception is the nannoflora observed in the uppermost Messinian sediments at Sites 978A, 975B and 967A (Levant Basin; Fig. 2b). Here, among the plethora of reworked and long-ranging Neogene taxa, Castradori (1998) reported the anomalous abundance of *Sphenolithus* spp (mostly *Sphenolithus gr abies/moriformis*). Although the assemblage points to the absence of a primary marine signature, the unlikely possibility that reworking and/or sorting lies behind the observed peak of *Sphenolithus* spp. led Castradori (1998) to conclude that at least one incursion of marine water occurred during the (uppermost) Lago-Mare.

By contrast, some authors (i.e. Popescu et al., 2007, 2015; Do Couto et al., 2014; Clauzon et al., 2015; Pellen et al., 2017) described the nannofossil assemblage the Lago-Mare LM Unit in Malaga, the Zorreras Member in Sorbas, the uppermost di Tetto/Colombacci Fm. in some Apenninic localities and offshore in the Alborán Basin as having good preservation and showing no erratic fluctuations, all characteristics that led to their interpretation as autochthonous and to the conclusion that these sediments were deposited in a Mediterranean already replenished of Atlantic water (Fig. 4b). In addition, these authors reported the low abundance, but continuous presence of the biostratigraphic markers for the Zanclean *Triquetrorhabdulus rugosus* and *Ceratolithus acutus* (Fig. 9d) below the formally defined Miocene/Pliocene boundary (Van Couvering et al., 2000) in several onshore and offshore Mediterranean (as wells as Paratethyan) localities (see Popescu et al., 2017 for details and a complete list of finding locations).

Such findings (especially that of *C. acutus*) are in sharp disagreement with most of the existing literature and have resulted in an important debate amongst the MSC community (e.g. Popescu et al., 2007, 2008 vs Roveri et al., 2008c and Stoica et al., 2016 vs Popescu et al., 2017), not only for their paleoenvironmental implications (i.e. presence of Atlantic water in the Mediterranean), but also for the chronostratigraphic repercussions (Fig. 4b). The chronostratigraphic value of *C. acutus* lies in its short temporal distribution straddling the M/P boundary (astrochronologically calibrated at 5.332 Ma; Van Couvering et al., 2000; Lourens et al., 2004). However, the corresponding biozone is established in oceanic areas (Zone CNPL1: 5.36-5.05 Ma; Backman et al., 2012; Agnini et al., 2017) and is considered not applicable to the Mediterranean region during the MSC due to the harsh physicochemical conditions that are unsuitable for marine biota (Di Stefano and Sturiale, 2010). The interpretation of these nannofossil assemblages in the westernmost areas of the Mediterranean has been countered with several observations: (1) the observation of these age-diagnostic taxa is often not replicated by other studies (e.g. Roveri et al., 2008a; Van Baak et al., 2015; Krijgsman et al., 2020b); (2) *Ceratolithus acutus* is very rare also in fully marine open-ocean sediments (e.g. Di Stefano and Sturiale, 2010); (3) despite being rare in the late Messinian Mediterranean, this species has never been documented together with other long-range taxa, generally predominant in the assemblage, in Stage 3 deposits (see discussion in Krijgsman et al., 2020b). Recently, Golovina et al. (2019) showed that the morphology and size of *C. acutus* overlaps with the shape and dimensions of destroyed ascidian spicules (i.e. calcareous elements produced by benthic tunicates; Fig. 9d), providing an explanation for erroneous identification of *C. acutus* in the Black Sea Basin (Golovina et al., 2019) and perhaps in the western Mediterranean Lago-Mare sediments as well.

5.6. Fish

Fossil fish remains provide information about salinity and depth and have been used to contradict the brackish nature of the Lago-Mare deposits by Carnevale et al. (2006a, 2006b, 2008, 2018) and Grunert et al. (2016). Euryhaline fish species inhabit marine to brackish environments and dominate settings with strong salinity variations while stenohaline fish have specific salinity requirements (marine, brackish, or freshwater) and cannot survive under different conditions. Demersal fish (i.e. those living in or immediately above the sea floor) have specific depth requirements, whereas pelagic fish occupy the water column within a wide range of depth variable from species to species. Fossil fish remains are found either as articulated or disarticulated skeletal parts, including teeth and otoliths, which are identified to the species level. Articulated fish skeletons typically indicate autochthonous deposition because of the difficulty in reworking and transporting intact skeletons. Otoliths and fish teeth are much more likely to be transported.

Otoliths and rare articulated skeletons (Fig. 9e) of marine and Paratethyan species have been reported from Stage 3 deposits, but commonly huge volumes of sediment are required to find even quite small numbers of these fossils (e.g. 20 tons from Moncucco, 6 tons from Cava Serredi, 700 kg from Capanne di Bronzo; Schwarzhans et al., 2020), much more than what is expected for normal marine deposits (i.e. < 30 kg; Agiadi et al., 2017; Karakitsios et al., 2017b).

Substage 3.1 sediments contain articulated skeletons (Fig. 9e) of the marine fish species *Lampanyctus licatae* and *Maurolicus muelleri*, and the shallow water, euryhaline species *Aphanius crassicaudus* in the Lower Feos Member in the Nijar Basin (de la Chapelle and Gaudant, 1987) and the marls of the first UG cycle in the Polemi Basin (Manzi et al., 2016a; Fig. 3a). Cava Serredi (Tuscany), Verduno and Moncucco (Piedmont) are the only other localities in which fish remains (only otoliths) in (claimed) substage 3.1 sediments are known (Carnevale et al., 2006a, 2008, 2018; Grunert et al., 2016).

The more diverse and abundant ichtyofaunal record occurs in substage 3.2 in a few marginal sections on the Italian peninsula (Ciabot Cagna in the Piedmont Basin; Cava Serredi and Podere Torricella in Tuscany; Capanne di Bronzo, La Vicenne and Ca' Ciuccio in thrust-top basins of the Northern and Central Apennines). The Lago-Mare fish

remains mainly comprise otoliths of both euryhaline and stenohaline taxa indicative of marine, brackish, and freshwater habitats (Carnevale et al., 2018). Three articulated skeletons of the euryhaline marine taxa *Mugil* cf. *cephalus* (Fig. 9e), the marine Indo-Pacific species *Spratelloides gracilis* and of *Gobius* sp. have been identified at Cava Serredi in a horizon < 1 m below the Miocene/Pliocene boundary (Carnevale et al., 2006b). The dominant stenohaline families in these assemblages are Gobiidae, a family of demersal fish occupying shallow-water marine, brackish and freshwater environments, and Myctophidae, which are marine mesopelagic fish that live below 200 m depth during the day, but feed at night in surface waters. A recent review of the Tortonian-Zanclean Gobiidae of the Mediterranean (Schwarzhans et al., 2020) showed that the otoliths of this family, described by Carnevale et al. (2006a, 2008, 2018) and Grunert et al. (2016) as belonging to marine Atlantic species, instead belong to brackish and freshwater species of Paratethyan affinity inhabiting sheltered prodelta environments. In fact, no normal marine demersal taxa were recognized in these assemblages by Schwarzhans et al. (2020). As for the Myctophidae, the vast majority of the taxa belonging to this family were recovered in Moncucco and Verduno from alluvial plain silty mudstones along with terrestrial mammals (Dela Pierre et al., 2011; Colombero et al., 2017 and references therein), pointing to a physically reworked origin. When $^{87}Sr/^{86}Sr$ isotope ratios are measured (Carnevale et al., 2008; Grunert et al., 2016), the resulting Sr-based age of the otoliths is > 7 Ma, therefore further arguing against their in-situ origin. Since the good preservation of the otoliths suggests they did not suffer physical reworking (Carnevale et al., 2006a, 2006b, 2008, 2018; Grunert et al., 2016), predators foraging in open marine settings and migrating to marginal environments are proposed as a way out of the enigma (Carnevale et al., 2008, 2018; Grunert et al., 2016; Colombero et al., 2017). However, Carnevale et al. (2006a) also rule out that so well preserved otoliths may have suffered post-mortem transport and action of the digestive acids in the stomach of predators. Rare findings of Myctophidae from Ciabot Cagna (3 species), Cava Serredi (1 species), Capanne di Bronzo (1 species) and Podere Torricella (6 species) (Carnevale et al., 2018) are all from sections where the host sediments have not been studied in sufficient detail to be clear about the *in situ* or reworked nature of the fossil assemblage. This lack of sedimentological uncertainty also extends to the stratigraphic position of many samples, because a stratigraphic log is provided for only a few sections (i.e. Ca' Ciuccio, Cava Serredi and Moncucco; Carnevale et al., 2006a, 2006b). What this stratigraphic information suggests is that euryhaline fish taxa are widespread throughout substage 3.2, whereas strictly Myctophidae, which are an oceanic, marine stenohaline species, only occur very close to the base of the Pliocene, plausibly corresponding to the uppermost lithological cycle in substage 3.2 (~5.35-5.33 Ma; Carnevale et al., 2018).

5.7. Summary of the Stage 3 paleontological record

The aquatic fossil record of MSC Stage 3 indicates that substage 3.1 in onshore sections is mostly barren, while diverse assemblages characterize substage 3.2 deposits. By contrast, the deep record as a whole contains relatively few, low diversity assemblages. This might be as a consequence either of the limited sample locations recovered from the offshore areas (see Fig. 2b) or because the environmental conditions in the intermediate-deep basins were less favorable for sustaining the life forms typical of the onshore domain. Nevertheless, the assemblages that are found in both marginal and deep locations comprise mixed brackish and marine species.

Brackish species are mostly represented by ostracods and dinocysts (and mollusks here not addressed because poorly studied; see Esu, 2007 and Guerra-Merchán et al., 2010). Prominent is the affinity of these late Messinian Mediterranean brackish species with the same species that were simultaneously dwelling in the Eastern Paratethyan basins (Dacian, Euxinic and Caspian) and in the North Aegean. Since these organisms were not present in the Mediterranean at any time before the MSC, they are considered, with a broad consensus, as *in situ*. This conclusion is further corroborated by the mixing of adult and juvenile forms in the ostracod assemblages and by the good preservation of the specimens, which do not show typical evidence of physical reworking like abrasion, dissolution, or fragmentation. Still problematic is the time of their arrival in the Mediterranean and their likelihood as biostratigraphic tool. From our review it seems more likely that truly Paratethyan species of ostracods entered the Mediterranean already during substage 3.1, when they colonized intermediate-deep settings, while they entered the marginal basins at different times during substage 3.2. As for dinocysts, characteristic is their occurrence only in the uppermost Messinian. However, it must be noted that samples from the substage 3.1 interval are rarely processed for dinocysts, especially in age model-equipped sections (Fig. 3a). The route followed by the Paratethyan immigrants is equally contested and important for paleoenvironmental and paleohydrological interpretations. In view of a desiccated Mediterranean, their migration can only have taken place passively by means of aquatic migratory birds. Conversely, the homogeneity of the ostracod assemblages throughout the Mediterranean marginal basins is more indicative of the presence of a water body fed by Eastern Paratethys and connecting all Mediterranean subbasins, therefore implying relatively high water-level conditions (at least at times when ostracod-bearing sediments deposited; see Andreetto et al., 2021).

Marine assemblages are composed by foraminifera, nannofossils, dinocysts and calcareous nannofossils. Their reworked or *in situ* nature is in many cases contested but critical for paleoenvironmental interpretation. The picture that emerges from our review is that an open marine signature is questionable in the foraminifera, nannofossils, dinocyst and fish records, as well as in other biotic groups (e.g. corals, echinoids and mammals) here not tackled (and for which we refer the reader to Dominici et al., 2018 and Carnevale et al., 2019). All marine representatives of the above mentioned categories were reintroduced into the Mediterranean only at the beginning of the Pliocene and at the expense of the Paratethys species that, instead, disappeared. Collectively, these observations lead us to conclude that the marine model as conceived by Carnevale et al. (2006a, 2006b, 2008, 2018) and Grunert et al. (2016) has no foundation and therefore will not be further discussed.

6. The geochemical perspective

Variations in the water sources draining into the Mediterranean are expected to be reflected also in (geo)chemical properties of the paleodepositional environments. Important information about the nature of the connectivity framework of the Mediterranean can be gained by interpreting geochemical signals that respond to the presence or absence of an exchange with a chemically-unique water body. Four main geochemical proxies have been applied so far to MSC Stage 3 sedimentary and paleontological records. These includes both radiogenic (Sr isotope ratios) and stable isotopes (sulfate and oxygen) measured on fossils and minerals and hydrogen isotopes on molecular biomarkers. This section summarizes the dataset available for geochemical proxies (Fig. 10; Supplementary material 1) and its interpretation(s) for MSC Stage 3.

6.1. Strontium isotope ratios ($^{87}Sr/^{86}Sr$)

The available strontium isotope data for Stage 3 (Fig. 10a; Supplementary material 1) derive from measurements on both Ca-bearing fossils (ostracod valves, mollusk shells, fish otoliths; Fig. 9a) and minerals (calcite and gypsum), where Sr^{2+} dissolved in an aqueous solution substitutes Ca atoms due to their similar ionic radius (e.g. Hajj et al., 2017). Here we screen the available dataset and discuss only results that (1) reflect the original primary isotopic signal, i.e. the isotopic signal of the fluid at time of shell calcification or mineral precipitation, and (2) for which timing of mineral precipitation can be constrained. This screening excludes bulk carbonate samples (e.g. *Colombacci* limestones;

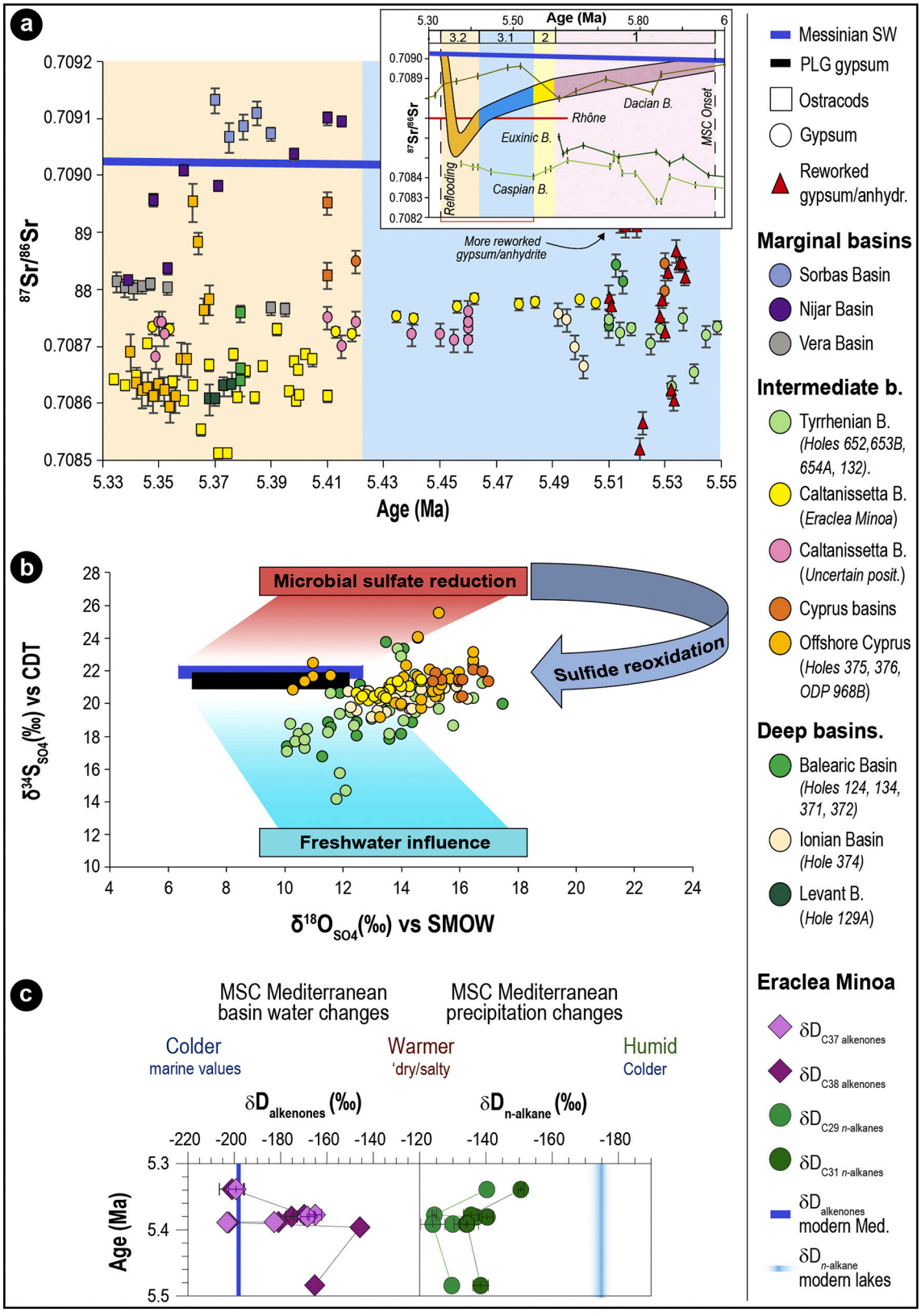

(caption on next page)

Fig. 10. Isotopic record of MSC Stage 3 for the Mediterranean Basin. (a) Compilation of MSC Stage 3 $^{87}Sr/^{86}Sr$ isotope data sourced from ostracod valves and gypsum crystals (see Supplementary material 1 and subsection 6.1 for references). Data are plotted with the global $^{87}Sr/^{86}Sr$ seawater curve (McArthur et al., 2012). Error bars indicate analytical error, which is so small in some cases that no error bars are visible at this scale. To not complicate the figure, horizontal error bars have not been added for the sections/cores unprovided of a chronostratigraphic framework and for which age uncertainties are present (i.e. all but Nijar and Vera basins, Eraclea Minoa and onshore Cyprus; see Fig. 3). Note that none of the $^{87}Sr/^{86}Sr$ isotope ratios but one from Nijar plot on the ocean curve. In the inset is shown the Mediterranean Sr record for the entire MSC as well as the time-equivalent Eastern Paratethys record (modified after Andreetto et al., 2021). (b) Plot of $\delta^{34}S_{SO4}$ and $\delta^{18}O_{SO4}$ in Stage 3 gypsum and anhydrite beds from onshore and offshore localities (see Supplementary material 1 and subsection 6.2 for references). No measures are available from the marginal basins, where gypsum did not deposit during Stage 3. The dark blue and black rectangles represent the sulfate isotopic composition of the Global Messinian ocean and Stage 1 (PLG) evaporites, respectively. The light blue area represents the sulfate isotopic composition of mixtures of Messinian marine waters with non-marine sources. The red area represents the isotopic composition of the residual sulfate ion in a basin where marine Messinian sulfate is consumed by microbial sulfate reduction to produce H_2S. The arrow represents the isotope trajectory of dissolved sulfate resulting from the mixing of residual ^{34}S-enriched sulfate produced by MSR and ^{34}S-depleted sulfate produced by H_2S oxidation. All the published $\delta^{34}S_{SO4}$ and $\delta^{18}O_{SO4}$ values are provided corrected with the fractionation factors $\delta^{34}S$=+1.65‰ and $\delta^{18}O$=+3.5‰ to smooth the isotopic fractionation effects experienced by dissolved sulfate and to reason on values reproducing the isotopic composition at the time of gypsum precipitation. (c) δD isotopes of C_{29} and C_{31}*n*-alkanes and C_{37} and C_{38} long chain alkenones recorded in the Stage 3 gypsums and marls of the Eraclea Minoa section (modified from Vasiliev et al., 2017). Blue lines indicate the values recorded in the present day lacustrine settings for the *n*-alkanes (Sachse et al., 2006) and in the alkenones from the Mediterranean in the recent times (Van der Meer et al., 2007). Error bars indicate standard errors of the mean.

Bassetti et al., 2004), which contain carbonate compounds of various and/or unknown provenance, measurements from mollusk shells and otoliths (e.g. Carnevale et al., 2008; Grunert et al., 2016; Roveri et al., 2019a), because they are made of mineral phases easily altered during diagenesis (e.g. aragonite; Marcano et al., 2015), and data coming from reworked material (e.g. all reworked gypsum or transported foraminifera). $^{87}Sr/^{86}Sr$ isotope ratios have also been measured by Müller and Mueller (1991) and Roveri et al. (2014b) on the halite beds recovered at Sites 134, 374 and 376 (Ryan et al., 1973; Hsü et al., 1978b). Although they provide interesting interpretative aspects, we do not consider these Sr measurements because the position of Sr in the crystal lattice of halite is unknown and the removal of all contaminants, that is not a straightforward procedure (see Meilijson et al., 2019), is not clear it was achieved by Müller and Mueller (1991) and Roveri et al. (2014b). As a matter of fact, there is no consistency between data generated from roughly the same interval in Core 134 by Müller and Mueller (1991) (0.708968) and Roveri et al. (2014b) (0.708800-0.708896). Added to this is the uncertainty over the provenance of halite in Sites 134 and 374 (see subsections 4.2 and 4.6.1), which violates both criteria mentioned above.

The general trend of the Mediterranean $^{87}Sr/^{86}Sr$ isotope ratio during the MSC deviates from the ocean curve towards the less radiogenic values of the major peri-Mediterranean rivers and Paratethys and returns abruptly to oceanic values at the Miocene/Pliocene boundary (Fig. 10a inset). This trend is regarded to reflect the progressive restriction of Mediterranean-Atlantic exchange and the relative increase in the proportion of non-marine source waters (Topper et al., 2011; Roveri et al., 2014a). At first glance it seems that each MSC Stage was characterized by a well-defined range of Sr ratios (Fig. 10a inset), an observation that led Roveri et al. (2014b) to attribute a chronostratigraphic value to MSC $^{87}Sr/^{86}Sr$ ratios. A closer look, however, shows that MSC substages are anything but homogeneous with respect to $^{87}Sr/^{86}Sr$ ratios. At least in the marginal basins, local lithological differences in the catchments (each lithology carries a unique $^{87}Sr/^{86}Sr$ fingerprint; see subsection 8.1.1) explain the different Sr isotopic compositions from basin to basin (see Schildgen et al., 2014; Modestou et al., 2017; Andreetto et al., 2021), therefore arguing against the use of $^{87}Sr/^{86}Sr$ ratios for chronostratigraphic purposes in the MSC record.

Most of the data characterizing substage 3.1 (Fig. 10a) are from the Eraclea Minoa gypsum (Fig. 5h). These data define a narrow range of Sr isotope ratios between 0.708747 and 0.708793 (García-Veigas et al., 2018). Similar values were reported from both Eraclea Minoa and the nearby Siculiana Marina section (0.708710-0.708760; Keogh and Butler, 1999; Fig. 5i). The dominance of Sicily samples gives the appearance of a consistent Sr isotope signal for gypsum beds. However, data points from elsewhere (Cyprus, Manzi et al., 2016a; DSDPs 122, 371 and 372 in the Algero-Balearic Basin, ODPs 652, 653 and 654 in the Tyrrhenian Basin, DSDP 374 in the Ionian Basin; Müller et al., 1990; Müller and Mueller, 1991; Roveri et al., 2014b) display a wider range (from ~0.7087 to 0.708847; Fig. 10a) that may indicate a different hydrological regime for each basin (e.g. Müller et al., 1990; Müller and Mueller, 1991; Ryan, 2009). The one published Sr isotope value for ostracods found within one of the marl interbeds at Eraclea Minoa also has a lower value outside the typical Sicily gypsum range (Grossi et al., 2015). This suggests that a different hydrological regime may also have characterised precession minima stages of the precessional cycle.

The Sr isotope dataset for the Lago-Mare phase includes the lowest values measured on MSC sediments (~0.7085 from between gypsum VI and VII at Eraclea Minoa; Fig. 3a; Grossi et al., 2015) and the widest range of ratios spanning from 0.7085 to 0.7091, which is above coeval oceanic values (Fig. 10a). Again, the conspicuously high Sr isotope values in substage 3.2 come from two areas, the marginal basins of southern Spain (Andreetto et al., 2021 and references therein; Figs. 5a-c) and the intermediate Polemi Basin on Cyprus (McCulloch and De Deckker, 1989). The lower values are drawn from right across the intermediate-deep Mediterranean (Algero-Balearic, Sicily, Levant; Fig. 2a) and are therefore more likely to represent a Mediterranean-wide Sr isotope signal.

New Sr isotope data from Eastern Paratethys (i.e. Dacian and Caspian basins; Fig. 2b) are now available for the interval corresponding to MSC Stage 3 (inset Fig. 10a). The $^{87}Sr/^{86}Sr$ ratios of the Dacian Basin (0.708865-0.708982; Vasiliev et al., 2010; Grothe, 2016) are slightly lower than coeval ocean water (0.709020), but much higher than coeval Mediterranean values. However, the Dacian Basin is regarded as highly restricted from the Mediterranean throughout the MSC (Vasiliev et al., 2010). By contrast, the Caspian has very low values (0.708402 to 0.708473, Grothe et al., 2020) which are thought to reflect both the very low Sr isotope ratio of the Volga river (0.708020; Vasiliev et al., 2010 and references therein) and some input from the Mediterranean (Grothe et al., 2020).

6.2. *Sulfate isotopes*

Sulfur isotopic investigations have been carried out only on sulfate minerals (gypsum and more rarely anhydrite) of the MSC Stage 3 deposits with samples drawn from both onshore intermediate sequences (Caltanissetta Basin and Cypriot basins) and deep basinal records (Sites 122, 124, 125A, 132, 134, 372, 374, 375, 376, 652, 653, 654, 968, 969, 970; Fig. 10b; Fontes et al., 1973; Pierre, 1974, 1982; Pierre and Fontes, 1978; Ricchiuto and McKenzie, 1978; Pierre and Rouchy, 1990; Blanc-Valleron et al., 1998). Because the incorporation of dissolved sulfate into gypsum produces a nearly constant fractionation of $\delta^{18}O$ (+3.5‰) and $\delta^{34}S$ (+1.65‰) at earth surface temperatures (Thode and Monster, 1965; Lloyd, 1968; Warren, 2016), $\delta^{18}O$ and $\delta^{34}S$ isotopic values measured in gypsum should be corrected with the above mentioned fractionation factors in order to reconstruct the sulfate isotopic composition of the

basin waters at the time of gypsum formation.

The deep Mediterranean samples exhibit a wide range of $\delta^{34}S_{SO4,}$ but the majority of samples display $\delta^{34}S_{SO4}$ values between 18 and 22‰, strongly indicative of a marine origin of the sulfate forming the gypsum (Fig. 10b; Fontes et al., 1973; Pierre, 1974, 1982; Pierre and Fontes, 1978; Pierre and Rouchy, 1990; Blanc-Valleron et al., 1998). The $\delta^{34}S_{SO4}$ values lower than marine sulfate in the dataset are generally considered to represent a greater influence of continental sulfate input to the basin (Fig. 10b; Pierre, 1974; Pierre and Fontes, 1978; Pierre and Rouchy, 1990). By contrast, the data display $\delta^{18}O_{SO4}$ isotopic values that deviate substantially from marine $\delta^{18}O_{SO4}$ values towards higher values (Fig. 10). This is consistent with the influence of sulfate produced by reoxidation of reduced sulfur compounds generated by microbial sulfate reduction (MSR; Kaplan and Rittenberg, 1964; Brunner and Bernasconi, 2005; Sim et al., 2011; Leavitt et al., 2013). The microbial use of SO_4^{2-} leads to an equilibration of $\delta^{18}O_{SO4}$ with ambient water oxygen, whereas the $\delta^{34}S_{SO4}$ returns towards its initial value as a higher fraction of sulfide produced by MSR is re-oxidated. This mechanism has been suggested for Sites in the Algero-Balearic, Tyrrhenian and Ionian basins and offshore Cyprus (Pierre, 1974; Pierre and Fontes, 1978; Pierre and Rouchy, 1990). Although some authors have suggested that partial equilibration of sulfate oxygen toward $\delta^{18}O_{H2O}$ values of the basin enriched in heavy oxygen isotopes by evaporation have led to an increase in $\delta^{18}O_{SO4}$ values without significant changes in $\delta^{34}S_{SO4}$ (Fontes et al., 1973; Pierre, 1974; Ricchiuto and McKenzie, 1978), this hypothesis seems highly unlikely as the abiotic equilibration between sulfate and water oxygen take about 20 Myr at normal marine pH (Lloyd, 1968; Longinelli and Craig, 1967; Turchyn et al., 2006). Moreover, the microbial sulfate reduction process is supported by the presence of pyrite at Sites 132, 654A and 968 (Pierre, 1982; Pierre and Rouchy, 1990; Blanc-Valleron et al., 1998) and the existence of filaments of possible microbial origin at Site 654A (Pierre and Rouchy, 1990).

The sulfate isotopic values reported by Longinelli (1979) and Pierre (1982) from the Upper Gypsum of Eraclea Minoa (Caltanissetta Basin, Sicily) are considerably more scattered than those from a recent study by García-Veigas et al., 2018; Fig. 10b). Such discrepancies are probably a consequence of different sample selection: García-Veigas et al. (2018) analyzed only pristine whitish selenite and balatino samples, while Longinelli (1979) and Pierre (1982) analyzed all types of gypsum-bearing samples such as "gypsiferous marl" and gypsum laminae intercalated in carbonate or diatomaceous intervals. These less pristine samples probably contain high quantities of ^{34}S-depleted solid sulfides or diagenetic gypsum formed by oxidation of sulfides (see Liu et al., 2017 for more details on this process) and are therefore unlikely to be representative of the primary gypsum facies. Once these data are excluded, the Eraclea Minoa sulfate values ($\delta^{18}O_{SO4}$ from 12.4 to 14.6‰ and $\delta^{34}S_{SO4}$ from 21.0 to 22.3‰) suggest a marine origin of the sulfate and stable redox conditions during gypsum deposition (Fig 9.b; García-Veigas et al., 2018). Interestingly, the Eraclea Minoa sulfate values are in compliance with the isotopic values ($\delta^{18}O_{SO4}$=15.2 to 16.8‰; $\delta^{34}S_{SO4}$= 20.4 to 21.9‰) measured by Pierre (1982) in the Polemi Basin (Cyprus).

6.3. Hydrogen isotopes on molecular biomarkers

From the point of view of the application of organic geochemistry proxies, the Miocene Mediterranean Basin received little attention so far, with biomarker-based proxies that have been mostly applied to (a limited number of) pre-MSC sequences (Tzanova et al., 2015; Herbert et al., 2016; Mayser et al., 2017; Natalicchio et al., 2017, 2019; Vasiliev et al., 2019) and pre-Stage 3 sedimentary records (Lower Evaporites on Sicily, Andersen et al., 2001; Vena del Gesso Basin, Sinninghe Damsté et al., 1995 and Vasiliev et al., 2017; Levant Basin, Meilijson et al., 2019). To date, only one study analyzed Stage 3 samples (Vasiliev et al., 2017). This study used compound specific hydrogen isotope (δD) analyses, measured on both terrestrial (long chain C_{29} and C_{31}*n*-alkanes; Sachse et al., 2006) and aquatic (alkenones; Englebrecht and Sachs, 2005) biomarkers from the gypsum beds of the Upper Gypsum at Eraclea Minoa to reconstruct the hydrological cycle during gypsum precipitation.

Both $\delta D_{C29n\text{-alkane}}$ and $\delta D_{alkenones}$ results (Fig. 10c) suggested that conditions in Sicily were significantly dryer than today, with highly enriched values of $\delta D_{C29n\text{-alkanes}}$ (up to −125‰). The $\delta D_{alkenones}$ varied between values suggesting evaporative conditions (−125‰) and values typical for present-day $\delta D_{alkenones}$ in the Mediterranean (−203‰) (Vasiliev et al., 2017).

No time-equivalent biomarker data from the open ocean settings are currently available. Instead, Vasiliev et al. (2017) compared their Mediterranean data with data from the Black Sea (DSDP 42B Hole 380 and Taman peninsula; Vasiliev et al., 2013, 2015). The Upper Gypsum $\delta D_{n\text{-alkanes}}$ were more enriched when compared to their time equivalent deposits of the DSDP 42B 380 borehole of the Black Sea (−180‰). This probably reflects the more intracontinental position of the Black Sea which commonly translates into more depleted values for $\delta D_{precipitation}$ used by the vegetation, resulting in more depleted $\delta D_{C29n\text{ -alkanes}}$. However, there is a 30 to 40‰ enrichment relative to present in the $\delta D_{n\text{-alkanes}}$ (i.e. $\delta D_{precipitation}$) in both Mediterranean and Paratethys domains, indicating concurrent changes in both areas during the latest phase of the MSC.

Both the Mediterranean and Paratethyan samples contain $\delta D_{alkenones}$ with low values (~-200‰) (Fig. 10c) leading Vasiliev et al. (2017) to suggest that either the surface water from the Upper Gypsum was derived from the Black Sea, or that the Mediterranean and Paratethys were exchanging surface water during gypsum precipitation. Similarity between the relative contribution of the C_{37}, C_{38} and C_{39} alkenones at Eraclea Minoa and one of the Black Sea samples may suggest common alkenone producers for the two areas, again supporting the idea of a Mediterranean-Paratethys connection during Stage 3 (Vasiliev et al., 2017).

A final speculative insight from this biomarker dataset is that the relative contribution of alkenones found in the Upper Gypsum of Eraclea Minoa is strikingly similar to present-day open marine samples, even though *Emiliania huxleyi*, the principal ocean alkenone producer today, did not exist in the late Miocene. Vasiliev et al. (2017) suggested that this could imply the existence of a connection to the open ocean during Upper Gypsum deposition in Sicily (i.e. throughout Stage 3; Fig. 3a).

6.4. Oxygen isotopes

Oxygen stable isotope data ($\delta^{18}O$) are available from bulk samples (Rouchy et al., 2001, 2003, 2007; Pierre et al., 2006; Cosentino et al., 2012), gypsum (Pierre and Fontes, 1978; Ricchiuto and McKenzie, 1978; Lugli et al., 2007), mollusk shells (Carnevale et al., 2008; Grunert et al., 2016) and ostracod valves (Cosentino et al., 2012; Grossi et al., 2015).

For all the sub-basins for which there is latest Messinian data (e.g. Sites 974 and 975; Eraclea Minoa section, Sicily; Aghios Stefanos section, Corfu; Kalamaki section, Zakynthos; Pissouri Basin, Cyprus; Rouchy et al., 2001, Pierre et al., 2006), each has its own range of oxygen isotopic compositions and its own degree of variability. Values from above the Miocene/Pliocene boundary regain seawater values of 0.3 to 1 ‰ (e.g. Pierre et al., 2006).

In marginal marine settings and lakes, the controls over $\delta^{18}O$ are poorly constrained as oxygen does not respond simply to the freshwater flux, but to a combination of variables such as temperature, rainfall and evaporation (e.g. Placzek et al., 2011). Freshwater input may contribute to the signal, resulting in $\delta^{18}O$ more negative than seawater (0.3‰ to 0.8‰ SMOW; Dettman et al., 2004), but under prevailing evaporating conditions it is likely that the $\delta^{18}O$ will be primarily influenced by evaporation, leading to $\delta^{18}O$ more positive than seawater (e.g. Dettman et al., 2004), making any data very difficult to interpret. Furthermore, the lack of a unique $\delta^{18}O$ signature for each water source makes oxygen isotopes a difficult tracer proxy to use.

6.5. Summary of the Stage 3 geochemical dataset

The variety of paleoenvironmental and connectivity proxies applied to MSC Stage 3 record provide valuable insights into the hydrological conditions during Stage 3. The more outstanding results from all discussed proxies are that:

1) Paleodepositional subaqueous environments where gypsum was precipitating and ostracods and biomarker-producers were thriving were strongly dominated by non-oceanic inputs;
2) an indisputable marine signal is absent and only regained above the M/P boundary.

Sulfate and oxygen isotopes are currently difficult to use for water provenance reconstruction because the non-marine sources (local and major rivers and Eastern Paratethys) that are likely to be of influence lack distinctive isotopic signatures and, especially for oxygen, respond to a combination of controls (e.g. temperature, rainfall, evaporation) with local variability. $\delta^{34}S_{SO4}$ are claimed by several authors to be an evidence of the presence of an Atlantic inflow ($\delta^{34}S_{SO4}$=22‰; Turchyn and Schrag, 2004) in a Mediterranean strongly affected by non-marine waters (Manzi et al., 2009, 2016a; García-Veigas et al., 2018 among others). However, the same values can be obtained by means of the recycling of PLG deposits (~23‰; Lu et al., 2001; Lugli et al., 2010; García-Veigas et al., 2018).

Similarities between the $\delta D_{alkenones}$ of the Upper Gypsum at Eraclea Minoa and coeval Black Sea sediments and $\delta D_{n\text{-alkanes}}$ similar to present-day marine settings, suggest that Eastern Paratethys and the Atlantic were simultaneously contributing to the Mediterranean hydrological budget. $^{87}Sr/^{86}Sr$ isotope ratios are a useful water-mass tracer because each water body carries a unique Sr isotope fingerprint (see subsection 8.1.1). Our plotting of Stage 3 $^{87}Sr/^{86}Sr$ isotope values (Fig. 10a) highlights the large geographical variability of the values and the sharp division between Sr isotope ratios measured in marginal basins versus those in intermediate-deep water locations. This is only noticeable in substage 3.2, since no (or not enough) material suitable for Sr analysis is present in substage 3.1 deposits from the marginal basins. Some authors see this variability as an indication of isolated subbasins with unique hydrological conditions driven by their catchment rivers (e.g. Müller et al., 1990; Müller and Mueller, 1991; Ryan, 2009). If some degree of connection was present, it involved only neighbouring basins (e.g. Tyrrhenian subbasins; Müller et al., 1990; Müller and Mueller, 1991). A recent comparison of the Sr isotope record of the Spanish marginal basins of Sorbas, Nijar and Vera with the Sr isotope ratios likely to have typified the local riverine sources demonstrated that a local sources-mixed signal expected from an endorheic lake in that location is absent. In this instance mixing of intrabasinal water sources with a non-marine Mediterranean water mass is used to explain the measured values (Andreetto et al., 2021). If this explanation is more widely applicable, then it may result in a re-interpretation of the spread of Sr isotope data from the latest Messinian interval.

To conclude, geochemical proxies have great potential to test the different scenarios, but data are currently too numerically and geographically limited to be robust.

7. Paleoenvironmental scenarios for freshening the salt giant: desiccated versus full Mediterranean

The riddle of the Mediterranean environmental and hydrological conditions during Stage 3 is a highly debated topic and it is key to understanding the means by which open marine conditions were restored at the base of the Zanclean and on the potential impact that the Atlantic-Mediterranean re-connection had on the Atlantic and global climate (Flecker et al., 2015; Capella et al., 2019). In this chapter, the paleoenvironmental scenarios, in terms of base-level position (desiccated or full Mediterranean) and hydrological configuration (connections to the Atlantic and/or Paratethys), proposed for the Mediterranean during Stage 3 are described, as well as the different timings of the reflooding (instantaneous, gradual, step-like increments). The low-salinity Stage 3 followed the hypersaline Stage 2 and the transition between the two likely influences the plausibility of the various paleoenvironmental scenarios proposed for the terminal stage. We therefore first summarize the current understanding of the configuration of the Mediterranean during Stage 2 and the enduring controversies (see Roveri et al., 2014a for a more extensive review).

7.1. Stage 2 (5.59-5.55 Ma): formation of the Mediterranean salt giant

Numerical modelling based on hydrological budget calculations shows that in order to reach salinity levels compatible with halite saturation and to accumulate the substantial thicknesses of halite observed in the seismic profiles (Ryan, 1973; Haq et al., 2020), the Atlantic-Mediterranean gateway needs to have permitted inflow from the Atlantic, but may have completely blocked outflow (Blanc, 2002; Krijgsman and Meijer, 2008). Numerical models also showed that without Atlantic inflow into the Mediterranean Sea its base level is forced to drop on time scales in the order of a few thousand years by virtue of the basin's negative hydrological budget, where more water is lost to the atmosphere by evaporation than is received from rainfall and river runoff (e.g. Meijer and Krijgsman, 2005; Krijgsman and Meijer, 2008; Simon et al., 2017). The idea of a drawdown is supported by several arguments: (1) the widespread presence, from the margins to the slopes, of the Messinian Erosional Surface cutting through Stage 1 and pre-MSC deposits and canyon incisions following today's drainage networks (e.g. Chumakov, 1973; Clauzon, 1982; Lofi et al., 2005, 2011a, 2011b; Loget et al., 2006; Maillard et al., 2006, 2020; Estrada et al., 2011; Just et al., 2011; Urgeles et al., 2011; Amadori et al., 2018; Lymer et al., 2018; Cazzini et al., 2020; Figs. 5e, 7e); (2) their morphology interpreted as subaerial in origin; (3) the clastic fans at the outlet of the valleys onlapped by Stage 3 deposits and interpreted as fluvial accumulations (e.g. Lofi et al., 2005; Maillard et al., 2006; Pellen et al., 2019). A number of studies have tried to quantify the magnitude of the sea-level fall by compensating for the isostatic vertical motion since the Messinian to obtain the original depth of the erosional features and Messinian deposits. However, this depends on the assumptions about when the drawdown occurred relative to the halite precipitation: before (e.g. Cartwright and Jackson, 2008; Bache et al., 2009, 2012), during (e.g. Ryan, 2008, 2009) or after (e.g. Ryan, 1978; Bertoni and Cartwright, 2007; Lofi et al., 2011a, 2011b). How shallow the Mediterranean became during Stage 2 is also a matter of disagreement. Estimates in the Western Mediterranean vary from a maximum drawdown of 2500 m (Ryan, 1976) to 1000-1500 m (Bache et al., 2012) in the Gulf of Lion, 800-1200 m in the Balearic promontory (Mas et al., 2018b) and 400 m in the Ebro delta region (Frey-Martinez et al., 2004). A later backstripping analysis of this delta yielded a drawdown of ~1300 m (Urgeles et al., 2011). East of the Sicily sill, backstripping studies estimated base-level drops of 1800-2000 m in the Ionian basin (Micallef et al., 2018, 2019; Camerlenghi et al., 2019; Spatola et al., 2020), 800-900 m in the Adriatic foredeep and Po plain (Ghielmi et al., 2013; Amadori et al., 2018), 800-1300 m (Ben-Gal et al., 2005), 600 (Druckman et al., 1995) and 800 m (Cartwright and Jackson, 2008) in the Levant Basin.

None of these quantifications could unequivocally constrain the timing of the drawdown within the MSC sequence, but numerical modeling studies show that, if the blocking of the outflow was controlled by a tectonic uplift counteracted by inflow erosion across the Strait of Gibraltar, then the expected drawdown of the Mediterranean Sea should be moderate (< 400 m; and possibly harmonic) due to an equilibrium between incision and uplift before the complete blocking of inflow and larger (up to complete desiccation) only after tectonic uplift overcame incision rates (Garcia-Castellanos and Villaseñor, 2011). The same model suggests that the initiation of halite precipitation might overlap in time with the late primary gypsum deposition, right before the full

disconnection from the Atlantic Ocean.

The interpretation of the deep evaporites and their associated seismic markers (erosional surfaces and deep engravings along the shelf-slope systems) is not straightforward. Recently, it was suggested that the deep evaporitic facies and the seismic morphological features could have been produced without a significant drop of the Mediterranean base-level, therefore promoting the persistence of a relatively deep-water Mediterranean basin even during halite deposition (Lugli et al., 2013, 2015; Roveri et al., 2014b). For example, Roveri et al. (2014c) proposed that downslope flows of dense, hypersaline waters sourced from evaporation in shallower water areas could have generated both the observed shelf-slope erosion and have created a deep brine, super-saturated in the ions necessary for precipitating halite. These subaqueous hyperpycnal flows are consistent with the observed clastic evaporites that filled the Levant margin canyons (Lugli et al., 2013) and, more generally, with the widespread presence of Complex Units at the outlet of the MES drainage systems (see Lofi et al., 2005, 2011a, 2011b; Lofi, 2018). These sediments are dominated by reworked PLG that would have been exposed by a sea-level fall as little as 200 m (Lugli et al., 2010). However, the hypersaline environment that is presumed to be established by these hyperpycnal flows during the deposition of the RLG is in contrast with the occurrence of the Paratethyan ostracod *L. muelleri* within the clastic evaporites (RLG) in several marginal sections (e.g. Adana Basin, Faranda et al., 2013; Radeff et al., 2016, 2017).

Whatever the state of Mediterranean base-level during Stage 2, the more commonly used chronostratigraphic model for the MSC (Fig. 1a; Roveri et al., 2014a) states that massive halite precipitation ceased at 5.55 Ma and was superseded by an environment that, with precession periodicity (Fig. 3a), cycled between gypsum precipitation and conditions that saw fresh-brackish organisms thriving. The question is whether these conditions cycled homogeneously in several isolated lakes or in basins largely connected to the same Atlantic and Eastern Paratethys-influenced water mass (Fig. 11).

7.2. Stage 3 (5.55-5.33 Ma): resumption of (upper) gypsum precipitation and Paratethys fauna invasion

7.2.1. An isolated Mediterranean dotted by sabkhas and lakes

The first and long-lasting paleoenvironmental interpretation of the evaporite-bearing UG/UU units and (possibly) time-equivalent evaporite-free units (e.g. LM Unit in Malaga, Sorbas and Zorreras Mb. in Sorbas, Feos Fm. in Nijar, Cassano Spinola Conglomerates in Piedmont, San Donato/Colombacci fms. in the Apennines, Handere Fm. in Turkey) envisaged their sedimentation in a Mediterranean mostly isolated from the Paratethys (which may have added water only to some basins in the Eastern Mediterranean) and totally isolated from the Atlantic where, in each subbasin, continental settings (e.g. alluvial plains, river channels, alluvial fans, playa lakes, sabkhas) alternated/interfingered with shallow, endorheic lakes (Figs. 11a, c; e.g. Ruggieri, 1962, 1967; Decima and Sprovieri, 1973; Decima and Wezel, 1973; Friedman, 1973; Hsü et al., 1973a, 1973b, 1973c, Hsü et al., 1978a, 1978b; Ryan et al., 1973; Selli, 1973; Sturani, 1973; Sissingh, 1976; Benson, 1978; Bossio et al., 1978; Cita et al., 1978, 1990; Ricchiuto and McKenzie, 1978; Ryan, 1978, 2008, 2009; Cita and Colombo, 1979; Orszag-Sperber and Rouchy, 1979; Ghibaudo et al., 1985; Müller et al., 1990; Benson and Rakic-El Bied, 1991; Benson et al., 1991; Müller and Mueller, 1991; Orszag-Sperber et al., 2000; Rouchy et al., 2001, 2003, 2007; Blanc, 2002; Lofi et al., 2005, Lofi et al., 2011b; Bassetti et al., 2006; Rouchy and Caruso, 2006; Bertoni and Cartwright, 2007; Cameselle and Urgeles, 2017; Amadori et al., 2018; Camerlenghi et al., 2019; Kartveit et al., 2019; Madof et al., 2019; Ben Moshe et al., 2020; Caruso et al., 2020; Cazzini et al., 2020; Raad et al., 2021). The full disconnection is also supported by observations that support an abrupt Zanclean reflooding (e.g. Blanc, 2002; Micallef et al., 2018, 2019; Garcia-Castellanos et al., 2020; Spatola et al., 2020), since a rapid outburst flood requires a large sea level difference prior to the flood that can only be developed in a scenario of a full Mediterranean-Atlantic disconnection (Garcia-Castellanos et al., 2009; Garcia-Castellanos and Villaseñor, 2011). Although rarely explicitly stated, all these studies must assume that:

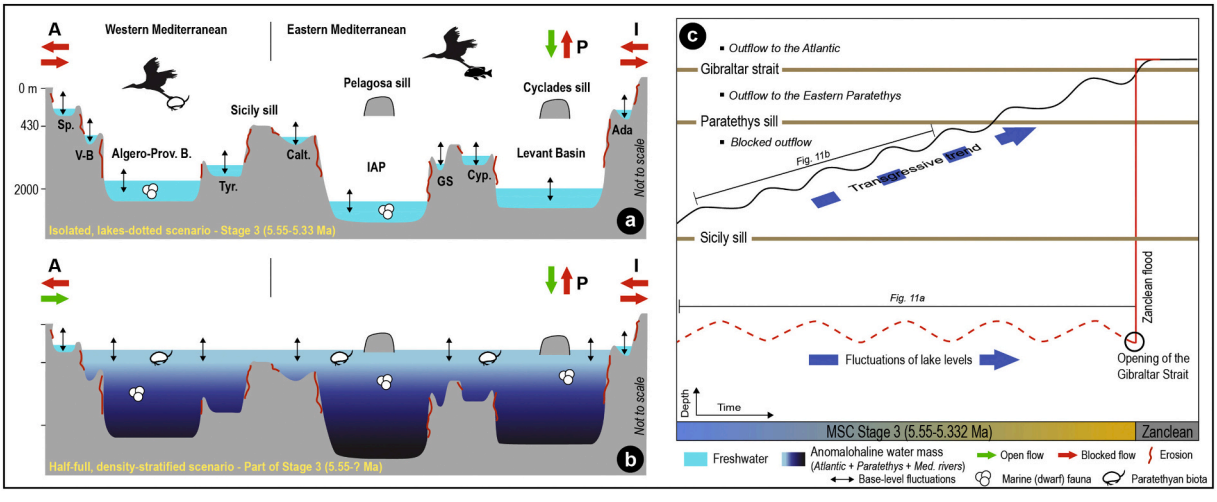

Fig. 11. (a), (b) Schematic W-E profiles across the Mediterranean Basin showing the contrasting paleoenvironmental, paleohydrological and paleoconnectivity interpretations proposed for Stage 3. When a water flow is present (green arrow) from and/or to an extra-Mediterranean water mass (i.e., A: Atlantic Ocean; I: Indian Ocean; P: Eastern Paratethys), the direction of the arrow gives the direction of flow. For simplicity, water added by the major and local rivers is not shown, but it adds to the hydrological budget at any time in each scenario. Note the main difference between the isolated (a) and density-stratified (b) scenario lies in the connectivity framework (Atlantic connection closed and negligible influence from the Paratethys in the isolated scenario; influence from both Atlantic and Paratethys in the density-stratified scenario), which affects the position of the base level of the Mediterranean water mass and its hydrochemistry (see extensive discussion in subsection 7.2). Abbreviations: Sp.: SE Spain; V-B: Valencia Basin; Tyr: Tyrrhenian Basin; Calt: Caltanissetta Basin; IAP: Ionian Abyssal Plain; GS: Gulf of Sirt; Cyp: Cyprus; Ada: Adana Basin. See Fig. 2 for the geographic position of each basin. (c) Schematic plot showing the evolution of the Mediterranean base-level during Stage 3 according to both the isolated (red line) and half-full (black line) scenarios. The critical sills for controlling intra- and extra-Mediterranean connectivity are also shown.

1) all Paratethyan biota (and possibly other organisms of undisclosed provenance like diatoms) migrated passively via aquatic migratory birds across the entire Mediterranean (Fig. 11a; Benson, 1978; Benson and Rakic-El Bied, 1991; Caruso et al., 2020);
2) chemical and physical conditions (brackish water and water depth not exceeding 100 m; e.g. Hajós, 1973; Gliozzi and Grossi, 2008) that allowed alternated conditions suitable for gypsum to precipitate and Paratethyan biota and euryhaline benthic foraminifera to thrive were related to changes in the local freshwater budget;
3) The marine isotopic signals in UU/UG gypsum (Fig. 10) are entirely the reflection of the lithologies that are leached by continental waters in surficial and/or underground drainage areas (e.g. Ryan, 2009; Raad et al., 2021);
4) Stage 3 gypsum precipitated in extremely shallow-water (playa lakes) to completely dried environments (sabkhas) and the excessive sulfate necessary is completely derived from "clastic reworking, dissolution, re-precipitation and diagenesis of materials belonging to the PLG and halite of the previous MSC Stage 2" (Ryan, 2009).

Observations supporting a Mediterranean isolated throughout Stage 3 and only at the mercy of local freshwater inputs (Fig. 11a) are: (1) the lack of evidence for in situ marine fauna and flora in UU (e.g. Ryan et al., 1973; Hsü et al., 1978a; Cita et al., 1990; Ryan, 2009; Lofi et al., 2011a); (2) the shallow-water mode of life and highly likely in-situ nature of ostracods and euryhaline, shallow-water benthic foraminifera observed in DSDP/ODP wells from intermediate and deep basins (e.g. Cita et al., 1978; Iaccarino and Bossio, 1999; Figs. 9a-c); (3) the bathymetric contrast (up to several hundred meters) between the late Messinian paleoenvironments and the marine Zanclean on top (e.g. Cita and Colombo, 1979; Bonaduce and Sgarrella, 1999; Caruso et al., 2020); (4) the presence of paleosols in Cyprus (Orszag-Sperber et al., 2000; Rouchy et al., 2001) and on the crest of the Eratosthenes seamount (Robertson, 1998a, 1998b); (5) the erosional features preserved both offshore on the continental shelves and lower-middle slope domain and interpreted in most seismic stratigraphic studies as the result of subaerial exposure (e.g. Lofi et al., 2005; Lofi et al., 2011b; Lymer et al., 2018; Ben Moshe et al., 2020); (6) the pinching out of the UU/BU units towards evaporite-free pre-Messinian structural highs (Figs. 7b-g; Figs. 8a, e; Ryan, 2009; Lymer et al., 2018; Camerlenghi et al., 2019; Raad et al., 2021); (7) the more abundant terrigenous clasts and reworked calcareous fossils in Stage 3 samples compared to the overlying, deep-water Pliocene (Ryan et al., 1973; Hsü et al., 1978b; Ryan, 2009); (8) the erosional nature of the M-reflector/TES/IMTS in the Levant Basin (Figs. 8e-g), by some linked to subaerial exposure of the Levant seafloor (e.g. Bertoni and Cartwright, 2007; Lofi et al., 2011a, 2011b; Maillard et al., 2011a) before the emplacement of deposits interpreted as fluvial from seismic observations (Bowman, 2012; Radeff et al., 2017; Leila et al., 2018; Kartveit et al., 2019; Madof et al., 2019). Furthermore, (9) isolated hydrological circuits with unique chemical composition are regarded by Camerlenghi et al. (2019) as the most plausible explanation for the W-E change in the MSC sedimentary expression in the deep basins, represented by the trilogy LU-MU-UU in the Algero-Balearic and Liguro-Provençal basins, missing the LU in the Tyrrhenian and (possibly) Ionian basins, by terrigenous deposits with hiatuses in the WAB and Adriatic foredeep and by halite, anhydrite and clastics in the Levant Basin (Interbedded and Argillaceous evaporites of Meilijson et al., 2019; Fig. 3b).

The main problems with the isolated scenario lasting throughout Stage 3 are: (1) it does not provide an explanation neither for the homogeneity of Paratethyan ostracod assemblages in the marginal basins (e.g. Gliozzi et al., 2007; Stoica et al., 2016), an aspect difficult to explain when fauna migration takes place passively via either birds or wind, nor for the biomarkers (Vasiliev et al., 2017), which cannot be transported effectively by aquatic birds; (2) it does not explain the mismatch between $^{87}Sr/^{86}Sr$ isotope ratios measured on marginal ostracods and Sr values expected from endorheic lakes fed with local freshwaters (e.g. Andreetto et al., 2021); 3) it misses to substantiate, with geochemical arguments, the precipitation of gypsum in lakes, a process that is everything but straightforward (see Warren, 2016 for insights); 4) except for the salt-bearing basins, the source(s) of solutes which makes freshwater-fed endorheic lakes brackish and causes similar physico-chemical conditions to exist in each lake is also difficult to explain in the context of a Mediterranean only at the mercy of local rivers.

7.2.2. *The half-full, density-stratified Mediterranean scenarios*

An alternative concept to the isolated scenario envisages the Mediterranean connected with the Atlantic and/or the Eastern Paratethys and relatively full of water connecting the different subbasins (Fig. 11b). To our knowledge, this scenario was first developed by McCulloch and De Deckker (1989) on the basis of the similar $^{87}Sr/^{86}Sr$ ratios from marginal (Spain and Cyprus) and deep (Levantine and Algero-Balearic) basins. This intuition was a significant departure from the far more in vogue desiccated scenario (see conclusion of Hsü et al., 1973b), and for this was long overlooked. Sr isotope ratios lower than contemporary ocean water led McCulloch and De Deckker (1989) to conclude that a brackish water mass created by the mixing of water from the peri-Mediterranean rivers (e.g. Nile, Rhône and African rivers that no longer flow today, etc.; see Griffin, 2002 and Gladstone et al., 2007) with water of the Eastern Paratethys filled the Mediterranean, resembling the Caspian Sea today. This conclusion is consistent with the impoverished (or absent) marine fauna and flora of Stage 3 sediments and the enhanced assemblage of fresh-brackish water biota (see subsection 5.7; Figs. 9a-c), but is problematic as a viable origin for Stage 3 gypsum to precipitate at depth. Furthermore, climate models for the late Miocene fail to fill the Mediterranean Basin with fluvial and Paratethys waters alone (Gladstone et al., 2007; Marzocchi et al., 2016, 2019; Simon et al., 2017). A marine contribution is therefore required to fill the Mediterranean (Marzocchi et al., 2016). In the event, the contribution is most likely to have derived from the Atlantic via the Gibraltar Corridor (Flecker et al., 2015; Booth-Rea et al., 2018; Krijgsman et al., 2018) either through a karst system (Krijgsman et al., 2018) or an emerged volcanic archipelago in the Alborán Basin (Booth-Rea et al., 2018). In fact, although an Indian Ocean contribution was proposed (Cita et al., 1978; Hsü et al., 1978a) and the possibility discussed (Ryan, 2009; Vai, 2016), palinspastic reconstructions concluded that the Neo-Tethys Mediterranean-Indian Ocean connection via southern Turkey and Iran already closed before the Tortonian (Rögl, 1998; Popov et al., 2004; Gargani et al., 2008; Bialik et al., 2019; Gülyüz et al., 2020), while a seaway via the Red Sea and Gulf of Aden, although not completely ruled out (e.g. Schütz, 1994; Bosworth et al., 2005; Gargani et al., 2008; Ryan, 2009), is highly contested (e.g. Meulenkamp and Sissingh, 2003; Segev et al., 2017).

In light of this, Roveri et al. (2014c), Gvirtzman et al. (2017), Vasiliev et al. (2017), García-Veigas et al. (2018) and Grothe et al. (2020) suggested that the Mediterranean was likely density-stratified during this interval as a result of the simultaneous influx of isotopically-different marine and non-marine (major Mediterranean rivers and Eastern Paratethys) water sources (Fig. 11b). This connectivity framework resulted in a brackish layer carrying low-salinity (mostly Paratethyan) biota (Gliozzi et al., 2007; Stoica et al., 2016; Grothe et al., 2018, 2020; Figs. 9a-b) to lay on top of a more saline layer formed by Atlantic-derived seawater from which UU/UG gypsum (Figs. 5h-j, 7b-g, 8a-d), that facies analyses demonstrated to result from subaqueous deposition (Hardie and Lowenstein, 2004; Lugli et al., 2015), precipitated at intermediate and greater depths (e.g. García-Veigas et al., 2018). A dense, anoxic deep-water mass, possibly inherited from Stage 2, is envisaged at the bottom of the Mediterranean by Marzocchi et al. (2016) and García-Veigas et al. (2018), albeit without conclusive arguments, and by Gvirtzman et al. (2017) following the observation that the tilted halite body of the Levant Basin was simultaneously eroded landward and preserved basinward (Fig. 8f).

This scenario accounts for the erosive/non-depositional features

(Figs. 5e, 6a, e) and continental/lacustrine facies (Figs. 5a-b, d-g) widespread around the margins and shelves and suggestive of a Mediterranean base-level somewhat lower than the Atlantic level suggesting a one-way inflow from both the Atlantic and the Eastern Paratethys after Stage 2 (e.g. Marzocchi et al., 2016; Figs. 11b, c), a connectivity configuration that effectively translates in a half-full Mediterranean (e.g. Krijgsman and Meijer, 2008). Refilling as a result of persistent Atlantic inflow, in part perhaps because of the latest Messinian deglaciation (see subsection 2.2; Van der Laan et al., 2006; Hilgen et al., 2007), would have resulted in the establishment of two-way exchange first with the Paratethys at some point during the Lago-Mare phase and later, i.e. slightly before or at the Messinian/Zanclean boundary, with the Atlantic Ocean (Fig. 11c; Marzocchi et al., 2016). The moment the Mediterranean base-level reached the sill with the adjacent water body (Paratethys and Atlantic) and a two-way exchange was initiated, the density contrast will have prompted an enhanced inflow into the Mediterranean (Marzocchi et al., 2016). The overall transgressive trend leading to the Zanclean marine replenishment was accompanied by base-level fluctuations in the order of 400±100 m every precessional cycle (Fig. 11c; Fortuin and Krijgsman, 2003; Ben Moshe et al., 2020; Andreetto et al., 2021). These fluctuations are ascribed to switch in the Mediterranean freshwater budget driven by the African summer monsoon and Atlantic winter storms (e.g. Marzocchi et al., 2015, 2019; Simon et al., 2017). Since higher freshwater discharge rates occur at precession minima times and their Stage 3 sedimentary expression is considered to be the mudstone intervals (Fig. 3a; Manzi et al., 2009), mudstone interbeds (both onshore and offshore; e.g. Figs. 5h-j) represent the highstand episodes (e.g. Manzi et al., 2009; Roveri et al., 2008a; Omodeo-Salé et al., 2012; Fig. 3), while continental facies onshore (e.g. conglomerates in the Apennines; Fig. 5g) and offshore (clastic beds in the Levant Basin) and gypsum beds (Algero-Balearic, Liguro-Provencal, CMD, Tyrrhenian, Caltanissetta, Ionian, Sirte and Polemi-Pissouri basins; Figs. 5h-j) represent the lowstand (e.g. Roveri et al., 2008a; Manzi et al., 2009; Meilijson et al., 2019; Fig. 3). If Atlantic was the major source of sulfate for Stage 3 gypsum (e.g. García-Veigas et al., 2018) and an intervening, relatively shallow (Sicily) sill was establishing Western and Eastern Mediterranean division during the MSC (e.g. Garcia-Castellanos et al., 2009, 2020; Micallef et al., 2018), the presence of Stage 3 gypsum to the east of the Sicily sill (Fig. 2b) implies that the Mediterranean base level never dropped below the (maximum estimated) paleodepth of the sill (i.e. ~430 m; Garcia-Castellanos et al., 2009) during Stage 3 and Western and Eastern Mediterranean remained connected also during the arid (lowstand) phases of the precession cycles.

A Mediterranean step-wise refilled and at times filled with water up to the marginal belt agrees with: (1) Paratethyan biota being present only in intermediate-deeper settings during substage 3.1, but more widespread including marginal settings during substage 3.2; (2) the W-E homogeneity of Paratethyan ostracod assemblages around the Mediterranean marginal belt (Gliozzi et al., 2007; Stoica et al., 2016; Sciuto et al., 2018; Sciuto and Baldanza, 2020; Fig. 9a); (3) the presence, in marginal basins, of Paratethyan fish (Bannikov et al., 2018; Schwarzhans et al., 2020), dinocysts (e.g. Pellen et al., 2017; Fig. 9b) and biomarkers (Vasiliev et al., 2017; Fig. 10c); (4) the occurrence of a monospecific assemblage of abundant *Sphenolithus* spp. just below the M/P boundary at ODP Sites 978, 975 and 967 (Castradori, 1998); (5) the requirement of water from the Mediterranean to explain the Sr isotope ratios of ostracods that inhabited marginal subaqueous environments (Andreetto et al., 2021); (6) the Atlantic-like sulfate values (although variably diluted and affected by microbial processes; Fig. 10b) of the UU/UG gypsum beds (García-Veigas et al., 2018); (7) the presence of long chain alkenones in the Sicilian UG beds similar to those observed in present-day marine settings (Fig. 10c; Vasiliev et al., 2017).

Major problems also exist with the half-full stratified scenario: (1) it does not provide a proper mechanism for gypsum precipitation at several hundreds, or thousands, meters water depth; (2) it fails to explain how unquestionable shallow-water (< 50 m) benthic organisms such as *Ammonia tepida* and *Cyprideis* sp. could survive at hundreds of meters of depth and beyond; (3) it does not provide an explanation for the high abundance of coarse-grained detritus at intermediate and deep-water locations, especially when compared to deep-water Pliocene samples, as well as for the broad absence of MSC deposits in the shelf domain; (4) a persistent Atlantic inflow without outflow seems to be a configuration that cannot be maintained stable for ~200 kyr. Indeed, models coupling the inflow of marine waters with the erosion of the gateway channel concluded that, if the Mediterranean level was lowered by at least several hundred meters below present sea level, any small overtopping of water from the Atlantic would inevitably trigger a fast refill of the basin that, if responsible for the erosion trough the Alborán Basin, should have involved an unprecedented water discharge and be completed within a few years or less (Garcia-Castellanos et al., 2020 and references therein). The scenario arising from Meilijson et al., 2019, Figs. 3b, 4a) is also problematic for a high base-level Mediterranean. In order to simultaneously reach precipitation of gypsum and halite in different basins sharing the same water, the water has to be of high salinity and stratified. Simon and Meijer (2017) demonstrated that this can be achieved with slow overturning circulation, but it is currently unclear how realistic this process is.

7.3. Demise of the MSC (5.33 Ma): the Zanclean marine replenishment

The conspicuous and abrupt transition to normal marine sediments in the Mediterranean is globally and historically important because it is the origin of the stratigraphic position of the Miocene/Pliocene boundary (Van Couvering et al., 2000). From an ocean perspective, it is not an ideal stratigraphic location being difficult to locate from biozone data even in the adjacent Atlantic (Hodell et al., 2001; Krijgsman et al., 2004; Van den Berg et al., 2015). However, from a Mediterranean perspective it provides a clear and unambiguous end to the MSC and the restoration of normal marine conditions. All evidence show that the onset of the Zanclean marine replenishment followed a period of relative lowstand that exposed all the Mediterranean margins (see subsection 3.12; Figs. 6a-b, f) and kept intermediate and deep basins underwater (see subsection 4.8). Yet again, the key dispute concerns the exact depth of the Mediterranean base level preceding the Miocene/Pliocene transition.

Building on the isolated Mediterranean scenario, base level immediately before the early Zanclean was more than thousand kilometers below eustatic sea level (Fig. 10e; e.g. Hsü et al., 1973a; Blanc, 2002; Loget et al., 2006; Garcia-Castellanos et al., 2009; Pérez-Asensio et al., 2012; García-Alix et al., 2016; Amadori et al., 2018; Micallef et al., 2018, 2019; Camerlenghi et al., 2019; Kartveit et al., 2019; Madof et al., 2019; Ben Moshe et al., 2020; Caruso et al., 2020; Cazzini et al., 2020; Mas and Fornós, 2020; Spatola et al., 2020). Hydrodynamic erosional models allowed a reinterpretation of the erosional features across the strait of Gibraltar (Campillo et al., 1992; Blanc, 2002) suggesting that a sudden breach of the Mediterranean-Atlantic divide at Gibraltar resulted in a vast cascade of Atlantic water that refilled the entire Mediterranean in less than 2 years (i.e. rates of ten meters per day) spilling first into the Western Mediterranean (see the extensive review in Garcia-Castellanos et al., 2020) and then, after reaching the level of the Sicily sill, pouring into the Eastern Mediterranean (Micallef et al., 2018, 2019; Ben Moshe et al., 2020; Spatola et al., 2020). This concept of catastrophic refilling has led to terms such as “Zanclean flood” or “deluge”. Evidence supporting the catastrophic flood mechanism mostly comes from the seismic reflection dataset and includes: 1) the presence of >250 m deep and 390-km-long incisions on both sides of the Gibraltar Strait (Garcia-Castellanos et al., 2020); 2) the detection of (allegedly) Pliocene-aged chaotic sedimentary bodies stretching for kilometers in the Alborán Basin (Garcia-Castellanos et al., 2020 and references therein) and Ionian Basin at the foot of the Malta Escarpment (Micallef et al., 2018, 2019; Spatola et al., 2020; Fig. 8c). A further argument is the bathymetric jump of several hundred meters between the late Messinian and the early

Pliocene sediments (e.g. Caruso et al., 2020; Fig. 6d).

Instantaneous sea level rise is not the only possible refilling model. Bache et al. (2012) suggested the reflooding occurred in two steps at ~5.60 Ma, accompanied by a moderate (≤ 500 m) rise, followed by a rapid rise of 600-900 m at around 5.46 Ma tracking the deposition of the deep basin evaporites and resulting from the collapse of the Gibraltar divide. There is also the reconnection model that follows from a Stage 3 Mediterranean that is already relatively full and with the base level possibly oscillating of 400 ± 100 m with precessional frequency (Fig. 10h; Fortuin and Krijgsman, 2003; Ben Moshe et al., 2020; Andreetto et al., 2021). In this case, only a sea level rise of a few hundred meters is required to restore the Mediterranean to the Atlantic level (Fig. 10h), which was hypothesized to have occurred in the last precessional cycle of the Messinian (Marzocchi et al., 2016; Fig. 3a).

In detail, the re-establishment of a fully marine faunal diversity and oceanic geochemistry (e.g. $^{87}Sr/^{86}Sr$ ratios and $\delta^{18}O$) occurred more gradually over one or more precessional cycles in the earliest Zanclean (e.g. Iaccarino et al., 1999; Pierre et al., 1998, 2006; Cipollari et al., 2013; Roveri et al., 2019a; Bulian et al., 2021). This suggests that stressed ecological conditions at first only suitable for opportunistic organisms to survive (e.g. Bulian et al., 2021) developed (or persisted) in the Mediterranean as marine replenishment occurred (e.g. Rouchy et al., 2003). One possible mechanism for achieving this may be the physico-chemical turnover in the water column triggered by the re-established two-way exchange with the Atlantic which, for reasons that are largely unknown, took time (at least oneprecession cycle; Pierre et al., 2006) to displace surficial Paratethyan water and restore normal marine conditions (Marzocchi et al., 2016).

8. Methods and proxies to better reconstruct base level and connectivity changes

Chronological uncertainty and spatial variability limit the use of both sedimentological and paleontological information to achieve a comprehensive and coherent basin-wide interpretation of the conditions and drivers of Stage 3 environments and water levels. Alternative methods are therefore required to clarify connectivity relationships and constrain base-level conditions. This section explores the principles and potential of geochemical, backstripping and numerical modelling techniques that could be used to further test existing hypotheses and enhance understanding of the complex environmental conditions experienced by the Mediterranean during the latest Messinian.

8.1. Geochemical proxies

Radiogenic strontium isotopes. Radiogenic strontium isotope ratio ($^{87}Sr/^{86}Sr$) is a widely applied geochemical tool in provenance studies, including the reconstruction of the hydrological circuit and connectivity of basins with little or null oceanic entries. Its potential to detect the provenance of the hydrological fluxes derives from the unique $^{87}Sr/^{86}Sr$ ratio that typifies each water source and from the negligible effects of isotopic fractionation during the liquid-solid transition (see Hajj et al., 2017).

Mineral phases precipitating in endorheic lakes uptake Sr with $^{87}Sr/^{86}Sr$ ratio that reflects the mixing of all feeding surficial and underground streams and whose $^{87}Sr/^{86}Sr$ fingerprint hinges on the composition and age of watershed bedrock (see Peucker-Ehrenbrink and Fiske, 2019; Andreetto et al., 2021 and references therein). When river water mixes with seawater such as in the oceans, semi-enclosed basins or estuaries, mineral phases uptake Sr with oceanic $^{87}Sr/^{86}Sr$ ratios because the high oceanic Sr concentration (~7.8 mg/l today; Veizer, 1989) masks the impact of the ~100 times lower concentrated continental Sr-sources (~0.0780 mg/l; Palmer and Edmond, 1992). This is valid as long as a certain ratio of continental-marine water mixing is fulfilled, beyond which $^{87}Sr/^{86}Sr$ ratios deviate towards the $^{87}Sr/^{86}Sr$ ratios of the non-marine source(s) (Ingram and Sloan, 1992). For the Mediterranean to attain non-marine $^{87}Sr/^{86}Sr$ ratios (like during the MSC), Topper et al. (2014) calculated a mixing of at least 1:4 (Atlantic: freshwater) to be required.

If Mediterranean subbasins hosted endorheic lakes (Figs. 10c, e), the $^{87}Sr/^{86}Sr$ isotope ratios measured on ostracod valves or gypsum crystals of each lake are expected to generate a scattered distribution by virtue of the different geology in the hinterland of each basin. By contrast, some degree of connection between different basins and the Mediterranean water mass (Figs. 10d, f) is expected to result in more homogeneous $^{87}Sr/^{86}Sr$ ratios because, although isotopically-different, local rivers mix with a water mass that has the same $^{87}Sr/^{86}Sr$ value and (much higher) Sr concentration for each basin (Andreetto et al., 2021). In this scenario, differences in the $^{87}Sr/^{86}Sr$ ratios between basins are likely the reflection of the different $^{87}Sr/^{86}Sr$ ratio of the local input in each basin (Andreetto et al., 2021). The application of numerical models assists to identify and quantify the different water sources feeding the basin(s) in question and (e.g. Placzek et al., 2011; Topper et al., 2011, 2014; Doebbert et al., 2014; Rossi et al., 2015b; Modestou et al., 2017; Grothe et al., 2020; Andreetto et al., 2021).

Sulfate isotopes. When sulfate-bearing minerals precipitate in a basin they uptake dissolved S and O with $\delta^{34}S_{SO4}$ and $\delta^{18}O_{SO4}$ isotopic composition that, once corrected for the fractionation effects during liquid-solid transition (see subsection 6.2), can be assimilated to that of the mother brine. The higher concentrated source of sulfate is seawater (with present-day $\delta^{34}S_{SO4}$=21.15±0.15‰ and $\delta^{18}O_{SO4}$=8.67±0.21‰, Johnston et al., 2014; with Messinian values of ~22±0.2‰ for the $\delta^{34}S_{SO4}$ and ~9±2‰ for the $\delta^{18}O_{SO4}$; Turchyn and Schrag, 2004; Markovic et al., 2016; Masterson et al., 2016). Significantly higher inputs from the ~1000 times less concentrated riverine freshwater (both surficial and underground) with respect to the ocean water (more than 1:5 according to Lu et al., 2001) can modify the marine $\delta^{34}S_{SO4}$ and $\delta^{18}O_{SO4}$ isotopic composition of the mother brine (Utrilla et al., 1992; Lu et al., 2001) and have it deviated from that of the ocean (Lu et al., 2001). This deviation is normally towards lower values, because river-derived dissolved sulfate is generally depleted in heavy isotopes ^{34}S and ^{18}O compared to oceanic sulfate because these isotopes mainly come from the oxidation of ^{34}S-depleted pyrite (FeS_2) on the continents and to a lesser extent from the dissolution of older sulfate-bearing minerals (Claypool et al., 1980; Turchyn and Schrag, 2004; Burke et al., 2018). However, when marine sulfate is preferentially leached in the catchment, ^{34}S of the freshwater-dissolved sulfate and [SO_4^{2-}] likely increase, therefore reducing the continental-marine mixing ratio necessary to deviate the resulting sulfate isotopic signature away from marine values. Unfortunately, the sulfate isotopic composition is not provided for a number of major Mediterranean rivers (Burke et al., 2018) nor for the Eastern Paratethys and it is hardly assessed with the catchment-forming lithologies (Liu et al., 2017; Burke et al., 2018), making sulfate isotopes still an unsuitable tracer of non-marine water provenance in Mediterranean subbasins.

Deviation of $\delta^{34}S_{SO4}$ and $\delta^{18}O_{SO4}$ from the marine average can also be the result of isotopic fractionation during microbial sulfate reduction (MSR; Fritz et al., 1989; Berner, 1999). MSR produces ^{34}S-depleted hydrogen sulfide (~0 to 70‰ lighter than initial sulfate; Brunner and Bernasconi, 2005; Sim et al., 2011; Leavitt et al., 2013) and induces the enrichment in ^{34}S and ^{18}O of the residual sulfate pool (Kaplan and Rittenberg, 1964; Thode and Monster, 1965; Turchyn et al., 2006; Wortmann et al., 2007). Therefore, if isotopically light H_2S produced by MSR leaves the system as a sulfide mineral (most likely pyrite), the resulting dissolved sulfate would have $\delta^{34}S_{SO4}$ and $\delta^{18}O_{SO4}$ isotopic signatures higher than the oceanic one (Brunner et al., 2005). However, if the MSR-produced H_2S is re-oxidized back to sulfate through abiotic or microbial sulfide oxidation, isotopically light sulfate will be brought back to the ^{34}S-enriched sulfate pool, producing little or no enrichment in ^{34}S observed in the resulting sulfate (Gomes and Johnston, 2017 and references therein; Pellerin et al., 2019). Slight deviations from marine $\delta^{18}O_{SO4}$ and $\delta^{34}S_{SO4}$ values of sulfate reflect both biological sulfur

cycling and/or freshwater riverine inputs (e.g. Utrilla et al., 1992; Lu et al., 2001; Turchyn et al., 2009) (Fig. 10b). Untangling the relative importance of these processes is key to understanding the Mediterranean sulfur isotope record and gleaning paleoenvironmental insights into Stage 3.

Hydrogen isotopes. Organic geochemistry biomarker-based tools can be used as independent proxies for reconstructing sea surface temperatures, relative changes in the basin hydrology and, indirectly, salinity. Basin water properties are reflected in a variety of life forms. Different types of organisms produce specific organic compounds that serve as molecular biomarkers. These large biomolecules record the changes in the hydrogen isotopic composition of the water used by different groups of biomarker producers (i.e. different organisms). The principle behind the method is to measure δD on biomarkers produced in Mediterranean Sea waters (e.g. alkenones, produced by a few species of haptophyte coccolithophores algae) during the MSC and compare the results with the δD signals retrieved from biomarkers produced in the open ocean ideally at the same time intervals. The influence of precipitation on the changes in hydrological budget can be monitored by measuring the δD of long chain *n*-alkanes (Sachse et al., 2006), biomarkers predominantly produced by higher terrestrial plants that rely on precipitation for plant growth, therefore reflecting the changes in the δD of the precipitation. The extreme base level drop(s) suggested for the Mediterranean during the MSC would, in principle, indicate a negative precipitation (P) + runoff (R) – evaporation (E) ratio. Such a negative water budget (E>P+R) results in waters increasingly enriched in δD whereas, a positive water balance (E<P+R) results instead in a negative shift of δD values. The analysis of compound specific δD of alkenones, long and short chain *n*-alkanes can be used to constrain E/(P+E) relationships.

8.2. Backstripping analyses

Backstripping uses paleobathymetry, sea level and sediment thickness to quantify the tectonic and isostatic components of subsidence. If tectonic subsidence or uplift history are known relative to the current position and depth of paleoshoreline markers, an inverse approach allows base level to be estimated. A number of approaches have been applied to the MSC, using erosional surfaces (e.g. Amadori et al., 2018), terraces (Micallef et al., 2018) or fluvial network characteristics (Urgeles et al., 2011) as paleoshoreline indicators. The relief on erosional features has also been used to estimate minimum base-level variation (Frey-Martinez et al., 2004).

Apart from the quantitative constraints on base level that backstripping provides, consideration of the regional implications of isostatic subsidence and the gravitational impact of redistributing water masses (such as in the cascading model of Roveri et al., 2014c; Fig. 10b) and evaporite precipitation is important in gateway regions like Gibraltar, which due to their shallow and restricted nature are exceptionally sensitive to vertical motions. Here, both flexural effects and gravitational effects on local sea level on the Atlantic side of the strait has the potential to influence Mediterranean-Atlantic connectivity driving paleoenvironmental changes in the basin itself (Coulson et al., 2019).

8.3. Modelling

Numerical models can be used complementary to lab- and field-based studies, or to find answers to open questions by testing the physical plausibility of hypotheses and their compatibility with the available sedimentological/stratigraphic/paleontological/geochemical data, which have to constrain model results and not adjust to it. For example, whether gypsum beds in marginal/intermediate basins can precipitate at the same time as the halite in deep basins is an intriguing question that circulates in the MSC literature (e.g. Van Couvering et al., 1976), but whether this is physically and geochemically possible is yet to be answered. In a first model analysis, Simon and Meijer (2017) found that the required stratification can indeed be achieved for specific conditions including a slow overturning circulation. A different approach is needed to determine whether such slow circulation is to be expected or if other scenarios should be considered. A thermo-haline stratification that enables coeval precipitation of two evaporites for a considerable time span might also influence the degree of heterogeneity of other parameters, such as strontium concentration. Previous models showed the influence of the Atlantic Ocean and major rivers (Topper et al., 2014) and of evaporation (Flecker et al., 2002) on the Sr value of a basin with restricted oceanic inflow and assuming a homogeneous distribution of strontium throughout the water column (Flecker et al., 2002; Topper et al., 2011, 2014; Modestou et al., 2017), but it is uncertain if this holds true in conditions of water stratification. New insights into this behavior would have consequences for the way the strontium dataset (Fig. 10a) must be interpreted. Another loose end where the model approach can provide insight relates to the question whether a high water level could have been reached without an inflow from the Atlantic. Climate simulations conducted by Gladstone et al. (2007), Simon et al. (2017) and Marzocchi et al. (2019) indicate that this is not possible with today's bathymetry. A quantitative analysis exploring the Mediterranean water level reached in different situations (i.e. with or without an Atlantic or Paratethys in and outflow) and with information on the Mediterranean hypsometry that may be provided by isostatic restoration of the seafloor topography (flexural backstripping) could help understanding how the Messinian Salinity Crisis ended.

9. Certainties, open problems and future directions

Our understanding of the nature of MSC Stage 3 has evolved considerably over the last fifty years. However, there are still such disparate models for the paleoenvironmental conditions and basin connectivity that led to Stage 3 deposition and that express the challenges that the study of this interval presents: it is a relatively short interval and its sedimentary expression varies spatially. It is no surprise that the main point of contention lies in reconciling the observations from seismic profiles and well data, which are largely interpreted as favoring the desiccated scenario, with the sedimentological, paleontological and geochemical data from the marginal basins record, largely discontinuous and unaddressed from seismic-based and computational-based studies and mainly supporting the full-Mediterranean hypothesis.

To a large extent this mismatch is the result of the lack of intersection of the two datasets. Some Stage 3 onshore localities are meticulously studied from the stratigraphic, sedimentological, paleontological and geochemical point of view, showing remarkably consistent and homogenous trends and patterns (as previously highlighted by Roveri et al., 2008a). However, changes at precessional and subprecessional scale are difficult to trace from one exposure to another and are well below the level of seismic resolution, making onshore-offshore correlation at this scale impossible. Even correlation between onshore sections is problematic since most of the stratigraphic sections are incomplete, with erosion surfaces at the bottom and/or top (i.e. the Miocene/Pliocene boundary), and this lack of stratigraphic continuity frustrates attempts to constrain ages by cyclostratigraphy. A future focus on strengthening the available chronostratigraphic framework (Fig. 3) and making it inclusive of the fragmented outcrops is required to better understand the paleoenvironmental and paleohydrological changes suffered by the Mediterranean marginal belt through time. The successful drilling of the three IODP proposals currently in the scheduling pool (see Camerlenghi and Aloisi, 2020), all of which propose to recover Stage 3 sediments, will also provide transformative information enabling far better offshore-onshore correlation and interpretation of currently enigmatic seismic data. In the meantime, re-evaluation of existing DSDP and ODP material, particularly through the application of more novel geochemical techniques and, where possible, access to material collected during industrial drilling would be helpful for understanding the deep Mediterranean Basin during this interval.

Extensive paleontological studies have established that Stage 3

contains *in situ* biota assemblages of Paratethyan provenance implying brackish water conditions. More problematic is the differentiation of in situ and reworked marine microfauna and flora and the paleoecological significance of dwarfism in marine calcareous microfossils/algae. These have important repercussions for the Mediterranean connectivity and base-level reconstruction.

The geochemical dataset for Stage 3, particularly strontium isotopes and hydrogen isotopes on biomarkers, is both demonstrably valuable in providing key constraints on connectivity and environmental conditions, and frustratingly inadequate in terms of data distribution. It has great potential as a constraint on quantitative sensitivity analysis of the different hydrochemistry scenarios that follow from the endmember Stage 3 hypotheses, but substantially more data is required.

An approach which combines geological, geochemical, geophysical and paleontological data with numerical modelling (e.g. climate simulations, backstripping analyses and paleoceanographic models) will provide a more accurate reconstruction of Mediterranean paleogeography and the processes that occurred during the final phase of the Messinian Salinity Crisis.

Data availability

The compilation of strontium, sulfate and hydrogen isotope data plotted in figure 9, as well as some of the available, and here not (graphically) shown, oxygen isotope values is accessible in separate excel spreadsheets (Supplementary material 1).

Declaration of Competing Interest

The authors whose names are listed immediately below certify that they have NO affiliations with or involvement in any organization or entity with any financial interest (such as honoraria; educational grants; participation in speakers' bureaus; membership, employment, consultancies, stock ownership, or other equity interest; and expert testimony or patent-licensing arrangements), or non-financial interest (such as personal or professional relationships, affiliations, knowledge or beliefs) in the subject matter or materials discussed in this manuscript.

Acknowledgments

We thank the entire SALTGIANT community for many profitable workshops that inspired the development of this manuscript. This research was supported by the project SALTGIANT-Understanding the Mediterranean Salt Giant, a European project which has received funding from the European Union's Horizon 2020 research and innovation program, under the Marie Sklodowska-Curie [grant agreement No 765256]. We greatly thank the two reviewers Domenico Cosentino and William Ryan and the editor Alessandra Negri for the fruitful comments provided that led to a substantial improvement of the manuscript.

Appendix A. Supplementary data

Supplementary data to this article can be found online at https://doi.org/10.1016/j.earscirev.2021.103577.

References

Abdel Aal, A., El Barkooky, A., Gerrits, M., Meyer, H., Schwander, M., Zaki, H., 2000. Tectonic evolution of the eastern Mediterranean Basin and its significance for hydrocarbon prospectivity in the ultradeepwater of the Nile Delta. Lead. Edge 19, 1086–1102. https://doi.org/10.1190/1.1438485.

Abdel-Fattah, M.I., 2014. Petrophysical characteristics of the messinian abu madi formation in the baltim east and north fields, offshore Nile delta, Egypt. J. Pet. Geol. 37 (2), 183–195.

Agiadi, K., Antonarakou, A., Kontakiotis, G., Kafousia, N., Moissette, P., Cornée, J.-J., Manoutsoglou, E., Karakitsios, V., 2017. Connectivity controls on the late Miocene eastern Mediterranean fish fauna. Int. J. Earth Sci. 106, 1147–1159. https://doi.org/10.1007/s00531-016-1355-7.

Agnini, C., Monechi, S., Raffi, I., 2017. Calcareous nannofβossil biostratigraphy: historical background and alication in Cenozoic chronostratigraphy. Lethaia 50 (3), 447–463.

Aguirre, J., Sánchez-Almazo, I.M., 2004. The Messinian post-evaporitic deposits of the Gafares area (Almeria-Nijar basin, SE Spain). A new view of the "Lago-Mare" facies. Sediment. Geol. 168, 71–95.

Amadori, C., Garcia-Castellanos, D., Toscani, G., Sternai, P., Fantoni, R., Ghielmi, M., Di Giulio, A., 2018. Restored topography of the Po Plain-Northern Adriatic region during the Messinian base level drop-Implications for the physiography and compartmentalization of the paleo-Mediterranean basin. Basin Res. 30 (6), 1247–1263. https://doi.org/10.1111/bre.12302.

Andersen, N., Paul, H.A., Bernasconi, S.M., McKenzie, J.A., Behrens, A., Schaeffer, P., Albrecht, P., 2001. Large and rapid climate variability during the Messinian salinity crisis: evidence from deuterium concentrations of individual biomarkers. Geology 29, 799–802.

Andreetto, F., Matsubara, K., Beets, C.J., Fortuin, A.R., Flecker, R., Krijgsman, W., 2021. High Mediterranean water-level during the Lago-Mare phase of the Messinian Salinity Crisis: insights from the Sr isotope records of Spanish marginal basins (SE Spain). Paleogeogr. Paleoclimatol. Paleoecol. 562.

Andrusov, D., 1890. Les Dreissenidae fossiles et actuelles d'Eurasie. Geol. Min. 25, 1–683 (in Russian).

Arab, M., Rabineau, M., Déverchère, J., Bracene, R., Belhai, D., Roure, F., Marok, A., Bouyahiaoui, B., Granjeon, D., Andriessen, P., Sage, F., 2016. Tectonostratigraphic evolution of the eastern Algerian margin and basin from seismic data and onshore-offshore correlation. Mar. Pet. Geol. 77, 1355–1375. https://doi.org/10.1016/j.marpetgeo.2016.08.021.

Arenas, C., Pomar, L., 2010. Microbial deposits in upper Miocene carbonates, Mallorca, Spain. Paleogeogr. Paleoclimatol. Paleoecol. 297 (2), 465–485.

Aufgebauer, A., McCann, T., 2010. Messinian to Pliocene transition in the deep part of the Sorbas Basin, SE Spain-a new description of the depositional environment during the Messinian Salinity Crisis. Neues Jahrbuch für Geologie und Paläontologie-Abhandlungen 259 (2), 177–195.

Azdimousa, A., Poupeau, G., Rezqi, H., Asebriy, L., Bourgois, J., Ait Brahim, L., 2006. Geodynamique des bordures meridionales de la mer d'Alboran; alication de la stratigraphie sequentielle dans le bassin neogene de Boudinar Rif oriental. Maroc. Bull. Inst. Sci. Rabat 28, 9–18.

Bache, F., Olivet, J.-L., Gorini, C., Rabineau, M., Baztan, J., Aslanian, D., Suc, J.-P., 2009. Messinian erosional and salinity crisis: view from the Provence basin (Gulf of Lions, western Mediterranean). Earth Planet. Sci. Lett. 286, 139–157.

Bache, F., Popescu, S.-M., Rabineau, M., Gorini, C., Suc, J.-P., Clauzon, G., Olivet, J.-L., Rubino, J.-L., Melinte-Dobrinescu, M.C., Estrada, F., Londeix, L., Armijo, R., Meyer, B., Jolivet, L., Jouannic, G., Leroux, E., Aslanian, D., Reis, A.T.D., Mocochain, L., Dumurdžanov, N., Zagorchev, I., Lesić, V., Tomić, D., Namık Çağatay, M., Brun, J.-P., Sokoutis, D., Csato, I.T., Ucarkus, G., Çakır, Z., 2012. A two-step process for the reflooding of the Mediterranean after the Messinian Salinity Crisis. Basin Res. 24, 125–153. https://doi.org/10.1111/j.1365-2117.2011.00521.x.

Backman, J., Raffi, I., Rio, D., Fornaciari, E., Pälike, H., 2012. Biozonation and biochronology of Miocene through Pleistocene calcareous nannofossils from low and middle latitudes. Newsl. Stratigr. 45, 221–244.

Bannikov, A.F., Schwarzhans, W., Carnevale, G., 2018. Neogene Paratethyan croakers (Teleostei, Sciaenidae). Riv. Ital. Paleontol. Stratigr. 124, 535–571.

Barra, D., Bonaduce, G., Sgarrella, E., 1998. Paleoenvironmental bottom water conditions in the early Zanclean of the Capo Rossello area (Agrigento, Sicily). Boll. Soc. Paleontol. Ital. 37, 61–88.

Bassetti, M.A., Miculan, P., Lucchi, F.R., 2003. Ostracod faunas and brackish-water environments of the late Messinian Sapigno section (northern Apennines, Italy). Paleogeogr. Paleoclimatol. Paleoecol. 198 (3-4), 335–352.

Bassetti, M.A., Manzi, V., Lugli, S., Roveri, M., Longinelli, A., Lucchi, F.R., Barbieri, M., 2004. Paleoenvironmental significance of Messinian post-evaporitic lacustrine carbonates in the northern Apennines, Italy. Sediment. Geol. 172 (1–2), 1–18.

Bassetti, M.A., Miculan, P., Sierro, F.J., 2006. Evolution of depositional environments after the end of Messinian Salinity Crisis in Nijar basin (SE Betic Cordillera). Sediment. Geol. 188-189, 279–295.

Ben Moshe, L., Ben-Avraham, Z., Enzel, Y., Schattner, U., 2020. Estimating drawdown magnitudes of the Mediterranean Sea in the Levant basin during the Lago Mare stage of the Messinian Salinity Crisis. Mar. Geol. 106215 https://doi.org/10.1016/j.margeo.2020.106215.

Ben-Gal, Y., Ben-Avraham, Z., Buchbinder, B., Kendall, C.G.S.C., 2005. Post-Messinian evolution of the Southeastern Levant Basin based on two-dimensional stratigraphic simulation. Mar. Geol. 221 (1-4), 359–379.

Benson, R.H., 1978. The paleoecology of the ostracods of DSDP Leg 42A. In: Hsü, K., Montadert, L. (Eds.), Initial Reports of the Deep-Sea Drilling Project, 42. U.S. Government Printing Office, Washington, pp. 777–787.

Benson, R.H., Rakic-El Bied, K., 1991. The Messinian parastratotype at Cuevas de Almanzora, Vera Basin, SE Spain; refutation of the deep-basin, shallow-water hypothesis? Micropaleontology 37 (3), 289–302.

Benson, R.H., Rakic-El Bied, K., Bonaduce, G., 1991. An important current reversal (influx) in the Rifian Corridor (Morocco) at the Tortonian-Messinian boundary: the end of Tethys Ocean. Paleoceanography 6 (1), 165–192.

Berner, R.A., 1999. Atmospheric oxygen over Phanerozoic time. Proc. Natl. Acad. Sci. 96, 10955.

Bertini, A., 2006. The Northern Apennines palynological record as a contribute for the reconstruction of the Messinian paleoenvironments. Sediment. Geol. 188, 235–258.

Bertini, A., Corradini, D., 1998. Biostratigraphic and paleoecological significance of Galeacysta etrusca in the "Lago-Mare" facies from the Mediterranean area (Neogene). Dino NTNU Vitensk. Mus. Rapp. Bot. ser. 6, 15–16. Abstract.
Bertoni, C., Cartwright, J., 2007. Major erosion at the end of the Messinian Salinity Crisis: evidence from the Levant Basin, Eastern Mediterranean. Basin Res. 19, 1–18.
Bessis, F., 1986. Some remarks on the study of subsidence of sedimentary basins. Application to the Gulf of Lions margin (Western Mediterranean). Mar. Pet. Geol. 3, 37–63.
Bialik, O.M., Frank, M., Betzler, C., Zammit, R., Waldmann, N.D., 2019. Two-step closure of the Miocene Indian Ocean Gateway to the Mediterranean. Sci. Rep. 9 (1), 1–10. https://doi.org/10.1038/s41598-019-45308-7.
Biscaye, P.E., Ryan, W.B.F., Wezel, F.C., 1972. Age and nature of the Pan-Mediterranean subbottom reflector M. The Mediterranean Sea 83–90.
Blanc, P.L., 2002. The opening of the Plio-Quaternary Gibraltar Strait: assessing the size of a cataclysm. Geodin. Acta 15, 303–317.
Blanc-Valleron, M.-M., Rouchy, J.-M., Pierre, C., Badaut-Trauth, D., Schuler, M., 1998. Evidence of Messinian nonmarine deposition at site 968 (Cyprus lower slope). In: Proceedings of the Ocean Drilling Program, Scientific Results. ODP Sci. Results 160, Texas, USA, pp. 43–445.
Bonaduce, G., Sgarrella, F., 1999. Paleoecological interpretation of the latest Messinian sediments from southern Sicily (Italy). Soc. Geol. Ital. Mem. 54, 83–91.
Booth-Rea, G., Ranero, R., Grevemeyer, I.C., 2018. The Alboran volcanic-arc modulated the Messinian faunal exchange and salinity crisis. Sci. Rep. 8 https://doi.org/10.1038/s41598-018-31307-7.
Borsetti, A.M., Curzi, P.V., Landuzzi, V., Mutti, M., Ricci Lucchi, F., Sartori, R., Tomadin, L., Zuffa, G.G., 1990. Messinian and pre-Messinian sediments from ODP Leg 107 Sites 652 and 654 in the Tyrrhenian Sea: sedimentologic and petrographic study and possible comparisons with Italian sequences. In: Kastens, K.A., Mascle, J., et al. (Eds.), Proceedings of the Ocean Drilling Program, Scientific Results, 107, pp. 169–186.
Bossio, A., Esteban, M., Giannelli, L., Longinelli, A., Mazzanti, R., Mazzei, R., Ricci Lucchi, F., Salvatorini, G., 1978. Some aspects of the upper Miocene in Tuscany. In: Messinian Seminar, vol. 4. Pacini, Pisa, 88 pp.
Bossio, A., Costantini, A., Lazzarotto, A., Liotta, D., Mazzanti, R., 1993. Rassegna delle conoscenze sulla stratigrafia del Neoautoctono toscano. Mem. Soc. Geol. Ital. 49, 17–98.
Bosworth, W., Huchon, P., Mc Clay, K., 2005. The Red Sea and Gulf of Aden Basins. J. Afr. Earth Sci. 43, 334–378.
Bowman, S.A., 2012. A comprehensive review of the MSC facies and their origins in the offshore Sirt Basin, Libya. Pet. Geosci. 18, 457–469. https://doi.org/10.1144/petgeo2011-070.
Braga, J.C., Martín, J.M., Riding, R., Aguirre, J., Sanchez-Almazo, I.M., Dinares-Turell, J., 2006. Testing models for the Messinian salinity crisis: the Messinian record in Almería, SE Spain. Sediment. Geol. 188-189, 131–154. https://doi.org/10.1016/j.sedgeo.2006.03.002.
Brolsma, M.J., 1975. Lithostratigraphy and Foraminiferal assemblages of the Miocene/Pliocene transitional strata at Capo Rossello and Eraclea Minoa (Sicily, Italy): Kon. Ned. Akad. Wetensch. Amsterdam Proc 78, 1–40.
Brunner, B., Bernasconi, S.M., 2005. A revised isotope fractionation model for dissimilatory sulfate reduction in sulfate reducing bacteria. Geochim. Cosmochim. Acta 69, 4759–4771.
Brunner, B., Bernasconi, S.M., Kleikemper, J., Schroth, M.H., 2005. A model for oxygen and sulfur isotope fractionation in sulfate during bacterial sulfate reduction processes. Geochim. Cosmochim. Acta 69, 4773–4785.
Bulian, F., Sierro, F.J., Santiago, L., Jiménez-Espejo, F.J., Bassetti, M.A., 2021. Messinian West Alboran Sea record in the proximity 1 of Gibraltar: early signs of Atlantic-Mediterranean gateway restriction. Mar. Geol. 434.
Burke, A., Present, T.M., Paris, G., Rae, E.C.M., Sandilands, B.H., Gaillardet, J., Peucker-Ehrenbrink, B., Fischer, W.W., McClelland, J.W., Spencer, R.G.M., Voss, B.M., Adkins, J.F., 2018. Sulfur isotopes in rivers: Insights into global weathering budgets, pyrite oxidation, and the modern sulfur cycle. Earth Planet. Sci. Lett. 496, 168–177.
Butler, R.W.H., Likhorish, W.H., Grasso, M., Pedley, H.M., Ramberti, L., 1995. Tectonics and sequence stratigraphy in Messinian Basins, Sicily: constraints on the initiation and termination of the Mediterranean salinity crisis. Geol. Soc. Am. Bull. 107, 425–439.
Butler, R.W.H., Maniscalco, R., Sturiale, G., Grasso, M., 2015. Stratigraphic variations control deformation patterns in evaporite basins: Messinian examples, onshore and offshore Sicily (Italy). J. Geol. Soc. 172, 113–124.
Camerlenghi, A., Aloisi, V., 2020. Uncovering the Mediterranean Salt Giant (MEDSALT)-Scientific Networking as Incubator of Cross-disciplinary Research in Earth Sciences. Eur. Rev. 28 (1), 40–61. https://doi.org/10.1017/S1062798719000255.
Camerlenghi, A., Accettella, D., Costa, S., Lastras, G., Acosta, J., Canals, M., Wardell, N., 2009. Morphogenesis of the SW Balearic continental slope and adjacent abyssal plain, Western Mediterranean Sea. Int. J. Earth Sci. 98, 735–750.
Camerlenghi, A., Del Ben, A., Hübscher, C., Forlin, E., Geletti, R., Brancatelli, G., Micallef, A., Saule, M., Facchin, L., 2019. Seismic markers of the Messinian salinity crisis in the deep Ionian Basin. Basin Res bre.12392. https://doi.org/10.1111/bre.12392.
Cameselle, A.L., Urgeles, R., 2017. Large-scale margin collapse during Messinian early sea-level drawdown: the SW Valencia trough, NW Mediterranean. Basin Res. 29, 576–595. https://doi.org/10.1111/bre.12170.
Cameselle, A.L., Urgeles, R., De Mol, B., Camerlenghi, A., Canning, J.C., 2014. Late Miocene sedimentary architecture of the Ebro Continental Margin (Western Mediterranean): implications to the Messinian Salinity Crisis. Int. J. Earth Sci. 103 (2), 423–440.
Campillo, A.C., Maldonado, A., Mauffret, A., 1992. Stratigraphic and Tectonic evolution of the Western Alboran Sea late Miocene to recent. Geo-Mar. Lett. 12, 165–172.
Capella, W., Flecker, R., Hernández-Molina, F.J., Simon, D., Meijer, P.T., Rogerson, M., Sierro, F.J., Krijgsman, W., 2019. Mediterranean isolation preconditioning the Earth System for late Miocene climate cooling. Sci. Rep. 9 (1), 1–8. https://doi.org/10.1038/s41598-019-40208-2.
Capella, W., Spakman, W., van Hinsbergen, D.J., Chertova, M.V., Krijgsman, W., 2020. Mantle resistance against Gibraltar slab dragging as a key cause of the Messinian Salinity Crisis. Terra Nova 32 (2), 141–150. https://doi.org/10.1111/ter.12442.
Capellini, G., 1880. Gli strati a Congerie o la formazione gessoso solfifera nella provincia di Pisa e nei dintorni di Livorno. Mem. R. Accad. Lincei., Cl. Sci. Fis. Mat. Nat. 5, 1–64.
Carbonnel, G., 1978. La zone à Loxoconcha djaffarovi Schneider (ostracodes, Miocène supérieur) ou le Messinien de la vallée du Rhône. Rev. Micropaleontol. 21 (3), 106–118.
Carnevale, G., Landini, W., Sarti, G., 2006a. Mare versus Lago-mare: marine fishes and the Mediterranean environment at the end of the Messinian Salinity Crisis. J. Geol. Soc. 163 (1), 75–80. https://doi.org/10.1144/0016-764904-158.
Carnevale, G., Caputo, D., Landini, W., 2006b. Late Miocene fish otoliths from the Colombacci Formation (Northern Apennines, Italy): implications for the Messinian 'Lago-mare'event. Geol. J. 41 (5), 537–555. https://doi.org/10.1002/gj.1055.
Carnevale, G., Longinelli, A., Caputo, D., Barbieri, M., Landini, W., 2008. Did the Mediterranean marine reflooding precede the Miocene/Pliocene boundary? Paleontological and geochemical evidence from upper Messinian sequences of Tuscany, Italy. Paleogeogr. Paleoclimatol. Paleoecol. 257, 81–105. https://doi.org/10.1016/j.paleo.2007.09.005.
Carnevale, G., Dela Pierre, F., Natalicchio, M., Landini, W., 2018. Fossil marine fishes and the "Lago Mare" event: Has the Mediterranean ever transformed into a brackish lake? Newsl. Stratigr. 51, 57–72. https://doi.org/10.1127/nos/2016/0343.
Carnevale, G., Gennari, R., Lozar, F., Natalicchio, M., Pellegrino, L., Dela Pierre, F., 2019. Living in a deep desiccated Mediterranean Sea: An overview of the Italian fossil record of the Messinian salinity crisis. Boll. Soc. Paleontol. Ital. 58, 109–140. https://doi.org/10.4435/BSPI.2019.04.
Cartwright, J.A., Jackson, M.P.A., 2008. Initiation of gravitational collapse of an evaporitic basin margin: the Messinian saline giant, Levant Basin, eastern Mediterranean. Geol. Soc. Am. Bull. 120, 399–413.
Caruso, A., Pierre, C., Blanc-Valleron, M.M., Rouchy, J.M., 2015. Carbonate deposition and diagenesis in evaporitic environments: the evaporative and sulphur-bearing limestones during the settlement of the Messinian Salinity Crisis in Sicily and Calabria. Palaeogeogr. Palaeoclimatol. Palaeoecol. 429, 136–162. https://doi.org/10.1016/j.palaeo.2015.03.035.
Caruso, A., Blanc-Valleron, M.M., Da Prato, S., Pierre, C., Rouchy, J.M., 2020. The late Messinian "Lago-Mare" event and the Zanclean Reflooding in the Mediterranean Sea: new insights from the Cuevas del Almanzora section (Vera Basin, South-Eastern Spain). Earth Sci. Rev. 200, 102993 https://doi.org/10.1016/j.earscirev.2019.102993.
Casati, P., Bertozzi, P., Cita, M.B., Longinelli, A., Damiani, V., 1976. Stratigraphy and paleoenvironment of the Messinian "Colombacci" Formation in the periadriatic trough. A pilot study. Memorie della Società Geologica Italiana 16, 173–195.
Castradori, D., 1998. Calcareous nannofossils in the basal Zanclean of the Eastern Mediterranean Sea: remarks on paleoceanography and sapropel formation. In: Robertson, A.H.F., Emeis, K.C., Richter, C., Camerlenghi, A. (Eds.), Proceedings of the Ocean Drilling Program. US Government Printing Office, Washington, pp. 113–123. Scientific Results 160.
Catalano, R., Valenti, V., Albanese, C., Accaino, F., Sulli, A., Tinivella, U., Morticelli, M. G., Zanolla, C., Giustiniani, M., 2013. Sicily's fold–thrust belt and slab roll-back: the SI. RI. PRO. seismic crustal transect. J. Geol. Soc. 170 (3), 451–464.
Cazzini, F.F., Amadori, C., Bosino, A., Fantoni, R., 2020. New seismic evidence of the Messinian paleomorphology beneath Lake Maggiore area (Italy). Ital. J. Geosci. 139 (2), 195–211. https://doi.org/10.3301/IJG.2019.26.
Chumakov, I.S., 1973. Pliocene and Pleistocene deposits of the Nile valley in Nubia and upper Egypt. In: Ryan, W.B.F., Hsu, K.J., et al. (Eds.), Initial Reports of the Deep Sea Drilling Project, 13. US Govern. Print. Office, Washington, DC, pp. 1242–1243.
Cipollari, P., Cosentino, D., Gliozzi, E., 1999. Extension-and compression-related basins in central Italy during the Messinian Lago-Mare event. Tectonophysics 315 (1-4), 163–185.
Cipollari, P., Cosentino, D., Radeff, G., Schildgen, T.F., Faranda, C., Grossi, F., Gliozzi, E., Smedile, A., Gennari, R., Darbas, G., Dudas, F.Ö., Gürbüz, K., Nazik, A., Echtler, H., 2013. Easternmost Mediterranean evidence of the Zanclean flooding event and subsequent surface uplift: Adana Basin, southern Turkey. Geol. Soc. Lond., Spec. Publ. 372 (1), 473–494. https://doi.org/10.1144/SP372.5.
Cita, M.B., 1973. Inventory of biostratigraphical findings and problems. Init. Rep. Deep-Sea Drill. Proj. 13 (2), 1045–1065.
Cita, M.B., Colombo, L., 1979. Sedimentation in the latest Messinian at Capo Rossello (Sicily). Sedimentology 26, 497–522.
Cita, M.B., Wright, R.C., Ryan, W.B.F., Longinelli, A., 1978. Messinian paleoenvironments. In: Hsü, K.J., Montadert, L., et al. (Eds.), Initial Reports of the Deep Sea Drilling Project, 42. U.S. Government Printing Office, Washington D.C, pp. 1003–1035.
Cita, M.B., Santambrogio, S., Melillo, B., Rogate, F., 1990. Messinian Paleoenvironments: New Evidence from the Tyrrhenian Sea (ODP LEG 107). In: Proceedings of the Ocean Drilling Program, Scientific Results, 107, pp. 211–227.
Clauzon, G., 1982. Le canyon messinien du Rhône: Une preuve decisive du "dessicated deep basin model" (Hsu¨, Cita et Ryan, 1973). Bull. Soc. Geol. Fr. 24, 231–246.

Clauzon, G., Suc, J.-P., Gautier, F., Berger, A., Loutre, M.F., 1996. Alternate interpretation of the Messinian salinity crisis, controversy resolved? Geology 24, 363–366.
Clauzon, G., Suc, J.P., Popescu, S.M., Marunteanu, M., Rubino, J.L., Marinescu, F., Melinte, M.C., 2005. Influence of Mediterranean sea-level changes on the Dacic Basin (Eastern Paratethys) during the late Neogene: the Mediterranean Lago Mare facies deciphered. Basin Res. 17 (3), 437–462. https://doi.org/10.1111/j.1365-2117.2005.00269.x.
Clauzon, G., Suc, J.-P., Do Couto, D., Jouannic, G., Melinte-Dobrinescu, M.C., Jolivet, L., Quillévéré, F., Lebret, N., Mocochain, L., Popescu, S.-M., Martinell, J., Doménech, R., Rubino, J.-L., Gumiaux, C., Warny, S., Bellas, S.M., Gorini, C., Bache, F., Rabineau, M., Estrada, F., 2015. New insights on the Sorbas Basin (SE Spain): the onshore reference of the Messinian salinity crisis. Mar. Pet. Geol. 66, 71–100. https://doi.org/10.1016/j.marpetgeo.2015.02.016.
Claypool, G.E., Holser, W.T., Kaplan, I.R., Sakai, H., Zak, I., 1980. The age curves of sulfur and oxygen isotopes in marine sulfate and their mutual interpretation. Chem. Geol. 28, 199–260.
Colalongo, M.L., Cremonini, G., Farabegoli, E., Sartori, R., Tampieri, R., Tomadin, L., 1976. Paleoenvironmental study of the "Colombacci" Formation in Romagna (Italy): the cella section. Mem. Soc. Geol. Ital. 16, 197–216.
Colombero, S., Alba, D.M., D'Amico, C., Delfino, M., Esu, D., Giuntelli, P., Harzhauser, M., Mazza, P.P.A., Mosca, M., Neubauer, T.A., Pavia, G., Pavia, M., Villa, A., Carnevale, G., 2017. Late Messinian mollusks and vertebrates from Moncucco Torinese, north-western Italy. Paleoecological and paleoclimatological implications. Palaeontol. Electron. 1–66, 20.1.10A.
Comas, M.C., Zahn, R., Klaus, A., et al., 1996. Proceedings of the Ocean Drilling Program, Initial Reports, v. 161: College Station, Texas, Ocean Drilling Program.
Comas, M.C., Platt, J.P., Soto, J.I., Watts, A.B., 1999. 44. The origin and tectonic history of the Alboran Basin: Insights from leg 161 results: Proceedings of the Ocean Drilling Program. Sci. Res. 161, 555–580.
Consorti, L., Sabbatino, M., Parente, M., 2020. Insights on the paleoecology of Ammonia (Foraminifera, Rotalioidea) from Miocene carbonates of central and southern Apennines (Italy). Palaeogeogr. Palaeoclimatol. Palaeoecol. 110105 https://doi.org/10.1016/j.palaeo.2020.110105.
Corbí, H., Soria, J.M., 2016. Late Miocene-early Pliocene planktonic foraminifer event-stratigraphy of the Bajo Segura basin: a complete record of the western Mediterranean. Mar. Pet. Geol. 77, 1010–1027. https://doi.org/10.1016/j.marpetgeo.2016.08.004.
Corbí, H., Soria, J.M., Lancis, C., Giannetti, A., Tent-Manclús, J.E., Dinarès-Turell, J., 2016. Sedimentological and paleoenvironmental scenario before, during, and after the Messinian Salinity Crisis: The San Miguel de Salinas composite section (western Mediterranean). Mar. Geol. 379, 246–266. https://doi.org/10.1016/j.margeo.2016.05.017.
Corbí, H., Soria, J.M., Giannetti, A., Yébenes, A., 2020. The step-by-step restriction of the Mediterranean (start, amplification, and consolidation phases) preceding the Messinian Salinity Crisis (climax phase) in the Bajo Segura basin. Geo-Mar. Lett. 1–21. https://doi.org/10.1007/s00367-020-00647-7.
Cornée, J.J., Munch, P., Achalhi, M., Merzeraud, G., Azdimousa, A., Quillevere, F., Melinte-Dobrinescu, M., Chaix, C., Ben Moussa, A., Lofi, J., Seranne, A., Moissette, P., 2016. The Messinian erosional surface and early Pliocene reflooding in the Alboran Sea: new insights from the Boudinar basin. Morocco. Sediment. Geol. 333, 115–129. https://doi.org/10.1016/j.sedgeo.2015.12.014.
Corradini, D., Biffi, U., 1988. Etude des dinokystes a la limite Messinien-Pliocene dans la coupe Cava Serredi, Tos cane, Italie. Bulletin des Centres de Recherche Exploration-Production Elf-Aquitaine 12 (1), 221–236.
Cosentino, D., Cipollari, P., Mastro, S.L., Giampaolo, C., 2005. High-frequency cyclicity in the latest Messinian Adriatic foreland basin: insight into paleoclimate and paleoenvironments of the Mediterranean Lago-Mare episode. Sediment. Geol. 178 (1–2), 31–53. https://doi.org/10.1016/j.sedgeo.2005.03.010.
Cosentino, D., Federici, I., Cipollari, P., Gliozzi, E., 2006. Environments and tectonic instability in central Italy (Garigliano Basin) during the late Messinian Lago-Mare episode: new data from the onshore Mondragone 1 well. Sediment. Geol. 188, 297–317. https://doi.org/10.1016/j.sedgeo.2006.03.010.
Cosentino, D., Gliozzi, E., Pionzi, G., 2007. The late Messinian Lago-Mare episode in the Mediterranean Basin: preliminary report on the occurrence of Paratethyan ostracod fauna from central Crete (Greece). Geobios 40 (3), 339–349. https://doi.org/10.1016/j.geobios.2007.01.001.
Cosentino, D., Darbaş, G., Gürbüz, K., 2010. The Messinian salinity crisis in the marginal basins of the peri-Mediterranean orogenic systems: examples from the central Apennines (Italy) and the Adana Basin (Turkey). EGUGA 2462.
Cosentino, D., Bertini, A., Cipollari, P., Florindo, F., Gliozzi, E., Grossi, F., Lo Mastro, S., Sprovieri, M., 2012. Orbitally forced paleoenvironmental and paleoclimate changes in the late postevaporitic Messinian of the central Mediterranean Basin. GSA Bull. 124 (3-4), 499–516. https://doi.org/10.1130/B30462.1.
Cosentino, D., Buchwaldt, R., Sampalmieri, G., Iadanza, A., Cipollari, P., Schildgen, T.F., Hinnov, L.A., Ramezani, J., Bowring, S.A., 2013. Refining the Mediterranean "Messinian gap" with high-precision U-Pb zircon geochronology, central and northern Italy. Geology 41, 323–326. https://doi.org/10.1130/G33820.1.
Cosentino, D., Bracone, V., D'Amico, C., Cipollari, P., Esu, D., Faranda, C., Frezza, V., Gliozzi, E., Grossi, F., Gupperrieri, P., Iadanza, A., Kotsakis, D., Soulié-Märsche, I., 2018. The record of the Messinian salinity crisis in mobile belts: insights from the Molise allochthonous units (southern Apennines, Italy). Paleogeogr. Paleoclimatol. Paleoecol. 503, 112–130. https://doi.org/10.1016/j.paleo.2018.04.028.
Coulson, S., Pico, T., Austermann, J., Powell, E., Moucha, R., Mitrovica, J.X., 2019. The role of isostatic adjustment and gravitational effects on the dynamics of the Messinian salinity crisis. Earth Planet. Sci. Lett. 525, 115760.
Dal Cin, M., Del Ben, A., Mocnik, A., Accaino, F., Geletti, R., Wardell, N., Zgur, F., Camerlenghi, A., 2016. Seismic imaging of late Miocene (Messinian) evaporites from western Mediterranean back-arc basins. Pet. Geosci. 22, 297–308. https://doi.org/10.1144/petgeo2015-096.
De Benedetti, A., 1982. The problem of the origin of the salt deposits in the Mediterranean and of their relations to other salt occurrences in the Neogene formations of the contiguous regions. Mar. Geol. 49, 91–114.
de la Chapelle, G., Gaudant, J., 1987. Decouverte de deux nouveaux gisements de poissons fossiles messiniens dans le bassin de Nijar-Carboneras (Andalousie Orientale): Signification paleoecologique et implications paleogeographiques.
de la Peña, L.G., Ranero, C.R., Gràcia, E., Booth-Rea, G., 2020. The evolution of the westernmost Mediterranean basins. Earth Sci. Rev. 103445.
Decima, A., 1964. Ostracodi del Gen. Cyprideis JONES del Neogene e del Quaternario italiani. Paleont. Italica, 57, p. 81.
Decima, A., Sprovieri, R., 1973. Comments on late Messinian microfaunas in several sections from Sicily. In: Drooger, C.W. (Ed.), Messinian Events in the Mediterranean. North-Holland Pub. Co, Amsterdam, pp. 229–234.
Decima, A., Wezel, F.C., 1971. Osservazioni sulle evaporiti Messiniane della Sicilia centro-meridionale. Rivista Mineraria Siciliana 130-134, 172–187.
Decima, A., Wezel, F.C., 1973. Late Miocene evaporites of the Central Sicilian Basin. In: Ryan, W.B.F., Hsu, K.J. (Eds.), Initial Reports of the Deep Sea Drilling Project, vol. 13. U.S. Gov. Print. Off, Washington, DC, pp. 1234–1240.
Decima, A., Schreiber, B.C., McKenzie, J.A., 1988. The origin of "evaporative" limestones: an example from the Messinian of Sicily (Italy). J. Sediment. Petrol. 58-2, 256–272.
Del Olmo, W.M., 2011. The Messinian in the Gulf of Valencia and Alboran Sea (Spain): paleogeography and paleoceanography implications. Rev. Soc. Geol. Esp. 24, 1–22.
Del Olmo, W.M., Martín, D., 2016. The Messinian record of Spanish onshore and offshore data (Atlantic Ocean and Western Mediterranean Sea). Pet. Geosci. 22 (4), 291–296.
Dela Pierre, F., Bernardi, E., Cavagna, S., Clari, P., Gennari, R., Irace, A., Lozar, F., Lugli, S., Manzi, V., Natalicchio, M., Roveri, M., Violanti, D., 2011. The record of the Messinian salinity crisis in the Tertiary Piedmont Basin (NW Italy): The Alba section revisited. Paleogeogr. Paleoclimatol. Paleoecol. 310, 238–255. https://doi.org/10.1016/j.paleo.2011.07.017.
Dela Pierre, F., Clari, P., Bernardi, E., Natalicchio, M., Costa, M., Cavagna, S., Lozar, F., Lugli, S., Manzi, V., Roveri, M., Violanti, D., 2012. Messinian carbonate-rich beds of the Tertiary Piedmont Basin (NW Italy): microbially-mediated products straddling the onset of the salinity crisis. Palaeogeogr. Palaeoclimatol. Palaeoecol. 34, 78–93. https://doi.org/10.1016/j.palaeo.2012.05.022.
Dela Pierre, F., Clari, P., Natalicchio, M., Ferrando, S., Giustetto, R., Lozar, F., Lugli, S., Manzi, V., Roveri, M., Violanti, D., 2014. Flocculent layers and bacterial mats in the mudstone interbeds of the Primary Lower Gypsum unit (Tertiary Piedmont Basin, NW Italy): archives of paleoenvironmental changes during the Messinian salinity crisis. Mar. Geol. 335, 71–87. https://doi.org/10.1016/j.margeo.2014.05.010.
Dela Pierre, F., Natalicchio, M., Lozar, F., Bonetto, S., Carnevale, G., Cavagna, S., Clari, P., Colombero, S., Violanti, D., 2016. The northermost record of the Messinian salinity crisis (Piedmont Basin, NW Italy). Geol. F. Trips 8, 1–58. https://doi.org/10.3301/GFT.2016.03.
Delrieu, B., Rouchy, J.M., Foucault, A., 1993. La surface d'erosion finimessinienne en Crète centrale (Grèce) et sur le pourtour méditerranéen: Rapports avec la crise de salinité méditerranéenne. Comptes rendus de l'Académie des sciences. Série 2, Mécanique, Physique, Chimie, Sciences de l'univers, Sciences de la Terre 316, no. 4, pp. 527–533.
Dettman, D.L., Flessa, K.W., Roopnarine, P.D., Schöne, B.R., Goodwin, D.H., 2004. The use of oxygen isotope variation in shells of estuarine mollusks as a quantitative record of seasonal and annual Colorado River discharge. Geochim. Cosmochim. Acta 68 (6), 1253–1263.
Di Stefano, A., Sturiale, G., 2010. Refinements of calcareous nannofossil biostratigraphy at the Miocene/Pliocene Boundary in the Mediterranean region. Geobios 43 (1), 5–20.
Do Couto, D., Popescu, S.-M., Suc, J.-P., Melinte-Dobrinescu, M.C., Barhoun, N., Gorini, C., Jolivet, L., Poort, J., Jouannic, G., Auxietre, J.-L., 2014. Lago Mare and the Messinian salinity crisis: evidences from the Alboran Sea (S. Spain). Mar. Pet. Geol. 52, 57–76. https://doi.org/10.1016/j.marpetgeo.2014.01.018.
Doebbert, A.C., Johnson, C.M., Carroll, A.R., Beard, B.L., Pietras, J.T., Carson, M.R., Norsted, B., Throckmorton, L.A., 2014. Controls on Sr isotopic evolution in lacustrine systems: Eocene green river formation, Wyoming. Chem. Geol. 380, 172–189. https://doi.org/10.1016/j.chemgeo.2014.04.008.
Dominici, S., Danise, S., Benvenuti, M., 2018. Pliocene stratigraphic paleobiology in Tuscany and the fossil record of marine megafauna. Earth Sci. Rev. 176, 277–310.
Driussi, O., Maillard, A., Ochoa, D., Lofi, J., Chanier, F., Gaullier, V., Briais, A., Sage, F., Sierro, F., Garcia, M., 2015. Messinian Salinity Crisis deposits widespread over the Balearic Promontory: insights from new high-resolution seismic data. Mar. Pet. Geol. 66, 41–54. https://doi.org/10.1016/j.marpetgeo.2014.09.008.
Druckman, Y., Buchbinder, B., Martinotti, G.M., Tov, R.S., Aharon, P., 1995. The buried Afiq Canyon (eastern Mediterranean, Israel): a case study of a Tertiary submarine canyon exposed in Late Messinian times. Mar. Geol. 123 (3–4), 167–185.
Drury, A.J., Westerhold, T., Hodell, D., Röhl, U., 2018. Reinforcing the North Atlantic backbone: revision and extension of the composite splice at ODP Site 982. Clim. Past 14 (3), 321–338.
Emeis, K.-C., Robertson, A.H.F., Richter, C., et al., 1996. Proc. ODP, Initial Reports, 160: College Station, TX (Ocean Drilling Program).
Englebrecht, A.C., Sachs, J.P., 2005. Determination of sediment provenance at drift sites using hydrogen isotopes and unsaturation ratios in alkenones. Geochim. Cosmochim. Acta 69, 4253–4265.

Estrada, F., Ercilla, G., Gorini, C., Alonso, B., Vazquez, J.T., García-Castellanos, D., Juan, C., Maldonado, A., Ammar, A., Elabbassi, M., 2011. Impact of pulsed Atlantic water inflow into the Alboran Basin at the time of the Zanclean flooding. GeoMar. Lett. 31, 361–376.

Esu, D., 2007. Latest Messinian "Lago-Mare" Lymnocardiinae from Italy: close relations with the Pontian fauna from the Dacic Basin. Geobios 40 (3), 291–302. https://doi.org/10.1016/j.geobios.2006.10.003.

Faranda, C., Gliozzi, E., Cipollari, P., Grossi, F., Darbaş, G., Gürbüz, K., Cosentino, D., 2013. Messinian paleoenvironmental changes in the easternmost Mediterranean Basin: Adana Basin, southern Turkey. Turk. J. Earth Sci. 22 (5), 839–863. https://doi.org/10.3906/yer-1205-11.

Feng, Y.E., Yankelzon, A., Steinberg, J., Reshef, M., 2016. Lithology and characteristics of the Messinian evaporite sequence of the deep Levant Basin, Eastern Mediterranean. Mar. Geol. 376, 118–131. https://doi.org/10.1016/j.margeo.2016.04.004.

Feng, Y.E., Steinberg, J., Reshef, M., 2017. Intra-salt deformation: implications for the evolution of the Messinian evaporites in the levant basin, eastern Mediterranean. Mar. Pet. Geol. 88, 251–267.

Fiduk, J.C., 2009. Evaporites, petroleum exploration, and the Cenozoic evolution of the Libyan shelf margin, central North Africa. Mar. Pet. Geol. 26 (8), 1513–1527.

Flecker, R., de Villiers, S., Ellam, R.M., 2002. Modelling the effect of evaporation on the salinity-$^{87}Sr/^{86}Sr$ relationship in modern and ancient marginal-marine systems: the Mediterranean Messinian Salinity Crisis. Earth Planet. Sci. Lett. 203, 221–233.

Flecker, R., Krijgsman, W., Capella, W., de Castro Martíns, C., Dmitrieva, E., Mayser, J.P., Marzocchi, A., Modestu, S., Ochoa, D., Simon, D., Tulbure, M., van den Berg, B., van der Schee, M., de Lange, G., Ellam, R., Govers, R., Gutjahr, M., Hilgen, F., Kouwenhoven, T., Lofi, J., Meijer, P., Sierro, F.J., Bachiri, N., Barhoun, N., Alami, A. C., Chacon, B., Flores, J.A., Gregory, J., Howard, J., Lunt, D., Ochoa, M., Pancost, R., Vincent, S., Yousfi, M.Z., 2015. Evolution of the late Miocene Mediterranean-Atlantic gateways and their impact on regional and global environmental change. Earth Sci. Rev. 150, 365–392. https://doi.org/10.1016/j.earscirev.2015.08.007.

Fontes, J.-C., Letolle, R., Nesteroff, D., Ryan, W.B.F., 1973. Oxygen, Carbon, Sulfur and Hydrogen stable isotopes in carbonate and sulfate mineral phases of Neogene evaporites, sediments and in interstitial waters. Texas A.M University, O.D.P.C.S., TX, United States (Ed.). In: Initial Reports of the Deep Sea Drilling Project, Covering Leg 13 of the Cruises of the Drilling Vessel Glomar Challenger Lisbon, Portugal to Lisbon, Portugal, August-October 1970., United States, pp. 788–796.

Fortuin, A.R., Krijgsman, W., 2003. The Messinian of the Nijar basin (SE Spain): sedimentation, depositional environments and paleogeographic evolution. Sediment. Geol. 160, 213–242.

Fortuin, A.R., Kelling, J.M.D., Roep, T.B., 1995. The enigmatic Messinian -Pliocene section of Cuevas del Almanzora (Vera Basin, SE Spain) revisited-erosional features and strontium isotope ages. Sediment. Geol. 97, 177–201.

Frey-Martinez, J.F., Cartwright, J.A., Burgess, P.M., Bravo, J.V., 2004. 3D seismic interpretation of the Messinian Unconformity in the Valencia Basin, Spain. Geol. Soc. Lond. Mem. 29 (1), 91–100.

Friedman, G.M., 1973. Petrographic data and comments on the depositional environment of the Miocene sulfates and dolomites at Sites 124, 132, and 134, western Mediterranean Sea. In: Ryan, W.B.F., Hsü, K.J., et al. (Eds.), Initial Reports of the Deep Sea Drilling Project 13. U. S. Government Printing Office, Washington, pp. 695–708.

Frigui, M., Youssef, M.B., Ouaja, M., 2016. Evidences of "Lago-Mare" episode around the Messinian-Pliocene boundary in eastern Tunisia (central Mediterranean). J. Afr. Earth Sci. 123, 57–74. https://doi.org/10.1016/j.jafrearsci.2016.07.007.

Fritz, P., Basharmal, G.M., Drimmie, R.J., Ibsen, J., Qureshi, R.M., 1989. Oxygen isotope exchange between sulphate and water during bacterial reduction of sulphate. Chem. Geol. 79, 99–105.

Gallais, F., Gutscher, M.A., Graindorge, D., Klaeschen, D., 2018. 12.B&E- Ionian Basin. In J. Lofi (Ed.), Seismic Atlas of the Messinian salinity crisis markers in the Mediterranean sea. Volume 2. - Mémoires de la Société géologique de France, n.s., 2018, t. 181, and Commission for the Geological Map of the World, pp. 41–44.

García-Alix, A., Minwer-Barakat, R., Martín Suárez, E., Freudenthal, M., Aguirre, J., Kaya, F., 2016. Updating the Europe-Africa small mammal exchange during the late Messinian. J. Biogeogr. 43 (7), 1336–1348.

Garcia-Castellanos, D., Villaseñor, A., 2011. Messinian salinity crisis regulated by competing tectonics and erosion at the Gibraltar arc. Nature 480, 359–363. https://doi.org/10.1038/nature10651.

Garcia-Castellanos, D., Estrada, F., Jiménez-Munt, I., Gorini, C., Fernàndez, M., Vergés, J., De Vicente, R., 2009. Catastrophic flood of the Mediterranean after the Messinian salinity crisis. Nature 462, 10. https://doi.org/10.1038/nature08555.

Garcia-Castellanos, D., Micallef, A., Estrada, F., Camerlenghi, A., Ercilla, G., Periáñez, R., Abril, J.M., 2020. The Zanclean megaflood of the Mediterranean-Searching for independent evidence. Earth Sci. Rev. 201, 103061. https://doi.org/10.1016/j.earscirev.2019.103061.

García-García, F., Corbí, H., Soria, J.M., Viseras, C., 2011. Architecture analysis of a river flood-dominated delta during an overall sea-level rise (Early Pliocene, SE Spain). Sediment. Geol. 237, 102–113.

García-Veigas, J., Orti, F., Rosell, L., Ayora, C., Rouchy, J.M., Lugli, S., 1995. The Messinian salt of the Mediterranean: geochemical study of the salt from the Central Sicily Basin and comparison with the Lorca Basin (Spain). Bull. Soc. Géol. Fr 166, 699–710.

García-Veigas, J., Cendón, D.I., Gibert, L., Lowenstein, T.K., Artiaga, D., 2018. Geochemical indicators in Western Mediterranean Messinian evaporites: Implications for the salinity crisis. Mar. Geol. 403, 197–214. https://doi.org/10.1016/j.margeo.2018.06.005.

Gargani, J., Moretti, I., Letouzey, J., 2008. Evaporite accumulation during the Messinian Salinity Crisis: the Suez rift case. Geophys. Res. Lett. 35 (2) https://doi.org/10.1029/2007GL032494.

Gaullier, V., Chanier, F., Lymer, G., Vendeville, B., Maillard, A., Thinon, I., Lofi, J., Sage, F., Loncke, L., 2014. Salt tectonics and crustal tectonics along the Eastern Sardinian margin, Western Tyrrhenian: new insights from the «METYSS 1» cruise. Tectonophysics. https://doi.org/10.1016/j.tecto.2013.12.015.

Geletti, R., Zgur, F., Del Ben, A., Buriola, F., Fais, S., Fedi, M., Forte, E., Mocknik, A., Paoletti, V., Pipan, M., Ramella, R., Romeo, R., Romi, A., 2014. The Messinian Salinity Crisis: new seismic evidence in the West-Sardinian Margin and Eastern Sardo-Provençal basin (West Mediterranean Sea). Mar. Geol. 351, 76–90. https://doi.org/10.1016/j.margeo.2014.03.019.

Gennari, R., Iaccarino, S.M., Di Stefano, A., Sturiale, G., Cipollari, P., Manzi, V., Roveri, M., Cosentino, D., 2008. The Messinian–Zanclean boundary in the Northern Apennine. Stratigraphy 5, 307–322.

Gennari, R., Manzi, V., Angeletti, L., Bertini, A., Biffi, U., Ceregato, A., Rosso, A., 2013. A shallow water record of the onset of the Messinian salinity crisis in the Adriatic foredeep (Legnagnone section, Northern Apennines). Paleogeogr. Paleoclimatol. Paleoecol. 386, 145–164.

Ghibaudo, G., Clari, P., Perello, M., 1985. Litostratigrafia, sedimentologia ed evoluzione tettonico-sedimentaria dei depositi miocenici del margine sud-orientale del bacino terziario ligure-piemontese (Valli Borbera, Scrivia e Lemme). In memoria di Carlo Sturani. Boll. Soc. Geol. Ital. 104 (3), 349–397.

Ghielmi, M., Minervini, M., Nini, C., Rogledi, S., Rossi, M., Vignolo, A., 2010. Sedimentary and tectonic evolution in the eastern Po-Plain and northern Adriatic Sea area from Messinian to Middle Pleistocene (Italy). Rendiconti Lincei 21 (1), 131–166. https://doi.org/10.1007/s12210-010-0101-5.

Ghielmi, M., Minervini, M., Nini, C., Rogledi, S., Rossi, M., 2013. Late Miocene-Middle Pleistocene sequences in the Po Plain-Northern Adriatic Sea (Italy): the stratigraphic record of modification phases affecting a complex foreland basin. Marine and Petroleum Geology, Special Issue: The Geology of the Periadriatic Basin and of the Adriatic Sea 42, 50–81. https://doi.org/10.1016/j.marpetgeo.2012.11.007.

Gignoux, M., 1936a. Géologie stratigraphique, 2°édition. Masson, Paris.

Gignoux, M., 1936b. Géologie stratigraphique, 2°édition. Masson, Paris.

Gillet, S., 1932. Essai de classification du Miocène superieur et du Pliocene inferieur de Roumanie. La Transylvanie et le Banat. Comptes Rendus Hebdomadaires des séances de l'Académie des sciences. Séance 27 Decembre, 1932. Académie des Sciences, Paris.

Gillet, S., 1933. Essai de classification du Miòcene supérieur et du Pliocène inférieur de Roumanie. Le bassin dacique. Comptes Rendus Hebdomadaires des séances de l'Académie des sciences. 01/1933. Académie des Sciences, Paris.

Gladstone, R., Flecker, R., Valdes, P., Lunt, D., Markwick, P., 2007. The Mediterranean hydrologic budget from a Late Miocene global climate simulation. Paleogeogr. Paleoclimatol. Paleoecol. 251 (2), 254–267. https://doi.org/10.1016/j.paleo.2007.03.050.

Gliozzi, E., 1999. A late Messinian brackish water ostracod fauna of Paratethyan aspect from Le Vicenne Basin (Abruzzi, central Apennines, Italy). Paleogeogr. Paleoclimatol. Paleoecol. 151 (1-3), 191–208.

Gliozzi, E., Grossi, F., 2008. Late Messinian lago-mare ostracod paleoecology: a correspondence analysis aroach. Paleogeogr. Paleoclimatol. Paleoecol. 264 (3-4), 288–295. https://doi.org/10.1016/j.paleo.2007.03.055.

Gliozzi, E., Ceci, M.E., Grossi, F., Ligios, S., 2007. Paratethyan ostracod immigrants in Italy during the Late Miocene. Geobios 40 (3), 325–337. https://doi.org/10.1016/j.geobios.2006.10.004.

Golovina, L.A., Radionova, E.P., van Baak, C.G., Krijgsman, W., Palcu, D.V., 2019. A Late Maeotian age (6.7-6.3 Ma) for the enigmatic "Pebbly Breccia" unit in DSDP Hole 380A of the Black Sea. Paleogeogr. Paleoclimatol. Paleoecol. 533, 109269. https://doi.org/10.1016/j.paleo.2019.109269.

Gomes, M.L., Johnston, D.T., 2017. Oxygen and sulfur isotopes in sulfate in modern euxinic systems with implications for evaluating the extent of euxinia in ancient oceans. Geochim. Cosmochim. Acta 205, 331–359.

Gorini, C., Lofi, J., Duvail, C., Dos Reis, A.T., Guennoc, P., Lestrat, P., Mauffret, A., 2005. The Late Messinian salinity crisis and Late Miocene Tectonism: interaction and consequence on the physiography and post-rift evolution of the gulf of Lions margin. Mar. Pet. Geol. 22, 695–712.

Griffin, D.L., 2002. Aridity and humidity: two aspects of the late Miocene climate of North Africa and the Mediterranean. Paleogeogr. Paleoclimatol. Paleoecol. 182 (1-2), 65–91.

Grossi, F., Cosentino, D., Gliozzi, E., 2008. Late Messinian Lago-Mare ostracods and paleoenvironments of the central and eastern Mediterranean Basin. Boll. Soc. Paleontol. Ital. 47 (2), 131–146.

Grossi, F., Gliozzi, E., Cosentino, D., 2011. Paratethyan ostracod immigrants mark the biostratigraphy of the Messinian Salinity Crisis. Joannea Geologie und Paleontologie 11, 66–68.

Grossi, F., Gliozzi, E., Anadón, P., Castorina, F., Voltaggio, M., 2015. Is Cyprideis agrigentina Decima a good paleosalinometer for the Messinian Salinity Crisis? Morphometrical and geochemical analyses from the Eraclea Minoa section (Sicily). Paleogeogr. Paleoclimatol. Paleoecol. 419, 75–89. https://doi.org/10.1016/j.paleo.2014.09.024.

Grothe, A., 2016. The Messinian Salinity Crisis: a Paratethyan perspective (Doctoral dissertation, University Utrecht).

Grothe, A., Sangiorgi, F., Mulders, Y.R., Vasiliev, I., Reichart, G.-J., Brinkhuis, H., Stoica, M., Krijgsman, W., 2014. Black Sea desiccation during the Messinian Salinity Crisis: fact or fiction? Geology 42 (7), 563–566. https://doi.org/10.1130/G35503.1.

Grothe, A., Sangiorgi, F., Brinkhuis, H., Stoica, M., Krijgsman, W., 2018. Migration of the dinoflagellate Galeacysta etrusca and its implications for the Messinian Salinity Crisis. Newsl. Stratigr. 51 (1), 73–91. https://doi.org/10.1127/nos/2016/0340.

Grothe, A., Andreetto, F., Reichart, G.J., Wolthers, M., Van Baak, C.G., Vasiliev, I., Stoica, M., Sangiorgi, F., Middelburg, J.J., Davies, G.R., Krijgsman, W., 2020. Paratethys pacing of the Messinian Salinity Crisis: low salinity waters contributing to gypsum precipitation? Earth Planet. Sci. Lett. 532, 116029 https://doi.org/10.1016/j.epsl.2019.116029.

Grunert, P., Harzhauser, M., Rosenthal, Y., Carnevale, G., 2016. Estuarine Lago Mare fauna from the Tertiary Piedmont Basin indicates episodic Atlantic/Mediterranean exchange during the final stage of the Mediterranean Salinity Crisis. Paleogeogr. Paleoclimatol. Paleoecol. 457, 70–79. https://doi.org/10.1016/j.paleo.2016.06.005.

Guennoc, P., Réhault, J.P., Thinon, I., 2011. West-Corsica Margin: MSC basinal units. In: Lofi, J., et al. (Eds.), Mémoires de la Société géologique de France and World Geological Map Commission ed, pp. 1–72.

Guerra-Merchán, A., Serrano, F., Garcés, M., Gofas, S., Esu, D., Gliozzi, E., Grossi, F., 2010. Messinian Lago-Mare deposits near the strait of Gibraltar (Malaga basin, S Spain). Paleogeogr. Paleoclimatol. Paleoecol. 285 (3-4), 264–276. https://doi.org/10.1016/j.paleo.2009.11.019.

Guerra-Merchán, A., Serrano, F., Hlila, R., El Kadiri, K., de Galdeano, C.S., Garcés, M., 2014. Tectono-sedimentary evolution of the peripheral basins of the Alboran Sea in the arc of Gibraltar during the latest Messinian-Pliocene. J. Geodyn. 77, 158–170. https://doi.org/10.1016/j.jog.2013.12.003.

Gülyüz, E., Durak, H., Özkaptan, M., Krijgsman, W., 2020. Paleomagnetic constraints on the early Miocene closure of the southern Neo-Tethys (Van region; East Anatolia): Inferences for the timing of Eurasia-Arabia collision. Glob. Planet. Chang. 185, 103089. https://doi.org/10.1016/j.gloplacha.2019.103089.

Güneş, P., Aksu, A.E., Hall, J., 2018. Internal seismic stratigraphy of the Messinian evaporites across the northern sector of the eastern Mediterranean Sea. Mar. Pet. Geol. 91, 297–320. https://doi.org/10.1016/j.marpetgeo.2018.01.016.

Gvirtzman, Z., Reshef, M., Buch-Leviatan, O., Ben-Avraham, Z., 2013. Intense salt deformation in the Levant Basin in the middle of the Messinian salinity crisis. Earth Planet. Sci. Lett. 379, 108–119.

Gvirtzman, Z., Reshef, M., Buch-Leviatan, O., Groves-Gidney, G., Karcz, Z., Makovsky, Y., Ben-Avraham, Z., 2015. Bathymetry of the Levant basin: interaction of salt-tectonics and surficial mass movements. Mar. Geol. 360, 25–39. https://doi.org/10.1016/j.margeo.2014.12.001.

Gvirtzman, Z., Manzi, V., Calvo, R., Gavrieli, I., Gennari, R., Lugli, S., Reghizzi, M., Roveri, M., 2017. Intra-Messinian truncation surface in the Levant Basin explained by subaqueous dissolution. Geology 45 (10), 915–918. https://doi.org/10.1130/G39113.1.

Hajj, F., Poszwa, A., Bouchez, J., Guérold, F., 2017. Radiogenic and "stable" strontium isotopes in provenance studies: a review and first results on archaeological wood from shipwrecks. J. Archaeol. Sci. 86, 24–49. https://doi.org/10.1016/j.jas.2017.09.005.

Hajós, M., 1973. 34.5. The Mediterranean diatoms. In: Proceedings of the Ocean Drilling Program: Initial report. Part A, 944.

Hallett, D., 2002. Petroleum Geology of Libya. Elsevier Inc., New York, 503 pp.

Haq, B., Gorini, C., Baur, J., Moneron, J., Rubino, J.L., 2020. Deep Mediterranean's Messinian evaporite giant: how much salt? Glob. Planet. Chang. 184, 103052 https://doi.org/10.1016/j.gloplacha.2019.103052.

Hardie, L.A., Lowenstein, T.K., 2004. Did the Mediterranean Sea dry out during the Miocene? A reassessment of the evaporite evidence from DSDP Legs 13 and 42A cores. J. Sediment. Res. 74, 453–461.

Harzhauser, M., Neubaupper, T.A., Georgopoulou, E., Esu, D., D'Amico, C., Pavia, G., Giuntelli, P., Carnevale, G., 2015. Late Messinian continental and Lago-Mare gastropods from the Tertiary Piedmont Basin. NW Italy. Boll. Soc. Paleontol. Ital. 54, 1–53. https://doi.org/10.4435/BSPI.2015.1.

Herbert, T.D., Lawrence, K.T., Tzanova, A., Peterson, L.C., Caballero-Gill, R., Kelly, C.S., 2016. Late Miocene global cooling and the rise of modern ecosystems. Nat. Geosci. 9, 843–847. https://doi.org/10.1038/ngeo2813.

Hilgen, F.J., 1991. Astronomical calibration of Gauss to Matuyama sapropels in the Mediterranean and implication for the geomagnetic polarity time scale. Earth Planet. Sci. Lett. 104 (2-4), 226–244.

Hilgen, F.J., Krijgsman, W., Langereis, C.G., Lourens, L.J., Santarelli, A., Zachariasse, W.J., 1995. Extending the astronomical (polarity) time scale into the Miocene. Earth Planet. Sci. Lett. 136, 495–510.

Hilgen, F., Kuiper, K., Krijgsman, W., Snel, E., van der Laan, E., 2007. Astronomical tuning as the basis for high resolution chronostratigraphy: the intricate history of the Messinian Salinity Crisis. Stratigraphy 4 (2-3), 231–238.

Hodell, D.A., Benson, R.H., Kent, D.V., Boersma, A., Rakic-el Bied, K., 1994. Magnetostratigraphic, biostratigraphic, and stable isotope stratigraphy of an Upper Miocene drill core from the Salé Briqueterie (northwest Morocco): a high-resolution chronology for the Messinian stage. Paleoceanography 9, 835–855.

Hodell, D.A., Curtis, J.H., Sierro, F.J., Raymo, M.E., 2001. Correlation of late Miocene to early Pliocene sequences between the Mediterranean and North Atlantic. Paleoceanography 16, 164–178.

Hsü, K.J., 1972. Origin of Saline Giants: a critical review after the discovery of the Mediterranean evaporite. Earth-Sci. Rev. 8, 371–396.

Hsü, K.J., Ryan, W.B.F., Cita, M., 1973a. Late Miocene desiccation of the Mediterranean. Nature 242, 240.

Hsü, K.J., Cita, M.B., Ryan, W.B.F., 1973b. The origin of the Mediterranean evaporites. In: Ryan, W.B.F., Hsü, K.J., et al. (Eds.), Initial Reports of the Deep Sea Drilling Project, 13. U. S. Government Printing Office, Washington, pp. 1203–1231.

Hsü, K.J., Montadert, L., Bernouilli, D., Cita, M.B., Erikson, A., Garrison, R.G., Kidd, R.B., Mélières, F., Müller, C., Wright, R., 1978a. History of the Mediterranean salinity crisis. In: Hsü, K.J., Montadert, L., et al. (Eds.), Initial Reports of the Deep Sea Drilling Project. U.S. Government Printing Office, Washington, DC.

Hsü, K.J., Montadert, L., Bernoulli, D., Bizon, G., Cita, M., Erickson, A., Fabricius, F., Garrison, R.E., Kidd, R.B., Mélières, F., Müller, C., Wright, R.C., 1978b. Initial reports of the deep sea drilling project: DSDP volume XLII Part 1.

Iaccarino, S., Bossio, A., 1999. Paleoenvironment of uppermost Messinian sequences in the western Mediterranean (Sites 974, 975, and 978). In: Proceedings of the Ocean Drilling Program, Scientific Results (Vol. 161, 529-541). College Station, TX: Ocean Drilling Program.

Iaccarino, S.M., Cita, M.B., Gaboardi, S., Gruppini, G.M., 1999. 15. High-Resolution Biostratigraphy at the Miocene/Pliocene boundary in Holes 974b and 975b, Western Mediterranean. In: Proceedings of the Ocean Drilling Program: Scientific Results, Vol. 161, p. 197.

Hsü, K.J., Ryan,, W.B.F., Schreiber, B.C., 1973c. Petrography of a halite sample from Hole 134-Balearic Abyssal Plain. In: Ryan, W.B.F., Hsü, K.J., et al. (Eds.), Initial Reports of the Deep Sea Drilling Project, 13. U. S. Government Printing Office, Washington, pp. 708–711.

Iaccarino, S.M., Bertini, A., Di Stefano, A., Ferraro, L., Gennari, R., Grossi, F., Lirer, F., Manzi, V., Menichetti, E., Ricci Lucchi, M., Taviani, M., Sturiale, G., Angeletti, L., 2008. The Trave section (Monte dei Corvi, Ancona, central Italy): an integrated paleontological study of the Messinian deposits. Stratigraphy 5 (3–4), 281–306.

Ingram, B.L., Sloan, D., 1992. Strontium isotopic composition of estuarine sediments as paleosalinity-paleoclimate indicator. Science 255, 68–72.

Jagger, L.J., Bevan, T.G., McClay, K.R., 2020. Tectono-stratigraphic evolution of the SE Mediterranean passive margin, offshore Egypt and Libya. Geol. Soc. Lond., Spec. Publ. 476 (1), 365–401.

Johnston, D.T., Gill, B.C., Masterson, A., Beirne, E., Casciotti, K.L., Kna, A.N., Berelson, W., 2014. Placing an upper limit on cryptic marine sulphur cycling. Nature 513, 530–533.

Jolivet, L., Augier, R., Robin, C., Suc, J.-P., Rouchy, J.-M., 2006. Lithospheric-scale geodynamic context of the Messinian Salinity Crisis. Sediment. Geol. 188–189, 9–33. https://doi.org/10.1016/j.sedgeo.2006.02.004.

Just, J., Hübscher, C., Betzler, C., Lüdmann, T., Reicherter, K., 2011. Erosion of continental margins in the Western Mediterranean due to sea-level stagnancy during the Messinian Salinity Crisis. Geo-Mar. Lett. 31 (1), 51–64.

Kaplan, I.R., Rittenberg, S.C., 1964. Microbiological fractionation of sulphur isotopes. Microbiology 34, 195–212.

Karakitsios, V., Cornée, J., Tsourou, T., Moissette, P., Kontakiotis, G., Agiadi, K., Manoutsoglou, E., Triantaphyllou, M., Koskeridou, E., 2017a. Messinian salinity crisis record under strong freshwater input in marginal, intermediate, and deep environments: the case of the North Aegean. Paleogr. Paleoclimatol. Paleoecol. 485, 316–335. https://doi.org/10.1016/j.palaeo.2017.06.023.

Karakitsios, V., Roveri, M., Lugli, S., Manzi, V., Gennari, R., Antonarakou, A., Triantaphyllou, M., Agiadi, K., Kontakiotis, G., Kafousia, N., de Rafelis, M., 2017b. A record of the Messinian salinity crisis in the eastern Ionian tectonically active domain (Greece, eastern Mediterranean). Basin Res. 29, 203–233. https://doi.org/10.1111/bre.12173.

Kartveit, K.H., Ulsund, H.B., Johansen, S.E., 2019. Evidence of sea level drawdown at the end of the Messinian salinity crisis and seismic investigation of the Nahr Menashe unit in the northern Levant Basin, offshore Lebanon. Basin Res. 31 (5), 827–840. https://doi.org/10.1111/bre.12347.

Kastens, K.A., Mascle, J., 1990. The geological evolution of the Tyrrhenian Sea: An introduction to the scientific results of ODP Leg 107. In: Proceedings of the Ocean Drilling Program, Scientific Results (Vol. 107, No. 3), p. 26. College Station, TX (Ocean Drilling Program).

Kastens, K.A., Mascle, J., Auroux, C., et al., 1987. Proc. ODP, Init. Repts., 107. College Station, TX (Ocean Drilling Program). https://doi.org/10.2973/odp.proc.ir.107.1987.

Keller, G., Abramovich, S., 2009. Lilliput effect in late Maastrichtian planktic foraminifera: response to environmental stress: Paleogeography. Paleoclimatol. Paleoecol. 284, 47–62.

Keogh, S.M., Butler, R.W.H., 1999. The Mediterranean water body in the late Messinian: interpreting the record from marginal basins on Sicily. J. Geol. Soc. 156 (4), 837–846.

Kirkham, C., Bertoni, C., Cartwright, J., Lensky, N.G., Sirota, I., Rodriguez, K., Hodgson, N., 2020. The demise of a 'salt giant' driven by uplift and thermal dissolution. Earth Planet. Sci. Lett. 531, 115933 https://doi.org/10.1016/j.epsl.2019.115933.

Kováč, M., Andreyeva-grigorovich, A., Bajraktarević, Z., Brzobohatý, R., Filipescu, S., Fodor, L., Harzhauser, M., Nagymarosy, A., Oszczypko, N., Pavelić, D., Rögl, F., Saftić, B., Sliva, U., Studencka, B., 2007. Badenian evolution of the Central Paratethys Sea: paleogeography, climate and eustatic sea-level changes. Geol. Carpathica 58, 579–606.

Krijgsman, W., Meijer, P.T., 2008. Depositional environments of the Mediterranean "Lower Evaporites" of the Messinian salinity crisis: constraints from quantitative analyses. Mar. Geol. 253 (3–4), 73–81. https://doi.org/10.1016/j.margeo.2008.04.010.

Krijgsman, W., Hilgen, F.J., Raffi, I., Sierro, F.J., Wilson, D.S., 1999a. Chronology, causes, and progression of the Messinian salinity crisis. Nature 400, 652–655.

Krijgsman, W., Hilgen, F.J., Marabini, S., Vai, G.B., 1999b. New paleomagnetic and cyclostratigraphic age constraints on the Messinian of the Northern Apennines (Vena del Gesso Basin, Italy). Mem. Soc. Geol. Ital. 54, 25–33.

Krijgsman, W., Fortuin, A.R., Hilgen, F.J., Sierro, F.J., 2001. Astrochronology for the Messinian Sorbas basin (SE Spain) and orbital (precessional) forcing for evaporite cyclicity. Sediment. Geol. 140, 43–60.

Krijgsman, W., Gaboardi, S., Hilgen, F.J., Iaccarino, S., Kaenel, E.D., Laan, E.V.D., 2004. Revised astrochronology for the Ain el Beida section (Atlantic Morocco): no glacio-eustatic control for the onset of the Messinian Salinity Crisis. Stratigraphy 1, 87–101.
Krijgsman, W., Stoica, M., Vasiliev, I., Popov, V.V., 2010. Rise and fall of the Paratethys Sea during the Messinian Salinity Crisis. Earth Planet. Sci. Lett. 290 (1-2), 183–191. https://doi.org/10.1016/j.epsl.2009.12.020.
Krijgsman, W., Capella, W., Simon, D., Hilgen, F.J., Kouwenhoven, T.J., Meijer, P.Th., Sierro, F.J., Tulbure, M.A., van den Berg, B.C.J., van der Schee, M., Flecker, R., 2018. The Gibraltar Corridor: watergate of the Messinian Salinity Crisis. Mar. Geol. 403, 238–246. https://doi.org/10.1016/j.margeo.2018.06.008.
Krijgsman, W., Palcu, D., Andreetto, F., Stoica, M., Mandic, O., 2020a. Changing seas in the late Miocene Northern Aegean: a Paratethyan aroach to Mediterranean basin evolution. Earth Sci. Rev. 103386 https://doi.org/10.1016/j.earscirev.2020.103386.
Krijgsman, W., Stoica, M., Hoyle, T.M., Jorissen, E.L., Lazarev, S., Rausch, L., Bista, D., Alçiçek, M.C., Ilgar, A., van den Hoek Ostende, L.W., Mayda, S., Raffi, I., Flecker, R., Mandic, O., Neubauer, T.A., Wesselingh, F.P., 2020b. The myth of the Messinian Dardanelles: Late Miocene stratigraphy and paleogeography of the ancient Aegean-Black Sea gateway. Paleogeogr. Paleoclimatol. Paleoecol. 110033 https://doi.org/10.1016/j.paleo.2020.110033.
Van der Laan, E., Gaboardi, S., Hilgen, F.J., Lourens, L.J., 2005. Regional climate and glacial control on high-resolution oxygen isotope records from Ain El Beida (latest Miocene, NW Morocco): a cyclostratigraphic analysis in the depth and time domain. Paleoceanography 20. https://doi.org/10.1029/2003PA000995. PA1001.
Van der Laan, E., Snel, E., de Kaenel, E., Hilgen, F.J., Krijgsman, W., 2006. No major deglaciation across the Miocene-Pliocene boundary: integrated stratigraphy and astronomical tuning of the Loulja sections (Bou Regreg area, NW Morocco). Paleoceanography 21. https://doi.org/10.1029/2005PA001193. PA3011.
Laskar, L.J., Robutel, P., Joutel, F., Gastineau, M., Correia, A.C.M., Levrard, B., 2004. A long term numerical solution for the insolation quantities of the Earth. Astron. Astrophys. 428, 261–285.
Lazarev, S., de Leeuw, A., Stoica, M., Mandic, O., van Baak, C.G.C., Vasiliev, I., Krijgsman, W., 2020. From Khersonian drying to Pontian "flooding": Late Miocene stratigraphy and paleoenvironmental evolution of the Dacian Basin (Eastern Paratethys). Glob. Planet. Chang. 103224 https://doi.org/10.1016/j.gloplacha.2020.103224.
Leavitt, W.D., Halevy, I., Bradley, A.S., Johnston, D.T., 2013. Influence of sulfate reduction rates on the Phanerozoic sulfur isotope record. Proc. Natl. Acad. Sci. 110, 11244.
Leila, M., Moscariello, A., Šegvić, B., 2018. Depositional facies controls on the diagenesis and reservoir quality of the Messinian Qawasim and Abu Madi formations, onshore Nile Delta, Egypt. Geol. J. 54 (3), 1797–1813.
Liu, J., Li, S., Zhong, J., Zhu, X., Guo, Q., Lang, Y., Han, X., 2017. Sulfate sources constrained by sulfur and oxygen isotopic compositions in the upper reaches of the Xijiang River, China. Acta Geochimica 36, 611–618.
Lloyd, R.M., 1968. Oxygen isotope behavior in the Sulfate-Water System. J. Geophys. Res. 1896-1977 (73), 6099–6110.
Lofi, J., 2018. Seismic Atlas of the Messinian salinity crisis markers in the Mediterranean sea. Volume 2 - Mémoires de la Société géologique de France, n.s., 2018, t. 181, and Commission for the Geological Map of the World, 72 p. + DVD. https://doi.org/10.10682/2018M ESSINV2.
Lofi, J., Gorini, C., Berne, S., Clauzon, G., Dos Reis, A.T., Ryan, W.B.F., Steckler, M.S., 2005. Erosional processes and paleo-environmental changes in the Western Gulf of Lions (SW France) during the Messinian Salinity Crisis. Mar. Geol. 217, 1–30. https://doi.org/10.1016/j.margeo.2005.02.014.
Lofi, J., Sage, F., Déverchère, J., Loncke, L., Maillard, A., Gaullier, V., Thinon, I., Gillet, H., Guennoc, P., Gorini, C., 2011a. Refining our knowledge of the Messinian salinity crisis records in the offshore domain through multi-site seismic analysis. Bulletin de la Société géologique de France 182 (2), 163–180.
Lofi, J., Déverchère, J., Gaullier, V., Gillet, H., Gorini, C., Guennoc, P., Loncke, L., Maillard, A., Sage, F., Thinon, I., 2011b. Seismic atlas of the "Messinian Salinity Crisis" markers in the Mediterranean and Black seas. Commission for the Geological Map of the World and Memoires de la Société Géologique de France. Nouv. Ser. 72.
Loget, N., Davy, P., Van Den Driessche, J., 2006. Mesoscale fluvial erosion parameters deduced from modelling the Mediterranean sea-level drop during the Messinian (late Miocene). J. Geophys. Res. 111. F03005.
Loncke, L., Gaullier, V., Mascle, J., Vendeville, B., Camera, L., 2006. The Nile deep-sea fan: An example of interacting sedimentation, salt tectonics, and inherited subsalt paleotopographic features. Mar. Pet. Geol. 23, 297–315. https://doi.org/10.1016/j.marpetgeo.2006.01.001.
Londeix, L., Benzakour, M., Suc, J.P., Turon, J.L., 2007. Messinian paleoenvironments and hydrology in Sicily (Italy): the dinoflagellate cyst record. Geobios 40 (3), 233–250. https://doi.org/10.1016/j.geobios.2006.12.001.
Longinelli, A., 1979. Isotope geochemistry of some Messinian evaporates: paleoenvironmental implications. Paleogeogr. Paleoclimatol. Paleoecol. 29, 95–123.
Longinelli, A., Craig, H., 1967. Oxygen-18 variations in sulfate ions in sea water and saline lakes. Science 156 (3771), 56–59.
López-Garrido, A.C., Sanz de Galdeano, C., 1999. Neogene sedimentation and tectonic-eustatic control of the Malaga basin, South Spain. J. Pet. Geol. 22 (1), 81–96.
Loreto, M.F., Zitellini, N., Ranero, C.R., Palmiotto, C., Prada, M., 2020. Extensional tectonics during the Tyrrhenian back-arc basin formation and a new morpho-tectonic map. Basin Res. 33 (1), 138–158.
Lourens, L., Hilgen, F., Shackleton, N.J., Laskar, J., Wilson, D., 2004. The Neogene period. In: Gradstein, F.M., Ogg, J.G., Smith, A.G. (Eds.), A Geologic Time Scale 2004. Cambridge Univ. Press, Cambridge, pp. 409–440.
Lozano, D.O., 2016. Astrobiochronological Constraints on Margin to deep basin correlations across the Balearic Promontory and the Valencia basin (Doctoral dissertation, Universidad de Salamanca).
Lu, F.H., 2006. Lithofacies and water-body record of Messinian evaporites in Nijar Basin, SE Spain. Sediment. Geol. 188, 115–130.
Lu, F.H., Meyers, W.J., Schoonen, M.A., 2001. S and O (SO4) isotopes, simultaneous modeling, and environmental significance of the Nijar Messinian gypsum, Spain. Geochim. Cosmochim. Acta 65, 3081–3092.
Lugli, S., Schreiber, B.C., Triberti, B., 1999. Giant polygons in the Realmonte mine (Agrigento, Sicily): evidence for the desiccation of a Messinian halite basin. J. Sediment. Res. 69, 764–771.
Lugli, S., Bassetti, M.A., Manzi, V., Barbieri, M., Longinelli, A., Roveri, M., 2007. The Messinian "Vena del Gesso" evaporites revisited: characterization of isotopic composition and organic matter. In: Schreiber, B.C., Lugli, S., Bąbel, M. (Eds.), Evaporites through Space and Time. Special Publications, 285. Geological Society, London, pp. 143–154.
Lugli, S., Manzi, V., Roveri, M., Schreiber, B.C., 2010. The Primary Lower Gypsum in the Mediterranean: a newfacies interpretation for the first stage of the Messinian salinity crisis. Paleogeogr. Paleoclimatol. Paleoecol. 297, 83–99. https://doi.org/10.1016/j.paleo.2010.07.017.
Lugli, S., Gennari, R., Gvirtzman, Z., Manzi, V., Roveri, M., Schreiber, B.C., 2013. Evidence of clastic evaporites in the canyons of the Levant Basin (Israel): implications for the Messinian Salinity Crisis. J. Sediment. Res. 83, 942–954. https://doi.org/10.2110/jsr.2013.72.
Lugli, S., Manzi, V., Roveri, M., Schreiber, B.C., 2015. The deep record of the Messinian salinity crisis: evidence of a non-desiccated Mediterranean Sea. Paleogeogr. Paleoclimatol. Paleoecol. 433, 201–218. https://doi.org/10.1016/j.paleo.2015.05.017.
Lymer, G., Lofi, J., Gaullier, V., Maillard, A., Thinon, I., Sage, F., Chanier, F., Vendeville, B.C., 2018. The Western Tyrrhenian Sea revisited: New evidence for a rifted basin during the Messinian Salinity Crisis. Mar. Geol. 398, 1–21. https://doi.org/10.1016/j.margeo.2017.12.009.
Madof, A.S., Connell, S.D., 2018. Northern Levant Basin. In: Lofi, et al. (Eds.), Atlas of the Messinian Salinity Crisis markers in the Mediterranean and Black SeasMémoires de la Société géologique de France 179. World Geological Map Commission, pp. 60–62.
Madof, A.S., Bertoni, C., Lofi, J., 2019. Discovery of vast fluvial deposits provides evidence for drawdown during the late Miocene Messinian salinity crisis. Geology 47 (2), 171–174. https://doi.org/10.1130/G45873.1.
Magyar, I., Geary, D.H., Lantos, M., Müller, P., Süto-Szentai, M., 1999a. Integrated biostratigraphic, magnetostratigraphic and chronostratigraphic correlations of the Late Miocene Lake Pannon deposits. Acta Geol. Hung. 42 (1), 5–31.
Magyar, I., Geary, D.H., Müller, P., 1999b. Paleogeographic evolution of the late miocene Lake Pannon in Central Europe. Paleogeogr. Paleoclimatol. Paleoecol. 147 (3–4), 151–167.
Maillard, A., Mauffret, A., 2006. Relationship between erosion surfaces and Late Miocene Salinity Crisis deposits in the Valencia Basin (northwestern Mediterranean): evidence for an early sea-level fall. Terra Nova 18 (5), 321–329. https://doi.org/10.1111/j.1365-3121.2006.00696.x.
Maillard, A., Mauffret, A., 2011. Valencia through. In: Lofi, et al. (Eds.), Atlas of the Messinian Salinity Crisis markers in the Mediterranean and Black SeasMémoires de la Société géologique de France 179. World Geological Map Commission (72 pp.).
Maillard, A., Mauffret, A., 2013. Structure and present-day compression in the offshore area between Alicante and Ibiza Island (Eastern Iberian Margin). Tectonophysics 591, 116–130.
Maillard, A., Gorini, C., Mauffret, A., Sage, F., Lofi, J., Gaullier, V., 2006. Offshore evidence of polyphase erosion in the Valencia Basin (Northwestern Mediterranean): scenario for the Messinian Salinity Crisis. Sediment. Geol. 188–189, 69–91.
Maillard, A., Hübscher, C., Benkhelil, J., Tahchi, E., 2011a. Deformed Messinian markers in the Cyprus Arc: tectonic and/or Messinian Salinity Crisis indicators? Basin Res. 23, 146–170.
Maillard, A., Lofi, J., Déverchère, J., Gaullier, V., Loncke, L., Sage, F., Thinon, I., Guennoc, P., Gillet, H., Gorini, C., 2011b. Synthesis. In: Lofi, J., Déverchère, J., et al. (Eds.), Seismic Atlas of the Messinian Salinity Crisis Markers in the Offshore Mediterranean Domain. – CCGM & Mém. Soc. géol. Fr., n.s., 179, 72 p.
Maillard, A., Driussi, O., Lofi, J., Briais, A., Chanier, F., Hübscher, C., Gaullier, V., 2014. Record of the Messinian Salinity Crisis in the SW Mallorca area (Balearic Promontory, Spain). Mar. Geol. 357, 304–320. https://doi.org/10.1016/j.margeo.2014.10.001.
Maillard, A., Gaullier, V., Lézin, C., Chanier, F., Odonne, F., Lofi, J., 2020. New onshore/offshore evidence of the Messinian Erosion Surface from key areas: The Ibiza-Balearic Promontory and the Orosei-Eastern Sardinian margin. Découverte de la surface d'érosion messinienne onshore/offshore dans deux lieux clés: le Promontoire Baléares (Ibiza) et la marge est-sarde (Orosei). Bulletin de la Société Géologique de France 191 (1). https://doi.org/10.1051/bsgf/2020007.
Maniscalco, R., Casciano, C.I., Distefano, S., Grossi, F., Di Stefano, A., 2019. Facies analysis in the Second Cycle Messinian evaporites predating the early Pliocene reflooding: the Balza Soletta section (Corvillo Basin, central Sicily). Ital. J. Geosci. 138 (3), 301–316. https://doi.org/10.3301/IJG.2019.06.
Manzi, V., Lugli, S., Ricci Lucchi, F., Roveri, M., 2005. Deep-water clastic evaporites deposition in the Messinian Adriatic foredeep (northern Apennines, Italy): did the Mediterranean ever dry out? Sedimentology 52, 875–902.
Manzi, V., Roveri, M., Gennari, R., Bertini, A., Biffi, U., Giunta, S., Iaccarino, S.M., Lanci, L., Lugli, S., Negri, A., Riva, A., Rossi, M.E., Taviani, M., 2007. The deep-water counterpart of the messinian lower evaporites in the apennine foredeep: the fanantello section (northern Apennines, Italy). Paleogeogr. Paleoclimatol. Paleoecol. 251, 470–499.

Manzi, V., Lugli, S., Roveri, M., Schreiber, B.C., 2009. A new facies model for the Upper Gypsum of Sicily (Italy): chronological and paleoenvironmental constraits for the Messinian salinity crisis in the Mediterranean. Sedimentology 56. https://doi.org/10.1111/j.1365-3091.2009.01063.x, 1937-1960.

Manzi, V., Lugli, S., Roveri, M., Schreiber, B.C., Gennari, R., 2011. The Messinian CdB (Sicily, Italy) revisited. Geol. Soc. Am. Bull. 123, 347–370. https://doi.org/10.1130/B30262.1.

Manzi, V., Gennari, R., Hilgen, F., Krijgsman, W., Lugli, S., Roveri, M., Sierro, F.J., 2013. Age refinement of the Messinian salinity crisis onset in the Mediterranean. Terra Nova 25 (4), 315–322.

Manzi, V., Lugli, S., Roveri, M., Dela, Pierre F., Gennari, R., Lozar, F., Natalicchio, M., Schreiber, B.C., Taviani, M., Turco, E., 2016a. The Messinian salinity crisis in Cyprus: A further step towards a new stratigraphic framework for Eastern Mediterranean. Basin Res. 28, 207–236. https://doi.org/10.1111/bre.12107.

Manzi, V., Gennari, R., Lugli, S., Minelli, N., Reghizzi, M., Roveri, M., Schreiber, B.C., 2016b. Comment on "Carbonate deposition and diagenesis in evaporitic environments: the evaporative and sulphur-bearing limestones during the settlement of the Messinian Salinity Crisis in Sicily and Calabria" by Caruso et al., 2015. Palaeo3, 429, 136e162. Palaeogeogr. Palaeoclimatol. Palaeoecol. 459, 585–596.

Manzi, V., Gennari, R., Lugli, S., Persico, D., Reghizzi, M., Roveri, M., Schreiber, B.C., Calvo, R., Gavrieli, I., Gvirtzman, Z., 2018. The onset of the Messinian salinity crisis in the deep Eastern Mediterranean basin. Terra Nova 30 (3), 189–198. https://doi.org/10.1111/ter.12325.

Manzi, V., Argnani, A., Corcagnani, A., Lugli, S., Roveri, M., 2020. The Messinian salinity crisis in the Adriatic foredeep: evolution of the largest evaporitic marginal basin in the Mediterranean. Mar. Pet. Geol. 115, 104288 https://doi.org/10.1016/j.marpetgeo.2020.104288.

Marcano, M.C., Frank, T.D., Mukasa, S.B., Lohmann, K.C., Taviani, M., 2015. Diagenetic incorporation of Sr into aragonitic bivalve shells: Implications for chronostratigraphic and paleoenvironmental interpretations. Depositional Record 1 (1), 38–52. https://doi.org/10.1016/j.marpetgeo.2020.104288.

Markovic, S., Paytan, A., Li, H., Wortmann, U.G., 2016. A revised seawater sulfate oxygen isotope record for the last 4Myr. Geochim. Cosmochim. Acta 175, 239–251.

Marsaglia, K.M., Tribble, J.S., 1999. Petrography and mineralogy of the uppermost Messinian section and the Pliocene/Miocene boundary at Site 975, Western Mediterranean Sea. In: Proc. ODP, Sci. Results, Vol. 161, pp. 3–20. Ocean Drilling Program College Station, TX.

Martín-Suárez, E., Freudenthal, M., Krijgsman, W., Fortuin, R., 2000. On the age of the continental deposits of the Zorreras Member (Sorbas Basin, SE Spain). Géobios 33, 505–512.

Marzocchi, A., Lunt, D.J., Flecker, R., Bradshaw, C.D., Farnsworth, A., Hilgen, F.J., 2015. Orbital control on late Miocene climate and the North African monsoon: insight from an ensemble of sub-precessional simulations. Clim. Past 11 (10), 1271–1295. https://doi.org/10.5194/cpd-11-2181-2015.

Marzocchi, A., Flecker, R., Van Baak, C.G.C., Lunt, D.J., Krijgsman, W., 2016. Mediterranean outflow pump: an alternative mechanism for the Lago-mare and the end of the Messinian Salinity Crisis. Geology 44, 523–526. https://doi.org/10.1130/G37646.1.

Marzocchi, A., Flecker, R., Lunt, D.J., Krijgsman, W., Hilgen, F.J., 2019. Precessional drivers of late Miocene Mediterranean sedimentary sequences: African summer monsoon and Atlantic winter storm tracks. Paleoceanogr. Paleoclimatol. 34 (12), 1980–1994. https://doi.org/10.1029/2019PA003721.

Mas, G., 2013. Definició i caracterització de la Formació ses Olles (Lago mare, messinià terminal) a l'Illa de Mallorca (illes balears, mediterrània Occidental). Bolletí de la Societat d'Història Natural de Balears 56, 209–231.

Mas, G., 2015. El registre estratigr`afic del Messini`a terminal i del Pliocè a l'illa de Mallorca. Relacions amb la crisi de salinitat de la Mediterrània. PhD Tesis. Universitat de les Iles Balears. http://www.tdx.cat/handle/10803/375904.

Mas, G., Fornós, J.J., 2020. The messinian salinity crisis in Mallorca: New insights for a western mediterranean stratigraphic scenario. Mar. Pet. Geol. 104656 https://doi.org/10.1016/j.marpetgeo.2020.104656.

Mas, G., Bisconti, M., Torres-Roig, E., Juárez, J., Sacarès, J., 2018a. The last whale of the Messinian. First record of a mysticete cetacean from the Mediterranean Messinian Salinity Crisis. In: 1st Paleontological Virtual Congress. Book of Abstracts—Paleontology in the Virtual Era, Vol. 97.

Mas, G., Maillard, A., Alcover, J.A., Fornós, J.J., Bover, P., Torres-Roig, E., 2018b. Terrestrial colonization of the Balearic Islands: New evidence for the Mediterranean sea-level drawdown during the Messinian Salinity Crisis. Geology 46 (6), 527–530. https://doi.org/10.1130/G40260.1.

Masterson, A.L., Wing, B.A., Paytan, A., Farquhar, J., Johnston, D.T., 2016. The minor sulfur isotope composition of Cretaceous and Cenozoic seawater sulfate. Paleoceanography 31, 779–788.

Mather, A., Martín, J.M., Harvey, A.M., Braga, J.C., 2001. A Field Guide to the Neogene Sedimentary Basins of the Almería Province, South-East Spain., 186-189. Blackwell Science, Oxford.

Mayser, J.P., Flecker, R., Marzocchi, A., Kouwenhoven, T.J., Lunt, D.J., Pancost, R.D., 2017. Precession driven changes in terrestrial organic matter input to the Eastern Mediterranean leading up to the Messinian Salinity Crisis. Earth Planet. Sci. Lett. 462, 199–211. https://doi.org/10.1016/j.epsl.2017.01.029.

McArthur, J.M., Howarth, R.J., Shields, G.A., 2012. Strontium isotope stratigraphy. In: Gradstein, F.M., Ogg, J.G., Schmitz, M.D., Ogg, G.M. (Eds.), The Geological Time Scale 2012. Elsevier B.V, Oxford, pp. 127–144.

McCulloch, M.T., De Deckker, P., 1989. Sr isotope constraints on the Mediterranean environment at the end of the Messinian salinity crisis. Nature 342, 62–65.

McKenzie, J.A., 1999. From desert to deluge in the Mediterranean. Nature 400, 613–614.

McKenzie, J.A., Evans, N., Hodell, D., Aloisi, G., Vasconcelos, C., 2017. Subsurface dolomite formation during post-depositional flow of sulphate-bearing fluids from underlying salt giants: Early Pliocene example at DSDP Leg 42A, Site 374, Ionian Abyssal Plain. EGUGA 10166.

Medaouri, M., Déverchère, J., Graindorge, D., Bracene, R., Badji, R., Ouabadi, A., Yelles, K., Bendib, F., 2014. The transition from Alboran to Algerian basins (Western Mediterranean Sea): chronostratigraphy, deep crustal structure and tectonic evolution at the rear of a narrow slab rollback system. J. Geodyn. 77, 186–205. https://doi.org/10.1016/j.jog.2014.01.003.

Meijer, P.T., Krijgsman, W., 2005. A quantitative analysis of the desiccation and re-filling of the Mediterranean during the Messinian Salinity Crisis. Earth Planet. Sci. Lett. 240 (2), 510–520.

Meilijson, A., Steinberg, J., Hilgen, F., Bialik, O.M., Waldmann, N.D., Makovsky, Y., 2018. Deep-basin evidence resolves a 50-year-old debate and demonstrates synchronous onset of Messinian evaporite deposition in a non-desiccated Mediterranean. Geology 46 (3), 243–246. https://doi.org/10.1130/G39868.1.

Meilijson, A., Hilgen, F., Sepúlveda, J., Steinberg, J., Fairbank, V., Flecker, R., Waldmann, N.D., Spaulding, S.A., Bialik, O.M., Boudinot, F.G., Illner, P., Makovsky, Y., 2019. Chronology with a pinch of salt: integrated stratigraphy of Messinian evaporites in the deep Eastern Mediterranean reveals long-lasting halite deposition during Atlantic connectivity. Earth-Sci. Rev. 194, 374–398. https://doi.org/10.1016/j.earscirev.2019.05.011.

Melinte-Dobrinescu, M.C., Suc, J.-P., Clauzon, G., Popescu, S.-M., Armijo, R., Meyer, B., Biltekin, D., Çağatay, M.N., Ucarkus, G., Jouannic, G., Fauquette, S., Çakir, Z., 2009. The Messinian salinity crisis in the Dardanelles region: Chronostratigraphic constraints. Paleogeogr. Paleoclimatol. Paleoecol. 278, 24–39. https://doi.org/10.1016/j.paleo.2009.04.009.

Merzeraud, G., Achalhi, M., Cornee, J.J., Münch, P., Azdimousa, A., Moussa, A.B., 2019. Sedimentology and sequence stratigraphy of the late-Messinian-Early pliocene continental to marine deposits of the Boudinar basin (North Morocco). J. Afr. Earth Sci. 150, 205–223. https://doi.org/10.1016/j.jafrearsci.2018.11.002.

Meulenkamp, J.E., Sissingh, W., 2003. Tertiary paleogeography and tectonostratigraphic evolution of the Northern and Southern Peri-Tethys platforms and the intermediate domains of the African-Eurasian convergent plate boundary zone. Paleogeogr. Paleoclimatol. Paleoecol. 196 (1-2), 209–228.

Meulenkamp, J.E., Dermitzakis, M., Georgiades-Dikeoulia, E., Jonkers, H.A., Boger, A., 1979. Field Guide to the Neogene of Crete. Publication of the Department of Geology and Paleontology, University of Athens, A, 32, pp. 1–32.

Micallef, A., Camerlenghi, A., Garcia-Castellanos, D., Cunarro Otero, D., Gutscher, M.-A. M.A., Barreca, G., Spatola, D., Facchin, L., Geletti, R., Krastel, S., Gross, F., Urlaub, M., Sulli, A., Basilone, L., Basilone, G., 2018. Evidence of the Zanclean megaflood in the eastern Mediterranean Basin. Sci. Rep. 8, 1–8. https://doi.org/10.1038/s41598-018-19446-3.

Micallef, A., Camerlenghi, A., Georgiopoulou, A., Garcia-Castellanos, D., Gutscher, M.-A., Lo Iacono, C., Huvenne, V.A.I., Mountjoy, J.J., Paull, C.K., Le Bas, T., Spatola, D., Facchin, L., Accettella, D., 2019. Geomorphic evolution of the Malta Escarpment and implications for the Messinian evaporative drawdown in the eastern Mediterranean Sea. Geomorphology 327, 264–283. https://doi.org/10.1016/j.geomorph.2018.11.012.

Milker, Y., Schmiedl, G., 2012. A taxonomic guide to modern benthic shelf foraminifera of the western Mediterranean Sea. Palaeontol. Electron. 15 (2), 1–134. https://doi.org/10.26879/271.

Mocnik, A., Camerlenghi, A., Del Ben, A., Geletti, R., Wardell, N., Zgur, F., 2014. The Messinian Salinity Crisis in the West-Mediterranean Basins: comparison between two rifted margins. In: Proceedings of the 33rd GNGTS Conference, Bologna, Vol. 1, pp. 156–163.

Mocnik, A., Del Ben, A., Camerlenghi, A., Geletti, R., Saule, M., 2018. 12. Ionian Basin. In J. Lofi (Ed.), Seismic Atlas of the Messinian salinity crisis markers in the Mediterranean sea. Volume 2. - Mémoires de la Société géologique de France, n.s., 2018, t. 181, and Commission for the Geological Map of the World, pp. 41–44.

Modestou, S., Simon, D., Gutjahr, M., Marzocchi, A., Kouwenhoven, T.J., Ellam, R.M., Flecker, R., 2017. Precessional variability of $^{87}Sr/^{86}Sr$ in the late miocene sorbas basin: An interdisciplinary study of drivers of interbasin exchange. Paleoceanography 32 (6), 531–552.

Montadert, L., Letouzey, J., Mauffret, A., 1978. Messinian event: seismic evidence. In: Hsü, K.J., Montadert, L., et al. (Eds.), Initial Reports of the Deep Sea Drilling Project, 1. US Government Printing Office, Washington, DC, pp. 1037–1050.

Mudie, P.J., Marret, F., Mertens, K.N., Shumilovskikh, L., Leroy, S.A., 2017. Atlas of modern dinoflagellate cyst distributions in the Black Sea Corridor: from Aegean to Aral Seas, including Marmara, Black, Azov and Caspian Seas. Mar. Micropaleontol. 134, 1–152.

Müller, D.W., Mueller, P.A., 1991. Origin and age of the Mediterranean Messinian evaporites: implications from Sr isotopes. Earth Planet. Sci. Lett. 107 (1), 1–12.

Müller, D.W., Mueller, P.A., McKenzie, J.A., 1990. Strontium isotopic ratios as fluid tracers in Messinian evaporites of the Tyrrhenian Sea (western Mediterranean Sea). In: Proceedings of the Ocean Drilling Program, Scientific Results (Vol. 107, 603-614). College Station, Tex.: Ocean Drill. Program.

Natalicchio, M., Birgel, D., Peckmann, J., Lozar, F., Carnevale, G., Liu, X., Hinrichs, K.-U., Dela Pierre, F., 2017. An archaeal biomarker record of paleoenvironmental change across the onset of the Messinian salinity crisis in the absence of evaporites (Piedmont Basin, Italy). Org. Geochem. 113, 242–253.

Natalicchio, M., Dela Pierre, F., Birgel, D., Brumsack, H., Carnevale, G., Gennari, R., Gier, S., Lozar, F., Pellegrino, L., Sabino, M., Schnetger, B., Peckmann, J., 2019. Paleoenvironmental change in a precession-paced succession across the onset of the Messinian salinity crisis: insight from element geochemistry and molecular fossils.

Paleogeogr. Paleoclimatol. Paleoecol. 518, 45–61. https://doi.org/10.1016/j.paleo.2019.01.009.
Nesteroff, W.D., 1973. Un modéle pour les évaporites messinienne en Méditerranée, bassins peu profonds avec dépot d'évaporites lagunaires. In: Drooger, C.W. (Ed.), Messinian Events in the Mediterranean. North-Holland Publ. Co., Amsterdam, pp. 68–81.
Netzeband, G., Hübscher, C., Gajewski, G., 2006. The structural evolution of the Messinian evaporites in the Levantine Basin. Mar. Geol. 230, 249–273.
Ochoa, D., Sierro, F.J., Lofi, J., Maillard, A., Flores, J.A., Suárez, M., 2015. Synchronous onset of the Messinian evaporite precipitation: First Mediterranean offshore evidence. Earth Planet. Sci. Lett. 427, 112–124. https://doi.org/10.1016/j.epsl.2015.06.059.
Ochoa, D., Sierro, F.J., Hilgen, F.J., Cortina, A., Lofi, J., Kouwenhoven, T., Flores, J.A., 2018. Origin and implications of orbital-induced sedimentary cyclicity in Pliocene well-logs of the Western Mediterranean. Mar. Geol. 403, 150–164. https://doi.org/10.1016/j.margeo.2018.05.009.
Odin, G.S., Vai, G.B., Cosca, M., Tateo, F., Hunziker, J.C., 1997. Integrated stratigraphy of the Maccarone section. In: Montanari, A., Odin, G.S., Coccioni, R. (Eds.), Miocene Stratigraphy: An Integrated Aroach: Developments in Paleontology and Stratigraphy, 15. Elsevier Science B.V, Amsterdam, Netherlands, pp. 531–545.
Ogniben, L., 1955. Le argille scagliose del Crotonese. Memorie e Note dell'Istituto di Geologia Alicata di Napoli 6, 1–72.
Omodeo-Salé, S., Gennari, R., Lugli, S., Manzi, V., Roveri, M., 2012. Tectonic and climatic control on the Late Messinian sedimentary evolution of the Nijar Basin (Betic Cordillera, Southern Spain). Basin Res. 24, 314–337. https://doi.org/10.1111/j.1365-2117.2011.00527.x.
Orszag-Sperber, F., 2006. Changing perspectives in the concept of "Lago-Mare" in Mediterranean Late Miocene evolution. Sediment. Geol. 188, 259–277. https://doi.org/10.1016/j.sedgeo.2006.03.008.
Orszag-Sperber, F., Rouchy, J.M., 1979. Le Miocène terminal et le Pliocène inférieur au sud de Chypre, livret-guide, 5e séminaire sur le Messinien. Chypre, 60 p.
Orszag-Sperber, F., Rouchy, J.M., Blanc-Valleron, M.M., 2000. La transition Messinien-Pliocène en Méditerranée orientale (Chypre): la période du Lago-Mare et sa signification. Comptes Rendus de l'Académie des Sciences-Series IIA-Earth and. Planet. Sci. 331 (7), 483–490.
Orszag-Sperber, F., Caruso, A., Blanc-Valleron, M.M., Merle, D., Rouchy, J.M., 2009. The onset of the Messinian salinity crisis: insights from Cyprus sections. Sediment. Geol. 217 (1-4), 52–64. https://doi.org/10.1016/j.sedgeo.2009.03.006.
Palcu, D.V., Golovina, L.A., Vernyhorova, Y.V., Popov, S.V., Krijgsman, W., 2017. Middle Miocene paleoenvironmental crises in Central Eurasia caused by changes in marine gateway configuration. Glob. Planet. Chang. 158, 57–71. https://doi.org/10.1016/j.gloplacha.2017.09.013.
Palmer, M.R., Edmond, J.M., 1992. Controls over the strontium isotope composition of river water. Geochim. Cosmochim. Acta 56 (5), 2099–2111.
Pellen, R., Popescu, S.-M., Suc, J.-P., Melinte-Dobrinescu, M.C., Rubino, J.-L., Rabineau, M., Marabini, S., Loget, N., Casero, P., Cavazza, W., Head, M.J., Aslanian, D., 2017. The Apennine foredeep (Italy) during the latest Messinian: Lago Mare reflects competing brackish and marine conditions based on calcareous nannofossils and dinoflagellate cysts. Geobios 50, 237–257. https://doi.org/10.1016/j.geobios.2017.04.004.
Pellen, R., Aslanian, D., Rabineau, M., Suc, J.P., Gorini, C., Leroux, E., Blanpied, C., Silenziario, C., Popescu, S.M., Rubino, J.L., 2019. The Messinian Ebro River incision. Glob. Planet. Chang. 181, 102988 https://doi.org/10.1016/j.gloplacha.2019.102988.
Pellerin, A., Antler, G., Holm, S.A., Findlay, A.J., Crockford, P.W., Turchyn, A.V., Jørgensen, B.B., Finster, K., 2019. Large sulfur isotope fractionation by bacterial sulfide oxidation. Sci. Adv. 5 eaaw1480-eaaw1480.
Pérez-Asensio, J.N., Aguirre, J., Schmiedl, G., Civis, J., 2012. Impact of restriction of the Atlantic-Mediterranean gateway on the Mediterranean Outflow Water and eastern Atlantic circulation during the Messinian. Paleoceanography 27 (3). https://doi.org/10.1029/2012PA002309.
Peucker-Ehrenbrink, B., Fiske, G.J., 2019. A continental perspective of the seawater 87Sr/86Sr record: A review. Chem. Geol. 510, 140–165. https://doi.org/10.1016/j.chemgeo.2019.01.017.
Pierre, C., 1974. Contribution ~ l'Jtude sgdimentologique et isotopique des evaporites messiniennes de la Mediterrane; implications geodynamiques. Thesis, University of Paris.
Pierre, C., 1982. Teneurs en isotopes stables (18O,2H,13C,34S) et conditions de génèse des évaporites marines : Alication à quelques milieux actuels et au Messinien de la Mediterrannée, Ecole Normale Supérieure. Université Paris Sud Orsay, p. 262.
Pierre, C., Fontes, J.-C., 1978. Isotope Composition of Messinian sediments from the Mediterranean Sea as indicators of paleoenvironments and diagenesis, in: Texas A M University, O.D.P.C.S., TX, United States (Ed.), Initial reports of the Deep Sea Drilling, covering Leg 42 of the cruises of the drilling Vessel Glomar Challenger Malaga Spain to Itanbul Turkey. April-May 1975. University of California. Scris Institution of Oceanography. National Science Foundation. National Ocean Sediment Coring Program, pp. 635–650.
Pierre, C., Rouchy, J.M., 1990. Stable isotope composition of carbonates in the Tyrrhenian Sea, Sulement to: Pierre, C; Rouchy, JM (1990): Sedimentary and diagenetic evolution of Messinian evaporites in the Tyrrhenian Sea (ODP Leg 107, Sites 652, 653, and 654): petrographic, mineralogical, and stable isotope records. In: Kastens, K.A., Mascle, J., et al. (Eds.), Proceedings of the Ocean Drilling Program, Scientific Results, College Station, TX (Ocean Drilling Program), 107, pp. 187–210. https://doi.org/10.2973/odp.proc.sr.107.131.1990. PANGAEA.
Pierre, C., Rouchy, J.M., Blanc-Valleron, M.-M., 1998. Sedimentological and stable isotope changes at the Messinian-Pliocene boundary in the eastern Mediterranean. In: Robertson, A.H.F., Emeis, K.-C., Richter, C., Camerlenghi, A. (Eds.), Proc. O.D.P., Sci. Res, vol. 160. Ocean Drilling Program, College Station, TX, pp. 3–8.
Pierre, C., Caruso, A., Blanc-Valleron, M.M., Rouchy, J.M., Orzsag-Sperber, F., 2006. Reconstruction of the paleoenvironmental changes around the Miocene-Pliocene boundary along a West-East transect across the Mediterranean. Sediment. Geol. 188, 319–340. https://doi.org/10.1016/j.sedgeo.2006.03.011.
Placzek, C.J., Quade, J., Patchett, P.J., 2011. Isotopic tracers of paleohydrologic change in large lakes of the Bolivian Altiplano. Quat. Res. 75 (1), 231–244. https://doi.org/10.1016/j.yqres.2010.08.004.
Polonia, A., Torelli, L., Mussoni, P., Gasperini, L., Artoni, A., Klaeschen, D., 2011. The Calabrian Arc subduction complex in the Ionian Sea: Regional architecture, active deformation, and seismic hazard. Tectonics 30 (5).
Popescu, S.M., Melinte, M.C., Suc, J.P., Clauzon, G., Quillévéré, F., Süto-Szentai, M., 2007. Earliest Zanclean age for the Colombacci and uppermost Di Tetto formations of the "latest Messinian" northern Apennines: New paleoenvironmental data from the Maccarone section (Marche Province, Italy). Geobios 40 (3), 359–373. https://doi.org/10.1016/j.geobios.2006.11.005.
Popescu, S.-M., Melinte, M.-C., Suc, J.-P., Clauzon, G., Quillévéré, F., Süto-Szentai, M., 2008. Marine reflooding of the Mediterranean after the Messinian Salinity Crisis predates the Zanclean GSSP. Reply to the "Comment on 'Earliest Zanclean age for the Colombacci and uppermost Di Tetto formations of the "latest Messinian" northern Apennines: new paleoenvironmental data from the Maccarone section (Marche Province, Italy)'" by Popescu et al. (2007). Geobios 40 (359-373) authored by Roveri et al. Geobios 41, 657-660.
Popescu, S.M., Dalesme, F., Jouannic, G., Escarguel, G., Head, M.J., Melinte-Dobrinescu, M.C., Sütö-Szentai, M., Bakrac, K., Clauzon, G., Suc, J.P., 2009. Galeacysta etrusca complex: dinoflagellate cyst marker of Paratethyan influxes to the Mediterranean Sea before and after the peak of the Messinian Salinity Crisis. Palynology 33 (2), 105–134.
Popescu, S.-M., Dalibard, M., Suc, J.-P., Barhoun, N., Melinte-Dobrinescu, M.C., Bassetti, M.A., Deaconu, F., Head, M.J., Gorini, C., Do Couto, D., Rubino, J.-L., Auxietre, J.-L., Floodpage, J., 2015. Lago Mare episodes around the Messinian-Zanclean boundary in the deep southwestern Mediterranean. Mar. Pet. Geol. 66, 55–70. https://doi.org/10.1016/j.marpetgeo.2015.04.002.
Popescu, S.M., Melinte-Dobrinescu, M.C., Suc, J.P., Do Couto, D., 2017. Ceratolithus acutus (= C. armatus), calcareous nannofossil marker of the marine reflooding that terminated the Messinian salinity crisis: Comment on "Paratethyan ostracods in the Spanish Lago-Mare: More evidence for interbasinal exchange at high Mediterranean sea level" by. Paleogeogr., Paleoclimatol., Paleoecol. 441, 854-870. Paleogeogr. Paleoclimatol. Paleoecol. 485, 986–989. https://doi.org/10.1016/j.paleo.2016.07.011.
Popov, S.V., Rögl, F., Rozanov, A.Y., Steininger, F.F., Shcherba, I.G., Kovac, M., 2004. Lithological-paleogeographic maps of Paratethys-10 maps late Eocene to pliocene.
Popov, S.V., Shcherba, I.G., Ilyina, L.B., Nevesskaya, L.A., Paramonova, N.P., Khondkarian, S.O., Magyar, I., 2006. Late Miocene to Pliocene paleogeography of the Paratethys and its relation to the Mediterranean. Paleogeogr. Paleoclimatol. Paleoecol. 238 (1-4), 91–106.
Raad, F., Lofi, J., Maillard, A., Tzevahirtzian, A., Caruso, A., 2021. The Messinian Salinity Crisis deposits in the Balearic Promontory: an undeformed analog of the MSC Sicilian basins?? Mar. Pet. Geol. 104777 https://doi.org/10.1016/j.marpetgeo.2020.104777.
Radeff, G., Cosentino, D., Cipollari, P., Schildgen, T.F., Iadanza, A., Strecker, M.R., Darbas, G., Gurbuz, K., 2016. Stratigraphic architecture of the upper Messinian deposits of the Adana Basin (southern Turkey): implications for the Messinian salinity crisis and the Taurus petroleum system. Ital. J. Geosci. 135, 408–424.
Radeff, G., Schildgen, T.F., Cosentino, D., Strecker, M.R., Cipollari, P., Darbaş, G., Gürbüz, K., 2017. Sedimentary evidence for late Messinian uplift of the SE margin of the Central Anatolian Plateau: Adana Basin, southern Turkey. Basin Res. 29, 488–514. https://doi.org/10.1111/bre.12159.
Reiche, S., Hübscher, C., Ehrhardt, A., 2016. The impact of salt on the late Messinian to recent tectonostratigraphic evolution of the Cyprus subduction zone. Basin Res. 28 (5), 569–597. https://doi.org/10.1111/bre.12122.
Ricchiuto, T.E., McKenzie, J.A., 1978. Stable Isotopic investigation of Messinian sulfate samples from DSDP. LEG 42. Eastern Mediterranean Sea. In: Texas A M University, O.D.P.C.S., TX, United States (Ed.), Initial reports of the Deep Sea Drilling covering Leg 42 of the cruises of the drilling vessel Glomar Challenger. Malaga, Spain to Istanbul, Turkey. April-May 1975. University of California. Scris Institution of Oceanography, National Science Foundation. National Ocen Sediment Coring Program, pp. 657–660.
Rio, D., Negri, A., 1988. Calcareous nannofossils (Monticino Quarry, Faenza). In: De Giuli, C., Vai, G.B. (Eds.), Fossil Vertebrates in the Lamone Valley, Romagna Apennines. Field Trip Guidebook of the International Workshop "Continental faunas at the Miocene/Pliocene boundary", Faenza, pp. 55–57.
Robertson, A.H.F., 1998a. Late Miocene paleoenvironments and tectonic settings of the southern margin of Cyprus and the Eratosthenes Seamount. In: Robertson, A.H.F., Emeis, K.C., Richter, C., Camerlenghi, A. (Eds.), Proc. ODP, Sci. Res., vol. 160 Ocean Drilling Program, College Station, TX, pp. 453–463.
Robertson, A.H., 1998b. Tectonic significance of the Eratosthenes Seamount: a continental fragment in the process of collision with a subduction zone in the eastern Mediterranean (Ocean Drilling Program Leg 160). Tectonophysics 298 (1-3), 63–82.
Robertson, A.H.F., Eaton, S., Follows, E.J., Payne, A.S., 1995. Depositional processes and basin analysis of Messinian evaporites in Cyprus. Terra Nova 7, 233–253.
Roca, E., Guimera, J., 1992. The Neogene structure of the eastern iberian margin: structural constraints on the crustal evolution of the Valencia trough (western mediterranean). Tectonophysics 203, 203–218.

Roep, Th.B., Van Harten, D., 1979. Sedimentological and ostracodological observations on Messinian post-evaporite deposits in some southeastern Spanish basins. Annales Géologiques des Pays Helleniques 3, 1037–1044.
Roep, T.B., Dabrio, C.J., Fortuin, A.R., Polo, M.D., 1998. Late highstand patterns of shifting and steing coastal barriers and washover-fans (Late Messinian, Sorbas Basina, SE Spain). Sediment. Geol. 116, 27–56.
Rögl, F., 1998. Paleogeographic considerations for Mediterranean and Paratethys seaways (Oligocène to Miocene). Ann. Naturhist. Mus. Wien 9 9 A, 279310.
Rosenfeld, A., 1977. The sieve pores of Cyprideis torosa (Jones, 1850) from the Messinian Mavqi'im Formation in the coastal plain and continental shelf of Israel as an indicator of paleoenvironment. Isr. J. Earth Sci. 26, 89993.
Rossi, M., 2017. Outcrop and seismic expression of stratigraphic patterns driven by accommodation and sediment suly turnarounds: Implications on the meaning and variability of unconformities in syn-orogenic basins. Mar. Pet. Geol. 87, 112–127. https://doi.org/10.1016/j.marpetgeo.2017.03.032.
Rossi, M., Rogledi, S., 1988. Relative sea-level changes, local tectonic setting and basin margin sedimentation in the interference zone between two orogenic belts: seismic stratigraphic examples from Padan foreland basin, northern Italy. In: Fan Deltas: Sedimentology and Tectonic Settings, pp. 368–384.
Rossi, M., Minervini, M., Ghielmi, M., Rogledi, S., 2015a. Messinian and Pliocene erosional surfaces in the Po Plain-Adriatic Basin: Insights from allostratigraphy and sequence stratigraphy in assessing play concepts related to accommodation and gateway turnarounds in tectonically active margins. Marine Petroleum Geol. The Messinian events and hydrocarbon exploration in the Mediterranean 66, 192–216. https://doi.org/10.1016/j.marpetgeo.2014.12.012.
Rossi, C., Vilas, L., Arias, C., 2015b. The Messinian marine to nonmarine gypsums of Jumilla (Northern Betic Cordillera, SE Spain): Isotopic and Sr concentration constraints on the origin of parent brines. Sediment. Geol. 328, 96–114. https://doi.org/10.1016/j.sedgeo.2015.08.007.
Rouchy, J.M., 1982. La crise evaporitique messinienne de Mediterranee: nouvelles propositions pour une interpretation genetique. Thesis, Mem, p. 280. Mus. Natn. Hist. Nat, Paris.
Rouchy, J.M., Caruso, A., 2006. The Messinian salinity crisis in the Mediterranean basin: a reassessment of the data and an integrated scenario. Sediment. Geol. 188, 35–67. https://doi.org/10.1016/j.sedgeo.2006.02.005.
Rouchy, J.M., Orszag-Sperber, F., Blanc-Valleron, M.M., Pierre, C., Rivière, M., Combourieu-Nebout, N., Panayides, I., 2001. Paleoenvironmental changes at the Messinian-Pliocene boundary in the eastern Mediterranean (southern Cyprus basins): significance of the Messinian Lago-Mare. Sediment. Geol. 145 (1-2), 93–117.
Rouchy, J.M., Pierre, C., Et-Touhami, M., Kerzazi, K., Caruso, A., Blanc-Valleron, M.M., 2003. Late Messinian to Early Pliocene paleoenvironmental changes in the Melilla Basin (NE Morocco) and their relation to Mediterranean evolution. Sediment. Geol. 163 (1-2), 1–27.
Rouchy, J.M., Caruso, A., Pierre, C., Blanc-Valleron, M.M., Bassetti, M.A., 2007. The end of the Messinian salinity crisis: evidences from the Chelif Basin (Algeria). Paleogeogr. Paleoclimatol. Paleoecol. 254 (3–4), 386–417. https://doi.org/10.1016/j.paleo.2007.06.015.
Roveri, M., Manzi, V., Bassetti, M.A., Merini, M., Ricci Lucchi, F., 1998. Stratigraphy of the Messinian post-evaporitic stage in eastern-Romagna (northern Apennines, Italy). G. Geol. 60, 119–142.
Roveri, M., Bassetti, M.A., Ricci Lucchi, F., 2001. The Mediterranean Messinian salinity crisis: an Apennines foredeep perspective. Sediment. Geol. 140, 201–214.
Roveri, M., Boscolo Gallo, A., Rossi, M., Gennari, R., Iaccarino, S.M., Lugli, S., Manzi, V., Negri, A., Rizzini, F., Taviani, M., 2005. The Adriatic foreland record of Messinian events (central Adriatic sea, Italy). GeoActa 4 (139), 158.
Roveri, M., Bertini, A., Cosentino, D., Di Stefano, A., Gennari, R., Gliozzi, E., Grossi, F., Iaccarino, S.M., Lugli, S., Manzi, V., Taviani, M., 2008a. A high-resolution stratigraphic framework for the latest Messinian events in the Mediterranean area. Stratigraphy 5 (3-4), 323–342.
Roveri, M., Lugli, S., Manzi, V., Schreiber, B.C., 2008b. The Messinian Sicilian stratigraphy revisited: new insights for the Messinian salinity crisis. Terra Nova 20 (6), 483–488. https://doi.org/10.1111/j.1365-3121.2008.00842.x.
Roveri, M., Bertini, A., Cipollari, P., Cosentino, D., Di Stefano, A., Florindo, F., Gennari, R., Gliozzi, E., Grossi, F., Iaccarino, S., Lugli, S., Manzi, V., 2008c. Comment on "Earliest Zanclean age for the Colombacci and uppermost Di Tetto formations of the "latest Messinian" northern Apennines: new palaeoenvironmental data from the Maccarone section (Marche Province, Italy)" by Popescu et al. (2007) Geobios 40 (359–373). Geobios 41, 669-675.
Roveri, M., Gennari, R., Lugli, S., Manzi, V., 2009. The Terminal Carbonate Complex: the record of sea-level changes during the Messinian salinity crisis. GeoActa 8 (63), 63–77.
Roveri, M., Flecker, R., Krijgsman, W., Lofi, J., Lugli, S., Manzi, V., Sierro, F.J., Bertini, A., Camerlenghi, A., De Lange, G., Govers, R., Hilgen, F.J., Hübscher, C., Meijer, P.Th., Stoica, M., 2014a. The Messinian salinity crisis: past and future of a great challenge for marine sciences. Mar. Geol. 349, 113–125. https://doi.org/10.1016/j.margeo.2014.02.002.
Roveri, M., Lugli, S., Manzi, V., Gennari, R., Schreiber, B.C., 2014b. High resolution strontium isotope stratigraphy of the Messinian deep Mediterranean basins: implications for marginal to central basins correlation. Mar. Geol. 349, 113–125. https://doi.org/10.1016/j.margeo.2014.01.002.
Roveri, M., Manzi, V., Bergamasco, A., Falcieri, F., Gennari, R., Lugli, S., 2014c. Dense shelf water cascading and Messinian canyons: a new scenario for the Mediterranean salinity crisis. Am. J. Sci. 314, 751–784. https://doi.org/10.2475/05.2014.03].
Roveri, M., Gennari, R., Persico, D., Rossi, F.P., Lugli, S., Manzi, V., Reghizzi, M., Taviani, M., 2019a. A new chronostratigraphic and paleoenvironmental framework for the end of the Messinian salinity crisis in the Sorbas Basin (Betic Cordillera, southern Spain). Geol. J. 54 (3), 1617–1637. https://doi.org/10.1002/gj.3256.
Roveri, M., Gennari, R., Ligi, M., Lugli, S., Manzi, V., Reghizzi, M., 2019b. The synthetic seismic expression of the Messinian salinity crisis from onshore records: implications for shallow-to deep-water correlations. Basin Res. 31 (6), 1121–1152. https://doi.org/10.1111/bre.12361.
Roveri, M., Lugli, S., Manzi, V., Reghizzi, M., Rossi, F.P., 2020. Stratigraphic relationships between shallow-water carbonates and primary gypsum: insights from the Messinian succession of the Sorbas Basin (Betic Cordillera, Southern Spain). Sediment. Geol. 105678 https://doi.org/10.1016/j.sedgeo.2020.105678.
Ruggieri, G., 1962. La serie marine pliocenica e quaternaria della Val Marecchia: Atti Accad. Sci. Lett. Arti Palermo 19, 1–169.
Ruggieri, G., 1967. The Miocene and later evolution of the Mediterranean sea. Adams and Ager (Eds.). In: Aspects of Tethyan Biogeography: Syst. Ass. Publ. 7, p. 238.
Ryan, W.B.F., 1973. Geodynamic implications of the Messinian crisis of salinity. In: Drooger, C.W. (Ed.), Messinian Events in the Mediterranean. North-Holland Publ. Co., Amsterdam, Netherlands, pp. 26–38.
Ryan, W.B.F., 1976. Quantitative evaluation of the depth of the western Mediterranean before, during and after the late Miocene salinity crisis. Sedimentology 23, 791–813.
Ryan, W.B.F., 1978. Messinian badlands on the southeastern margin of the Mediterranean Sea. Mar. Geol. 27, 349–363.
Ryan, W.B.F., 2008. Modeling the magnitude and timing of evaporative drawdown during the Messinian salinity crisis. Stratigraphy 5, 227–243.
Ryan, W.B.F., 2009. Decoding the Mediterranean salinity crisis. Sedimentology 56 (1), 95–136.
Ryan, W.B.F., Hsü, K.J., Cita, M.B., Dumitrica, P., Lort, P., Maync, W., Nesteroff, W.D., Pautot, P., Stradner, H., Wezel, F.C., 1973. In: Ryan, W.B.F., Hsü, K.J. (Eds.), Initial Reports of the Deep Sea Drilling Project, Vol. 13. U.S. Government Printing Office, Washington, DC, p. 1447.
Sabat, F., Gelabert, B., Rodriguez-Perea, A., Giménez, J., 2011. Geological structure and evolution of Majorca: implications for the origin of the Western Mediterranean. Tectonophysics 510, 217–238.
Sabato Ceraldi, T., Kamel, M., Mason, T., Poole, A., Hossack, J., Slack, J., Fraser, A., 2010. Messinian seismic facies in offshore Sirt Basin Libya and implications for sub-Messinian seismic imaging. In: Paper presented at TOG 2008-Technology of Oil and Gas, Forum and Exhibition, 21-23 October, Tripoli.
Sachse, D., Radke, J., Gleixner, G., 2006. δD values of individual n-alkanes from terrestrial plants along a climatic gradient - implications for the sedimentary biomarker record. Org. Geochem. 37, 469–483.
Sage, F., Von Gronefeld, G., Déverchère, J., Gaullier, V., Maillard, A., Gorini, C., 2005. A record of the Messinian salinity crisis on the western Sardinia margin, northwestern Mediterranean. Mar. Pet. Geol. 22, 757–773.
Sampalmieri, G., Iadanza, A., Cipollari, P., Cosentino, D., Lo Mastro, S., 2010. Paleoenvironments of the Mediterranean Basin at the Messinian hypersaline/hyposaline transition: evidence from natural radioactivity and microfacies of post-evaporitic successions of the Adriatic sub-basin. Terra Nova 22 (4), 239–250. https://doi.org/10.1111/j.1365-3121.2010.00939.x.
Sant, K., Palcu, V., Mandic, D., Krijgsman, O., 2017. Changing seas in the Early-Middle Miocene of Central Europe: a Mediterranean approach to Paratethyan stratigraphy. Terra Nova 29 (5), 273–281.
Schildgen, T.F., Cosentino, D., Frijia, G., Castorina, F., Dudas, F.Ö., Iadanza, A., Sampalmieri, G., Cipollari, P., Caruso, A., Bowring, S.A., Strecker, M.R., 2014. Sea level and climate forcing of the Sr isotope composition of Late Miocene Mediterranean marine basins. Geochem. Geophys. Geosyst. 15, 2964–2983. https://doi.org/10.1002/2014GC005332.
Schmalz, R.F., 1969. Deep-water evaporite deposition, a genetic model. Am. Assoc. Pet. Geol. Bull. 53, 798–823.
Schreiber, B.C., 1997. Field trip to Eraclea Minoa: Upper Messinian. "Neogene Mediterranean Paleoceanography", Excursion Guide Book Palermo-Caltanissetta-Agrigento-Erice (Sicily), 24-27 September 1997, pp. 72–80.
Schütz, K.I., 1994. Structure and stratigraphy of the Gulf of Suez, Egypt, in Interior Rift Basins, edited by S. M. Landon. AAPG Mem. 59, 57–96.
Schwarzhans, W., Agiadi, K., Carnevale, G., 2020. Late Miocene-Early Pliocene evolution of Mediterranean gobies and their environmental and biogeographic significance. Riv. Ital. Paleontol. Stratigr. 126 (3).
Sciuto, F., Baldanza, A., 2020. Full restoration of marine conditions after the late Messinian Mediterranean Lago-Mare phase in Licodia Eubea and Villafranca Tirrena areas (east Sicily). Carnets de géologie.
Sciuto, F., Baldanza, A., Temani, R., Privitera, G., 2018. New reports of Paratethyan ostracods affinity from the Mediterranean Basin (Sicily, Italy). Paleontologia Electronica 21 (1), 1. https://doi.org/10.26879/800.
Segev, A., Avni, Y., Shahar, J., Wald, R., 2017. Late Oligocene and Miocene different seaways to the Red Sea-Gulf of Suez rift and the Gulf of Aqaba-Dead Sea basins. Earth Sci. Rev. 171, 196–219. https://doi.org/10.1016/j.earscirev.2017.05.004.
Selli, R., 1954. Il Bacino del Metauro. Giorn. Geol. 24, 1–294.
Selli, R., 1960. Il Messiniano Mayer-Eymar 1867. Proposta di un neostratotipo. Giornale di Geologia 28, 1–33.
Selli, R., 1973. An outline of the Italian Messinian. In: Drooger, C.W. (Ed.), Messinian Events in the Mediterranean, pp. 150–171. Amsterdam (Kon. Nedl. Akad. Wetensch.).
Sgarrella, F., Sprovieri, R., Di Stefano, E., Caruso, A., 1997. Paleoceanographic conditions at the base of the Pliocene in the Southern Mediterranean Basin. Riv. Ital. Paleontol. Stratigr. 103, 207–220.
Sgarrella, F., Sprovieri, R., Di Stefano, E., Caruso, A., Sprovieri, M., Bonaduce, G., 1999. The Capo Rossello Bore-Hole (Agrigento, Sicily): cyclostratigraphic and

paleoceanographic reconstructions from quantitative analyses of the Zanclean foraminiferal assemblages. Riv. Ital. Paleontol. Stratigr. 105, 303–322.
Sierro, F.J., Flores, J.A., Civis, J., Gonza, J.A., France, G., 1993. Late Miocene globorotaliid event-stratigraphy and biogeography in the NE-Atlantic and Mediterranean. Mar. Micropaleontol. 21 (1-3), 143–167.
Sim, M.S., Bosak, T., Ono, S., 2011. Large sulfur isotope fractionation does not require disproportionation. Science 333, 74–77.
Simon, D., Meijer, P.T., 2017. Salinity stratification of the Mediterranean Sea during the Messinian crisis: A first model analysis. Earth Planet. Sci. Lett. 479, 366–376.
Simon, D., Marzocchi, A., Flecker, R., Lunt, D.J., Hilgen, F.J., Meijer, P.T., 2017. Quantifying the Mediterranean freshwater budget throughout the late Miocene: New implications for sapropel formation and the Messinian Salinity Crisis. Earth Planet. Sci. Lett. 472, 25–37.
Sinninghe Damsté, J.S., Frewin, N.L., Kenig, F., De Leeuw, J.W., 1995. Molecular indicators for palaeoenvironmental changes in a Messinian evaporitic sequence (Vena del Gesso, Italy). I: Variations in extractable organic matter of ten cyclically deposited marl beds. Org. Geochem. 23, 471–483.
Sissingh, W., 1976. Aspects of late Cenozoic evolution of the South Aegean ostracode fauna. Paleogeogr., Paleoclimatol., Paleoecol 20, 131–146.
Snel, E., Mărunţeanu, M., Meulenkamp, J.E., 2006. Calcareous nannofossil biostratigraphy and magnetostratigraphy of the upper Miocene and lower Pliocene of the Northern Aegean (Orphanic Gulf-Strimon Basin areas), Greece. Paleogeogr. Paleoclimatol. Paleoecol. 238 (1-4), 125–150. https://doi.org/10.1016/j.paleo.2006.03.022.
Soria, J.M., Caracuel, J.E., Yébenes, A., Fernández, J., Viseras, C., 2005. The stratigraphic record of the Messinian salinity crisis in the northern margin of the Bajo Segura basin (SE Spain). Sediment. Geol. 179 (3), 225–247. https://doi.org/10.1016/j.sedgeo.2005.05.011.
Soria, J.M., Caracuel, J.E., Corbí, H., Dinarès-Turell, J., Lancis, C., Tent-Manclús, J.E., Yébenes, A., 2007. Estratigrafía y biomagnetoestratigrafía del Messiniense en la sección del Garruchal (Cuenca del Bajo Segura). Implicaciones para la Crisis de Salinidad del Mediterráneo. Geogaceta 41, 215–218.
Soria, J.M., Caracuel, J.E., Corbí, H., Dinarès-Turell, J., Lancis, C., Tent-Manclús, J.E., Yébenes, A., 2008a. The Bajo Segura basin (SE Spain): implications for the Messinian Salinity Crisis in the Mediterranean margins. Stratigraphy 5, 259–265.
Soria, J.M., Caracuel, J.E., Corbí, H., Dinarès-Turell, J., Lancis, C., Tent-Manclús, J.E., Viseras, C., Yébenes, A., 2008b. The Messinian-Early Pliocene stratigraphic record in the southern Bajo Segura basin (Betic Cordillera, Spain). Implications for the Mediterranean salinity crisis. Sediment. Geol. 203, 267–288.
Spatola, D., del Moral-Erencia, J.D., Micallef, A., Camerlenghi, A., Garcia-Castellanos, D., Gupta, S., Bohorquez, P., Gutscher, M.A., Bertoni, C., 2020. A single-stage megaflood at the termination of the Messinian salinity crisis: geophysical and modelling evidence from the eastern Mediterranean Basin. Mar. Geol. 106337 https://doi.org/10.1016/j.margeo.2020.106337.
Stampfli, J., Höcker, C.F.W., 1989. Messinian paleorelief from a 3D seismic survey in the Tarrasco concession area (Spanish Mediterranean Sea). Geologie in Minjbouw 68, 201–210.
Stoica, M., Lazăr, I., Krijgsman, W., Vasiliev, I., Jipa, D., Floroiu, A., 2013. Paleoenvironmental evolution of the East Carpathian foredeep during the late Miocene-early Pliocene (Dacian Basin; Romania). Glob. Planet. Chang. 103, 135–148. https://doi.org/10.1016/j.gloplacha.2012.04.004.
Stoica, M., Krijgsman, W., Fortuin, A., Gliozzi, E., 2016. Paratethyan ostracods in the Spanish Lago-Mare: More evidence for intra-basinal exchange at high Mediterranean sea level. Paleogeogr. Paleoclimatol. Paleoecol. 441, 854–870. https://doi.org/10.1016/j.paleo.2015.10.034.
Strasser, A., Hilgen, F.J., Heckel, P.H., 2006. Cyclostratigraphy-concepts, definitions, and alications. Newsl. Stratigr. 42 (2), 75–114.
Sturani, C., 1973. A fossil eel (Anguilla sp.) from the Messinian of Alba (Tertiary Piedmont Basin). Paleoenvironmental and paleogeographic implications. In: Messinian Events in the Mediterranean. K. Nederl. Akad. Wetensch, Amsterdam, pp. 243–255.
Suárez-González, P., Arenas, C., Benito, M.I., Pomar, L., 2019. Interplay between biotic and environmental conditions in presalt Messinian microbialites of the western Mediterranean (Upper Miocene, Mallorca, Spain). Palaeogeogr. Palaeoclimatol. Palaeoecol. 533, 109–242.
Suc, J.-P., Do Couto, D., Melinte-Dobrinescu, M.C., Macaleţ, R., Quillévéré, F., Clauzon, G., Csato, I., Rubino, J.-L., Popescu, S.-M., 2011. The Messinian salinity crisis in the Dacic Basin (SW Romania) and early Zanclean Mediterranean-Paratethys high sea-level connection. Paleoecol. 310, 256–272. https://doi.org/10.1016/j.paleo.2011.07.018.
Suc, J.-P., Popescu, S.-M., Do Couto, D., Clauzon, G., Rubino, J.-L., Melinte-Dobrinescu, M.C., Quillévéré, F., Brun, J.-P., Dumurdžanov, N., Zagorchev, I., Lesić, V., Tomić, D., Sokoutis, D., Meyer, B., Macalet, R., Rifelj, H., 2015. Marine gateway vs. fluvial stream within the Balkans from 6 to 5 Ma. Mar. Pet. Geol. 66 (1), 231–245. https://doi.org/10.1016/j.marpetgeo.2015.01.013.
Thinon, I., Guennoc, P., Serrano, O., Maillard, A., Lasseur, E., Réhault, J.P., 2016. Seismic markers of the Messinian Salinity Crisis in an intermediate-depth basin: data for understanding the Neogene evolution of the Corsica Basin (Northern Tyrrhenian Sea). Mar. Pet. Geol. 77, 1274–1296. November 2016. https://doi.org/10.1016/j.marpetgeo.2016.02.017.
Thode, H.G., Monster, J., 1965. Sulfur-Isotope Geochemistry of Petroleum, Evaporites, and Ancient Seas1. In: Young, A., Galley, J.E. (Eds.), Fluids in Subsurface Environments. American Association of Petroleum Geologists, p. 0.
Topper, R.P.M., Meijer, P.T., 2015. The precessional phase lag of Messinian gypsum deposition in Mediterranean marginal basins. Palaeogeogr. Palaeoclimatol. Palaeoecol. 417, 6–16.
Topper, R.P.M., Flecker, R., Meijer, P.T., Wortel, M.J.R., 2011. A box model of the Late Miocene Mediterranean Sea: implications from combined 87Sr/86Sr and salinity data. Paleoceanography 26. https://doi.org/10.1029/2010PA002063. PA3223.
Topper, R.P.M., Lugli, S., Manzi, V., Roveri, M., Meijer, P.T., 2014. Precessional control of Sr ratios in marginal basins during the Messinian salinity crisis? Geochem. Geophys. Geosyst. 15-5, 1926–1944. https://doi.org/10.1002/2013GC005192.
Trenkwalder, S., Violanti, D., D'Atri, A., Lozar, F., Dela Pierre, F., Irace, A., 2008. The Miocene/Pliocene boundary in the Early Pliocene micropaleontological record: new data from the Tertiary Piedmont Basin (Moncucco quarry, Torino Hill, northwestern Italy). Boll. Soc. Paleontol. Ital. 47, 87–103.
Turchyn, A.V., Schrag, D.P., 2004. Oxygen Isotope Constraints on the Sulfur Cycle over the Past 10 Million Years. Science 303, 2004.
Turchyn, A.V., Sivan, O., Schrag, D.P., 2006. Oxygen isotopic composition of sulfate in deep sea pore fluid: evidence for rapid sulfur cycling. Geobiology 4, 191–201.
Turchyn, A.V., Schrag, D.P., Coccioni, R., Montanari, A., 2009. Stable isotope analysis of the Cretaceous sulfur cycle. Earth Planet. Sci. Lett. 285, 115–123.
Tzanova, A., Herbert, T.D., Peterson, L., 2015. Cooling Mediterranean Sea surface temperatures during the Late Miocene provide a climate context for evolutionary transitions in Africa and Eurasia. Earth Planet. Sci. Lett. 419, 71–80. https://doi.org/10.1016/j.epsl.2015.03.016.
Urgeles, R., Camerlenghi, A., Garcia-Castellanos, D., De Mol, B., Garces, M., Verges, J., Haslam, I., Hardman, M., 2011. New constraints on the Messinian sealevel drawdown from 3D seismic data of the Ebro margin, western Mediterranean. Basin Res. 23, 123–145. https://doi.org/10.1111/j.1365-2117.2010.00477.x.
Utrilla, R., Pierre, C., Orti, F., Pueyo, J.J., 1992. Oxygen and sulphur isotope compositions as indicators of the origin of Mesozoic and Cenozoic evaporites from Spain. Chem. Geol. 102, 229–244.
Vai, G.B., 1997. Chapter E3 Cyclostratigraphic estimate of the messinian stage duration. In: Montanari, A., Odin, G.S., Coccioni, R. (Eds.), Miocene Stratigraphy: An Integrated Approach. Dev. Paleontol. Stratigr. 15, 463–476.
Vai, G.B., 2016. Over half a century of Messinian salinity crisis. Bol. Geol. Min. 127 (2), 625–641.
Van Baak, C.G.C., Radionova, E.P., Golovina, L.A., Raffi, I., Kuiper, K.F., Vasiliev, I., Krijgsman, W., 2015. Messinian events in the Black Sea. Terra Nova 27, 433–441. https://doi.org/10.1111/ter.12177.
Van Baak, C.G., Stoica, M., Grothe, A., Aliyeva, E., Krijgsman, W., 2016. Mediterranean-Paratethys connectivity during the Messinian salinity crisis: The Pontian of Azerbaijan. Glob. Planet. Chang. 141, 63–81. https://doi.org/10.1016/j.gloplacha.2016.04.005.
Van Baak, C.G., Krijgsman, W., Magyar, I., Sztanó, O., Golovina, L.A., Grothe, A., Hoyle, T.M., Mandic, O., Patina, I.S., Popov, S.V., Radionova, E.P., Stoica, M., Vasiliev, I., 2017. Paratethys response to the Messinian salinity crisis. Earth Sci. Rev. 172, 193–223. https://doi.org/10.1016/j.earscirev.2017.07.015.
Van Couvering, J.A., Berggren, W.A., Drake, R.E., Aguirre, E., Curtis, G.H., 1976. The terminal Miocene event. Mar. Micropaleontol. 1, 263–286.
Van Couvering, J.A., Castradori, D., Cita, M.B., Hilgen, F.J., Rio, D., 2000. The base of the Zanclean Stage and of the Pliocene Series. Episodes 23, 179–187.
Van den Berg, B.C.J., Sierro, F.J., Hilgen, F.J., Flecker, R., Larrasoaña, J.C., Krijgsman, W., Flores, J.A., Mata, M.P., Martín, E.B., Civis, J., González-Delgado, J. A., 2015. Astronomical tuning for the upper Messinian Spanish Atlantic margin: disentangling basin evolution, climate cyclicity and MOW. Glob. Planet. Chang. 135, 89–103.
Van der Meer, M.T.J., Baas, M., Rijpstra, I.C., Marino, G., Rohling, E.J., Sinninghe Damsté, J.S., Schouten, S., 2007. Hydrogen isotopic compositions of long-chain alkenones record freshwater flooding of the Eastern Mediterranean at the onset of sapropel deposition. Earth Planet. Sci. Lett. 262, 594–600.
Van Hinsbergen, D.J., Meulenkamp, J.E., 2006. Neogene supradetachment basin development on Crete (Greece) during exhumation of the South Aegean core complex. Basin Res. 18 (1), 103–124.
Vasiliev, I., Reichart, G.-J., Davies, G.R., Krijgsman, W., Stoica, M., 2010. Strontium isotope ratios of the Eastern Paratethys during the Miocene/Pliocene transition; Implications for interbasinal connectivity. Earth Planet. Sci. Lett. 292, 123–131. https://doi.org/10.1016/j.epsl.2010.01.027.
Vasiliev, I., Reichart, G.J., Krijgsman, W., 2013. Impact of the Messinian Salinity Crisis on Black Sea hydrology - insights from hydrogen isotopes on molecular biomarkers. Earth Planet. Sci. Lett. 362, 272–282. https://doi.org/10.1016/j.epsl.2012.11.038.
Vasiliev, I., Reichart, G.-J., Grothe, A., Sinninghe Damsté, J.S., Krijgsman, W., Sangiorgi, F., Weijers, J.W.H., van Roij, L., 2015. Recurrent phases of drought in the upper Miocene of the Black Sea region. Paleogeogr. Paleoclimatol. Paleoecol. 423, 18–31.
Vasiliev, I., Mezger, E.M., Lugli, S., Reichart, G.J., Manzi, V., Roveri, M., 2017. How dry was the Mediterranean during the Messinian salinity crisis? Paleogeogr. Paleoclimatol. Paleoecol. 471, 120–133. https://doi.org/10.1016/j.paleo.2017.01.032.
Vasiliev, I., Karakitsios, V., Bouloubassi, I., Agiadi, K., Kontakiotis, G., Antonarakou, A., Triantaphyllou, M., Gogou, A., Kafousia, N., de Rafélis, M., Zarkogiannis, S., Kaczmar, F., Parinos, C., Pasadakis, N., 2019. Large sea surface temperature, salinity, and productivity preservation changes preceding the onset of the Messinian Salinity Crisis in the eastern Mediterranean Sea. Paleoceanogr. Paleoclimatol. 34, 182–202. https://doi.org/10.1029/2018PA003438.
Veizer, J., 1989. Strontium isotopes in seawater through time. Annu. Rev. Earth Planet. Sci. 17 (1), 141–167.
Violanti, D., Trenkwalder, S., Lozar, F., Gallo, L.M., 2009. Micropaleontological analyses of the Narzole core: biostratigraphy and paleoenvironment of the late Messinian and early Zanclean of Piedmont (Northwestern Italy). Boll. Soc. Paleontol. Ital. 48, 167–181.

Warren, J.K., 2016. Evaporites: A geological compendium. Springer.
Winterberg, S., Picotti, V., Willett, S.D., 2020. Messinian or Pleistocene valley incision within the Southern Alps. Swiss J. Geosci. 113 (1), 1–14. https://doi.org/10.1186/s00015-020-00361-7.
Wortmann, U.G., Chernyavsky, B., Bernasconi, S.M., Brunner, B., Böttcher, M.E., Swart, P.K., 2007. Oxygen isotope biogeochemistry of pore water sulfate in the deep biosphere: Dominance of isotope exchange reactions with ambient water during microbial sulfate reduction (ODP Site 1130). Geochim. Cosmochim. Acta 71, 4221–4232.
Zachariasse, W.J., van Hinsbergen, D.J.J., Fortuin, A.R., 2008. Mass wasting and uplift on Crete and Karpathos (Greece) during the Early Pliocene related to beginning of South Aegean left-lateral, strike slip tectonics. Geol. Soc. Am.Bull. 120, 976–993.
Zachariasse, W.J., van Hinsbergen, D.J., Fortuin, A.R., 2011. Formation and fragmentation of a late Miocene supradetachment basin in central Crete: implications for exhumation mechanisms of high-pressure rocks in the Aegean forearc. Basin Res. 23 (6), 678–701. https://doi.org/10.1111/j.1365-2117.2011.00507.x.
Ziveri, P., Baumann, K.H., Bockel, B., Bollmann, J., Young, J., 2004. Present day coccolithophore-biogeography in the Atlantic Ocean. In: Coccolithophores: From Molecular Processes to Global Impact. Springer Verlag, pp. 403–428.
Zonneveld, K.A., Marret, F., Versteegh, G.J., Bogus, K., Bonnet, S., Bouimetarhan, I., Crouch, I.E., Esper, O., 2013. Atlas of modern dinoflagellate cyst distribution based on 2405 data points. Rev. Paleobot. Palynol. 191, 1–197.